FACULDADE DE ENGENHARIA DA UNIVERSIDADE DO PORTO

Antenna Design for Underwater Applications

Oluyomi Aboderin

Doctoral Program in Telecommunications

Supervisor: Prof. H. M. Salgado

Second Supervisor: Dr. L. M. Pessoa

July 29, 2019

Antenna Design for Underwater Applications

Oluyomi Aboderin

Doctoral Program in Telecommunications

July 29, 2019

Resumo

A investigação no campo das comunicações subaquáticas continua a gerar bastante interesse em todo o mundo, devido à ampla gama de aplicações que esta tecnologia cobre, que incluem: monitorização de campos de petróleo e gás no mar, proteção e vigilância costeira, recolha de dados oceanográficos que necessitam de troca de dados entre dois ou mais Veículos Submarinos Autónomos (AUVs) e observação ambiental subaquática para exploração. A este respeito, a tecnologia de ondas de rádio subaquáticas é proposta como um meio de fornecer comunicações de alta velocidade a uma curta distância entre dois corpos subaquáticos. Isto será de grande importância para mergulhadores, fotógrafos subaquáticos ou cinegrafistas, mergulhadores científicos e outros exploradores subaquáticos. No entanto, esta tecnologia sofre bastante com a atenuação em ambientes subaquáticos. Consequentemente, neste trabalho foram consideradas principalmente frequências mais baixas na banda de alta frequência onde o efeito da atenuação é mínimo.

Logo, com base em cálculos matemáticos e considerações para a condutividade e permitividade do meio, foram desenvolvidas antenas subaquáticas para uso em ambientes aquosos. As antenas desenvolvidas podem ser agrupadas em relação à sua largura de banda e às suas características de radiação. Nestas incluem-se antenas de banda estreita, banda dupla e de banda larga, bem como aquelas com características de radiação omnidirecional, bidirecional e direcional. Finalmente, os ganhos obtidos com as antenas subaquáticas para sistemas de comunicações subaquáticas são também apresentados.

Este trabalho de investigação pode ser resumidamente dividido em quatro categorias, que são: investigação de análises teóricas relevantes de propagação de ondas de rádio em meios com perdas, extensa simulação computacional usando o software de simulação eletromagnética FEKO, fabrico de antenas com resultados positivos e validação experimental do trabalho realizado, que inclui a medição das características de radiação das antenas no meio.

Assim, a fabricação das antenas projetadas com bons resultados foi realizada nas instalações do INESC TEC. Além disso, as antenas fabricadas foram caracterizadas com o auxílio do analisador de quadripolos recorrendo a uma tanque de água doce localizada no INESC TEC, com as antenas a uma profundidade de 2.5 m da superfície e colocadas no centro do tanque (que tem dimensões de 10 m x 6 m x 5.5 m e a condutividade da água foi de 0.0487 S/m a 25^{o}C).

Abstract

Research in the field of underwater communications continues to generate a lot of interest worldwide, due to a wide range of applications that this technology covers, which include: offshore oil and gas field monitoring, coastline protection and surveillance, oceanographic data collection which will require data exchange between two or more Autonomous Underwater Vehicles (AUVs) and underwater environmental observation for exploration. In this regard, underwater radio waves technology is proposed as a means to deliver high-speed communications at a short range between two underwater bodies. This will be of great importance to scuba divers, underwater photographers or videographers, scientific divers and other underwater explorers. Though this technology suffers greatly from attenuation in the underwater environment. Consequently this work has been considered mainly in lower frequencies in the high-frequency band where the attenuation effect is minimal.

Therefore, based on mathematical calculations and considerations for the conductivity and permittivity of the medium, underwater antennas were developed in this work for usage in aqueous environments. The developed antennas can be grouped into two with respect to bandwidth and their radiation characteristics. These includes narrow, dual and wideband antennas as well as those with omnidirectional, bi-directional and directional radiation characteristics. Finally, realized gains of underwater antennas for underwater communication systems are as well presented.

This research work can be summarily divided into four categories, which are: investigation of relevant theoretical analyses of radio waves propagation in lossy medium, extensive computer simulation using FEKO electromagnetic simulation software, fabrication of antennas and experimental validation of the work done, which include measurement of radiation characteristics of the antennas in the medium.

Hence, fabrication of the designs with good results was performed in the INESC TEC facilities. Also the manufactured antennas were measured with the aid of Vector Network Analyzer (VNA) and these were carried out in a freshwater tank located at INESC TEC, with the antennas at a depth of 2.5 m from the surface and placed on the centre of the tank (which has dimensions of 10 m $\times$ 6 m $\times$ 5.5 m and the conductivity of water was 0.0487 S/m at 25°C).

Acknowledgments

My foremost gratitude goes to the Almighty God, the creator of Heaven and Earth, for the gift of life and the grace I receive from him prior to the start of the research work till date. I am also very grateful to my supervisor Prof. Henrique Salgado and my co-supervisor Dr. Luís Pessoa for their combined effort, support, guidance and time spent on my research work and in every means that they have assisted me during my program. I am also deeply indebted to Dr. Mario Pereira for his untiring effort to assist all through when we were together in our laboratory. Not forgetting everyone in our -1 floor (Hugo, Joana, Erick and Ricardo), who have assisted in one way or the other and staff of the Robotic units in FEUP and INESC TEC building in ISEP.

I am extremely grateful to the Director General and Chief Executive and the Management Staff of the National Space Research and Development Agency (NASRDA) for granting the study leave that enabled my participation in the MAP-tele doctoral degree program. I am also not ungrateful to friends that were very helpful at the various junction in the course of my studies in Portugal. I will specifically mention; Dr. Abayomi Otebolaku and his family, Dr. Isiaka Alimi and his family, a friend more than a brother. Not forgetting fellow NASRDA colleagues and the entire Nigerian friends that made Portugal be home away from home.

This page will be incomplete without appreciating the members of my family. I am grateful to my parents, Rev. Dr. Ezekiel Olajide Aboderin and Mrs. Esther Olufunmilayo Aboderin, who provided the platform for my educational journey and set me on the right path, I need to say without you guys, there won't be me. I am as well very grateful to my second Mummy, Mrs. Busola Akinbaani for her unflinching support and prayer all through my journey here. I am also thankful to all my siblings and their family members for their efforts and encouragement throughout my academic pursuit till date. I will like to specifically mention Oluwaseun and Samuel the children of my late sister.

Finally, I am grateful to my best friend, my wife, my "Real Mummy" and my "girl", Ololade Omolola Aboderin for her patience and support both when she was alone with the kids in Nigeria and many time she was alone with them here in Porto. I am also indebted to my "Super Heroes" Inioluwa and Olaoluwa who could not understand why Daddy cannot enjoy weekends, holidays and even anniversaries with them at home in Nigeria and even here in Porto. I salute you guys!! Not forgetting Morayooluwa Olivia, a "master cum Ph.D. graduate", who joined the family during the period that my wife and I were both students in FEUP.

Lastly, to every other individual that have been of assistance in one way or the other during this program, I say THANK YOU.

Oluyomi Aboderin

"I can do all things through Christ which strengthen me.
Philippians 4: 13"

Contents

List of Figures

List of Tables

Abbreviations and Symbols

AUV	Autonomous underwater vehicles
BCA	Buoyant cable antenna
CDMA	Code Division Multiple Access
CSA	Cavity-backed Slot Antenna
DARPA	Defence Advanced Research Projects Agency
DRA	Dielectric Resonator Antenna
EHF	Extremely High Frequency
EFL	Electric Field Line
ELF	Extremely Low Frequency
EM	Electromagnetic
FEUP	Faculty of Engineering University of Porto
GPS	Global Positioning Systems
GO	Geometrical Optics
GSM	Global System for mobile communications
GTD	Geometrical Theory of Diffraction
H2020	Horizon 2020
HDPE	High-density polyethylene
HF	High Frequency
HED	Horizontal Electric Dipole
HMD	Horizontal Magnetic Dipole
IEEE	Institute of Electrical and Electronics Engineers
INESCTEC	Institute for Systems and Computer Engineering, Technology and Science
IOT	Internet of Things
ISI	Inter Symbol Interference
LEO	Low Earth Orbit
LF	Low Frequency
LORAN-C	long range navigation-C
LOS	line-of-sight
LTE	Long term Evolution
MF	Medium Frequency
MFL	Magnetic Field Loop
MMIC	Monolithic Microwaves Integrated Circuit
OC	Optical Communication
PEC	Perfect Electric Conductor
PCS	Personal Communication Service

RADAR	Radio Detection and Ranging
RF	Radio Frequency
RFID	Radio Frequency Identification
ROV	Remotely Operated Vehicles
RR	Radio Regulations
SEAFARER	Surface ELF Antenna For Addressing REmotely-deployed Receivers
SI	International Standard
SINR	Signal to Interference plus Noise Ratio
SLF	Super Low Frequency
SNR	Signal to noise ratio
SQUID	Superconducting Quantum Interference Device
SHF	Super High Frequency
THF	Terahertz High Frequency
TWA	Traveling Wave Antenna
UHF	Ultra High Frequency
ULF	Ultra Low Frequency
UMTS	Universal Mobile Telecommunications System
URFC	Underwater Radio Frequency Communication
UTD	Uniform Theory of Diffraction
UWB	Ultrawideband
VAMOS	Viable Alternative Mine Operating System
VED	Vertical Electric Dipole
VEIN	velocity induced electrode noise
VHF	Very High Frequency
VLF	Very Low Frequency
VMD	Vertical Magnetic Dipole
WI-FI	Wireless Fidelity
WiMAX	Worldwide Interoperability for Microwave Access
WLAN	Wireless Local Area Network
WRC	World radiocommunication Conference
WWW	*World Wide Web*

Chapter 1

Introduction

Transmission and reception of signals in aqueous environments require intense study and understanding of various parameters that can cause impairments or degradation thereby altering the propagation phenomenon of signals and devices immersed in it. There has also been an increasing demand for high-speed wireless communication links for underwater applications, which include: oceanographic data collection which will require data exchange between two or more Autonomous Underwater Vehicles (AUVs) and other underwater sensors, coastline protection and surveillance, underwater environmental observation for exploration and off-shore oil and gas field monitoring. In these applications, communications require downloading of mission data from the AUV to the docking station, successful docking of the AUV at the station for recharging through wireless power transfer [1], exchange of data between AUVs and underwater wireless sensor nodes.

In underwater communication there are three established technologies through which underwater communications have been considered, they are; acoustics and ultrasonic signals, optical signals, and radio frequency (RF) signal [2]. Due to the various advantages of the technologies, each of these is most appropriate for different underwater applications. For instance, when long-range propagation (up to tens of kilometers) in fresh or sea water is of paramount concern, as seen in the case of submarines, which are submerged in hundreds of meters below the water surface and communicating with a location on the earth surface, acoustic and ultrasonic systems are the most appropriate technology [3, 4, 5]. Similarly, when the distance is considerably long and high data-rates with low latency is expected, optical communication systems remain the best technology [4, 5, 6]. On the other hand, for a short-range and relatively high-speed communication, which is important for real-time voice, video and data exchange, EM signals will ensure smooth communication in this regards [2]. Despite these advantages, each of the

technologies still has its disadvantages. The acoustic and ultrasonic signal is unfit for real-time and broadband underwater wireless sensor networks because of poor immunity to noise, low data-rates, and high channel latency. In like manner, optical communication requires very good alignment and are as well affected by suspended particles in water and marine fouling. The major disadvantage of EM signals is attenuation, which imposes limits on its usage for underwater communications, as it increases with increasing operating frequency [7, 8]. Thus, the main concern of this thesis is to present the design, simulation, construction and measurements of underwater antennas, which will be utmost useful in various underwater applications by scuba divers, oceanographers, underwater photographers, and underwater miners. The performance of these antennas is accessed in fresh water for maximum directivity which is important for propagation distance and bandwidths for the data rates at this distance.

1.1 Motivation

The motivation for this work is to improve short-range communications which may exist between transmitting/receiving devices on scuba divers on one hand and with underwater elements (AUV, ROV (Remotely Operated Vehicles), sensor nodes) on the other hand or between an AUV and docking station, through the usage of underwater radio frequency communications. Robotic based activities in the underwater environment required sufficient bandwidth, improved propagation distance, and minimal attenuation, for real-time transmission and reception of signals in the medium. Hence, what measure(s) can be taken to ensure that the system suffers minimal attenuation? How also can propagation distance be improved for the underwater antennas in the environment? Also, to provide a better alternative to the usage of acoustic communication in the underwater scenario and for the possibility of combining this technology with either acoustic or optical communications in a hybrid underwater network for improved long-range communications in deep water scenario.

1.2 Aims and Objectives

To improve communications between underwater users and equipment through underwater radio frequency communications (URFC), the objective of this work is the design of antennas for underwater communications, followed by fabrication of these antennas, test and measurement.

1.2.1 Objectives

- To develop portable underwater antennas suitable for installation on AUV for onward communication with underwater sensor nodes and docking station;
- To develop underwater antennas useful for scuba divers for data harvesting in the shallow water scenario;
- To develop an analytical method that can be used to determine the gain of these antennas, which will assist in analyzing their performance in a lossy medium;
- To validate these analytical methods through practical measurements of the underwater antennas;

1.3 Thesis Organization

Beside this introductory chapter, four other chapters and the concluding remarks were added thereafter.

Chapter 2 addresses the review of underwater antennas with respect to designs, developments, and usage. This chapter comprises:

- definitions of antennas, brief history, and types.
- Underwater technologies with a table showing similarities and differences of the technologies;
- Extensive review of the state of the art with respect to antenna design and EM propagation in underwater environments, spanning around a century.

In **chapter 3**, the propagation of electromagnetic waves in lossless and lossy media is presented. This includes theoretical information regarding propagation in water, determination of the radiation characteristics of antennas submerged in lossy medium and also factors that affect RF propagation in the medium.

In **chapter 4**, full analyses of underwater antennas regarding the effect of the change in materials of the wire, the coating of the wire of the designed antennas, change in conductivity of the medium and when the antennas are placed in an air-filled casing were presented. In the second part, the performance of designed narrow band antennas was also presented.

In **chapter 5**, the performance of antennas with dual and wideband capabilities are assessed with respect to their radiation characteristics and bandwidth. Also presented in

this chapter are the antennas designed in a European project that our team partnered with. Though these antennas were originally designed as wideband, in order to ensure that the antennas were secured against water waves in the medium, addition of materials with different permittivities and their final performance is further investigated. Final in this chapter, realized gain and link budget of underwater antennas is presented.

Chapter 6 is the final chapter of this thesis, where final conclusion is drawn and the future works were also presented.

1.4 Contributions

The main contributions of this research are summarized below

- Model approach to the usage of wire antennas for narrow, dual and wideband communication in the underwater environment;
- Designing of underwater antennas at a specified resonating frequency;
- Modeling of directional underwater antennas for improved propagation distance;
- Underwater antenna modeling around the body of Autonomous Underwater vehicles;
- Experimental measurements of the radiation pattern of underwater antennas;
- Determination of realized gains of underwater antennas;

1.5 Publications

The following publications are the results of these contributions:

1. S. I. Inacio, M. R. Pereira, H. M. Santos, L. M. Pessoa, F. B. Teixeira, M. J. Lopes, O. Aboderin and H. M. Salgado, "Antenna design for underwater radio communications" OCEANS, Shanghai China, 2016;
2. S. I. Inacio, M. R. Pereira, H. M. Santos, L. M. Pessoa, F. B. Teixeira, M. J. Lopes, O. Aboderin and H. M. Salgado, "Dipole Antenna for Underwater Radio Communication" Underwater Communications Network (UComms), Lerici Italy, 2016;
3. L. M. Pessoa, M. R. Pereira, O. Aboderin, H. M. Salgado, and S. I. Inácio, “Antenna for underwater radio communications,” patent ep 3 291 364A1;

4. O. Aboderin, S. I. Inacio, H. M. Santos, M. R. Pereira, L. M. Pessoa and H. M. Salgado, "Analysis of J-Pole Antenna Configurations for Underwater Communications" OCEAN, Monterey California, United States of America, 2016;

5. O. Aboderin and L. M. Pessoa and H. M. Salgado, "Performance evaluation of antennas for underwater applications" Wireless Days 2017, Porto Portugal;

6. O. Aboderin, L. M. Pessoa and H. M. Salgado, "Analysis of loop antenna with ground plane for underwater communications," OCEANS 2017 - Aberdeen, Aberdeen, 2017;

7. O. Aboderin, L. M. Pessoa and H. M. Salgado, "Wideband dipole antennas with parasitic elements for underwater communications" OCEANS 2017 - Aberdeen, Aberdeen, 2017;

8. O. Aboderin and L. M. Pessoa and H. M. Salgado, "Analysis of Antennas Designed for Fresh Water Applications" to be submitted to IEEE Access;

9. O. Aboderin and L. M. Pessoa and H. M. Salgado, "A Survey of Underwater Antennas: Designs, Developments and Applications" To be submitted to IEEE Communications Surveys & Tutorials.

Chapter 2

Review of Underwater Antennas: Designs, Developments and Usage

2.1 Introduction

The much breakthrough in modern-day scientific research and technology can be attributed to the military exploits mostly around the first and second world wars. Some of the technologies that benefited from military activities include the antenna designs and development, satellite communication, Internet network, underwater communications among others [9]. Antenna, therefore, has proven to be an integral part of other technologies as the reliant on its usage cuts across different applications in space science, terrestrial networks, and underwater communications. In space science, antenna remains one of the most important equipment that ensures respective transmission and reception of telecommand and telemetry data, to and from satellites launched into orbits that is thousands of kilometers away from the earth's surface. Similarly, terrestrial networks has witnessed evolution from; wired to wireless, copper wire to fiber optic where long-distance transmission and interference which are limited to the former are well resolved in the latter, analog to digital, which include metamorphosing from first generation (1G) to the most recent fifth generation (5G) networks, whilst still looking ahead to the sixth generation (6G) [10, 11]. The need for high-speed, short-range communication for relevant applications in the context of underwater exploration and mining makes the development of various antennas that are capable of meeting these requirements of great importance to scuba divers, underwater miners, and other users. Therefore, this chapter begins discussing antenna as a whole with respect to its definition, history and types. Also, major technologies that ensure smooth communications in the underwater environment are compared and extensive review of designing, developing and

usage of underwater antennas over many decades and for many services is finally given.

2.2 Antenna in Communication Systems

One of the most critical components importantly needed in the communication systems (mobile, wired and wireless) in any medium is an antenna. The increasing need of improving communication mechanism; in household equipment (including television antennas (loop or Yagi), multi-functional cell phones, hand-held portable devices, long-range communications, electronic chips (including Radio Frequency Identification (RFIDs)) and most recently Internet of Things (IoT) has made the entire globe to depend on antennas for day-to-day activities. In actual fact, antennas in their millions are so ubiquitous worldwide.

Many definitions have been used to describe an antenna in several pieces of literature, but in all, it involves radiating and receiving of radio waves. For instance, it is defined in IEEE Standard Definitions of terms for antennas as "a means of radiating or receiving electromagnetic (radio) waves [12]." Webster's dictionary also defines an antenna as a metallic device, which may be rod or wire for radiating or receiving radio waves. Several writers in books and articles also have their respective definition for an antenna. Balanis in [13] defined it as transitional equipment or device between free space and a guiding device, whilst in [14] it is defined as a transducer that converts a guided wave to a free space wave or vice-versa and is also defined as a device that converts bounded circuit field into propagating electromagnetic wave (Transmitting antenna) and by reciprocity is a device that collects power from passing electromagnetic waves (receiving antenna) [15]. Thus, in all these definitions, it is obvious that an antenna is a device for transmitting and/or receiving radio waves or electromagnetic waves. The basic description of an antenna in either transmitting or receiving form is presented in Fig. 2.1.

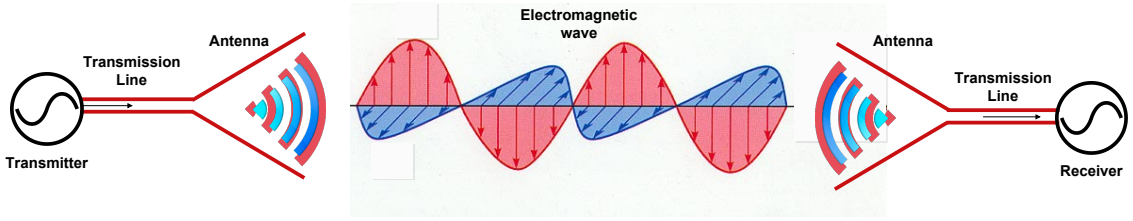

Figure 2.1: Antenna operation between the transmitter and the receiver [13]

Apart from the antenna, the medium where the antenna will be operated is also critical in the design analysis of such antennas. For instance, if an antenna is designed for usage in the air at a certain operating frequency, there will be frequency shift, when the same

antenna is encased in a glass or plastic box, due to change in its surrounding medium. There will be further shifting in the operating frequency when the antenna is immersed in water, which is also depending on whether it is fresh or sea water. All these frequency shifts depend on change in the permittivity and conductivity of the surrounding medium of the antenna.

2.2.1 Brief History of Antennas

James Clerk Maxwell's unified of the theories of electricity and magnetism into the electromagnetic theory in 1883, which was presented in a set of relations known as Maxwell's equations which forms the basic foundation for modern-day communication technologies. Four years later, Prof. Henrich Rudolf Hertz (1857-1894), (the SI (International Standard) unit of frequency is named after him) performed experiments to demonstrate the existence of electromagnetic radiation. This was done by connecting a dipole antenna to a variable voltage source as the transmitter and using a loop antenna as the receiver. A prototype of Hertz's experiment is presented in Fig. 2.2. The experiment confirmed that information can be transmitted between two locations through electromagnetic waves. Another important early contribution came from Guglielmo Marconi. He developed and commercialized wireless communication through the introduction of a radiotelegraph system. He was renown for the first Atlantic transmission in 1901 from Podhu, in the United Kingdom to St. John, Newfoundland in Canada, by employing un-tuned systems. His transmitting antenna is made up of 50 vertical wires, which were made to resemble fan and were connected to ground through a spark transmitter and the receiving antenna was a 200 m wire, is supported by a kite. It is important to note that Marconi used monopole antennas for most of his experiments, such that vertical monopole antennas are being referred to as Marconi antenna [16, 13, 17].

From Marconi's remarkable long range transmission up till the 1940s, other efforts in antenna development were restricted to usage of wires as radiating elements and operating at frequency up to Ultra High Frequency (UHF) bands. During World War (II), more antenna types like apertures, horns and reflector antennas were developed to cater for the need at that time. These resulted in the development of broadband, circularly polarized and other antennas for numerous applications. From the 1960s till date, advances were made in computer technology, mobile communications, wired and wireless communications among others, which also impacted positively in antenna developments for radio broadcasting, wireless communications (terrestrial, satellite and underwater) and RADAR (Radio Detection and Ranging) systems. Also, proliferation of emerging standards and applications (Global System for mobile communications

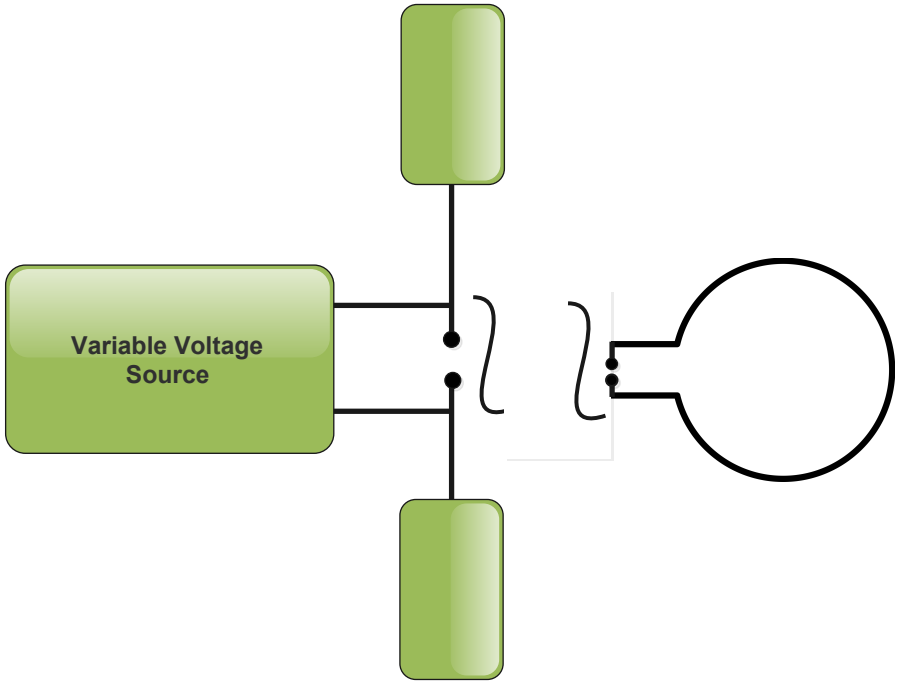

Figure 2.2: Hertz experiment of 1887 [17]

(GSM), Universal Mobile Telecommunications System (UMTS), Code Division Multiple Access (CDMA), Bluetooth, infrared, Personal Communication Service (PCS), Wireless Local Area Network (WLAN), Long term Evolution (LTE), Wireless Fidelity (WI-FI), Worldwide Interoperability for Microwave Access (WiMAX) and most recently Internet of Things (IoT)) require antennas that will match their service requirements, with respect to bandwidth (narrowband, wideband, ultrawideband (UWB)), high gain, directivity (omnidirectional and direction) and high efficiency.

2.2.2 Antenna Sizes

Antenna dimensions are usually expressed in terms of the wavelength (λ). It can be said that the frequency, wavelength, and size are related such that as the frequency decreases, the wavelength increases and the sizes increases. Thus for effective radiation of a named antenna, it is critical for its length to be a fraction of wavelength. Most common of these are half-wavelength ($\lambda/2$) and quarter-wavelength ($\lambda/4$). Hence, the length of a half-wave dipole antenna is approximately $\lambda/2$, whereas the length of the conductor for a monopole antenna is $\lambda/4$. Therefore the idea of antenna miniaturization is to ensure that a named antenna has its physical dimension shrink without any degradation on its performance nor affect the initial operating frequency, noting that a small antenna will always have to consider its size with respect to the operation wavelength [13]. In the underwater

environment, it is important to design an antenna that operates in the frequency band where attenuation effect is minimal, which should be below 400 MHz, as discussed later in section 3.3. Though it is expected that such an antenna might have a large physical dimension given the operation frequency ($\lambda = \frac{v}{f}$ in air) and the wavelength in free space equals 0.75 m. But in the underwater environment, the wavelength changes, which is due to the effect of permittivity (water relative permittivity is 81) and conductivity (0.005 S/m in fresh water and 4 S/m in sea water) in this medium and subsequently the dimension of the antenna. For instance, if a dipole antenna is designed to operate at 300 MHz; in the air, the wavelength is 1 m, whereas, at the same frequency, the wavelength is 0.124 m and 0.077m in fresh and sea water respectively.

2.2.3 Frequency Bands

Operating frequency is very important in any form of communication worldwide. It plays a significant role in the designing of equipment and providing services accordingly. It is fundamental in the design and developments of antennas for any services. To this end the International Telecommunication Union (ITU), an agency of the United Nation (UN) tasked with the responsibility of allocation, allotting, and management of frequency bands, which in conjunction with the International Union of Radio Science (URSI) designated the bands appropriately. It is therefore important for communication equipment manufacturers, antenna designers, network managers among others to be conversant with these allocations for proper design and management of equipment. In antenna design, for instance, the frequency of operation, as well as conductivity and permittivity, are important for determining the dimension of antennas depending on whether the medium is lossy or lossless. Thus, Table 2.1 gives details of the band designations as defined by the ITU in the radio regulations (RR), these documents contain four sub-documents (Articles, Appendices, Resolutions, and Recommendations) and the information therein are subject to review every four years during the World Radiocommunication Conference (WRC) [10, 18, 19, 20].

2.3 Types of Antennas

Antennas come in different forms (types, shapes, and configurations). This is depending on its usage, application and integration with other electronic devices. Thus, it can be grouped either by their physical structures or by various antenna parameters. For instance;

Table 2.1: ITU's table of frequency bands [18, 21]

Band Number	**Band Name**	**Symbols**	**Frequency range**	**Metric subdivision**
1	Extremely Low Frequency	ELF	3 - 30 Hz	
2	Super Low Frequency	SLF	30 - 300 Hz	
3	Ultra Low Frequency	ULF	300 - 3000 Hz	
4	Very Low Frequency	VLF	3 - 30 kHz	Myriametric waves
5	Low Frequency	LF	30 -300 kHz	Kilometric waves
6	Medium Frequency	MF	300 -3000 kHz	Hectometric waves
7	High Frequency	HF	3 - 30 MHz	Decametric waves
8	Very High Frequency	VHF	30 - 300 MHz	Metric waves
9	Ultra High Frequency	UHF	300 - 3000 MHz	Decimetric waves
10	Super High Frequency	SHF	3 - 30 GHz	Centimetric waves
11	Extremely High Frequency	EHF	30 - 300 GHz	Millimetric waves
12	Terahertz High Frequency	THF	300 - 3000 GHz	Decimillimetric waves

- if grouped with respect to bandwidth, they can be either narrowband or broadband (wideband, ultra-wideband (UWB));

- if organized with respect to their polarization, they can be circular, linearly (horizontal and vertical) or elliptically polarized;

- if divided with respect to their resonance, they can be traveling wave or resonant antennas;

- if classified with respect to the number of elements, they can be element antennas or antenna arrays.

Hence, physical structures have been used to classified antennas into 6 different groups.

2.3.1 Wire Antennas

Wire antennas are ubiquitous and seem to be more common than other antenna types and it is very familiar to a layman as they can be seen virtually everywhere. They are low cost, easy to construct and made from conducting wires. These antennas are used in automobiles, personal communications/applications, spacecraft, ships, and buildings. Various shapes of these antenna types include; Dipole, loop, Helix, J-pole, and spiral. Each of these may take different shapes, through which their performance can be optimized [17, 13]. Example of wire antennas are presented in Fig. 2.3. These antennas have been explored in the context of this thesis for underwater applications and are discussed in chapter 4. It is important to note that wire antennas are more suitable to use in the underwater environment, as it can go directly into the medium, without the need protect the antennas from water, unlike printed antennas that will require spraying of Epoxy resin on its either side, which will, therefore, alter the design frequency.

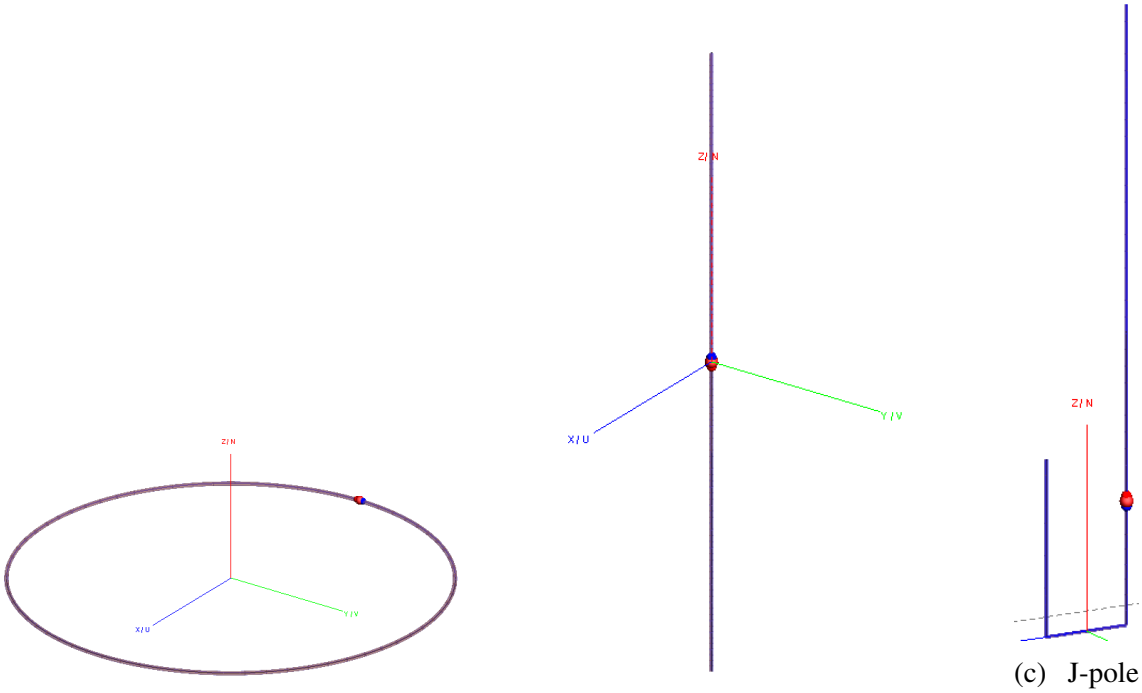

(a) Loop antenna (b) Dipole antenna (c) J-pole antenna

Figure 2.3: Examples of wire antennas

2.3.2 Aperture Antennas

These are antenna types with a physical opening that allows transmission and reception of electromagnetic waves. Aperture antennas can be flush-mounted, which made them suitable for use in spacecraft and aircraft. Example of antennas in this category includes;

horn antenna, a slot antenna, inverted-F antenna, and slotted waveguide antenna. Horns antennas are presented in Fig.2.4 comprises of pyramidal (rectangular) and conical (circular) shapes.

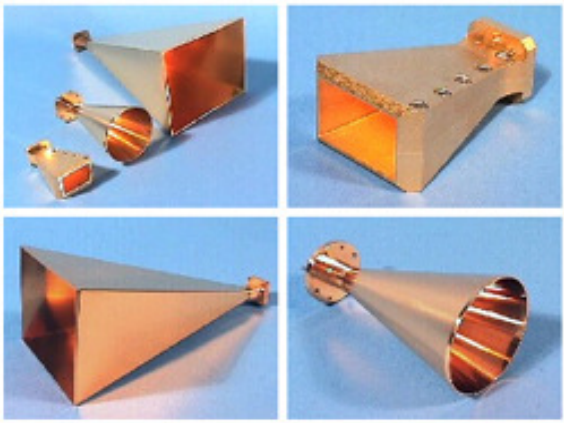

Figure 2.4: Different sizes of horn antennas [22]

2.3.3 Microstrip Antennas

Microstrip antennas consist of a metallic patch which can come in different shapes (circular, square, triangular), the substrate and the metallic ground plane. They are basically conformable to planar and non planar surfaces, low profile, simple or easy to design, low cost, when mounted on rigid surface they are mechanically robust, compatible with Monolithic Microwaves Integrated Circuit (MMIC) and as well very versatile with respect to their polarization, pattern, resonant frequency and impedance.

2.3.4 Antenna Arrays

Antenna arrays are sets of identical antennas that are radiating individually and are arranged in an electrical or geometrical form, in order to improve the overall performance over a single element antenna. It is also known as Phased arrays, which are used typically for military radar applications and in adaptive cruise control. The pattern of the array is determined by the relative amplitude and phase of the excitation fields of each source and the geometric spacing of the sources. Other antenna types like microstrip, wire, reflector antennas can form elements of an array antenna as seen Fig.2.5, where four elements microstrip antenna operating at 15 GHz, were used to form an array. Some of the advantages of this antenna include [23, 13];

- achieve diversity reception;

- increase the overall gain;
- improve Signal to Interference plus Noise Ratio (SINR);
- improve or reduce radiation characteristics in a particular direction(s);
- "Steer" the array to ensure that it is most sensitive in a particular direction;
- deduces the route of the incoming signals.

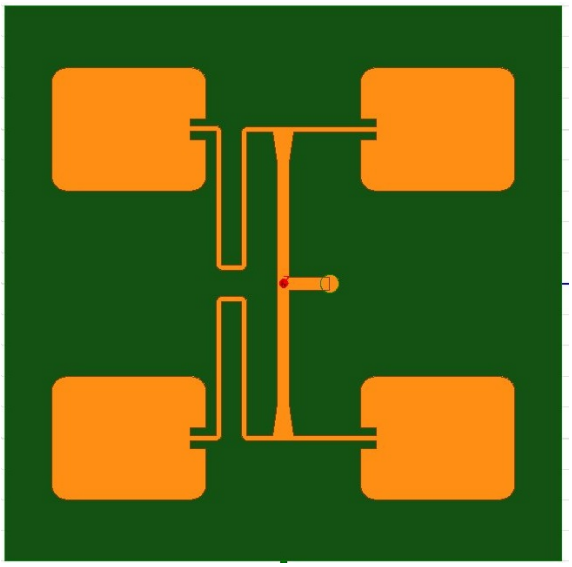

Figure 2.5: Four-element microstrip antenna array operating at 15 GHz band

2.3.5 Reflector Antennas

These are antennas with typically high gain (30 - 40 dBi), with a prospect to communicate over great distances, for radio communications, radio astronomy high-resolution radars and others. In principles, reflector antennas operate on the theory known as geometrical optics (GO). They are used in satellite communications and other outer space-related communications, where signals travel several thousands of kilometers between the transmitters and the receivers (satellite and ground receiving station). Fig. 2.6 shows the reflector antennas at the ground receiving center of the Nigerian Communication satellite in Abuja, Nigeria.

2.3.6 Lens Antennas

They are used primarily to collimate divergent energy and prevent it from radiating in an unwanted direction. This is achieved by proper shaping of the geometrical configuration

Figure 2.6: Nigerian Communication Satellite ground receiving antennas [24]

in addition to the choice of appropriate material of the lenses. This antenna can convert various form of divergent signals into plane waves. Typical configurations of lens antennas are given in Fig. 2.7.

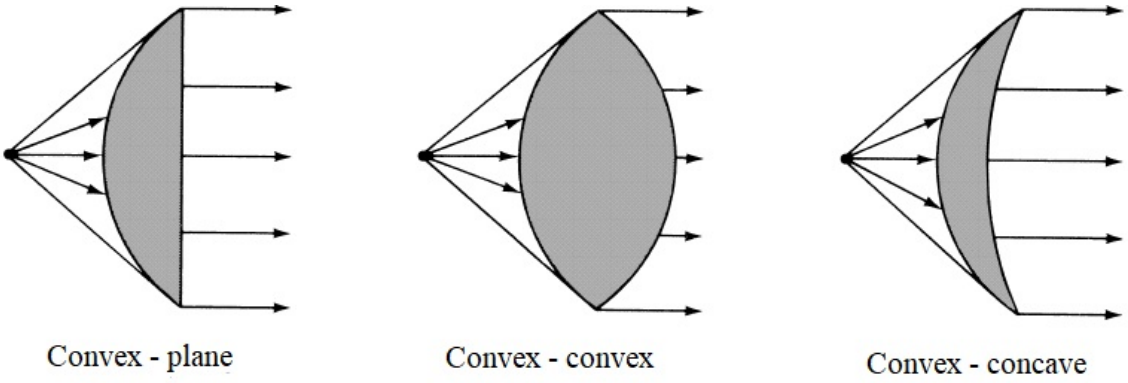

(a) Lens antennas with refractive index of n>1

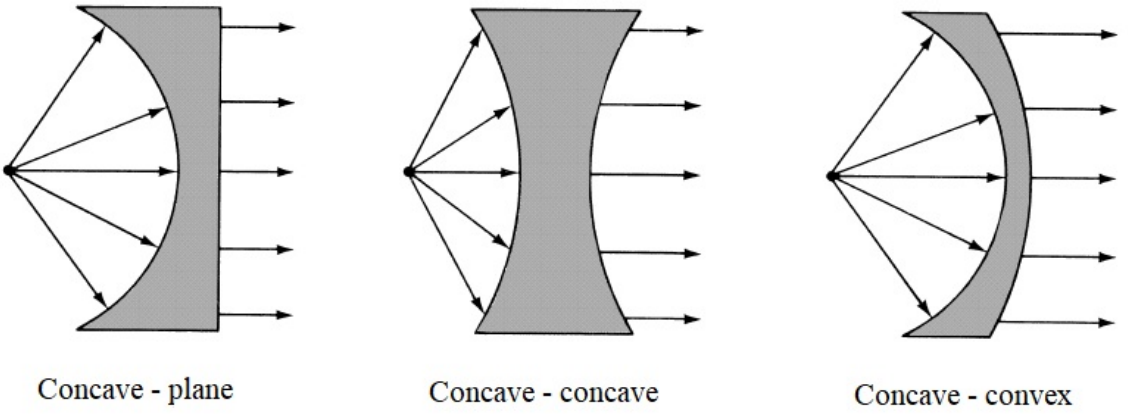

(b) Lens antennas with refractive index of n<1

Figure 2.7: Configurations of lens antennas [13]

2.4 Underwater Technologies

In underwater communications, there are three established technologies through which transmissions in this medium have been considered, they are [2]:

1. **Underwater acoustic communications;**
2. **Underwater optical communications and**
3. **Underwater radio frequency communications.**

Each of these has its merits and demerits in their usage for various applications in the medium. It is widely known that acoustic waves can propagate at a long range up to 20 km but at the expense of relatively low data rates, which can be around 1 b/s [2, 25]. Optical

communications, on the other hand, provide high data rates up to 1 Gbps, at seemingly propagation distance of about 100 m. On the other hand, wireless propagation of, the radio waves can achieve up to 1 km range with 100 b/s, but the data rates continue to decrease as the propagation distance increases. These three technologies are examined extensively and are presented as follows.

2.4.1 Underwater Acoustic Communications

Acoustic waves technology has been widely embraced worldwide as a viable solution for underwater communication because of its ability to establish long-distance links (up to tens of kilometers). Also, it is characterized by having low attenuation and can even operate in the absence of line-of-sight (LOS) between the terminals and in deep water [26, 27]. Despite these advantages, there are many disadvantages such as low data rates (propagates up to 20 Km at almost 1 b/s), high channel round trip delay (channel latency), poor immunity to noise and a high cost of nodes that have led to continuous research in alternative technologies. They are also not robust since they are easily affected by temperature, ambient noise, turbidity, and pressure gradients. Furthermore, they are dangerous to marine life and the ecosystem. Also, they offer poor propagation in shallow water due to interference [28]. The acoustic signals can also experience Inter-Symbol Interference (ISI), due to the multipath propagation effect [28]. In addition, this technology has low propagation velocity, when compared with other technologies, consequently, it suffers greatly from Doppler effects [29]. Thus, acoustic receivers often employ adaptive equalization [28, 30]. The ambient noise in acoustic communications is frequency dependent, which can be traced to a number of sources. For instance, at frequencies below 100 Hz, the noise is mainly due to marine traffic, whereas wind and rain are significantly responsible for noise at higher frequencies around 100 kHz, the noise level is dependent on the intensity of rain and wind. At frequencies beyond this, thermal noise, whose spectral density increases with frequency, is involved [28]. Despite these disadvantages, the technology is still being used around the world but other technologies are also gaining acceptance because of their advantages over acoustic systems.

2.4.2 Underwater Optical Communications

Apart from acoustic communications, another technology that has been widely used in the underwater environment is Optical Communication (OC). OC is as an alternative technology that provides ultra-high data rates up to the Gigabit per second (Gbps) and about 10-150 Mbps over moderate propagation distances (10-100 meters) [31]. It is

also immune to transmission round-trip delay, which is an advantage over acoustic communications. Likewise, it offers guaranteed signal fidelity (secured link) and low power consumption, among other things. However, this technology can only be used for short-range communications because of the strong backscatter from suspended particles and severe water absorption at the optical frequency band [32]. It also requires good alignment or line of sight for its propagation. Apart from these, optical waves are difficult to use for cross communications from seawater to air and vice versa, and they are also affected by scattering and absorption. They can also propagate at moderate link range (up to tens of meters) [31].

2.4.3 Underwater Radio Frequency Communications

The third technology, which can also be used for underwater communications is based on Electromagnetic (EM) waves in the radio frequency (RF) range. Usage of RF in the underwater environment began as a dream in the middle of the twentieth century, but further experiments have shown that when RF signal is coupled with digital signal compression, it has greater advantages than other technologies in the underwater scenario [25]. Apart from these, radio signals allow flexibility in the deployment of a wireless sensor network for coastal monitoring applications. This is nearly impossible with other technologies because of the high level of aeration and sediments present in coastal water. In water, EM waves propagate at a velocity that is about 4 times faster than that of the acoustic waves. This implies that Doppler shift and propagation delay or latency are significantly reduced and subsequently this technology is suitable for real-time data transfer [3, 26, 4, 5, 33].

Besides, it has also been proven that RF waves are less sensitive to reflection and refraction in shallow waters than the acoustic waves. This helps in reducing the multipath effect. In addition, the nature of water (dirty or clean) and suspended particles have very little or no impact on the RF waves. Also, it has no known effects on marine lives [34]. Furthermore, using the same technology, AUVs and ROVs can be charged at underwater docking station through wireless power transfer [1]. In terms of alignment, RF waves do not require strong alignment or LOS for propagating in any medium and are immune to acoustic noise. It also has the capability for cross-boundary transmission, that is water-to-air transmission or vice versa. This ensures long-range communication for the RF wave. In addition, out of the aforementioned technologies, it is the least affected by tidal waves or water turbulence [35, 25]. Moreover, RF waves do not require mechanical tunning, which is required with the acoustic communications and neither does it require surface repeaters especially when interfacing the water-air boundary [25, 6].

The similarities and differences including advantages and disadvantages of the three technologies are presented in Table 2.2.

Table 2.2: Comparison between three underwater technologies

Parameters	**Acoustics communications**	**Optical communications**	**EM/RF communications**
Data rates	Low data rates in kbps	High data rates in Gbps	Moderate data rates in Mbps
Latency (roundtrip delay)	High latency	Moderate latency	Low latency
Shallow water	affected by multi-path Propagation	Not affected	Not affected
Propagation speed	Low	High	High
Propagation Distance	Long range	Short range	Short range
Water condition (Turbidity and suspended particles)	affected by water condition	affected by water condition	not affected
Attenuation	Low	Low	High, which increases with frequency and water salinity
Cost	High cost of nodes	High cost	Relatively low cost
Line of sight (LOS)	Not required	Highly required	Not required

2.5 Underwater Antennas: Design, Development and Usage in Literatures

Antenna developments for underwater applications have been in the literature for more than a century. These developments have been considered in fresh and sea waters, with respect to the operations and usages in each medium. To this end, antenna design, developments and usage in sea water and fresh water are as presented in the subsections.

2.5.1 Antenna Developments for Usage in Sea Water

One of the earliest published work in an underwater antenna was by G. H. Clark in 1909. His experiment consisted of, two wires of 9.2 m long which were connected to the transmitting apparatus located at the Navy Yard Norfolk and also two insulated wires of 5.2 m long submerged below the surface of water at the depth of 1.2 m located at the Navy Yard Washington were connected to the receiving apparatus through a condenser of capacity 0.003 microfarad. Signals were received by the receiver, which was around 19 km away from the transmitter [36]. In furtherance of the work, experiments were also conducted on a boat located near Norfolk. Here, copper plates were attached to the insulated wires; while one plate was suspended over the stern into the water, the other was suspended over the bow into the water. Signals transmitted from the Navy Yard in Norfolk were received on this boat at a distance of up to 24 km. Despite the crude nature by which these experiments were conducted, it nonetheless became a remarkable achievement in the history of underwater antenna communication [36]. J. H. Rogers similarly transmitted from boat with underwater wires to a station in his home in 1916 [36]. About three years after, Rogers produced what can be tagged resounding breakthrough in the usage of antennas for underwater application, which was written by H. W. Secor and titled "American Greatest War Invention". The inventor based his idea on what should be a logical relationship between wireless transmission and reception of radio signals in the surface to those in the underwater environment. He believed that, since an antenna can transmit signal from a high altitude platform (mast) to a receiving antenna at a designated distance, then the same signal is transmitted appropriately through water, can be received by a receiving antenna submerged in underwater. In his work, he first used a heavily insulated stranded cable, stretched from stem to stern and attached to the submarines as a receiving antenna as presented in Fig. 2.8. This was later replaced by an insulated antenna placed in iron pipes located inside the submarines, probably to protect the antenna from the effect of the medium as shown in Fig. 2.9. The third is a long wire antenna attached to the last compartment of the submarine, thereby trailing it as presented in Fig. 2.10.

Based on these analyses and a couple of experiments, a wireless communication link was established with the submarines placed in seawater. This invention became an important tool that the American Navy used during the world war and the system he built paved ways for research in the usage of antennas in underwater environments. It was also reported that the submarines must be at a distance of less than 10 km to the transmitting antenna in seawater due to its conductive nature, whereas in fresh water the receiving antenna can be at any depth [37].

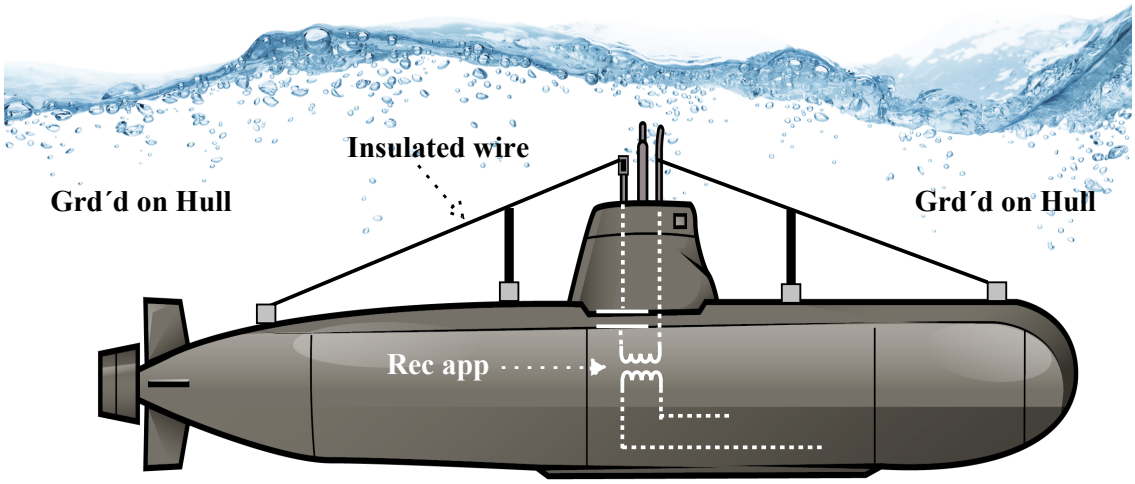

Figure 2.8: Insulated wired antenna on Submarine [37]

Shortly after Rogers's invention, Willoughby and Lowell also in the same year, performed further experiments on the detection of submarines. They discovered that loop antennas can likewise detect or receive radio signals transmitted through water [38, 39, 40]. The antenna system comprises of an insulated phosphorus bronze wire which was used to construct a single loop antenna that was firmly grounded by the hull of the submarine. This simply means hulls were part of the antenna and the prototype of their design is as presented in Fig. 2.11. The duo claimed that they were able to successfully establish communication links between two submarines, which were entirely submerged in seawater 20 Km apart at a wavelength of 952 m [38]. Though the communication distance between the two submarines was later disputed by V. R. Fisher [41], it was obvious that the loop antenna was similarly used to established communication in seawater between two submarines. Around the same time frame, Major General George O. Squier conducted experiments where he used an insulated wire for transmission of high-frequency signals through the water. His experiments confirmed

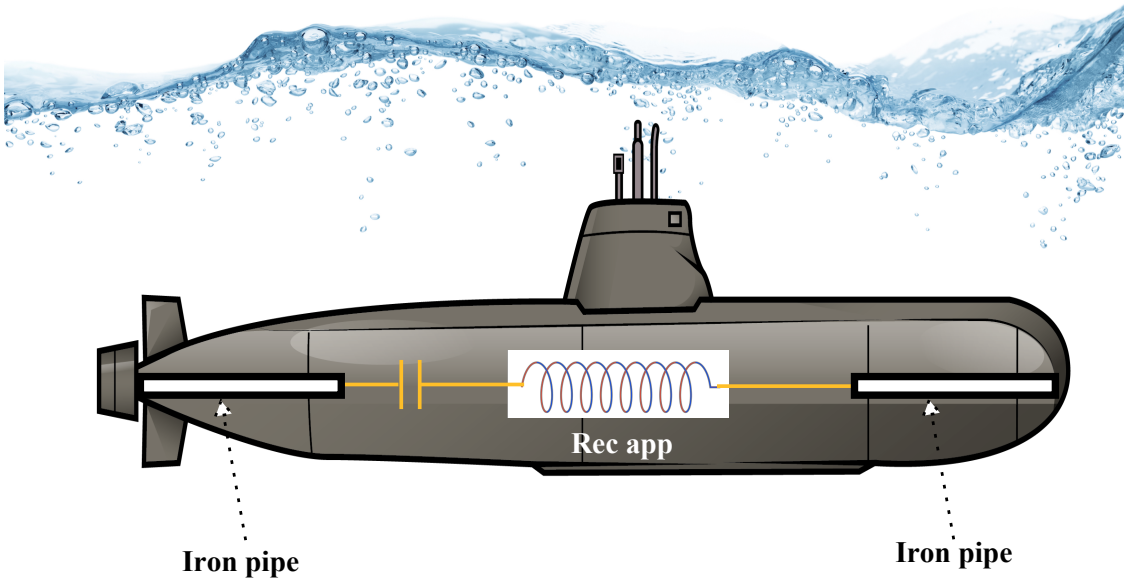

Figure 2.9: Antenna inside iron pipe on Submarine [37]

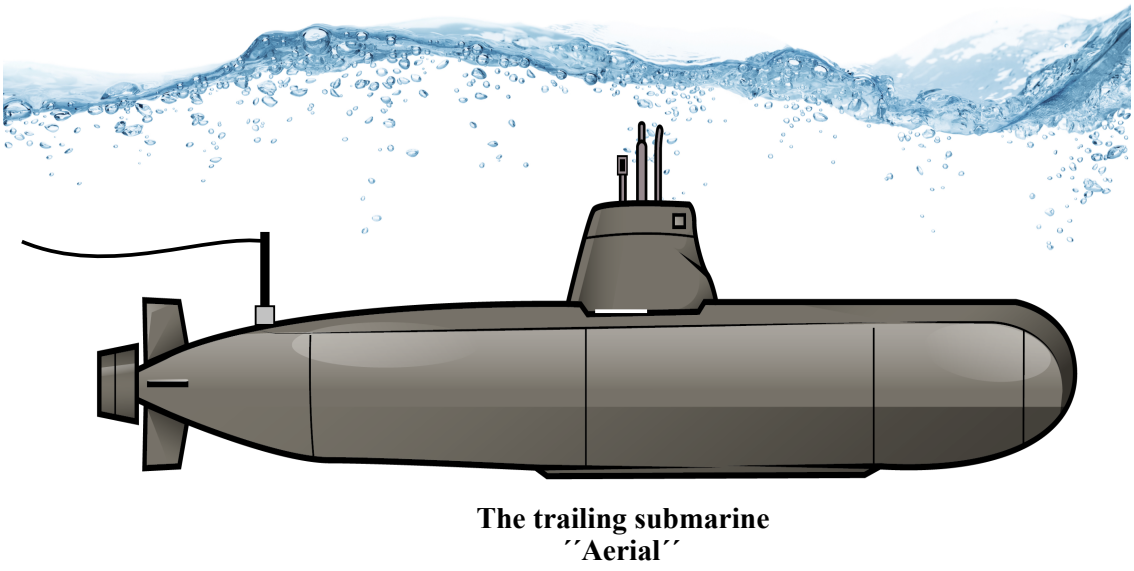

Figure 2.10: Long wire antenna trailing Submarine [37]

that EM waves can be transmitted through wires that were submerged in water [42]. Also, a US. Navy Lieutenant-Commander Taylor conducted experiments on underground and underwater antennas. He used a long wire of about 153 m long at a navy station in Washington and a submarine base [40, 39].

More discoveries were made during the post world war II era. For instance, Ronald K.

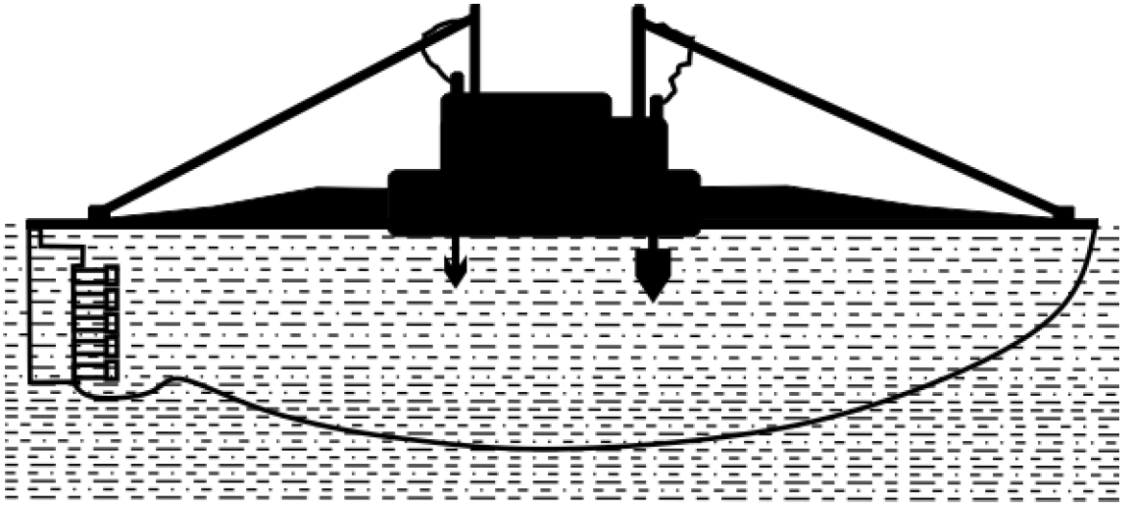

Figure 2.11: Loop antenna fixed on Submarine [38, 39]

Moore in 1951, was the first individual to present an electromagnetic theory of underwater antennas. This form the fulcrum of his doctoral program. Also between 1951 and 1957, James R. Wait conducted a series of studies on insulated loop, finite wire, magnetic dipole and Hertzian dipole antennas that were operating in conducting medium. Further tests were specifically conducted on Hertzian dipole by placing it perpendicular to the surface and immersing it in sea water. He concluded that the antenna radiation suffers attenuation of up to 20 dB when compared with the radiation on the surface at the operating frequency of 30 kHz and the antenna lowered to about 30 m in the medium [43, 44, 45, 46, 47]. Similarly in 1953, in the report submitted to the University of California by Banos and Wesley, mathematical solution to determine the electromagnetic field components generated by a horizontal electric dipole antenna was presented. In addition, four suitable integrals for the cartesian components of the Hertzian vectors and the cylindircal components of the field vextors ($\vec{E}$ *and* $\vec{H}$) were obtained [48]. In [49] the author examined the performance of small antennas operating at the VLF band in terms of signal reception when mounted on the submarine and submerged in a lossy medium. This was demonstrated by using the sketch in Fig. 2.12, where it can be seen that the signal is tilted downward and a fraction of the power radiated into the water. In this regard, the conductivity of the water play an important role in determining the index of refraction of the medium, consequently, the signal propagation is nearly vertical. Also, the propagated signal is greatly attenuated due to the effect of skin depth (this parameter will be discussed fully later) which affects conductors. Performance and characteristics of antennas submerged in the lossy medium were presented by Weeks and Fenwick in [50]. Mathematical expressions were derived for the input impedance, efficiency, current

distribution, and field strength of the horizontal dipole and vertical monopole antennas in the medium. The authors concluded that Signal to noise ratio (SNR) of horizontal dipole antennas doubled that of the vertical monopole when both are submerged in seawater, regardless of their respective depth in the medium.

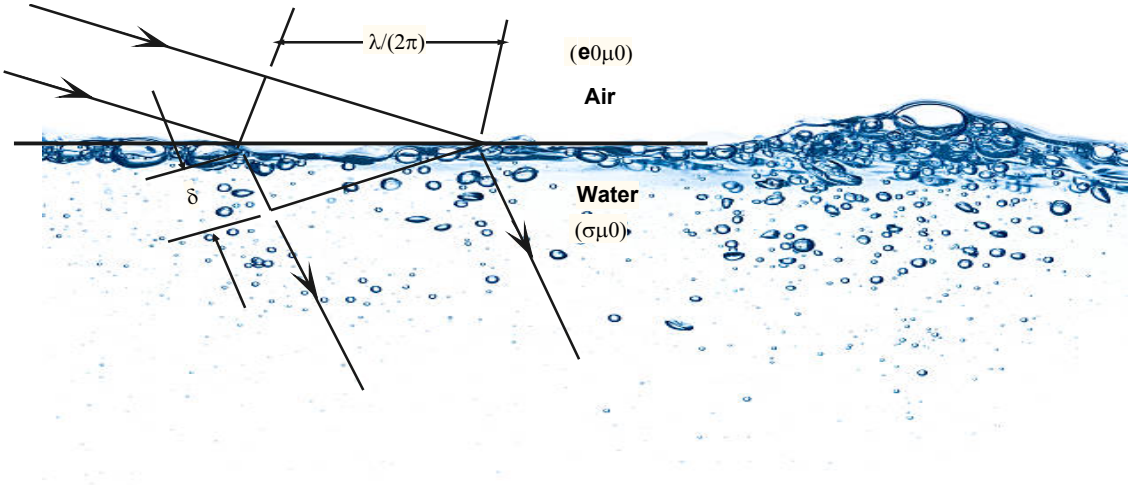

Figure 2.12: Refraction of radio wave at the surface of water [39, 49]

In 1959, Navy Research Laboratory developed an omnidirectional cross-loop antenna shortly after World war II. This antenna that operated in the VLF band, was embedded in plastics and mounted on a retractable mast [40, 51]. The antenna was part of the general overview of the loop antennas used in submarines communications that Turner gave en-route his own discovery. Other loop antennas presented in the paper operated at HF and UHF bands. However, his proposed solution is a hybrid antenna that worked at combined HF-UHF-IFF bands [51]. W. L. Anderson and R. K. Moore in 1960 calculated theoretically the energy density spectra of the transient electromagnetic fields at various distances between the field source and the medium. The source and the media are the magnetic dipole and seawater respectively. They concluded that as the distance increases to the critical value, the frequency on the other hand slowly shifts downward. Consequently, the electric and magnetic fields also decrease and are approximated as r^{-2} and r^{-3} respectively [52].

Moore and Blair also used dipole antennas in their studies of the problem associated with communication between antennas placed in a conducting medium like sea water. Expressions were presented for the fields of the horizontal and vertical dipole as well as electric and magnetic dipole antennas. It was concluded that the field of the horizontal dipole is stronger than that of the vertical dipole, due to the vertical nulls in the fields radiated from it [53]. In 1962, cross-boundary (water to air or vice versa) transmission became a subject of interest to the military. This was done by establishing

a communication link between a helicopter in the air and a submarine submerged in seawater. Here, vertical electric dipole (VED) antenna operating at 10 kHz in the air and a horizontal electric dipole (HED) antenna operating at 100 kHz in the sea were proposed. These two antennas were proposed based on their respective field strength in each medium. It was also presented that difference in their respective operating frequency is due to differences in the properties of the two media [54]. In 1963 Hansen presented analyses of three antennas namely; loop and dipole in insulating radomes and an insulated long wire antenna with end electrodes, in a lossy medium based on their merit factor. Relative gain is the main merit factor considered as it relates vertically polarized power per unit solid angle to the total input power. From the analyses, the relative gain factor of the long wire antenna in the medium is better than the other two antennas, as this antenna acts basically to feed current into the electrodes, which subsequently set up a vertical quadripole of the conduction current. [55]. In the same year, King and Iizuka analyzed electric and magnetic fields of a half-wave dipole antenna submerged in a homogeneous isotropic dissipative medium, in terms of their admittances and currents. The studies compared E and H-fields obtained from the theoretical analyses with those from the measurements. General formula was derived for the fields components (near and far) around the antenna. Similarly, experimental results obtained for the field components validated the theoretical as both results are in good agreement [56]. Still, in 1963, Hasserjian and Guy performed a series of experiments to validate the theoretical approximations for subsurface antennas in a lossy medium. Experimental results of the horizontal dipole antenna in a lossy medium and the theoretical approximation agrees well [57]. It was still in that same year that Fenwick and Weeks theoretical and experimental analyses and characteristics of antennas placed in a lossy medium. Dipole antennas (center fed, end fed grounded and center fed ground) were used in these analyses. Based on the results obtained for the input impedance and current distribution of the antennas, relative communication efficiency (RCE) of the submerged antennas is defined. Subsequently, the authors presented a table of RCE for common antennas and theoretical and experimental results of the field strength of the antennas are in good agreement [58].

Apart from his work on the electromagnetic theory of underwater antennas, Roland K. Moore also theoretically analyzed the performance of antennas on the surface and in a conducting medium. The antenna gain and its radiation pattern were the two parameters considered in these analyses. Also, biconical loop and two forms of straight wire antennas operating at VLF were used in the work. It was shown that there is no significant difference among the gains of the three antennas in the medium, as it is related to current (uniform or reduced) and their respective wavelength. The conclusion was that calculation of power radiated and radiation resistance of antenna submerged

in a conducting medium is dissimilar to the calculation for the same antenna in the air. In addition, the gain and radiation pattern of the antennas in this medium were affected by the energy dissipated in the medium [59]. Based on these results, extensive effort was made by the author on the propagation of radio communication in sea water. Three proposed communication links for antennas submerged in the sea water and were used in his experiments, these are; surface to submarine communication, submarine to submarine communication via surface and submarine to surface communication. It was demonstrated that if the antenna is lowered into depth of within 5 meters to the surface and the bandwidth not exceeding 1 Hz, a propagation range of up to 20 km can be achieved. In conclusion, it was stated that propagation in seawater will require antennas operating at VLF bands (precisely at frequencies well below 10 kHz) due to strong attenuation in the medium. Also, propagation distances (communication ranges) are affected by depth attenuation and atmospheric noise. The author finally submitted that communication link between surface vessels and ocean-bottom working parties could be established by usage of antennas operating at ELF bands [60]. In furtherance of the research on cross-boundary communications, Durrani in 1964 presented the study on the usage of the magnetic dipoles submerged in the sea water. In the paper, the theoretical analysis including the electric and magnetic components of the horizontal magnetic dipole (HMD) and vertical magnetic dipole (VMD) was thoroughly discussed. Also, undersea fields produced by different dipoles compared and it was concluded that electric and magnetic fields produced at large distances by HMD in the medium are stronger than those by VMD with the same excitation and size. Similarly, for a large number of turns, equal currents, and equal input powers, HMD still showing a superior performance over VMD [61]. In 1969, King et al presented theoretical analyses of the current, distribution of charge and the admittance of cylindrical antennas immersed in arbitrary homogeneous media, with the effective conductivity of the media greater than or equal to zero. Electrically short, half-wave and full wave dipole antennas were used in these analyses. The theoretical results obtained for the three antennas were compared with the measurement and the two shows good agreement [62].

A year later the work was extended basically to determine the EM fields of linear antennas immersed in the Atlantic ocean or buried in the earth. Here, three subdivisions of horizontal ranges were used to determine a measurement of EM fields in the dissipative medium. These are; the near field range, the intermediate range, and the asymptotic range. Finally, the numerical solutions were simulated and the results were compared with the results of the experiments. In their submission, experimental measurements of the fields in the near and intermediate field range matched the predicted results in the medium [63]. Also in 1971, Tsao derived an expression to determine the radiation resistance

and efficiency for antennas placed in a dissipative medium. This is similar to Moore's effort of 1963, but here clarification was given concerning radiation resistance, which was often referred to as input resistance for antennas in lossy media in Moore's work [64]. Trailed Electrode-pair or horizontal dipole antenna grounded at both ends with the operating frequency of 45 Hz and 75 Hz was used to develop design principles for long range ELF broadcasting system by M. L. Burrows and C. W. Niessen in 1972 [65]. The transmitter consists of 10 parallel 100 km long conductors (antenna arrays), which are spaced 10 km apart and can communicate with a receiver at 10 Mm (megameter) away with data delivery of 1 bit per second at a depth of 80 mm below the surface of the ocean. The power required by the transmitter was 4 mW and the current in the conductor was about 100 Amperes. In another series of experiments by Siegel and King they measured the EM field characteristics, driving-point impedance and current distribution of antennas submerged in the seawater. For these experiments, two sites locations and one laboratory test performed using the setup shown in Fig. 2.13. Two short dipole antennas operating at 100 kHz and 14 MHz, both placed at a depth of 150 mm below the water surface were used [66].

Project Sanguine was a secret research work initiated by the US Navy in 1959, in which many researchers worked assiduously in its various segments. The project aimed at developing a single transmitter that is capable of communicating with American submarines, when they are submerged in the ocean. The main objective of Sanguine is to operate at ELF band and establish one-way radio communication with submarines, from a transmitter located at Wisconsin regardless of the submarines' depths and distances [67, 68]. The project was eventually made public around the early 70s and there are a lot of publications mainly on it between 1972 and 1975. For instance, Moore in 1972 presented the theoretical estimation of the signal-to-noise ratio of antennas for Sanguine project and he concluded that the calculated bit rate appears adequate for communication between submarines and specified location(s) on the earth surface. The antenna he proposed operates at 45 Hz, with a transmitted power of 10 Mw and are grounded at both ends [69]. Also, Kruger gave a general overview of the Project Sanguine, which includes the transmitting and the receiving antennas alongside other system requirements. According to this author, the choice of ELF band for the project are based on;

- Low seawater attenuation;
- Global coverage;
- Better survivability against nuclear attacks;

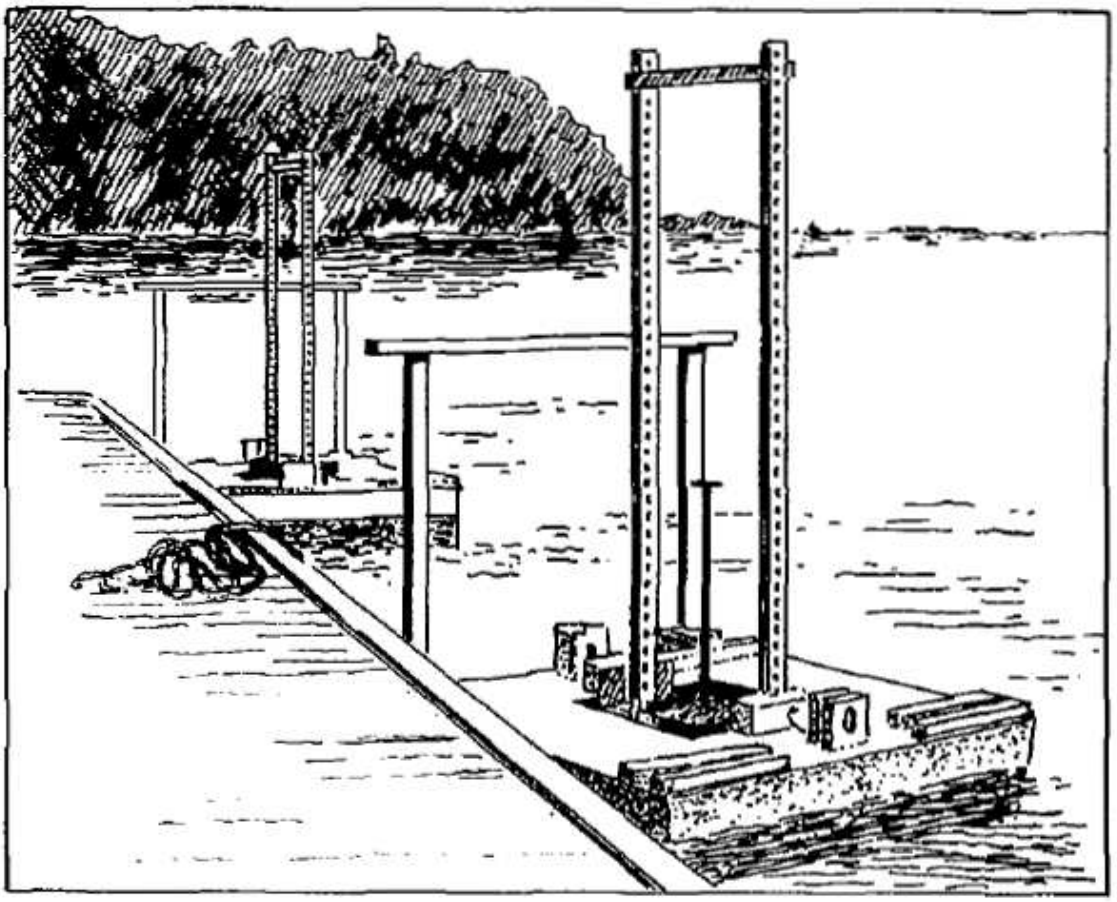

Figure 2.13: Polyfoam rafts supporting antennas with electronics systems as developed and used by the authors [66]

- Low atmospheric attenuation and disturbances.

In Fig. 2.14 a general overview of project Sanguine as presented by Kruger is shown. Additional reasons gave for engaging ELF band for the project is to counter C^3 (command, control, and communications) problems and to conserve energy, which will be an advancement to operating at VLF band which requires high-powered transmitter [70]. An improved breakdown of the composition of the project as shown by Llamas is presented in Fig. 2.15.

Buoyant cable antenna (BCA) operating at MF/HF, VLF/LF, and ELF/VLF frequencies were presented by Fessenden and Cheng in 1974. In the build-up to present their work, the authors looked into the use of BCA prior to 1965 and afterward. In the years before 1965, BCAs were designed to operate at VLF/LF frequencies, with a cable length of 610 m and a rigid electrode at the cable end. But after 1965, the same antenna was designed to operate in MF/HF frequencies with a cable length of 15 m long and placed between two electrodes which contain RF amplifier that is housed in a flexible

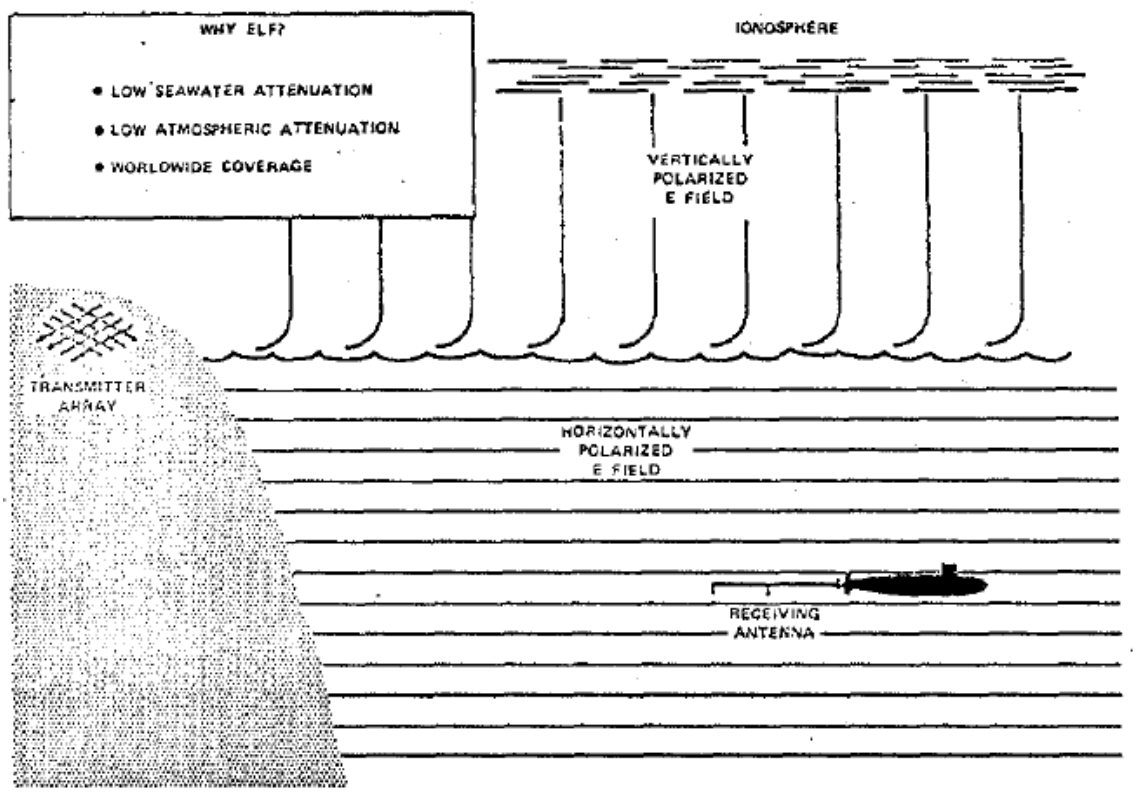

Figure 2.14: General overview of Project Sanguine [70]

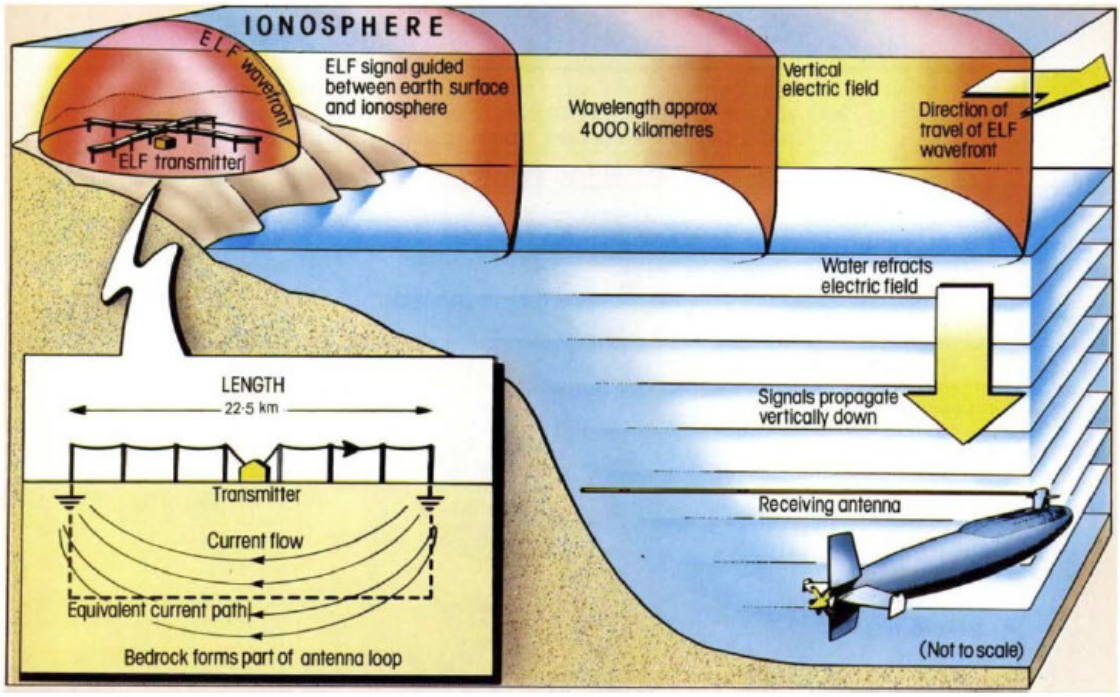

Figure 2.15: The proposed project Sanguine by U.S. Navy [39]

steel body. Another BCA design consists of 1.5 m length wire with a redundant electrode termination and a 32 m radiator that makes it possible for the antenna to operate at VLF/LF/MF/HF frequencies. Hence, the rest 520 m coaxial cable serves as a transmission line only. But these BCA antennas with polythene electrodes suffer from velocity induced electrode noise (VEIN) as the electrodes were noise generators, especially below 100 Hz. To address these, the authors proposed helical electrodes with new BCA antennas and the results obtained shows that the antennas had improved performance with the new electrode. Images of BCA at different operating frequencies are presented in Fig 2.16a, 2.16b and 2.16c [71].

Later in 1974, John Merrill gave a historical aspect of project sanguine, where he also presented the feasibility test conducted by the Navy in 1963. An experimental radio transmitter located at North Carolina with an antenna length of 176 Km, was used to communicate with receivers installed in fixed, land-portable and nuclear submarine at a range of 3200 Km. The intensive test measurements were carried out between January and April 1963, with the submarine located off US Atlantic coast, having a trailing antenna of about 304.8 m long. The data obtained from the test were used for further validation of the zero-order-mode propagation model at frequencies below 600 Hz, also accurate attenuation data down to 78 Hz were provided, these are interesting results for sanguine project [72]. Around the same time, J. R. Wait discussed the historical background of the usage of an ELF band in both terrestrial and underwater communications. Efforts by Conrad and Marcel Schlumberger before 1920 about wireless transmission in 100 Hz band was also presented [73]. Bernstein et al [74] also in the same year presented the results of experiments they performed, where a horizontal electric dipole with electrodes is used as the receiving antenna. The sizes, shapes, and spacing of the electrodes are important to counter the effect of motion-induced turbulence in the water. Also to cancel the problem associated with electromagnetic noise field enveloping the submarine hull, this antenna trails behind it. Long horizontal trailing wire with electrodes that are adequately gapped from the submarine, which minimized noise due to water turbulence around the hull and also onboard machinery is the preferred receiving antenna for project SANGUINE presented by Keiser also in 1974. This antenna similarly operates at ELF band to communicate with the preferred transmitting antenna [68].

Also, Wolf et al proposed the use of superconducting quantum interference device (SQUIDs) as a receiving antenna on the submarine to replace the ferromagnetic-core solenoids, which has communication deficiency when the submarine is deeply submerged in water. Theoretical analysis of the proposed antenna was given and SQUIDs is expected to achieve adequate dynamic range, adequate orthogonality among three planar sensors and refrigeration [75]. Momma and Tsuchiya in 1976 described a method of undersea

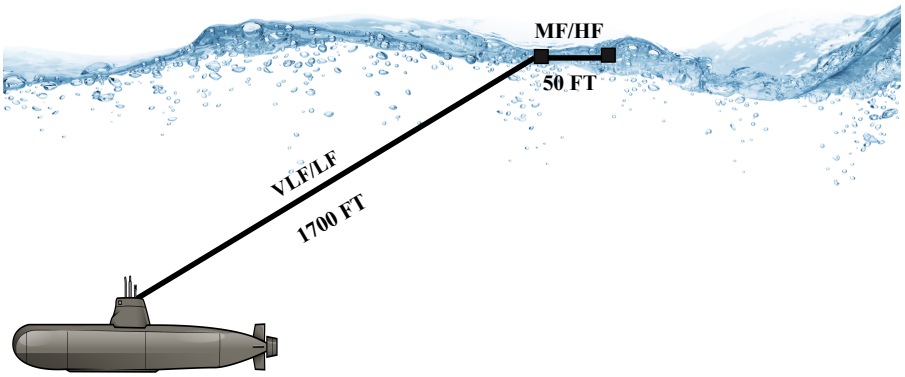

(a) BCA for MF/HF communication

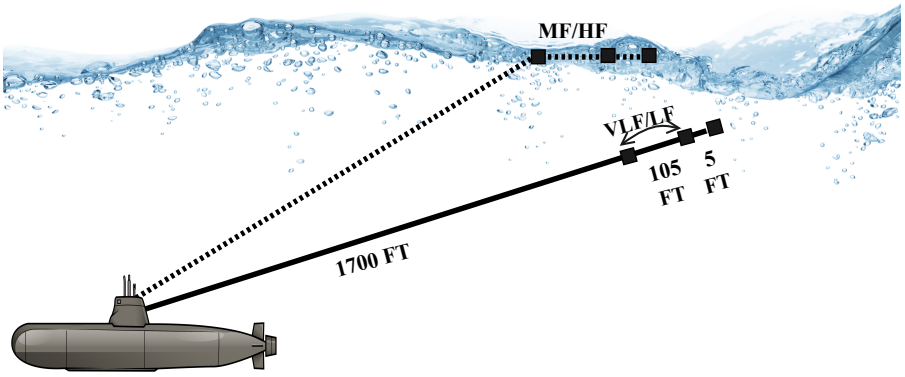

(b) BCA for VLF/LF communication

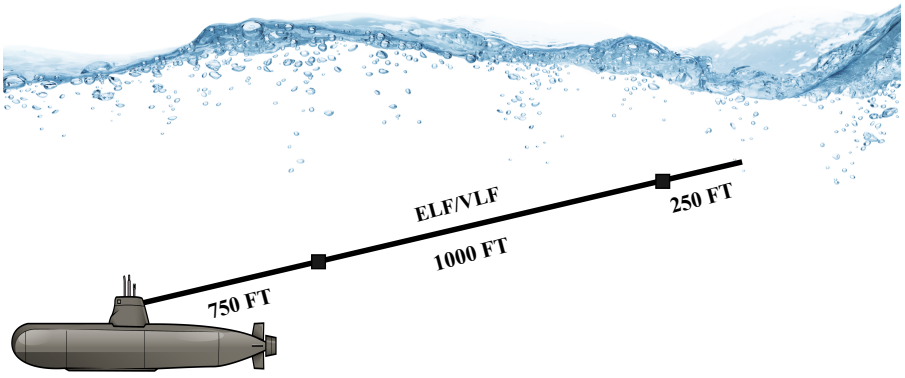

(c) BCA for ELF/VLF communication

Figure 2.16: BCA antennas [71]

wireless communication known as an electric current method. The writers gave an overview of studies that had been conducted in the undersea communication and detection and through experimental analysis were able to conclude that propagation range in the medium at this frequency can be expanded, only if the current output is increased, without increasing the power output [76]. The experiment was carried out in the Mystic Lakes in Massachusetts, the relative permittivity and conductivity of the lake are 81 and 0.06 S/m respectively. The measured electric field patterns at a distance of 50 m below the surface of the water from the transmitting antenna are quite directional. These were compared with the computed field patterns and their results are similar, with which the conclusion is drawn that traveling wave antenna can be appropriately used for subsurface communication in the lake and also that at 144 MHz bands, and that water behaves like a dielectric medium at this frequency. In [77], Davis et al presented results of research and experimental validation on SQUIDS antennas operating at ELF bands to demonstrate the feasibility of using the antenna in an underwater environment as well as overcoming the sub-problems associated with its performance. Each of these problems was typically analyzed through measurements and the conclusion as presented by the team shows that SQUIDs antenna is potentially capable to be used as an extremely sensitive ELF RF receiving element on a mobile platform. In addition, the antenna has the ability to operate at a depth of 100 m below the water surface and can also deal with anticipated buoy motions through motion-processing method. In the same year, J. R. Wait presented propagation of ELF electromagnetic waves for Surface ELF Antenna For Addressing REmotely-deployed Receivers (SEAFARER), research in this band had actually been a fertile field of investigation for many years. The project came to address some grays area of Project Sanguine that was fraught with some controversies. In principle the two projects are very alike as the frequency of operation for antennas for this project is the same as that of Project Sanguine. Only that in the latter project power requirements were better estimated, but the US Navy was not able to explain the influence of either project on physical and biological environments. Also, this project has striking similarities and fascinating developments with an early investigation by Nicola Tesla [78].

Descari in [79] which was presented in 1979, discussed the analysis of slot antenna that is buoyant, towable, certified seaworthy, which was designed for usage in the submarine-based communications. The antenna with other devices formed the prototype design by the author to provide VHF communication or send telemetry data from a; submarine placed at about 2000 feet below the water surface, stationary or moving object to a remote unit, satellite, or aircraft. In 1980, Arutaki and Chiba presented a theoretical analysis of vertical magnetic dipole (VMD) antenna immersed in a conducting medium. In the analysis, sea water is considered as three layers (air, sea, and ground)

media with which communication was established between the antenna and object in air, sea, and ground (seabed). The dominant term in their results agrees with Moore's results and they concluded that the VMD antenna is more advantageous for this type of communication than horizontal loop antenna [80]. Michael B. Callaham in 1981 described the transmission and reception of signals by submarines were mainly been done through UHF and VHF frequencies [81]. But the author also quick to point out that transmitting and receiving at these frequencies will require either deployment of small mast antenna that will remain above water surface or the entire submarine coming near the surface. In either case, it may be risky for the operation of the underwater bodies as it will mean exposing them to detection by enemies. Thus, for total concealment of the location of submarines from enemy's view, the author proved that communicating in ELF and ULF bands as well as through optical transmission will guarantee the signal penetrating deeply into the water. Thereby ensuring full protection of the submarines from any attacks.

In revealing the interest of British government to build a transmitter operating at ELF band and communicating with submarines, D. L. Jones recapped the developments in submarine communications over three decades which include; the danger of using VLF frequencies in communicating with submarines, different antennas that were designed to operate at required operating frequencies for deep-sea submarine communications and eventual breakthrough through ELF band, which made transmission and reception possible in tens of kilometers below the sea surface. References were made particularly to various stages of involvement of Project Sanguine, which was later upgraded to Seafarer [82]. Lloyd Butler in 1987 showed the importance of underwater communication to amateur radio by posing the following questions; How far can we communicate underwater in the sea or in a lake [83]. How large is the signal attenuation and what Frequency can be used? Could we use 1.8 MHz? These questions were answered through both theoretical and experimental results that were presented in his work. It was therefore affirmed that attenuation increases with increasing operating frequency, which is about 46 dB at 1.8 MHz in sea water and 27 dB in fresh water. It was also revealed that cross-boundary interface transmission will be very difficult in this band, as the attenuation in the outbound signal (water to air) and the inbound (air to water) add up to 54 dB in fresh water as shown in Fig. 2.17.

Dunbar gave two broad classes of antennas that can be used for subsea communications. These are the magnetic field loop (MFL) and electric field line (EFL) antennas. These were also known as passive reciprocal devices (can be used as either transmitting or receiving antennas). This is in contrast with SQUID, fluxgate and hall effect antennas that are only suited for receiving applications. examples of these antennas

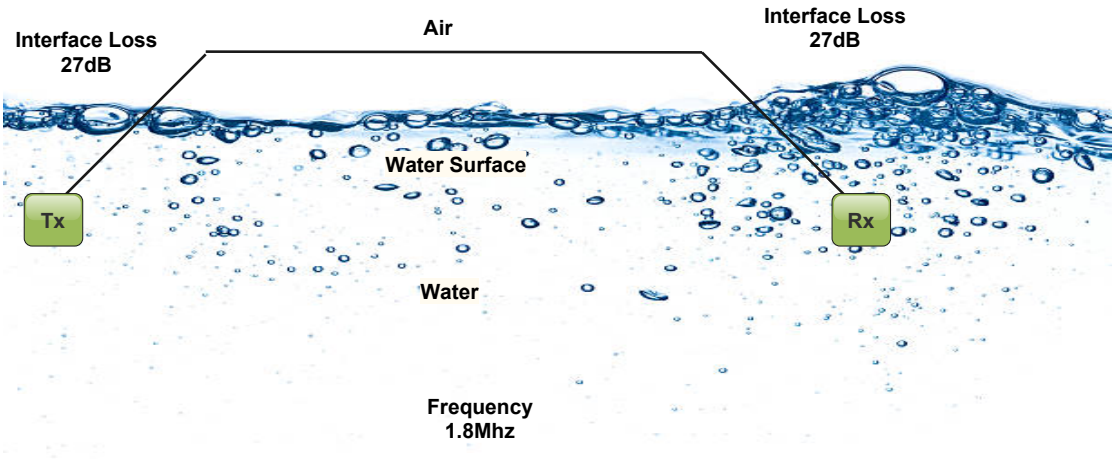

Figure 2.17: Air-Water Interface transmission in fresh water at 1.8 MHz through two submerged antennas [83]

include magnetic loop, short electric dipole, long line, disc monopole, and surface contour EM wave antennas. It is important to state that experimental analyses were used to validate the theoretical models of the antennas [84]. Benhabiles et al in 1996 used two physical models (the surface wave theory and the Fresnel formula) to derive a simple and closed-form expression for the propagation of electric field in sea water. Thus, a computer code was developed to monitor the scattered field and the expected voltage at the VLF band for the three wire antenna configurations. These results were compared with the experimental results in the literature and good agreement was reached for most of the configurations [85]. King et al presented formulas for the E-field of shore-based top-loaded monopole antennas operating at VLF band. The frequency range of the antennas is from 14 kHz to 30 kHz for radial distances around 10,000 Km along the spherical earth surface or sea. The E-field patterns of these antennas are omnidirectional shape [86]. In like manner, King in [87] presented a long horizontal wire traveling wave antenna, which is a beverage type operating at a frequency between 10 and 30 kHz. These antennas exhibit a unidirectional pattern and maintaining a large field over the sea and weak field over the land.

Bob Aldridge gave an overview of the usage of ELF band across some important underwater communication projects by the US Navy. Recap of both project Sanguine and Seafarer were given, both the technical analysis and reasons why the projects were step down. Shortly after the demise of Seafarer, which was terminated by President Jimmy Carter in February 1978, The Navy came up with an amended concept called Austere ELF, which was announced on 2 March 1978. This is closely followed by another modified version of Austere ELF called Project ELF in 1981. These two projects are similar with;

plan to upgrade the transmitting facility at Wisconsin, install second transmitting antennas at the K. I. Sawyer Air Force Base in Michigan and eventually install the receiving antennas on the submarines. The latter was eventually implemented due to a shorter cable length when compared with the Austere ELF [88]. Against the usage of ELF band for underwater applications, A. Monin in 2003 proposed an EM model for usage of a floating antenna (operating at VLF band) installed on the tail of submarines for communication with LORAN-C (long range navigation-C) radio navigation. A 700 m long insulated wire is the floating antenna and operating at VLF band. Various electrical characteristics of the antenna, which include radiation pattern, incident field, and current were fully analyzed. Also, an algorithm for estimating those parameters was proposed using parallel-extended Kalman filters and the results were validated with data set from General Army Direction of France (DGA). Finally, the performance of the antenna in terms of propagation distance was compared with that of Whip aerial. For incidence lower than 30^0, whip antenna returns good accuracy, whereas floating antenna's results were accurate all through the angles that were verified [89].

In 2004, the authors used four different experimental scenarios representing both horizontal and vertical propagation in seawater by employing loop, double loop, dipole and folded dipole antennas tuned to operate at 25 MHz, for a frequency range of 1 - 66 MHz. The four scenarios are types A, B, C, and D. In type A, the transmitter and receiver were placed some distance apart in seawater without insulation, transmission is impossible in this scenario. In B, both transmitting and receiving antennas were placed close to the walls of insulating container that contained sea water. Here horizontal propagation was established between the antennas. In C, the transmitter and the receiver were fully insulated and placed distance apart in sea water, again horizontal propagation was established. In D, the configuration in C was repeated but the two antennas were separated by vertical distances below the sea water. Subsequently, vertical transmission takes place between the antennas [90]. It was in the same year that, Anders Karlsson presented a theoretical analysis of the directivity, radiation efficiency and dissipated power gain of antennas placed in a lossy medium. In these derivations, the author optimized the quantities and also used electric and magnetic dipole antennas placed in the medium to analyze the impedance, efficiency and power gain. Thus, impedances of the two antenna types reached the expected asymptotic values as the radius of the sphere tends to infinity. Also, a magnetic dipole is about 10 dB more radiation efficient that the electric dipole antennas. It was concluded that larger gain is only obtainable by adding higher order multi-poles [91].

The world largest "Radio" station by Carlos A. Altgelt in 2005 gave more information about the project Sanguine research work both from the transmitting antenna on the earth

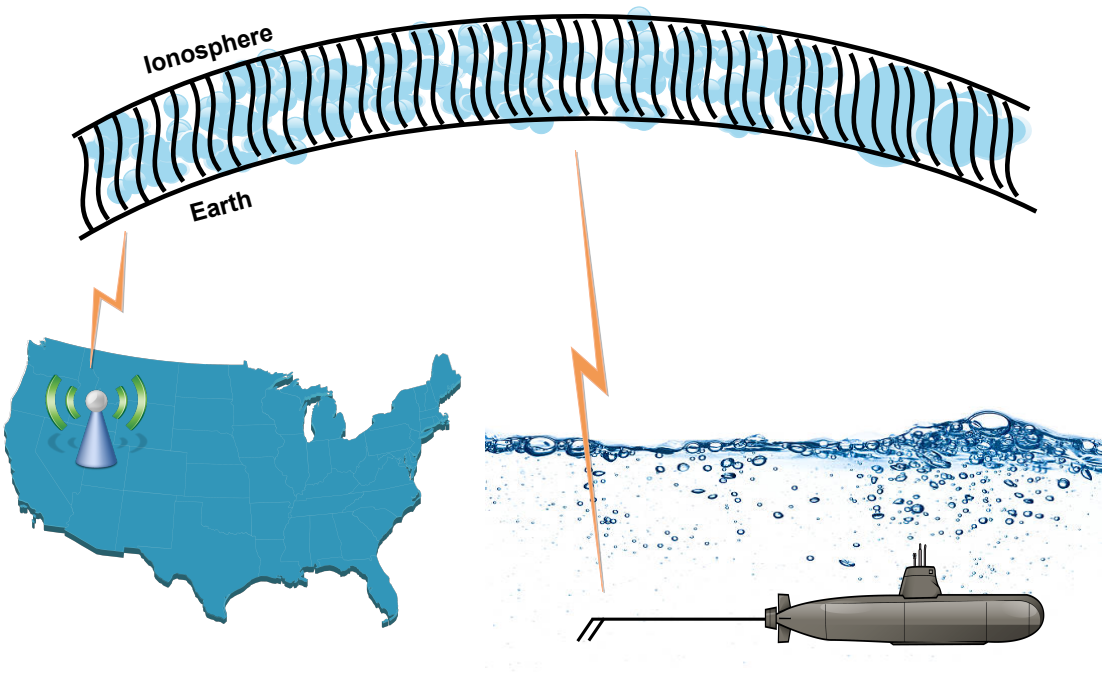

Figure 2.18: Communication between submarine and Nevada site [92]

situated in Nevada and the receiving antennas on the submarines. For the transmitter, it was observed that radio waves oscillating just above 60 Hz, and hit the ionosphere, this signal thus has the capacity to penetrate sea water sufficiently to communicate with antennas installed on deeply submerged submarines. The graphic analysis of the project showing the transmitting and the receiving antennas is presented in Fig. 2.18.

Still, in the same year, mutual coupling between shipborne antennas was evaluated so as to establish power and frequency restrain on the corresponding equipment. The antennas referred to in this regard are monopole antennas with a bounded ground plane. A hybrid selective method was used to select between several concepts like; geometrical theory of diffraction (GTD), the uniform theory of diffraction (UTD) and geometrical optics (GO), which eventually led to shorter computing time and as well preserving accuracy. This is a better alternative to the usage of fu1l-wave methods for calculating mutual coupling between shipborne antennas. Experiments were set up using two monopole antennas with a square ground plane, and the results are close to those obtained through numerical method [93]. Shaw et al in [94] presented the experimental results for EM wave propagation in seawater at MHz frequencies. A stand-alone, battery operated loop antenna and another loop shown in Fig. 2.19 and connected to the spectrum analyzer were used as transmitter and receiver respectively. The experiments were conducted in a laboratory test tank of 1.2 m deep. At an operating frequency of 5 MHz, propagation was

Figure 2.19: Standalone transmitting and receiving loop antenna [94]

measured as a function of distance after the antennas have been lowered to the bottom of the tank and propagation between the antennas was achieved up to the distance of 90 m. The results also show that as the distance between the antennas increases, attenuation also increases, which is rapid at low distances and relatively gradual at longer distances. Their conclusion is that EM propagation is possible in shallow sea water.

Frank Plonski and Charles Gyenes in 2008 built an HI-Q antenna (ultra small HF aperture submarine communications antenna) operating from 2-30 MHz in the HF band for submarine application. By employing unique tuning mechanism the antenna from 2-24 MHz behave like an inductively tuned cage capacity Hat element and from 24-30 MHz, it behaves like a broadband monopole antenna. Apart from the wide bandwidth of the antenna, it also achieved higher radiation efficiency, which is both important in RF signal transmission and reception. The antenna is given in 2.20 [95]. In 2009 Liu et al presented the results of theoretical analysis of an HED antenna submerged in seawater. Formulas were derived for ELF fields generated based on the three-layer model defined as the air-sea water-sea floor. It was observed that the horizontal component of the E-field and the vertical component of the H-field are strong, thereby very important for their respective propagation. The study also includes analyses of the effects of

Figure 2.20: HI-Q antenna [95]

seabed conductivity, depth of submerged antenna, frequency and sea depth on EM field distribution in the medium [96]. In the same year of 2009, three antennas operating at ELF bands were compared with reference to their performance in the underwater environment as presented in [97]. These antennas are SQUIDs, trailing wire and ferromagnetic-core solenoid antennas. It was discovered that the other two antennas apart from SQUID are limited to operation in shallow water as they have to operate close to the water surface. In addition to this, trailing antenna also has a peculiar disadvantage, because of the length of its cable, which is more than 600 m, the operability of this antenna is therefore restricted. Based on all these, the authors concluded that SQUID antenna stand out of the three antennas and make a prediction that this antenna will make remarkable progress in underwater communication.

Furthermore, Brian Austin discussed in detail a number of efforts by the US Navy to establish a one way signaling between a transmitting antenna buried in the earth and receiving antennas (both antennas operating in ELF band) on submarines. The report simply analyzed various projects, which are aimed at achieving these communication links. References were made to researchers and experts for their contributions in these projects, many of which had already been discussed in this work [98]. Aleix Garcia

Miquel also in 2009 in his thesis presented UWB antennas for underwater applications. These antennas were designed to operate between 150 MHz and 1 GHz. Dipole, circular loop, and bow tie were some of the shapes the author experimented with, before finally choosing a combination of loop and bow tie antennas based on their performance after several analyses [99].

In 2011, Dunbar et al considered some propagation conditions for underwater antennas. Three antennas that were investigated are; longline, magnetic loop and surface contour antennas. In the analysis, the antennas exhibited similar traits with respect to their measured and computed fields variation with range. The near fields vary with the inverse of the cube of the range $\frac{1}{r^3}$. The EM noise limitation on the propagation range of underwater antennas was also discussed, setting ITU maximum allowable noise level as reference value [100]. Still, in the same year, Zhang et al compared the performance of the J-pole vibrator with that of a double loop antenna at 7 MHz and 30 MHz bands. At 7 MHz, the results showed that the received voltage for the J-type antenna is higher than that of the double loop antenna. Also, the J-type antenna achieved higher communication distance, 12 m, while the double loop antenna only achieved a 10 m distance. At 30 MHz, the two antennas have similar performance in terms of the received voltage and the achieved transmission distance of the system was reported to be 11 m distance [5].

Efforts were also made to present a hybrid of technologies, which can be used for onward delivery of data between underwater bodies and locations above the water surface, regardless of the distance between the two sites. These were presented by the authors in 1999 and 2012, respectively. Thompson et al in [101] analyzed a proposed Buoyant Cable Antenna Array (BCAA), for a possible unified communication link between submarines and satellite networks, it is a project supported by Defense Advanced Research Projects Agency (DARPA) in conjunction with the US Navy. In the proposed concept, the antenna array will remain at the sea surface, while the fiber optic of the required length will be used to link the submarine's trailing antenna that is submerged in the sea with cavity-backed slot antenna (CSA) array as shown in Fig. 2.21. There will be a signal conversion in the forward and reverse communication from RF signal to the Optical signal and vice versa. The second phase of this concept will be to establish two-way communication links between the CSA and satellites in low earth orbit constellations, UHF SATCOM or even a commercial satellite network that operate within the frequency of interest. It is to this end that the proposed frequencies are UHF and L band. Details of the concept is presented in Fig. 2.22. All these are expected to enhance submarine performance in terms of depth, connectivity, and data exchange. Karim et al, on the other hand, proposed an underwater - Global Positioning Systems (GPS) communication network, using the fiber-optic signal transport link between submerged submarine and BCA which receives

the GPS signals, hence this yields a one-way communication with the GPS systems. One important conclusion from these proposals is that hybrid of the network (satellite, RF and optical or satellite, acoustic and Rf), will play a vital role in establishing unhindered underwater communications [102].

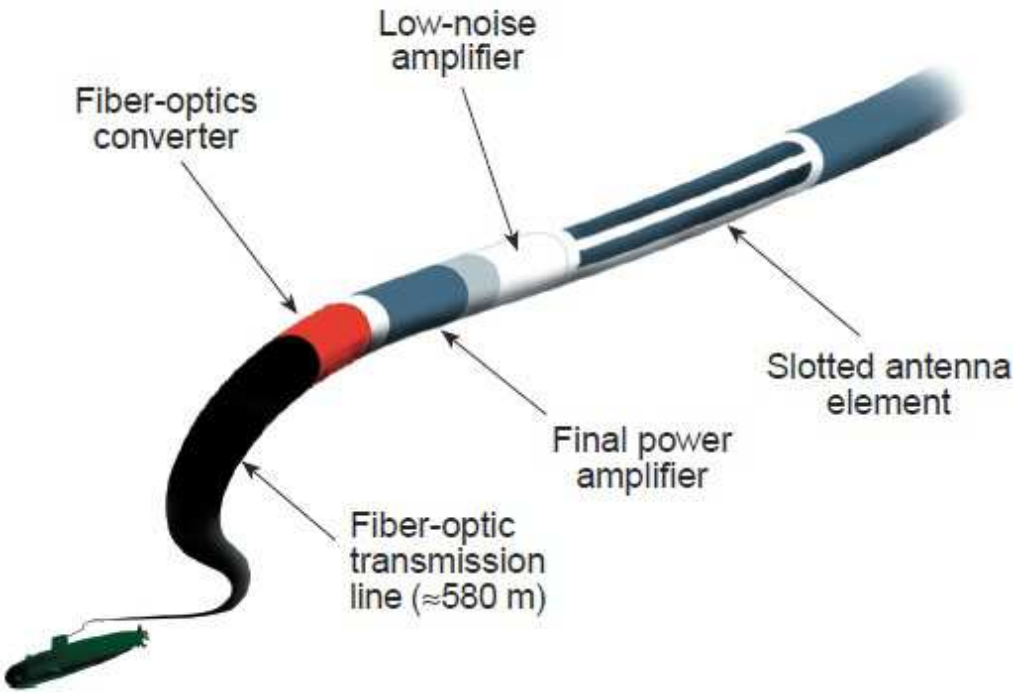

Figure 2.21: Connectivity between BCAA and submarine through fiber optic [101]

In 2014, Kelley and Naishadham presented their theoretical analyses of underwater broadband communication using loop antennas operating between 3 MHz and 30 MHz bands in shallow ocean zone. Through their model, they presented underwater RF data rate believed to be 1000 times that of acoustic by establishing a single communication link. Here theoretical Shannon capacity model and the software defined radio (SDR) were used to model the scenario in ocean environment [103]. In the same year, theoretical analysis of the near-field radiation characteristics around electric and magnetic dipole antennas operating in three lossy media which include salt water, human tissue and underground were presented in [104]. The authors concluded that magnetic antennas offer significant advantages over the electric antennas in terms of power lost in dielectric media to its surrounding. Still in 2014, Wang et al also investigated EM propagation from HMD antenna submerged in seawater and radiating into the air. Mathematical expressions were derived for the antenna operating in E and H fields at the frequency of 19 kHz in three media namely: air, seawater, and seabed. Results from numerical computations were compared with the experimental trials for the field components and the two are in

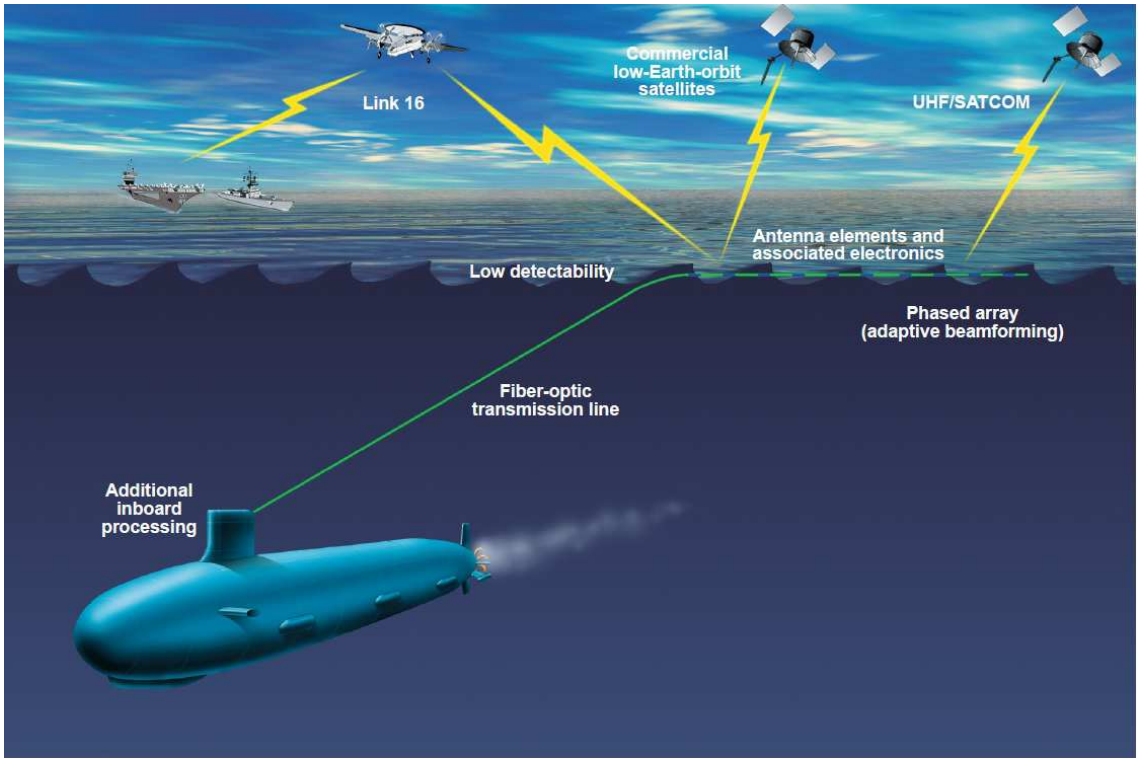

Figure 2.22: Proposed buoyant cable antenna array [101]

good agreement [105]. Their results show that there is a fundamental difference in the near field ohmic loss incurred within a lossy medium between Hertzian and magnetic antennas, which is more pronounced in electrically small antennas. They concluded at the operating frequency of 19 kHz, it is possible to establish cross-boundary (air-seawater) communication link as EM wave can propagate over a distance of 574 m across the media. In terms of power lost in dielectric and even where maximum efficiency is highly required, it has been shown that magnetic antennas will yield better results than electric antennas at that distance.

A further effort was presented in [106], where two Electrically Coupled Loop Antennas (ECLA) were designed for signal transmission and reception and were tuned to operate at a frequency of 2.95 MHz. The transmitting antenna is a circular loop with three turns of radius 35 cm, while the receiving antenna is a rectangular loop with four turns. The transmitting antenna was enclosed in a waterproof box with dimensions 54 cm x 42 cm x 20 cm. The measurement was performed with the antenna immersed in the water, while the receiving antenna remained in air for testing the water-air transmission performance. The prototype of the designed antennas are presented in 2.23.

The results obtained also showed that the received signal decays faster as the distance between the antennas exceeds the reactive near field zone. Analysis of half-wave dipole

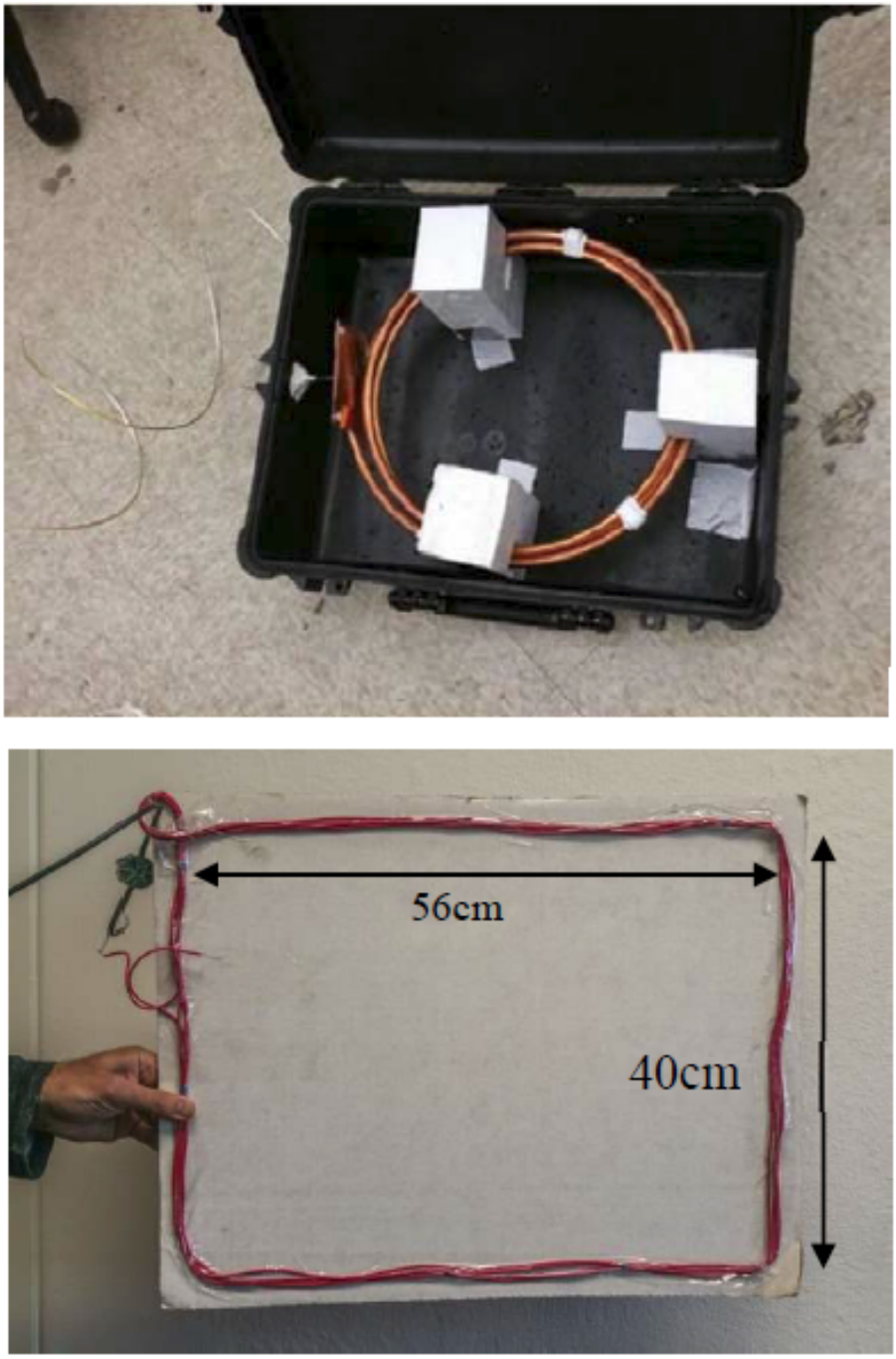

Figure 2.23: Proposed transmitting and receiving wire antennas [106]

antenna in fresh water at 433 MHz and short dipole antenna at the operating frequency of 30 kHz in seawater were presented in [107]. These were done to investigate the probability of using these antennas for communications between scuba divers. The electric fields and the power density radiated by the antenna in fresh and sea water were compared with the theoretical results presented by King-Iizuka and these were in good

agreement.

Hence, in table 2.3, a summary of some of the efforts in both theoretical and practical analyses of underwater antennas in the last century in sea water are given. This table includes the following information: antenna types, resonating frequency, propagating medium and the year the year the work was reported.

To conclude this chapter, we present in Table

Table 2.3: Antennas for underwater communications in sea water

S/No.	Antenna Types	Operating Frequency	Medium	Year
1	Wire antenna [36]	VLF	Sea water	1916
2	Wire antenna [37]	VLF	Sea water	1919
3	Loop antenna [38]	VLF	Sea water	1920
4	Insulated wire antenna [42]	VLF	Sea water	1920
5	Magnetic dipole antenna [43]	VLF	Sea water	1951
6	Insulated wire antenna [44]	VLF	Sea water	1952
7	Horizontal electric dipole antenna [48]	VLF	Sea water	1953
8	Insulated loop [47]	VLF	Sea water	1957
9	Horizontal dipole and vertical monopole antenna [50]	VLF	Sea water	1958
10	Cross-loop antenna [51]	VLF	Sea water	1959
11	Hybrid antenna [51]	HF-UHF-IFF	Sea water	1959
12	Magnetic Dipole [52]	VLF	Sea water	1960
13	Horizontal and vertical dipole [53]	VLF	Sea water	1961
14	HED and VED antennas [54]	LF	Seas water	1962
15	Biconical loop, dipole and insulated wire antenna [55]	VLF	Sea water	1963
16	Half-wave dipole [56]	VLF	Isotropic or Homogenous	1963
17	Dipole [57]	VLF	Sea water	1963
18	Short, Dipoles antenna (center fed, end fed grounded) [58]	VLF	Sea water	1963
19	Biconical loop and straight wire antennas [59]	VLF	Sea water	1963

Continued on next page

Table 2.3 – continued from previous page

S/No.	Antenna Types	Operating Frequency	Medium	Year
20	HMD and VMD antennas [61]	VLF	Sea water	1964
21	Short, Half-wave and full wave dipole antennas [62]	VLF	Isotropic or Homogenous	1969
22	Dipole [63]	ELF - MF	Sea water	1971
23	Linear dielectric antenna [64]	VLF	Sea water	1971
24	Trailed electrode pair antenna [65]	ELF	Sea water	1972
25	Wire antenna [69]	ELF	Sea water	1972
26	Trailing E-field antenna [67, 68]	ELF	Sea water	1972 & 1974
27	Short dipole antenna [66]	LF & HF	Sea water	1973
28	BCA with helical electrodes [71]	ELF	Sea water	1974
29	Horizontal electric dipole antenna [74]	ELF	Sea water	1974
30	Long horizontal trailing wire with electrodes [68]	ELF	Sea water	1974
31	SQUIDs antenna [75]	ELF	Sea water	1974
32	SQUIDs antenna [77]	ELF	Sea water	1977
33	Towable buoyant slot antenna [79]	VHF	Sea water	1979
34	VMD antenna [80]	LF	Sea water	1980
35	MFL and EFL antennas [84]	SLF - LF	Sea water	1994
36	Wire antenna [85]	VLF	Sea water	1996
37	Monopole antenna [86]	VLF	Sea water	1997
38	Long horizontal antenna [87]	VLF	Sea water	1997
39	BCA array [101]	UHF/L	Sea water	1999
40	Floating antenna [89]	VLF	Sea water	2003
41	Loop, double loop, dipole and folded dipole antennas [90]	HF	Sea water	2004

Continued on next page

Table 2.3 – continued from previous page

S/No.	Antenna Types	Operating Frequency	Medium	Year
42	Electric and magnetic dipole antenna [91]	UHF	Lossy medium	2004
43	Monopole antenna with square ground plane [93]	VHF	Sea surface	2005
44	Loop antennas [94]	HF	Sea water	2006
45	HI-Q antenna [95]	HF	Sea water	2008
46	HED antenna [96]	ELF	Sea water	2009
47	SQUIDs, Tailing wire and ferromagnetic-core solenoid antennas [97]	ELF	Sea water	2009
48	Dipole, circular loop and bow tie antenna [99]	VHF and UHF	Sea water	2009
49	Long line, magnetic loop and surface contour antennas [100]	VLF - UHF	Sea water	2011
50	J-pole vibrator and double loop antenna [5]	HF	Sea water	2011
51	Buoyant cable antenna [102]	UHF	Sea water	2012
52	Loop antenna [103]	HF	Sea water	2014
53	Electric and Magnetic dipole antennas [104]	UHF and SHF	Sea water	2014
54	HMD antenna [105]	VLF	Sea water	2014
55	Multiloop circular and rectangular antennas [106]	LF	Sea water	2016
56	Half-wave and short dipole antenna [107]	VLF and UHF	Fresh and sea water	2017

2.5.2 Antenna Developments for Usage in Fresh Water

The first notable works reported for fresh water applications are those of Saran and Held in 1960. Here, the field strength of monopole and loop antennas operating at 18.6 kHz on the surface of the water and at a different depth in a fresh water tank was measured. The theoretical and experimental results were compared, also the change in field strength

as the antennas were submerged at different depth in the liquid. Thus, as the submerged depth of the antennas increases, the field strength also attenuates exponentially. Similarly, in comparison with the results obtained at the surface, there is a decrease in the field strength to 1/10 and 1/100 at the depth of 164 m and 329 m respectively [108]. In 1970, Siegel and King in [109], presented numerical methods to determine the EM fields of a source (HED antenna) in a dissipative half-spaces propagating at either low or high frequencies. According to the authors, numerical solution is advantageous because it; requires only one general solution, fewer restrictions with the capability of being used in all media and frequencies. Also, a traveling wave antenna (TWA) operating at 144 MHz was used as a transmitter and placed at a distance of 17.5 cm below the water surface in an experiment to measure and compare field strength in water and in the surface by Shen et al in 1976. The antenna is made of a 0.32 cm diameter brass wire, insulated accordingly by an air-filled Plexiglas tube with the length of its arms equals one wavelength in the air and about 2.08 m long. Two dipole antennas were used as receivers, with one placed at about 50 m below the surface of the water, while the other was placed above the surface of the water. The dipole in water is half-wavelength, while that outside the water is quarter-wavelength long [110]. Similarly in 1977, Shen et al presented the theoretical analyses of the properties of two coupled horizontal-wire antennas over an electrically dense half-space region. Currents with arbitrary driving voltages were obtained by superposition the two identical parallel antennas with open ends. When these currents passed through the antennas, the power that can be transferred into freshwater propagates outward as radiant energy, whereas the same current into the sea water rapidly dissipated as heat [111]. Also in 1979 Hafez et al presented the attenuation rate of electromagnetic energy in fresh water for broadband measurements between 33 MHz and 363 MHz. For the experiments, freshwater samples were collected from lakes in Gatineau near Ottawa and the set up for the experiments is presented in Fig. 2.24. The results show that for frequencies below 100 MHz, the attenuation rate is dominated by ionic conductivity. It was also stated that attenuation at these frequencies is relatively independent of frequency, but above 100 MHz the attenuation increases rapidly. In addition, when the conductivity of water is 0.01 S/m, the attenuation at 100 MHz is 2.5 dB/m, which shows antennas operating around this frequency in the medium will surfer relatively from attenuation [112].

An and Smith presented theoretical analyses of horizontal circular loop antennas (transmitting and receiving) placed near a planar interface between two material regions, which are air and fresh water. The parameters analyzed for the transmitting antenna are current distribution, electric field, and admittance. For the receiving antenna, electromagnetic plane wave incident from either side of the interface was considered.

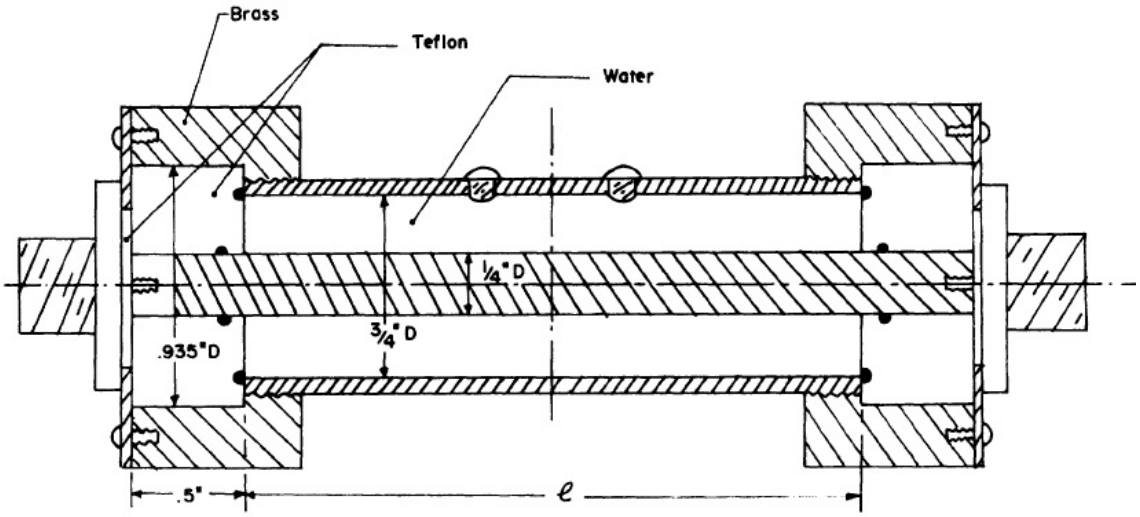

Figure 2.24: Attenuation measurements in fresh water at VHF band [112]

The numerical results show that when the transmitting antenna remain in the air, it produces a directive field pattern in water or any medium below the antenna. With this, the authors have drawn a preliminary conclusion that the resonant loop antenna will be useful for cross-boundary communications. Also, the theoretical results were validated with measurements of input admittance and field patterns of the antennas and the two results are in good agreement [113]. A year after, Smith and An presented analyses of a horizontal circular loop and a coaxial array of loop antennas placed above a material half-space medium. These antennas are designed for operating frequency of 900 MHz and optimum directivities of these antennas were determined through parametric analysis. The theoretical results were verified through measurements when the antennas were placed on the surface of fresh water [114]. In 1984, G. S. Smith investigated the directive properties such as gain, directivity and pattern function of an antenna, when it is transmitting into a material half-space. When antennas are placed in adjacent media, for instance, air (medium 1) and water (medium 2) it is referred to as half-space. Field patterns at different distances were measured using the apparatus shown in Fig. 2.25. In the studies, theoretical results for the infinitesimal electric and magnetic horizontal dipole antennas were presented with the directive transmission into the adjacent dielectric half-space. Similarly, the results of the theoretical analyses of a resonant circular loop and magnetic dipole antennas were compared with the experimental in a dielectric half-space and their results show good agreement. The conclusion is drawn that a single resonant circular loop and dipole antennas or simple arrays of these antennas will be useful for directive transmission into the lossy medium [115].

Travade et al in 1989 used underwater antennas and other devices for radio tracking

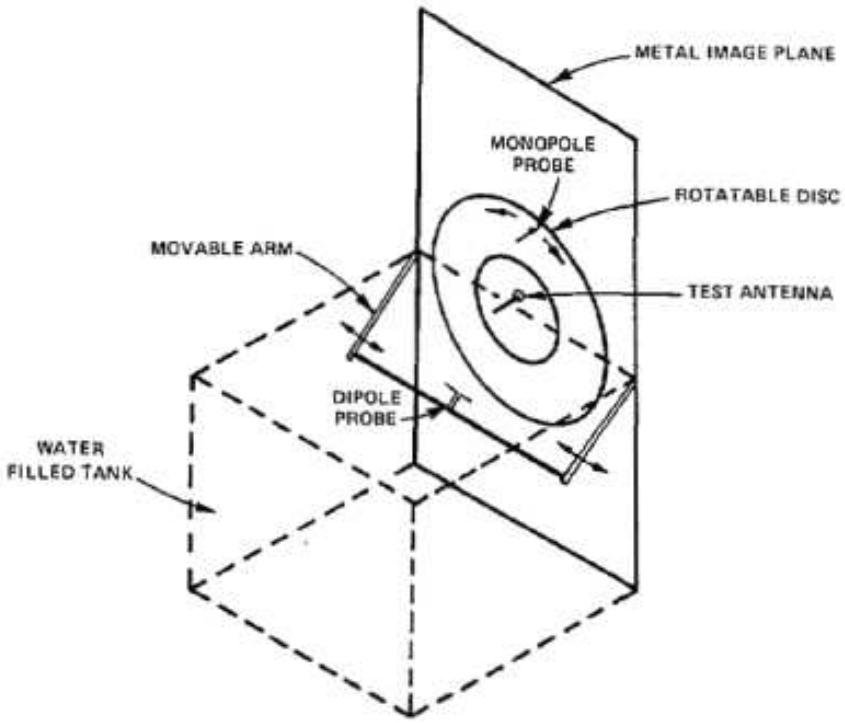

Figure 2.25: Apparatus for Smith's experiments [115]

of fishes. The conductivity of the water where these experiments were performed ranges from 0.005 S/m to 0.025 S/m. The antenna used is a small loop, yagi and wire antennas operating in the VHF band. It is important to note that their antenna selection is based on the selected tracking system [116]. Radiation pattern of three underwater radio-telemetry antennas was measured in an effort to compare their relative reception ranges in horizontal and vertical planes by Beeman et al in 2004. The antenna used is stripped coax and two versions of a dipole antenna (standard dipole and armored dipole). The experiments were conducted in Drano Lake because of its low water velocities and adequate depth. The results show that radiation patterns are similar between the antenna types and also similar to the half-wave dipole in the air. But their received signals strength differed, with the greatest reception achieved, when the transmitting and receiving antennas are parallel. Hence, to maximize detection ranges, appropriate transmit and receive antennas must be selected and as well ensure their proper orientation in the medium [117]. In 2009, Zhou et al presented their dielectric resonator (DR) antenna in [118]. DR antenna comprises of low loss dielectric container, a high permittivity material (permittivity of water is high) and a metal plate to avoid air gap. The one designed by the authors is presented in Fig 2.26. It comprises of a foam container having a thickness of 13.1 mm and relative permittivity of 1.03. The container is filled with distilled water at a temperature of 22°C and relative permittivity of 79.45. Also, a metal plate of 172 mm by 318 mm

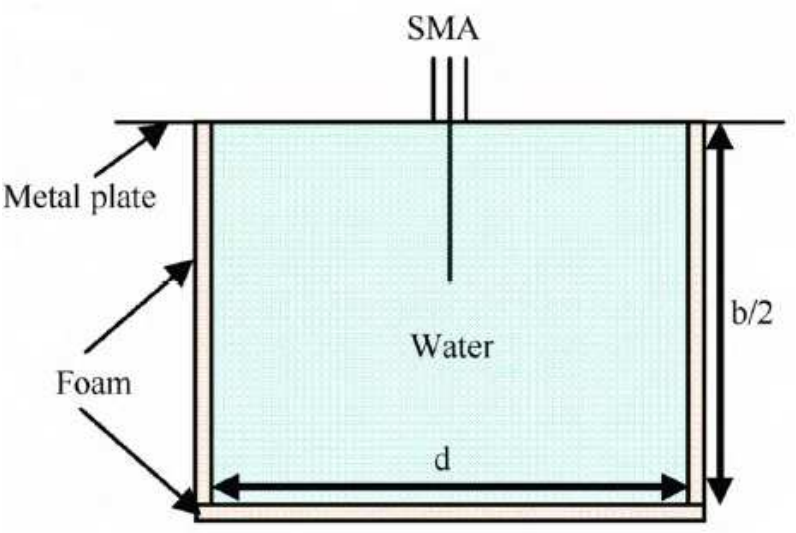

Figure 2.26: Side view of Dielectric Resonator antenna [118]

is placed on top of the container and an SMA connector is connected through the plate. Though the simulated and the measured reflection coefficient of the DR antenna are in good agreement, but the antennas were only able to achieve a bandwidth of about 10 MHz. Still in the same year, Connesa and Joisel designed an active wideband antenna for underwater tomography. The antenna is a short dipole with a frequency range from 100 MHz to 1 GHz [119]. Though this work opens path to new development, when an underwater antenna is designed for operating frequency above 400 MHz, it suffers from attenuation greatly.

In [120], three antennas namely dipole, loop and folded dipole operating at 433 MHz were investigated in a freshwater scenario. This piece of work focuses on measuring the transmitted and the received power of the antennas with and without insulating materials. The results showed that the performance of the antennas with coating materials perform better than those without coatings. In 2011, Mendez et al [121] presented a tin-can UHF radio antenna that is compatible with a deep underwater transmission. The center frequency of the designed antenna is 2.4 GHz, exhibiting a bandwidth of 100 MHz and a reflection coefficient below -10 dB in fresh and sea water. When the surface of the antenna was covered with glass, the bandwidth reduced to 70%, in seawater. The propagation distance of the antenna recorded in the paper was 200 mm which is too short and will eventually require more of these antenna elements for effective communication. In [122], RF waves propagation in water was investigated for the three ISM bands. The conclusion was that propagation at 6.7 MHz will yield positive results for a wireless sensor network for environmental monitoring. Similarly, in [123] ultrawideband (UWB) bow-tie antennas were designed for underwater communications. In that work, three modified types of the

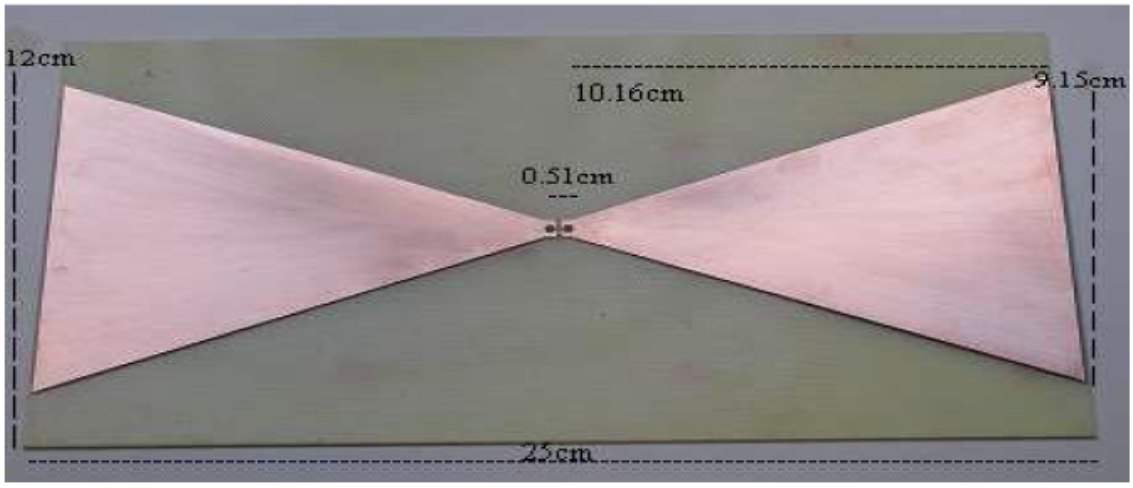

Figure 2.27: Angle-view of proposed Bow-tie patch antenna [124]

initial design were presented, but the best of these antennas achieved better results at low frequencies around 110 MHz.

In [124], a bow tie antenna was designed to operate at the second ISM band, 433 MHz in the air. The designed antenna, which is presented in Fig. 2.27 was made waterproof by spraying glue all over it and measured in water. This eventually made the antenna to resonate at 154 MHz in the medium and the results of transmission coefficient presented shows that the two bow-tie antennas lowered in the medium, can communicate beyond a separation distance of 45 cm. Also in the same year, Sendra et al established a communication link between underwater antennas to study the behavior of EM signals in a freshwater scenario. Two vertical monopole antennas operating at 2.4 GHz were placed inside sealed plastics box and submerged in the medium. Their results show a peak distance of 25 cm is achieved, for different data rates that were used. is that several data transfer rates Their results show that resonating frequency and modulation techniques determine the EM behavior in the medium [125].

In 2015 Evangelia A. Karagianni analyzed propagation speed and attenuation when EM waves propagate in a medium with non-zero conductivity. Here, a bow-tie patch antennas operating at 2.4 GHz and 5.1 GHz were designed and used for two ways WLAN communications. The conclusion was that the antennas produced good performance in pure water with respect to the reflection coefficient and the radiation pattern and due to the conductive nature of the sea water the signal remain unstable, though communication link is established as well [126]. Still, in 2015, Yoshida et al presented the theoretical and experimental analysis of EM wave propagation in an underwater environment. Small loop antennas which were placed in a water container filled with tap water as shown in Fig. 2.28 were used in the experiment. In tap water, they obtained stable results for both

theoretical and measurement, only that they quite differed from one another. On the other hand, the results obtained in seawater remain inconsistent [127].

Figure 2.28: Underwater Small loop antenna in a water container [127]

Also in the same year, a curved spiral antenna for freshwater applications was presented in [128] where the designed antenna operated between 250 MHz and 370 MHz. In 2016, Massaccessi and Pirinoli presented their preliminary results on designing and usage of cylindrical antennas for underwater communications. Three antennas namely dipole, folded dipole and monopole were designed to operate at 433 MHz. Based on their respective input impedance, the folded dipole antenna was preferred to the other two antennas as the real part of its input impedance is somewhat close to standard 50 Ω and therefore does not require matching network unlike the other two antennas [129].

Finally, in table 2.4 information regarding the theoretical and practical analyses of underwater antenna in fresh water scenario are presented. This is similar to the one presented for sea water in the previous subsection.

Table 2.4: Antennas for underwater communications in fresh water

S/No.	Antenna Types	Operating Frequency	Medium	Year
1	Monopole and loop [108]	VLF	Fresh water	1960
2	HED antenna [109]	ELF - MF	Fresh water Sea water	1970
3	TWA and dipole antennas [110]	VHF	Fresh water	1976
4	Coupled horizontal wire antennas [111]	VHF	Fresh and sea water	1977
5	Horizontal circular loop antenna [113]	VHF	Fresh water	1982
6	Loop antenna [114]	VHF	Fresh water	1983
7	Electric and magnetic dipole antennas [115]	UHF	Fresh water	1984
8	Small loop, Yagi wire antenna [116]	VHF	Fresh water	1989
9	Stripped coax, standard armoured dipole antennas [117]	HF and VHF	Fresh water	2004
10	DR antenna [118]	VHF	Fresh water	2009
11	Short dipole antenna [119]	HF, VHF and UHF	Fresh and sea water	2009
12	dipole, loop and folded dipole antennas [120]	UHF	Fresh water	2010
13	Tin-can antenna [121]	UHF	Fresh and sea water	2011
14	Ultrawideband cirucular bow-tie antenna [123]	VHF and UHF	Fresh water	2012
15	Bow-tie antenna [124]	HF	Fresh water	2013
16	Vertical Monopole antennas [125]	HF	Fresh water	2013
17	Printed bow-tie antenna [126]	UHF and SHF	Pure water	2015
18	Small loop [127]	HF	Tap water	2015
19	Curved spiral antenna [128]	VHF and UHF	Fresh water	2015
20	Dipole, folded dipole and monopole [129]	UHF	Fresh water	2016

2.6 Conclusion

In this chapter antenna definitions, types and usage in any known media (air, underwater, space) have been duly presented alongside with the three technologies employs in the underwater environment for operations in the medium. The advantages and disadvantages of these technologies were also given and it can be said that this research work only considers the use of electromagnetic waves in underwater environments. Based on this, a comprehensive review of underwater antenna development in the sea and fresh water in the last 100 years was as well presented. It is therefore important to note that more of the works published and presented till date have been in the seawater environment, but this research work which will be presented in the later chapters of this thesis are considered in both fresh and sea water for adequate comparison of propagation in waters with different conductivities. Lastly, it is important to note that antenna developments for usage in sea water have been considered mainly in the ELF, VLF and LF bands, whereas those of fresh water were considered in the HF, VHF and UHF bands.

Chapter 3

Propagation of Electromagnetic Waves in Lossless and Lossy Media

3.1 Introduction

Various mathematical derivations that help to determine the propagation of EM waves in any medium comes from the analyses of Maxwell's equations and their solutions. Indeed there are four fundamental electromagnetic field quantities, which when two or more are combined appropriately with necessary constants results in Maxwell's equations in different forms. These quantities and their units are presented in Table 3.1. Besides these field quantities, there are universal constants that are similarly very important in the description of electromagnetic waves as well as in other fields. These constants relate to the properties of free space (vacuum) and are presented in Table 3.2.

Table 3.1: Field Quantities

Symbols and Units for Field quantities	Field Quantity	Symbol	Unit
Electric	Electric Field intensity	E	V/m
	Electric Flux density	D	C/m^2
Magnetic	Magnetic flux density	B	T
	Magnetic field intensity	H	A/m

Table 3.2: Universal constants

Universal Constants	Symbol	Value	Unit
Speed of light in free space	c	3×10^8	m/s
Permeability of free space	μ_0	$4\pi \times 10^{-7}$	H/m
Permittivity of free space	ε_0	$\frac{1}{36\pi} \times 10^{-9}$	F/m

This chapter sought to shed light on some theoretical analyses behind EM propagation in any medium, but with clear emphasis to the propagation in the lossy medium. Also, some important concepts in underwater communications are briefly considered. These include Attenuation, Refraction Loss, Skin Depth and Water Properties.

3.2 Maxwell Equations

The fundamental phenomena for describing electromagnetic induction are simply summed together in four equations which are known as Maxwell's equations and presented as follows:

$$\nabla \times \vec{\mathcal{E}} = -\frac{\partial \vec{\mathcal{B}}}{\partial t} - \vec{\mathcal{M}}, \tag{3.1}$$

$$\nabla \times \vec{\mathcal{H}} = \frac{\partial \vec{\mathcal{D}}}{\partial t} + \vec{\mathcal{J}}, \tag{3.2}$$

$$\nabla \cdot \vec{\mathcal{D}} = \rho, \tag{3.3}$$

$$\nabla \cdot \vec{\mathcal{B}} = 0, \tag{3.4}$$

where $\vec{\mathcal{M}}$ is the fictitious magnetic current density V/m^2, $\vec{\mathcal{J}}$ is the electric current density in A/m^2 and ρ is the electric charge density in (C/m^3). Equations 3.1, 3.2, 3.3 and 3.4 are the Faraday law of electromagnetic induction, Ampere circuital law, Gauss' law and law of magnetism, respectively [8, 130, 131], which are otherwise known as Maxwell's equations in differential form. These equations with the continuity equation and the Lorentz force equation are the foundation of the electromagnetic theory. Also, the constitutive relations are given as,

$$\vec{\mathcal{D}} = \varepsilon \vec{\mathcal{E}}, \tag{3.5}$$

$$\vec{\mathcal{B}} = \mu \vec{\mathcal{H}}, \tag{3.6}$$

where the ε and μ are the permittivity and permeability of the medium respectively. These equations can be converted into integral form by using various vector integral theorems

yielding:

$$\oint_C \vec{\mathcal{E}}.\vec{dl} = -\frac{\partial}{\partial t}\int_S \vec{\mathcal{B}}.\vec{ds} - \int_S \vec{\mathcal{M}}.\vec{ds}, \tag{3.7}$$

$$\oint_C \vec{\mathcal{H}}.\vec{dl} = \frac{\partial}{\partial t}\int_S \vec{\mathcal{D}}.\vec{ds} + \int_S \vec{\mathcal{J}}.\vec{ds}, \tag{3.8}$$

$$\int_S \vec{\mathcal{B}}.\vec{ds} = 0; \tag{3.9}$$

$$\int_S \vec{\mathcal{D}}.\vec{ds} = \int_V \rho dv = Q, \tag{3.10}$$

where Q is the total charge in the close volume V. In a steady state sinusoidal time dependence, $\vec{\mathcal{E}}$ and $\vec{\mathcal{H}}$ will transform as:

$$\vec{\mathcal{E}}(x,y,z,t) = \mathbf{E}(x,y,z)e^{j\omega t}, \tag{3.11}$$

$$\vec{\mathcal{H}}(x,y,z,t) = \mathbf{H}(x,y,z)e^{j\omega t}, \tag{3.12}$$

where ω is the angular frequency in radians/second. Assuming linear and isotropic media and taking into consideration an $e^{j\omega t}$ time dependence, time derivatives in 3.1 to 3.4 can be replaced by $j\omega$. The output of these are Maxwell's equations in phasor form given as:

$$\nabla \times \mathbf{E} = -j\omega\mathbf{B}, \tag{3.13}$$

$$\nabla \times \mathbf{H} = \mathbf{J} + j\omega\mathbf{D}, \tag{3.14}$$

$$\nabla \cdot \mathbf{D} = \frac{\rho}{\varepsilon}, \tag{3.15}$$

$$\nabla \cdot \mathbf{B} = 0. \tag{3.16}$$

3.2.1 Wave Equations

To solve the problems of wave propagation, the concern is the behavior of an EM wave in a source-free region and also when there are no external current sources, which means ρ

and $\vec{J}$ are both zero. Hence, Maxwell's curl equations in phasor form are written as:

$$\nabla \times \mathbf{E} = -j\omega\mu\mathbf{H}, \tag{3.17}$$

$$\nabla \times \mathbf{H} = j\omega\varepsilon\mathbf{E}, \tag{3.18}$$

$$\nabla \cdot \mathbf{E} = 0, \tag{3.19}$$

$$\nabla \cdot \mathbf{H} = 0. \tag{3.20}$$

Considering that only equations 3.17 and 3.18 has two unknowns **E** and **H**, these can be solved either for one or the other. Thus, further analysis of these equations will involve taking the curl of these equations and combine them separately for an equation in each field. Hence, in the **E** field the resultant equation is:

$$\nabla \times \nabla \times \mathbf{E} = -j\omega\mu\nabla \times \mathbf{H} = \omega^2\mu\varepsilon\mathbf{E}. \tag{3.21}$$

Vector identities of the form $\nabla \times \nabla \times \mathbf{P} = \nabla(\nabla.\mathbf{P}) - \nabla^2\mathbf{P}$ was employed to simplify the result yielding:

$$\nabla(\nabla.\mathbf{E}) - \nabla^2\mathbf{E} = \omega^2\mu\varepsilon\mathbf{E}. \tag{3.22}$$

Substituting equation 3.19 and rearrange properly 3.22 becomes:

$$\nabla^2\mathbf{E} + \omega^2\mu\varepsilon\mathbf{E} = 0. \tag{3.23}$$

Similarly by employing the same mathematical derivatives on the **H** field component yield:

$$\nabla^2\mathbf{H} + \omega^2\mu\varepsilon\mathbf{H} = 0. \tag{3.24}$$

These two equations, 3.23 and 3.24 are known as Helmholtz equation or wave equation in **E** and **H** field respectively.

Further analyses of these equations yield the velocity of propagation of the wave in the medium which is $\frac{1}{\sqrt{\mu\varepsilon}}$. But:

$$\mu = \mu_0\mu_r, \tag{3.25}$$

and

$$\varepsilon = \varepsilon_0\varepsilon_r, \tag{3.26}$$

where μ_0 and ε_0 and the magnetic permeability and electrical permittivity of free space defined among the universal constants given in Table 3.2. Also μ_r ε_r are the relative magnetic permeability and electrical permittivity of the medium. In free space, $\mu_r = \varepsilon_r$ =1 and the resultant parameter is the third element among the universal constant, which is the speed of light. The propagation constant or wave number is another important parameter that can be derived from 3.23 and 3.24, and is defined as $k = \omega\sqrt{\mu\varepsilon}$.

Thus, the two equations are re-written as:

$$\nabla^2\mathbf{E} + k^2\mathbf{E} = 0. \tag{3.27}$$

$$\nabla^2\mathbf{H} + k^2\mathbf{H} = 0. \tag{3.28}$$

Hence, by squaring this propagation constant, the resulting element satisfies the component of $\vec{E}$ in equation 3.23.

3.2.2 Plane Waves in Lossless (Non-Conducting) Media

If the wave equation in 3.23 is considered in Cartesian coordinate, it will yield three scalar Helmholtz's equation, E_x, E_y and E_z and these components are written for E_x direction only we have:

$$\left(\frac{\partial^2}{\partial x^2} + \frac{\partial^2}{\partial y^2} + \frac{\partial^2}{\partial z^2} + k_0^2\right) E_x = 0. \tag{3.29}$$

Thus, for an electric field with only $\hat{x}$ component and no variation in x and y, then $\frac{\partial E}{\partial x}$ = $\frac{\partial E}{\partial y}$ =0, then wave equation reduces to:

$$\frac{\partial^2 E_x}{\partial z^2} + k_0^2 E_x = 0, \tag{3.30}$$

equation 3.30 is an ordinary differential equation, where E_x depends only on z. Thus, solution to this equation can be readily obtained in the form:

$$E_x(z) = E^+ e^{-jkz} + E^- e^{-jkz}, \tag{3.31}$$

where E^+ and E^- are arbitrary constant values representing the amplitudes of the forward and backward propagating waves, respectively. Also when equation 3.23 is applied to the

electric field in the last equation, the resultant solution is the magnetic field counterpart:

$$\mathbf{H}_x(z) = 0, \tag{3.32}$$

$$\mathbf{H}_z(z) = 0, \tag{3.33}$$

$$\mathbf{H}_y(z) = \frac{1}{\eta}\left[E^+ e^{-jkz} - E^- e^{-jkz}\right], \tag{3.34}$$

where η is the wave impedance, which can be expressed as $\eta = \omega\mu/k = \sqrt{\mu/\varepsilon}$ and is known as ratio of **E** and **H** fields. In planes waves, the wave impedance is equal to the intrinsic impedance. Thus, in free-space, the intrinsic impedance $\eta_0 = \sqrt{\mu_0/\varepsilon_0} = 377\,\Omega$. Full mathematical analysis of this derivation is not covered here, but can be found in [8, 132, 130]

3.2.3 Plane Waves in Lossy (Conducting) Media

This aspect is very important in this work because further research reported is practically based on wave propagation in this environment. The derivation for plane waves in a lossless medium can be modified to apply to wave propagation in a lossy medium. This is achieved by replacing k in equation 3.27 with k_c and the equation becomes:

$$\nabla^2\mathbf{E} + k_c^2\mathbf{E} = 0. \tag{3.35}$$

In this case k_c is a complex quantity, defined as:

$$k_c = \omega\sqrt{\mu\varepsilon_c}, \tag{3.36}$$

where ε_c is a complex electrical permittivity.

Based on the analysis presented in the Cole-Cole equation [133, 134] and Debye model [3, 135], complex permittivity in a conductive medium has been described mathematically [136] and can be presented as:

$$\varepsilon_c = \varepsilon - j\frac{\sigma}{\omega} = \text{ F/m}, \tag{3.37}$$

where σ is the conductivity measured in Siemens per meter, j is the imaginary unit ($=\sqrt{-1}$), and ε is already defined in 3.26.

This equation can be further expressed in line with Debye model, such that the complex relative permittivity is dependent on factors like frequency, temperature, and salinity. This is presented as:

$$\varepsilon_c = \varepsilon_0 \left[\varepsilon_\infty + \left[\frac{\varepsilon_s - \varepsilon_\infty}{1 + \left(j \frac{f}{f_{rel}} \right)} \right] \right] - \frac{j\sigma}{\omega}, \tag{3.38}$$

where ε_s and ε_∞ are the real part of the relative permittivity at low and high frequencies respectively, f_{rel} is the relaxation frequency and f is the operating frequency measured in Hertz.

Based on equation 3.37, equation 3.35 is re-written as:

$$\nabla^2 \mathbf{E} + \omega^2 \mu \varepsilon (1 - j \frac{\sigma}{\omega \varepsilon}) \mathbf{E} = 0 \tag{3.39}$$

and the conjugate in H plane is written as:

$$\nabla^2 \mathbf{H} + \omega^2 \mu \varepsilon (1 - j \frac{\sigma}{\omega \varepsilon}) \mathbf{H} = 0 \tag{3.40}$$

But the complex propagation constant, γ, can be written as:

$$\gamma = jk_c = j\omega \sqrt{\mu \varepsilon_c}, \tag{3.41}$$

which is the same component $\omega^2 \mu \varepsilon (1 - j \frac{\sigma}{\omega \varepsilon})$ in equation 3.39 and 3.40, and be can re-arranged as [3, 137]

$$\sqrt{j\omega\mu(j\omega\varepsilon + \sigma)} = \alpha + j\beta, \tag{3.42}$$

where α and β are respectively the real and the imaginary parts of γ and are also known as the attenuation constant in Neper per meter and the phase constant in radians per unit length respectively.

3.3 Impairments of Lossy Media on Wave Propagation

3.3.1 Water properties

In [8] the author classified propagating media into two different types which are: dielectric and conducting media. A medium is referred to as a dielectric or insulator lossy medium if $\sigma/\omega\varepsilon$ «1. This means that the displacement current is much greater than the conductive current. Conversely, when $\sigma/\omega\varepsilon$ »1, the media is considered to be a good conductor, meaning the conductive current is much greater than the displacement current. It is based on these analyses that the dependence of $\sigma/\omega\varepsilon$ as a function of operating frequency for fresh and sea water is presented in Fig. 3.1, which was obtained from the previous analysis, specifically from equation 3.37. From the plots, the horizontal line indicates the medium where $\sigma/\omega\varepsilon = 1$, but also serves as a demarcation between the conducting medium (region above the line) and the dielectric medium (the region below the line). It can also be seen that for frequencies below 10 MHz, freshwater behaves as a conductor, it thereafter behaves as a dielectric medium, whereas the change from conducting to dielectric occurs at 888 MHz in seawater [138]. This simply means it is only at lower frequencies that sea water behaves as a good conductor. Thus, the frequency at which fresh and seawater change from conducting to dielectric medium is known as transition frequency.

3.3.2 Attenuation

Attenuation in relation to underwater technology is defined as a gradual loss of signal intensity which is the resultant effect of scattering from the water, dissolved impurities (including organic and inorganic substance) and the intrinsic absorption by water [140]. Thus, it is important to note the full breakdown of the expression in the right hand side of equation 3.42 for α and β are given as equation 3.43 and 3.44 respectively [3], which are:

$$\alpha = \omega\sqrt{\mu\varepsilon}\sqrt{\frac{1}{2}\left(\sqrt{1+\left(\frac{\sigma}{\omega\varepsilon}\right)^2}-1\right)} \tag{3.43}$$

$$\beta = \omega\sqrt{\mu\varepsilon}\sqrt{\frac{1}{2}\left(\sqrt{1+\left(\frac{\sigma}{\omega\varepsilon}\right)^2}+1\right)} \tag{3.44}$$

where α is the attenuation coefficient and β the propagation constant. These two equations are vital for understanding the attenuation at various operating frequencies, which will be used in determining the best operating frequency of the underwater

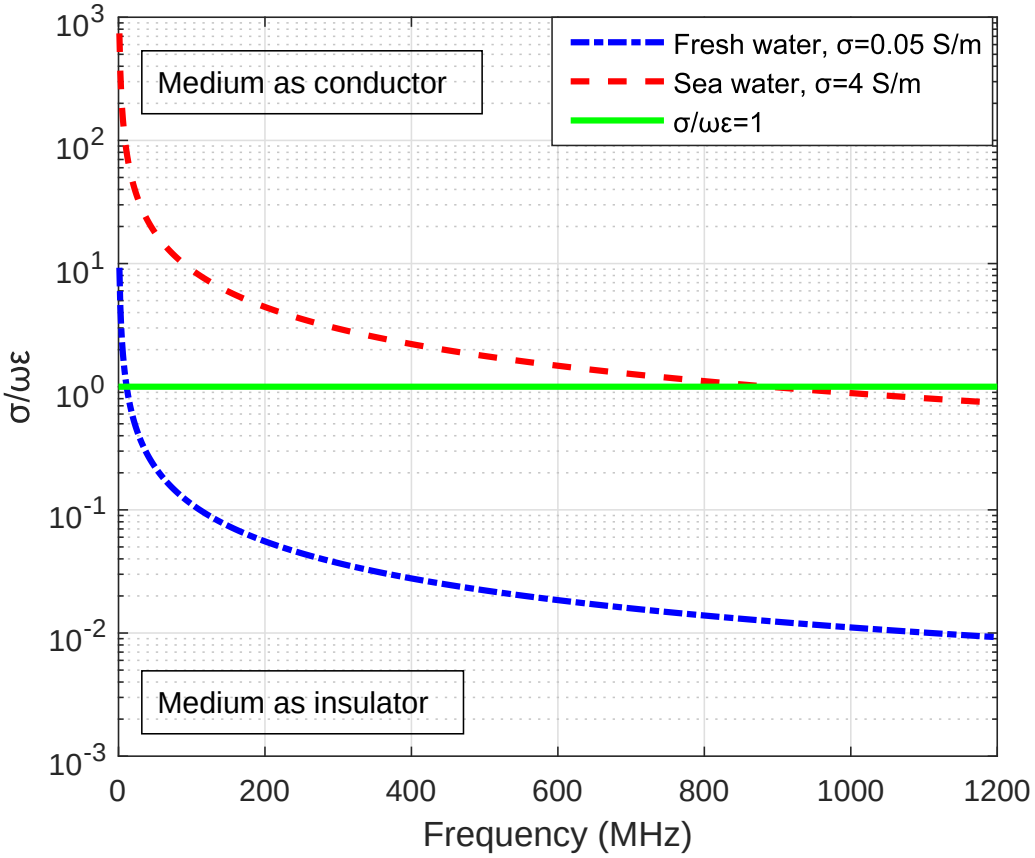

Figure 3.1: Behavior of $\sigma/\omega\varepsilon$ as a function of frequency in fresh and sea water [139]

antennas. Also, it will be employed in calculating the wavelength, λ, which is important for the antenna dimensioning, which can be expressed as:

$$\lambda = 2\pi/\beta. \tag{3.45}$$

The attenuation of an electromagnetic wave as a function of frequency for water with different conductivities is shown in Fig. 3.2. The plots comprises tap, fresh and sea water with conductivities of 0.01 S/m, 0.05 S/m and 4 S/m, respectively, which are plotted with and without complex permittivity. The discontinuous plots are without complex permittivity and therefore these does not depend on other parameters. These gives accurate results up to 80 MHz, but might be misleading at frequencies beyond this value, as the plots remained saturated despite increasing frequency. However, the continuous plots are those with complex permittivity. It can be deduced from these plots that attenuation increases with an increase in frequency, which shows the dependency of attenuation in any medium on complex permittivity as presented through Debye model in equation 3.38. In Table 3.3 some values of the attenuation coefficient measured in

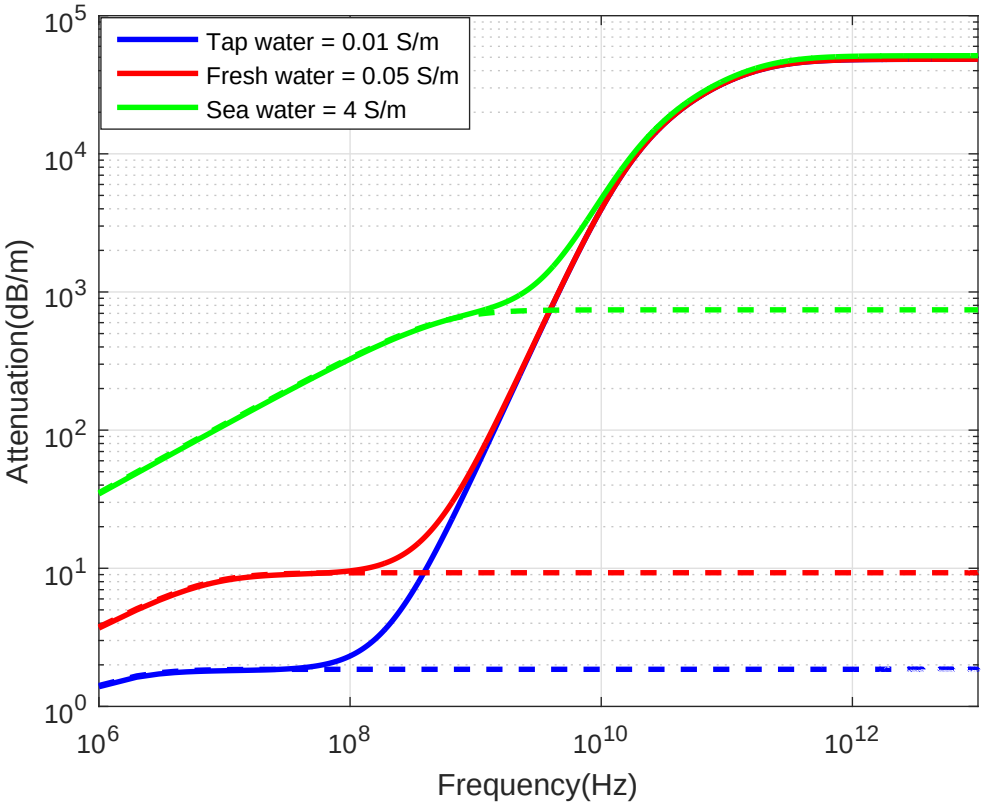

Figure 3.2: Attenuation coefficient of an electromagnetic wave propagating in water with different conductivity

decibel per meter, at several reference frequencies are presented. Also, it can be seen from these plots, that the values in tap and fresh water seems to remain almost steady between 10 MHz and 100 MHz. This is important, as there is less than 1 dB increase in attenuation spanning a 90 MHz bandwidth. It should be noted that as the frequency increases beyond VHF bands, attenuations increases astronomically as presented in [141], which makes it difficult to operate electromagnetic equipment at these frequencies. It was based on these analyses that the values of at the industrial, scientific, and medical radio band (ISM band) were deduced and presented in [122]. The only ISM band that falls within the range of this work is 6.7 MHz and the value in tap, fresh and sea water are 1.8 dB/m, 7.5 dB/m and 88.9 dB/m, respectively. It is remarkable that the attenuation is relatively manageable in the media up to 200 MHz. A reverberating conclusion is that EM waves can propagate efficiently in freshwater mostly at lower frequencies, whereas it will endure a severe propagation loss in sea water. Based on these conclusion this work focuses mainly on designing antennas within the High Frequency (HF) band and up to the lower part of the Very High Frequency (VHF) band.

Table 3.3: Attenuation values at different frequencies for tap, fresh and sea water

	Attenuation coefficient (dB/m) at different frequencies					
Medium	**1 MHz**	**10 MHz**	**100 MHz**	**200 MHz**	**433 MHz**	**2.4 GHz**
Tap water (0.01 S/m)	1.39	1.81	2.32	3.81	11.16	284.40
Fresh water (0.05 S/m)	3.69	8.15	9.58	11.09	18.43	291.70
Sea water (4 S/m)	34.51	108.60	326.60	437.50	573.40	987.90

3.3.3 Skin depth

Apart from the attenuation and the propagation characteristics as a function of frequency presented earlier, another a function that is also important for the antenna propagation in lossy media is the skin depth, δ. The attenuation presented earlier is specified for propagation mainly in water, but when there is air to water or water to air transitions, determination of the skin depth (SD) become also relevant. Skin depth refers to the measure of the penetration of the electromagnetic wave into the medium. The skin depth, δ, in fresh and sea water are compared given the difference in their respective conductivity. They can be calculated using the following expression [25, 60]:

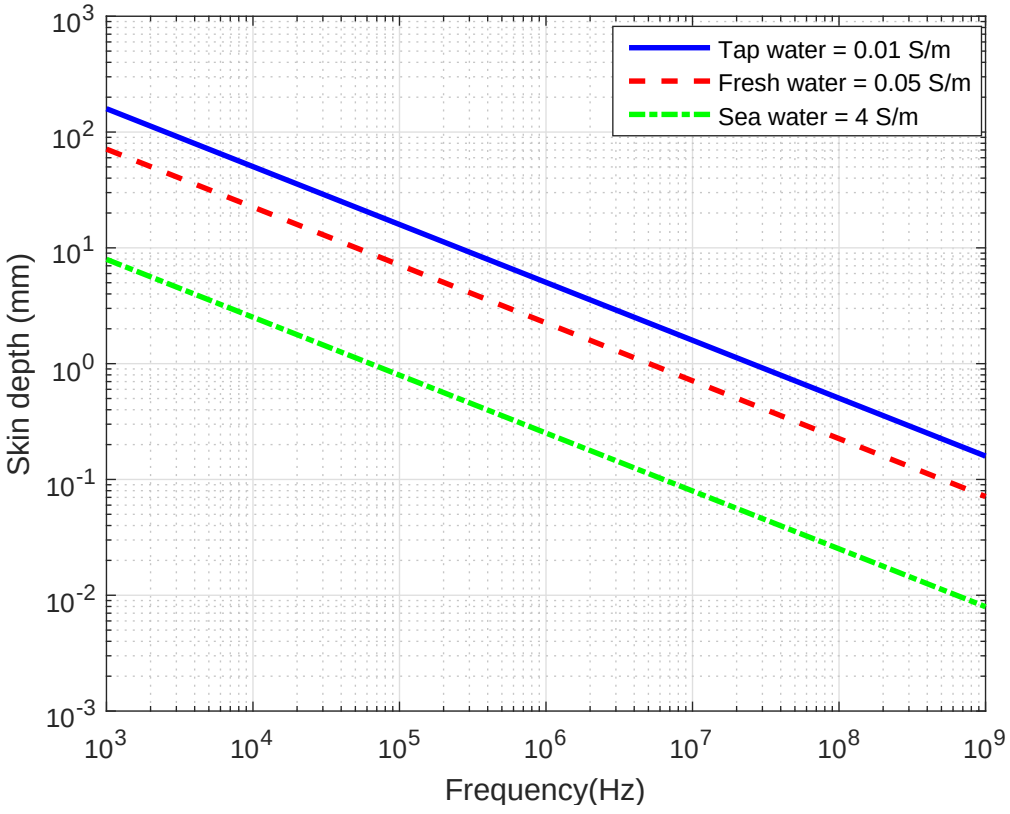

Figure 3.3: Skin depth as a function of frequency for tap, fresh and sea water

$$\delta = \frac{1}{\alpha} = \sqrt{\frac{2}{\mu\sigma\omega}}. \tag{3.46}$$

Also, when the value of permeability in free space is introduced, then this equation reduces to:

$$\delta = \frac{1}{2\pi\sqrt{f\sigma \times 10^{-7}}} \tag{3.47}$$

A plot of skin depth parameter with respect to frequency in tap, fresh and sea water is presented in Fig. 3.3. It can be seen from this figure that SD decreases as the frequency increases. Across media, it is lower in water with higher conductivity and conversely higher in water with lower conductivity.

3.3.4 Refraction or Interface Losses

Similarly, the refraction loss (RL) occurs due to the change in the medium experienced by the transmitted or received signal across the air to water or water to air interface. This can be calculated by employing the following formula [83, 142]:

$$RL\,(dB) = -20 \times log10\left\{\left(7.4586 \times 10^{-6}\sqrt{\frac{f}{\sigma}}\right)\right\} \tag{3.48}$$

Fig. 3.4 shows the refraction loss as a function of frequency. Its values decrease with increasing frequency up to the saturation point which occurs at 6.6 MHz, 29 MHz and 2.61 GHz in tap, fresh and seawater respectively. The figure also shows that at lower frequencies, the value is higher in highly conductive water and lower in low conductive water respectively.

3.3.5 Intrinsic Impedance

This is another important parameter for consideration in underwater propagation. It is literally defined as a ratio of the electric field strength to the magnetic field strength. The value in the air was given in subsection 3.2.2, in pure water when conductivity equals zero, the value is 42 Ω. But in water with different conductivities assuming that the propagating signal is perpendicular to the surface of the medium. It is defined mathematically as:

$$Z_{int} = \sqrt{\frac{j\omega\mu}{\sigma + j\omega\varepsilon}} \tag{3.49}$$

Using this equation, we plot the dependence of intrinsic impedance (real and imaginary) on conductivity which is presented in Figure 3.5. It is seen here that as the conductivity

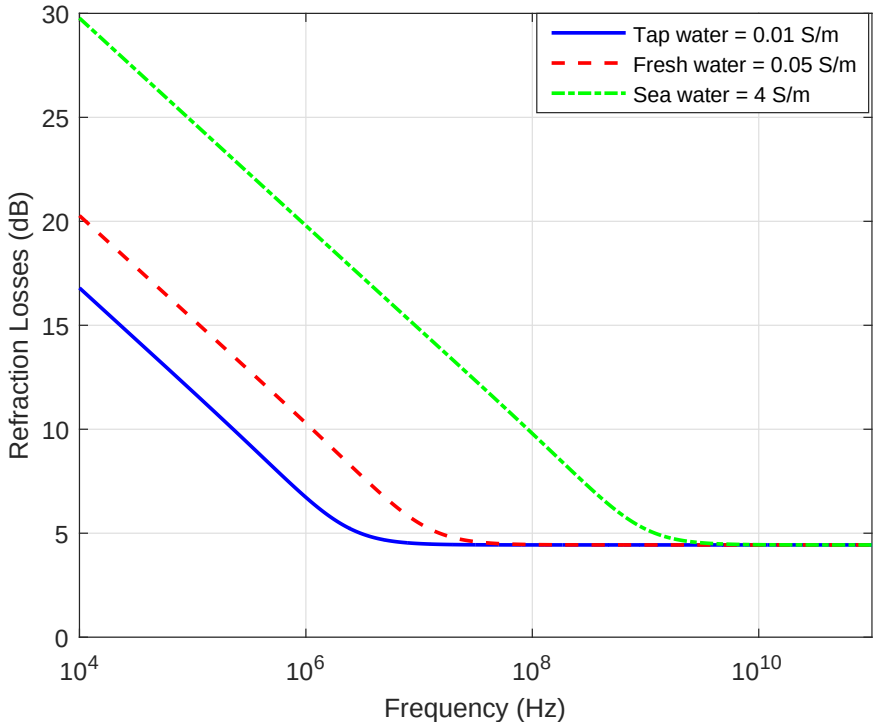

Figure 3.4: Refraction losses as a function of frequency for tap, fresh and sea water

increases the real part of the intrinsic impedance decreases, on the other hand, it increases with frequency. Similarly, for frequencies between 10 and 50 MHz, the imaginary part rises sharply to optimum before dropping again with increasing conductivity. But at higher frequencies, the imaginary part only rises and reach a saturation such that the plots remain unchanged with further increase in conductivity.

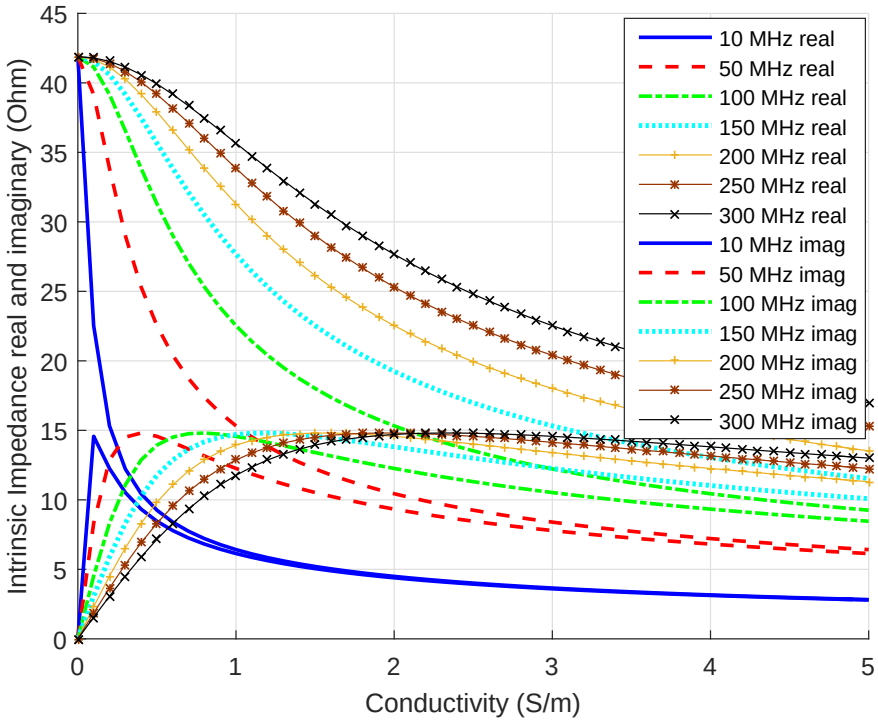

Figure 3.5: Intrinsic impedance as a function of conductivity

3.4 Radiation Theory

The radiation pattern of an antenna is the fundamental property that defines its performance in any medium. It can be calculated or computed through two different methods. The first method is by calculating the inhomogeneous wave equation in the E- and H- fields by means of Maxwell's equations. This procedure is cumbersome and will lead to tedious mathematical problems, which involves integration with complex integrand. An alternative and less complex approach is by breaking the procedure into two steps, here auxiliary functions known as vector potentials are introduced, which are then used to calculate the fields radiating from the antenna [13, 143]. Thus, methods one and two are jointly presented in Fig. 3.6, where path 1 with a single step involves only integration. On the other hand, the second path involves two, step one is integration and thereafter step two is differentiation. Despite having two steps, this method makes it easier to calculate radiated fields.

In Fig. 3.6, **J**, and **M** are the point source for the electric and magnetic fields respectively. Hence, to determine $\vec{E}$ and $\vec{H}$, the first step is to find the two vector potentials **A** (magnetic vector potential) and **F** (electric vector potential), which have

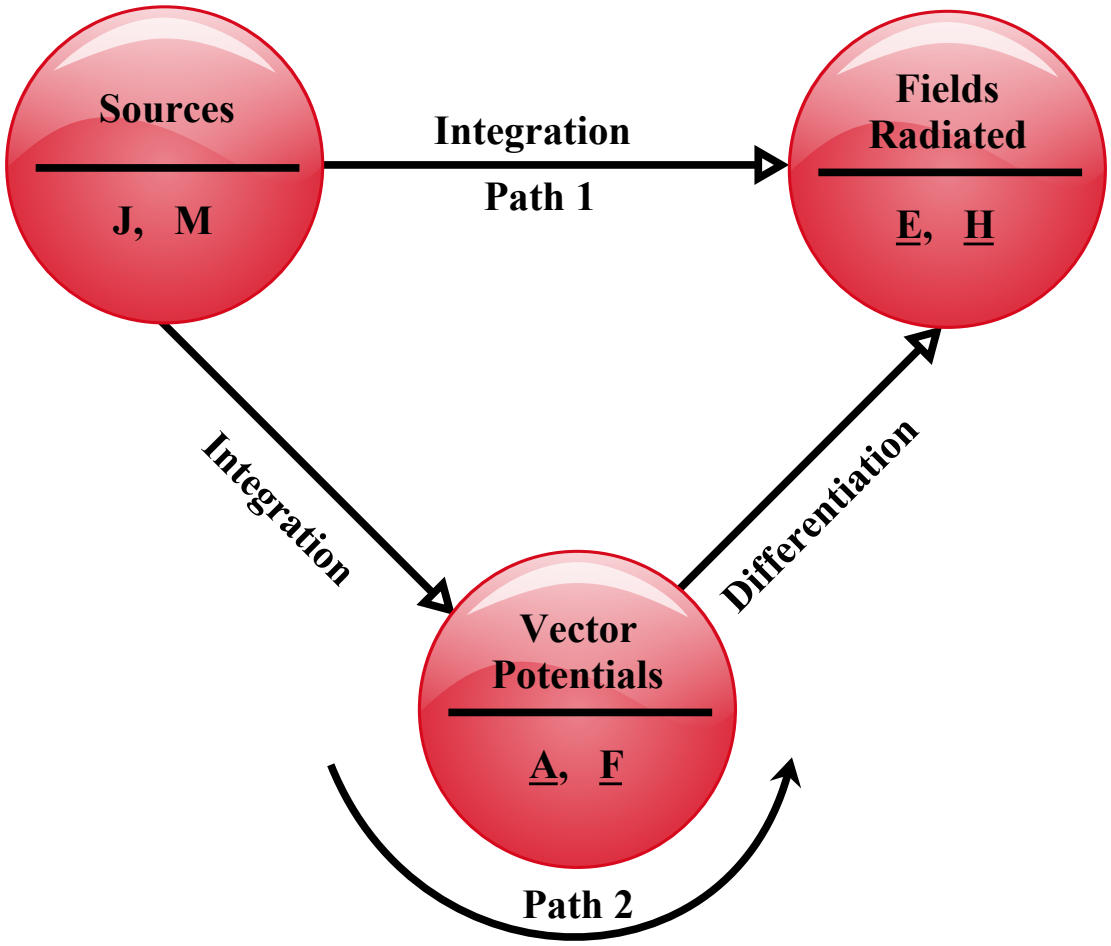

Figure 3.6: Block diagram for solving antenna radiation [13, 39, 143]

integral relations to the point sources **J** and **M** by

$$\nabla^2\mathbf{A} + k^2\mathbf{A} = -\mu\mathbf{J}, \tag{3.50}$$

$$\nabla^2\mathbf{F} + k^2\mathbf{F} = -\varepsilon\mathbf{M}, \tag{3.51}$$

details of the analyses that yield the respective solutions for **A** and **F** can be found in [13, 16, 8].

Based on these vector potentials, the components to be determined in the second step are $\mathbf{E}_A, \mathbf{H}_A$ and $\mathbf{E}_F, \mathbf{H}_F$, which are the corresponding electric and magnetic fields components. The total fields are then obtained by superposition of the individual fields which are due to **A** and **F** (**J** and **M**). Thus, the components are:

$$\mathbf{H}_A = \frac{1}{\mu}\nabla \times \mathbf{A} \tag{3.52}$$

$$\mathbf{E}_A = -j\omega\mathbf{A} - j\frac{1}{\omega\mu\varepsilon}\nabla(\nabla.\mathbf{A}) \tag{3.53}$$

$$\mathbf{E}_F = -\frac{1}{\varepsilon}\nabla\times\mathbf{F} \tag{3.54}$$

$$\mathbf{H}_F = -j\omega\mathbf{F} - \frac{j}{\omega\mu\varepsilon}\nabla(\nabla.\mathbf{F}) \tag{3.55}$$

In summary, the following steps are employed to determine the fields components from the point sources through the vector potentials:

- Specify the sources for the electric current density, **J** and the magnetic current density, **M** respectively;
- Using the Integral method, determine **A** (due to **J**) and **F** (due to **M**);
- and then the differential method to find $\mathbf{H}_A$ and $\mathbf{E}_A$ as well as $\mathbf{E}_F$ and $\mathbf{H}_F$;
- Finally determines the total fields which are the sum of the electric and magnetic components.

When current densities are distributed over a thin wire of a very short length as shown in Fig. 3.7, the line integral of the vector potentials of 3.50 and 3.51 are presented as:

$$\mathbf{A} = \frac{\mu}{4\pi}\int_C I_e\left(x^{'},y^{'},z^{'}\right)\frac{e^{-jkR}}{R}dl^{'}, \tag{3.56}$$

$$\mathbf{F} = \frac{\varepsilon}{4\pi}\int_C I_m\left(x^{'},y^{'},z^{'}\right)\frac{e^{-jkR}}{R}dl^{'}, \tag{3.57}$$

but if the wire carries only electric current I_e, it means the magnetic current I_m equals to zero thereby, the vector potential **F** also equal to zero, the vector potential **A**, which oriented from the source along the z axis such that $I_e\left(z^{'}\right) = \hat{a}_z I_e$ is presented as:

$$\mathbf{A} = \frac{\mu}{4\pi}\int_C \hat{\mathbf{a}}_z I_e\frac{e^{-jkR}}{R}dl^{'}, \tag{3.58}$$

these equations in phasor form can be presented as:

$$\mathbf{A} = \hat{\mathbf{a}}_z\frac{\mu_0 Idl}{4\pi}\left(\frac{e^{-jkR}}{R}\right) \tag{3.59}$$

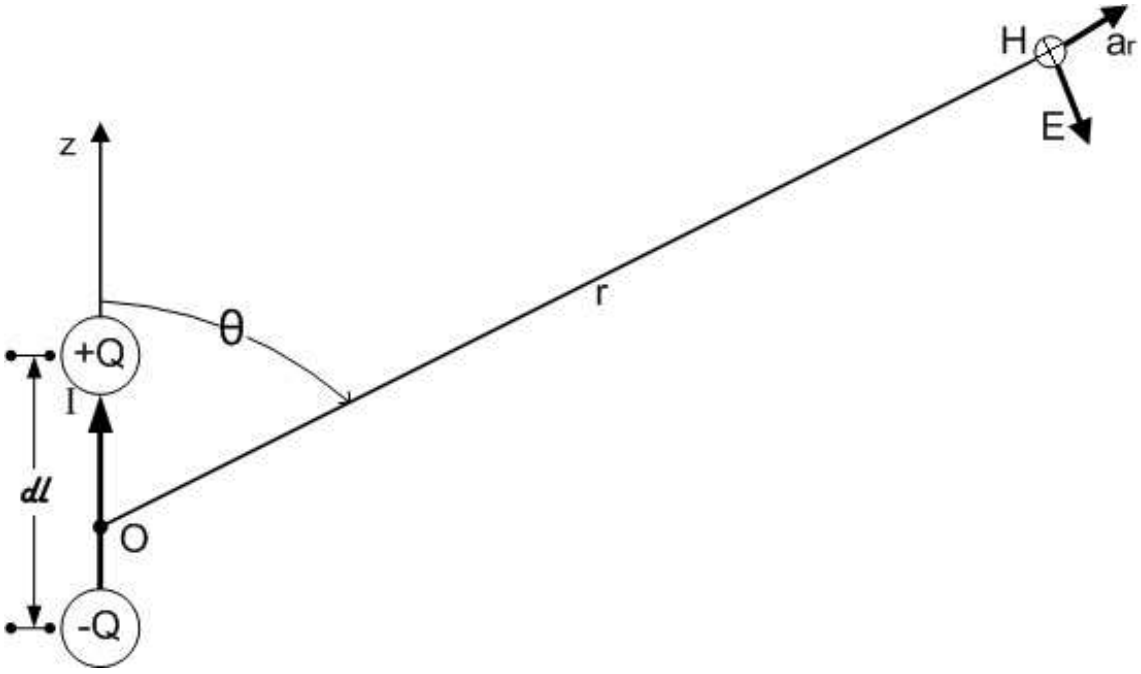

Figure 3.7: Geometrical arrangement showing the associated fields of an Hertzian dipole [8]

Thus, in deriving the field of a small current element which can be approximated with a point source, the use of spherical coordinate is most appropriate. This is given as:

$$\hat{\mathbf{a}}_z = \hat{\mathbf{a}}_r cos(\theta) - \hat{\mathbf{a}}_\theta sin(\theta) \tag{3.60}$$

The component of **A** in equation 3.58 in spherical coordinate is presented as:

$$\mathbf{A} = \hat{\mathbf{a}}_r A_r + \hat{\mathbf{a}}_\theta A_\theta + \hat{\mathbf{a}}_\phi A_\phi, \tag{3.61}$$

and the three components are:

$$A_r = A_z cos\theta = \frac{\mu_0 Idl}{4\pi}\left(\frac{e^{-jkR}}{R}\right) cos\theta, \tag{3.62}$$

$$A_\theta = -A_z sin\theta = -\frac{\mu_0 Idl}{4\pi}\left(\frac{e^{-jkR}}{R}\right) sin\theta, \tag{3.63}$$

$$A_\phi = 0. \tag{3.64}$$

If the symmetry of the hertizian dipole antenna in Fig. 3.7 is considered with no variations in ϕ, the equation as extended in spherical coordinates is presented in simplified

form as

$$\mathbf{H} = \hat{\mathbf{a}}_\phi \frac{1}{\mu r}\left[\frac{\partial}{\partial r}(rA_\theta) - \frac{\partial A_r}{\partial \theta}\right]. \tag{3.65}$$

By substituting equations 3.62 and 3.63 into 3.65, the equation reduces to

$$H_r = H_\theta = 0, \tag{3.66}$$

and

$$H_\phi = j\frac{kI_0 l sin\theta}{4\pi r}\left[1 + \frac{1}{jkr}\right]e^{-jkr}. \tag{3.67}$$

Recalling the relationship between **E** & **H** in equation 3.53, if **J** = 0, then

$$\mathbf{E} = \mathbf{E}_A = -j\omega\mathbf{A} - j\tfrac{1}{\omega\mu\varepsilon}\nabla(\nabla.A) = \frac{1}{j\omega\varepsilon}\nabla\times\mathbf{H}, \tag{3.68}$$

which means

$$\frac{1}{j\omega\varepsilon}\nabla\times\mathbf{H} = \frac{1}{j\omega\varepsilon_0}\left[\hat{a}_r\frac{1}{rsin\theta}\frac{\partial\left(H_{\phi sin\theta}\right)}{\partial\theta} - \hat{a}_\theta\frac{1}{r}\frac{\partial}{\partial r}\left(rH_\phi\right)\right]. \tag{3.69}$$

Therefore, the E-field components can be determined by substituting equations 3.62, 3.63 and 3.64 into equation 3.68, which reduces to

$$E_r = \eta\frac{I_0 l cos\theta}{2\pi r^2}\left[1 + \frac{1}{jkr}\right]e^{-jkr}, \tag{3.70}$$

$$E_\theta = j\eta\frac{kI_0 l sin\theta}{4\pi r}\left[1 + \frac{1}{jkr} - \frac{1}{(kr)^2}\right]e^{-jkr}, \tag{3.71}$$

$$E_\phi = 0. \tag{3.72}$$

3.5 Field Region of an Antenna

In principle, field regions of an antenna are divided into 3 namely: reactive near field (evanescent zone), radiating near field and far field. These three regions are as depicted in Fig. 3.8.

Further analysis regarding each of the zones, with respect to their definition and representation, mathematically are presented in the following subsections:

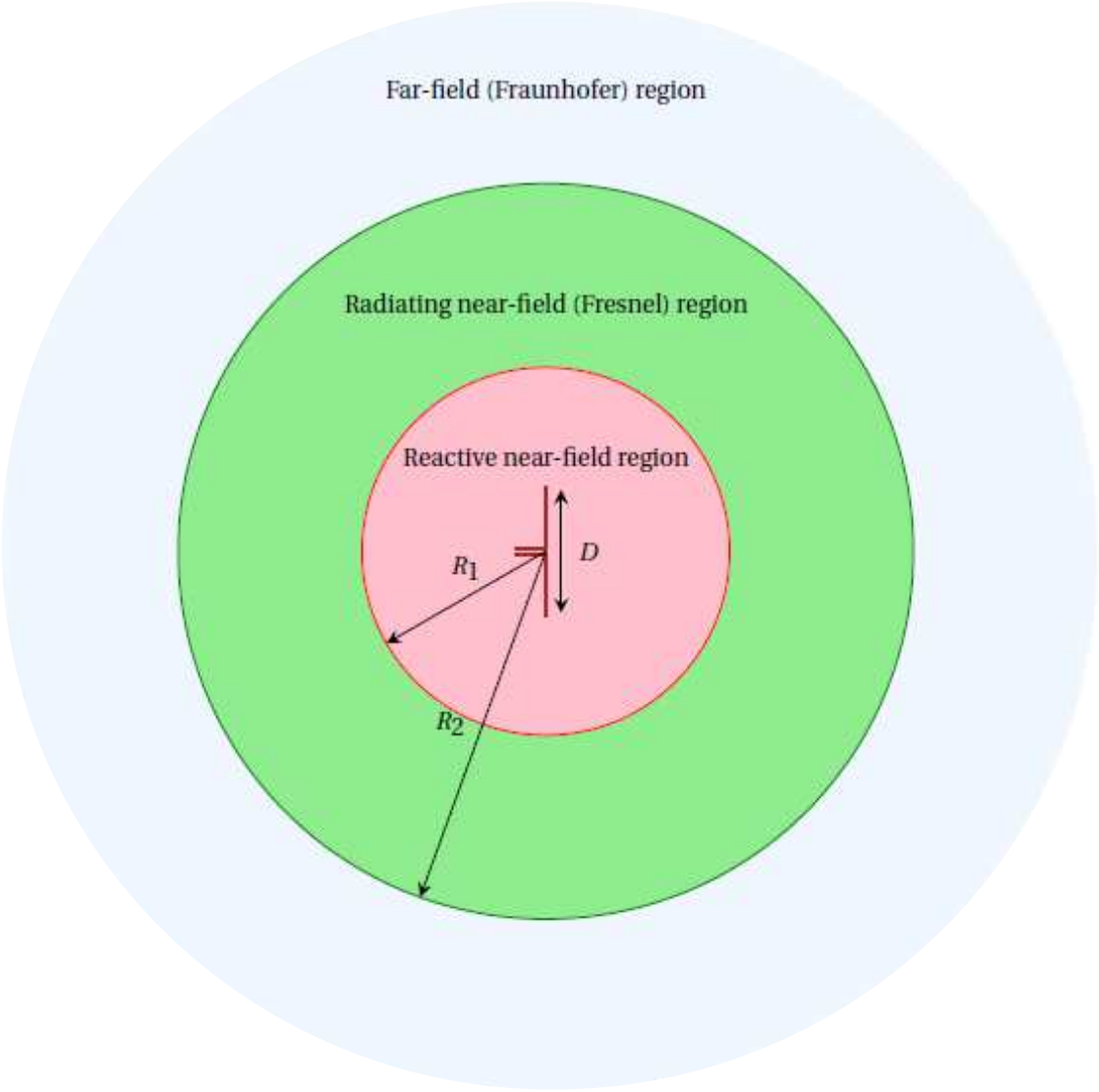

Figure 3.8: Antenna's Field Regions [13, 143]

3.5.1 Reactive Near Fields

This is the immediate area/environment of an antenna. The region is dominated by reactive fields. In other words, it means E-field and H-field are out of phase by 90° to each other. Mathematically, the boundary of the region is given as:

$$0.62\sqrt{\frac{l^3}{\lambda}} > r > 0, \tag{3.73}$$

where l is the length of a wire antenna which is equivalent to the largest dimension of the antenna, D. To present this in spherical coordinates, the conditions that must be satisfied are $kr << 1$ and when $kr << \lambda$ or $r << \lambda/2\pi$, the components of E-field and H-field

are:

$$E_r = -j\eta \frac{I_0 l e^{-jkr}}{2\pi k r^3} cos\theta, \tag{3.74}$$

$$E_\theta = -j\eta \frac{I_0 l e^{-jkr}}{4\pi k r^3} sin\theta, \tag{3.75}$$

$$E_\phi = H_r = H_\theta = 0, \tag{3.76}$$

$$H_\phi = \frac{I_0 l e^{-jkr}}{4\pi r^2} sin\theta. \tag{3.77}$$

3.5.2 Radiative Near Fields or Fresnel Region

This is the region sandwiched between the reactive near-field and the far-field. Here the radiation fields predominate and the angular field distribution depends largely upon the distance from the antenna. But in the case of antennas where D « λ the region may not exist. Thus, radiative near field region is presented as

$$\frac{2l^2}{\lambda} > r \geqslant 0.62\sqrt{\frac{l^3}{\lambda}} \tag{3.78}$$

This region is also called intermediate region, where the values of kr begin to increase and greater than unity. It is often called Fresnel region and the radiating near field parameters where $kr > 1$ can be presented in spherical coordinates as:

$$E_r = \eta \frac{I_0 l e^{-jkr}}{2\pi k r^2} cos\theta, \tag{3.79}$$

$$E_\theta = j\eta \frac{k I_0 l e^{-jkr}}{4\pi r} sin\theta, \tag{3.80}$$

$$E_\phi = H_r = H_\theta = 0, \tag{3.81}$$

$$H_\phi = \frac{k I_0 l e^{-jkr}}{4\pi r} sin\theta. \tag{3.82}$$

3.5.3 Farfields or Fraunhofer Region

This is the region that is farthest away from the antenna where the angular field distribution does not depend on the distance from the antenna (propagating waves). Hence the region is given mathematically as:

$$\infty \geqslant r \geqslant \frac{2l^2}{\lambda} \tag{3.83}$$

In this region, $kr >> 1$ and also $r > \lambda$. Hence, E_r is inversely proportional to r^2 and will be smaller than E_θ. Similarly, E_θ is inversely proportional to r and their field components

are given as:

$$E_\theta = j\eta \frac{kI_0 le^{-jkr}}{4\pi r} sin\theta, \tag{3.84}$$

$$E_r = E_\phi = H_r = H_\theta = 0, \tag{3.85}$$

$$H_\phi = j \frac{kI_0 le^{-jkr}}{4\pi r} sin\theta. \tag{3.86}$$

It can, therefore, be observed from Fig. 3.9 typical changes of antenna amplitude pattern shape of the field regions from reactive near field to the far field.

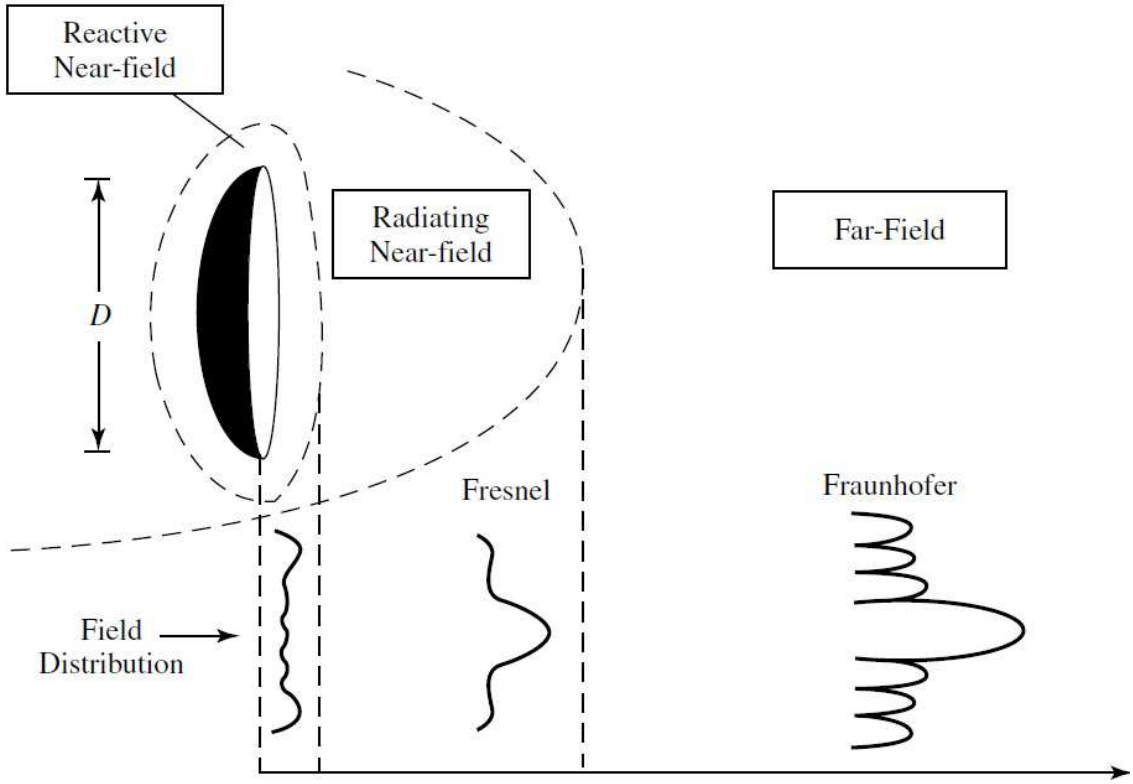

Figure 3.9: Near-Field (reactive near field and radiative near field) and Far-Field of an antenna[13, 144]

Hence, to conclude this chapter the calculated field regions of a half-wave dipole antenna operating at 40.00 MHz, 100 MHz, 315 MHz and 433 MHz in fresh water with relative permittivity of 81 and conductivity of 0.05 S/m are presented for the boundaries of the reactive near and the field radiative near field depicted as R1 and R2 respectively and tabulated in Table 3.4. Hence the region that exists beyond R2 is far-field, it is these results that were used in the set up of the FEKO simulation software during the designing of the antennas.

Table 3.4: Field regions of half-wave dipole antenna in fresh water

Frequency (MHz)	R1 (m)	R2 (m)
40	0.3826	0.7665
100	0.07301	0.1666
315	0.02319	0.05284
433	0.01687	0.03848

3.6 Conclusion

In this chapter, theoretical analyses of propagations of radio waves in lossy media have been presented. These also include the effect of increasing water conductivity on the signals been propagated in the medium. Indeed, it has been shown through the Debye model, that EM propagation in a lossy medium beyond an operating frequency of 250 MHz will suffer greatly from attenuation. Other parameters that can also affect the propagation in either fresh or sea water were also discussed. This chapter set the boundary or limitation for designing and operating underwater antennas, taking into consideration the conductivity and the permittivity of the medium. Similarly, the radiation characteristics of the underwater antennas in either reactive near-field, radiative near-field and the far-field scenario were defined. Finally, the equation related to propagation in the far-field region was adapted for calculating the required distance in the dipole antenna in the underwater environments. Hence, similar calculations will be required for any antenna designed to operate in the medium and this will also depend on whether the medium is fresh or sea water.

Chapter 4

Design and Analyses of Narrow band Underwater Antennas

4.1 Introduction

This chapter can be summarily divided into two sections, while the first part focuses on full analyses of underwater antennas with respect to the type of materials, change in conductivity, the coating of the wires, as well as when the antennas are placed in an air-filled casing. The second part is about design, construction, and testing of some named narrowband antennas that can be deployed with an AUV for data harvesting and also guiding the AUV to a docking station for recharging through wireless power transfer. These antennas are accessed in terms of their achievable bandwidth and directivity when they are submerged in both fresh and sea water. It is worth noting that these are narrow band antennas with bandwidth not exceeding 40 MHz.

4.2 Simulation Software

There are many simulation software used for antenna design and analysis. The top five are; High-Frequency Structure Simulator (HFSS), FEKO (it is acronym of German words translated into English as "field calculations involving bodies of arbitrary shape"), Computer Simulation Technology (CST), Antenna Magus, and Integral Equation Three-Dimensional (IE3D). In our laboratory, we only use HFSS and FEKO software. These differ in modeling, operation and solution set-up.

4.2.1 HFSS

It is known as Ansoft HFSS, a 3D electromagnetic (EM) simulation software for designing and simulating high-frequency electronic products. The simulator uses only one solver known as Finite Element Method (FEM) [145].

4.2.2 FEKO

FEKO is a computational electromagnetics software product developed by Altair Engineering [146]. This software uses a hybrid of solvers which include:

1. Method of Moment (MoM)
2. Finite Element Method (FEM)
3. Finite Difference Time Domain (FDTD)
4. Multilevel Fast Multipole Method (MLFMM)
5. Adaptive Cross Approximation (ACA)
6. Domain Green's Function Method (DGFM)

It is observed that HFSS simulations take longer time than FEKO to complete, for an underwater antenna setup. Typical simulation times for a dipole antenna are 15 minutes and 48 hours, for HFSS and FEKO, respectively. This is attributed to the hybrid solvers used by FEKO software, the convergence time being absolutely shorter than that of HFSS and therefore preferable for the simulation done in this work.

4.3 Analyses of Underwater Antennas

Two important parameters that make designing of antennas for underwater application completely different from those designed to operate in the air are conductivity and permittivity. Thus, the relative permittivity is important in determining the dimension of the designed antenna based on the operating frequency. The relative dielectric constant in either fresh or sea water is 81, which also has a significant effect on the angle of refraction at the air/water interface. However, conductivity is important in determining the attenuation at the desired frequency, its value ranging from 0.005 S/m to 0.05 S/m in freshwater and is about 4 S/m for typical seawater to 8 S/m in hot and saline red sea [4, 5, 147]. The third element is magnetic permeability, which is known as the degree of

magnetization of a medium/material with respect to the magnetic field. However, since water is a non-magnetic medium the relative permeability is approximately equal to the value in free space, which is 1. This simply means there is no direct or known effect of the magnetic field on the EM propagation in lossy media [148]. The respective values of conductivity, permittivity and permeability in fresh and sea water at 25°C are presented in Table 4.1 [147].

Table 4.1: Typical values of the major water properties @ 25°C

Parameters	Freshwater	Seawater
Conductivity, σ (S/m)	0.05	4
Relative Permittivity, ε_r	81	81
Relative Permeability, μ_r	1	1

4.3.1 Brief Introduction of the Antennas

The antennas considered for the analyses are a dipole, folded dipole, loop, and J-pole antennas. The prototypes of these antennas are presented in Fig. 4.1. Here the dipole, folded dipole, and J-pole antenna are half wave antennas and the loop can either be small or large in configuration with radius, r. These are simple to design from either a crop of wires or tubing and can also be printed on a desirable substrate. A brief discussion about these antennas are presented as follows:

1. **Dipole antenna**
   A dipole antenna made is up of two identical conductive elements or rods, which is fed at the center by a balanced transmission line, with equal and oppositely flowing currents [15, 149]. It has been used in several applications for many decades because of the simplicity in its design, flexibility and very effective for a wide range of communication needs, including underwater applications [147]. Dipole antennas also come in several types and shapes, which include short dipole, half-wave dipole, folded dipole, bow-tie, V-shaped and other configurations [13]. The input impedance of the dipole in free space is around 73 Ω, but it is about 19 Ω in fresh water, which is due to the high permittivity of the medium, therefore the antenna requires matching elements.

2. **Folded dipole antenna**
   A folded dipole antenna can be referred to as a basic dipole antenna with the two ends connected together and folded back thereby resembling a loop antenna. The characteristic input impedance of the folded dipole antenna in free space is about

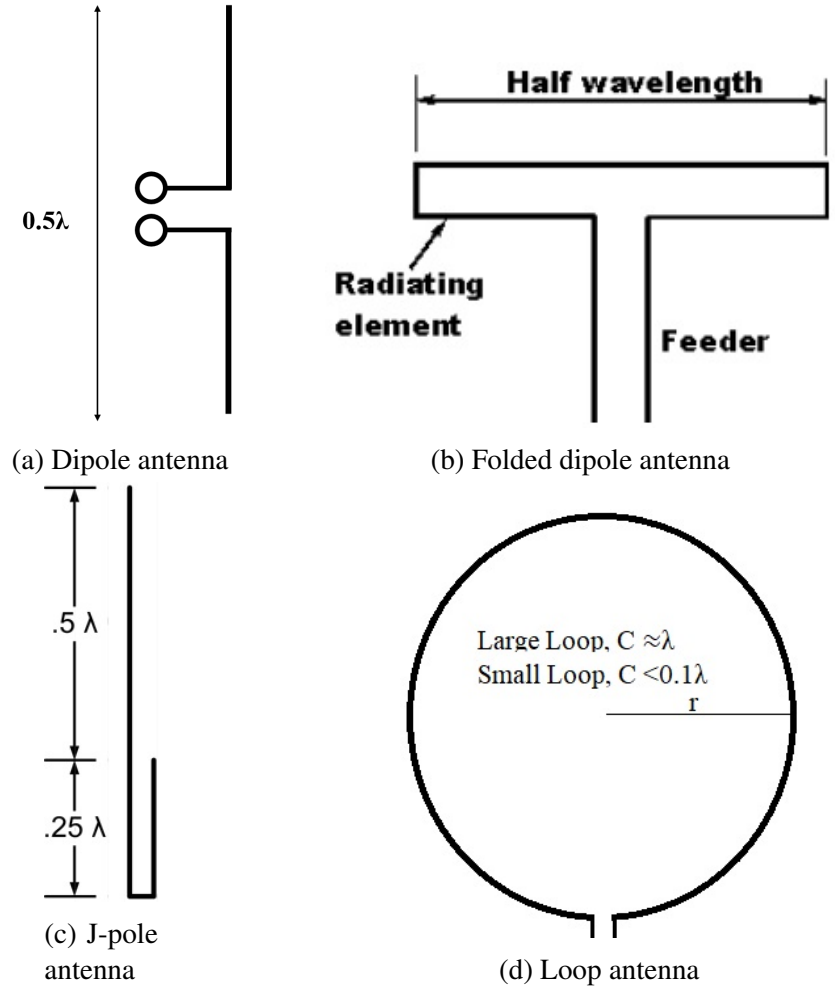

(a) Dipole antenna (b) Folded dipole antenna

(c) J-pole antenna (d) Loop antenna

Figure 4.1: Antenna geometry

300 Ω, which make this antenna to have input impedance around 50 Ω in freshwater thereby it does not require matching circuits. Another important attribute of the folded dipole is the possibility of varying the diameter of one of the two conductors, with which different impedance ratios of up to standard 4:1 can be implemented. Also, the currents in the two arms of the antenna reinforce one another instead of canceling out due to the folded nature of the antenna [13].

3. **Loop antenna**

The Loop antenna has drawn a lot of attention from radio frequency (RF) engineers across the globe; due to its simplicity in design, ease of fabrication, versatility, low cost, as well as ease of integration to other electronic components and devices [13]. This antenna is usually classified as an electrically small or large loop. When the circumference of the loop is less than the one-tenth wavelength ($C < \frac{\lambda}{10}$), such antenna is known as a small loop, on the other hand, when the circumference is

about one wavelength ($C \approx \lambda$), the antenna is known as a large loop. Indeed various shapes like a rectangular, triangular, circular, ellipse and other configurations have been designed but circular loop is believed to be more popular and more work has been done on this than any other shapes because of the simplicity in analysis and construction [13].

4. **J-pole antenna**
   This antenna comprises a half-wave vertical element end-fed by a quarter-wave matching stub, which makes the antenna in its entirety to resemble a letter J. Hans Beggerow in 1909 filed a patent for the invention of this antenna, which was then used in Zeppelin airships [150]. This antenna can exhibit high or low input impedance depending on the location of the port, hence, by sliding the port along the half-wave element the antenna can be matched to the feed-line.

4.3.2 Designing Antenna Models

The models of these antennas, as designed in FEKO simulation software, are shown in Fig. 4.2. For the loop antenna, the perimeter of the loop is approximately one wavelength (that is a large loop), where the wavelength has been expressed in equation 3.45 of the preceding chapter. Given that the phase constant (β) varies with the square root of the electrical permitivity for $\sigma/(\omega \times \varepsilon) \ll 1$, this means the antenna size is reduced proportionally that is by a factor of 9, with respect to its size in air. Yet from equation 3.44, it can be seen that both the permittivity of the water ($\varepsilon_r = 81$) and its conductivity will determine the final dimensions of the antennas. In this regards, the medium is fresh water and therefore the conductivity is 0.05 S/m. The antennas are designed for an operating frequency of 40 MHz. Thus, for such antennas to operate in fresh and sea water, different configurations of the antennas are required for each medium due to the different conductivities in order to achieve the desired operating frequency. The physical dimensions of the dipole, folded dipole, and J-pole antennas were calculated in a similar way. The dimensions of the antennas for fresh and sea water is given in Table 4.2. The thickness of the wires used in the design of the antennas is 3 mm, the wires are covered with insulating material with a thickness of 50 μm and relative permittivity of 3.

Thus, in the analyses of these antennas, it is important to determine various parameters that can affect their performance in any medium. Hence, several analyses were performed to determine the influence of material type (Perfect Electric Conductor (PEC), Copper, Brass, and Aluminum), wire size, change in a dielectric on wire (coating) and conductivity on the performance of underwater antennas. These were performed to ensure that the

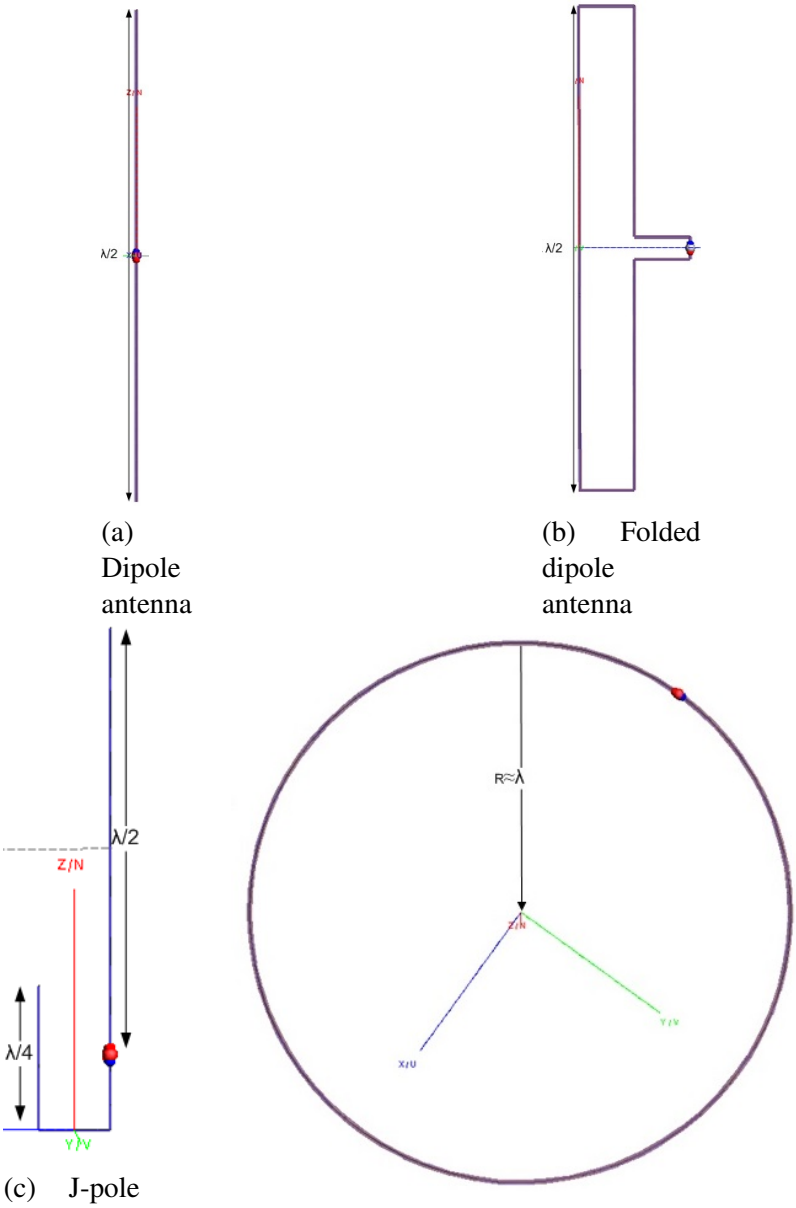

(a) Dipole antenna

(b) Folded dipole antenna

(c) J-pole antenna

(d) Loop antenna

Figure 4.2: Feko model of the antennas

antennas were designed for best performance and if and where needed, taking into account possible trade-offs of the antenna characteristics with respect to the different parameters.

4.3.2.1 Change in material type of the conductor

Efforts were made to determine the effect of changing the material used in the antenna design on its resonance frequency and input impedance in the underwater environment. Based on this, dipole and J-pole antennas were designed for an operating frequency of 40 MHz and analyzed accordingly. After several analyses, which include simulating of these

antennas in a freshwater scenario, while changing the materials, it is observed that change of the material of the conductor has no noticeable effect on the resonance frequency, bandwidths and the input impedance of the antennas as shown in Fig. 4.3. The results of the two antennas with different materials overlapped, which confirmed that irrespective of the material available, one can expect to achieve the same results with the desired material. The materials used in the simulations include aluminum, brass, copper, iron, and PEC. These analyses are important in that they allow us to conclude that the material selection is not that relevant, as long as it is a good conductor.

4.3.2.2 Change in medium conductivity

When there is a change in the propagating environment of an antenna it is expected that antenna parameters will also be altered. Thus, water as a propagation media has different conductivities starting with distilled water that is believed to have no dissolved salts with 0 S/m conductivity to highly saline water of about 5 S/m. Hence, the effect of a change in the propagating medium is verified in this section.

1. **Resonance Frequency:** It is also seen from the graph of the resonance frequency as a function of water conductivity, that changes in the conductivity of the medium brings about change in the resonance frequency of the designed antenna as presented in Fig. 4.4. This simply implies that it will be impossible to use the same antenna at two different medium and expect the resonating frequency to remain the same. The four antennas show similar responses as the water conductivity increases.

2. **Input Impedance:** The graph presented in Fig. 4.5 shows that the real and the imaginary parts of the input impedance of the antennas. The values for the real part starts at low value but rises sharply to an optimum value before dropping again as the conductivity increases. This optimum value occurs at 0.05 S/m for J-pole

Table 4.2: Dimension of the antennas

S /No.	Parameters	Fresh Water (σ=0.05 S/m)	sea Water (σ=4 S/m)
1	Radius of Loop Antenna (mm)	155.75	74.55
2	Dipole Antenna Arms (mm)	217.00	115.50
3	Short Arm of J-pole Antenna (mm)	161.13	42.50
4	Long Arm of J-pole Antenna (mm)	402.26	121.80
5	Base of J-pole Antenna (mm)	80.00	80.00
6	Width of folded dipole (mm)	20.00	20.00

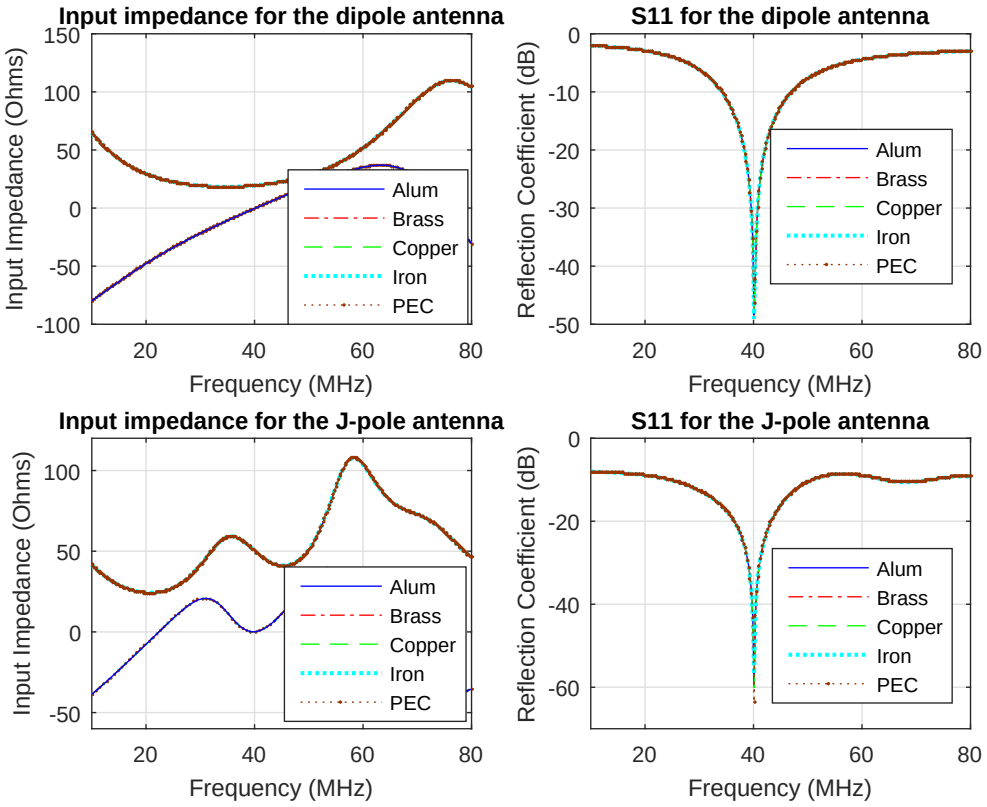

Figure 4.3: Simulations results for change in antenna materials

antenna, while that of other antennas occur at 0.2 S/m. The imaginary parts show a similar trend but as the conductivity increases, the values for the folded dipole antenna shows a capacitive characteristic whereas that of dipole shows inductive characteristics. This graph also indicates that the folded dipole and J-pole antennas may not require matching circuit when propagating in fresh water as their respective real part of input impedance is around 50 Ω when the conductivity is 0.05 S/m and the imaginary part is close to zero. But when these two antennas in addition to the dipole and loop are operating in the seawater, which is a medium with greater conductivity than that freshwater, different matching networks will be required. The sharp transition noticed may be due to change in the medium from dielectric to conducting and the reason for the J-pole antenna having its optimum value at a conductivity of 0.05 S/m, that is different from other antennas, is because the port is located such that the antenna resonates at the desired frequency.

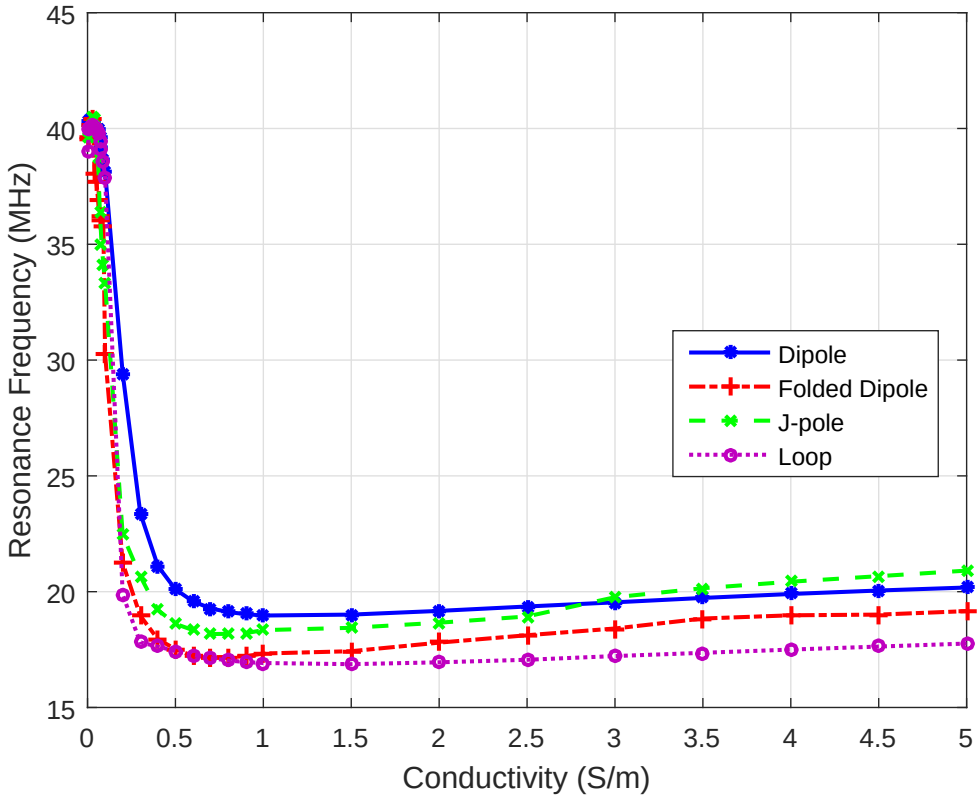

Figure 4.4: Resonance frequency as a function of conductivity

4.3.2.3 Coating Thickness

In this part, the effect of insulating thickness on the performance of the antennas in terms of the operating frequency and input impedance was verified. The need for this verification is to determine if coating materials have an impact on the operating frequency of an antenna vis-a-vis the input impedance. The dielectric material is important to ensure that the antenna is protected from direct contact with water, which can affect the results and alter the input impedance and the resonating frequency. In this analysis, dipole and loop antennas were used to verify the influence of the coating material on antenna performance. Thus, Fig. 4.6 and Fig. 4.7 show the dependence of the resonating frequency and input impedance on the coating or dielectric material (polyurethane, ε_r =2), respectively. It is seen from the plots that as the coating becomes thicker, the resonant frequency increase marginally. The increase is referred to as marginal because only a 6 MHz increase is noticed when the coating thickness change from 0.01 to 0.1. On the other hand, the input impedance decreases also marginally as the coating thickness increases. When the thickness is 0.05 mm, the input impedance is 19.4 Ω and 34.9 Ω for the dipole and loop antennas, respectively.

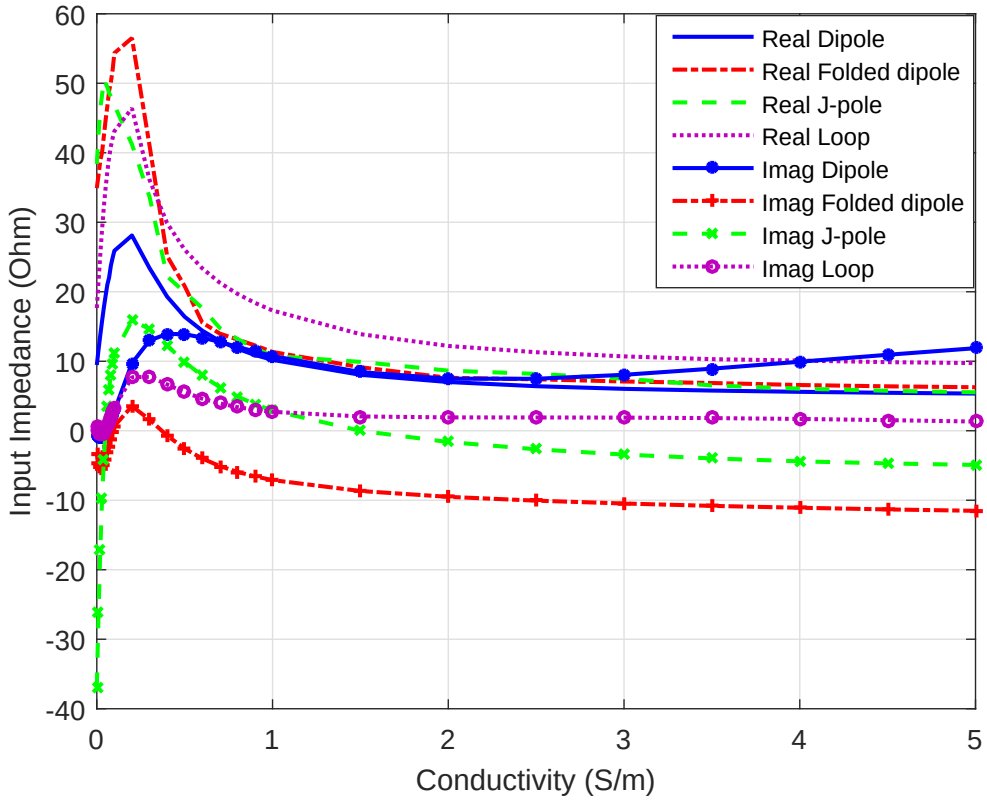

Figure 4.5: Input impedance as a function of conductivity

4.3.2.4 Antenna inside Air-filled Case

Another important analysis that we considered is the effect of putting the antenna in an air-filled plastics or glass container as shown in Fig 4.8. Here, the radius of the loop antenna use for these analyses is 155.75 mm and radiates at 40 MHz, when the wire is only covered with the coating material and simulated in a freshwater scenario. Then this antenna is inserted into air-filled container with a inner and outer radius of 170 mm and 180 mm, respectively, while its height is varied accordingly starting with 10 mm to 100 mm in 10 iterations. Plastic and borosilicate glass were the two materials considered in this analysis. The plastic is of a material known as High-density polyethylene (HDPE), its relative permittivity is 2.26 and its loss tangent ranges from 0.0000400 to 0.00100. Similarly, the other material used is borosilicate glass, which is made from quartz with dielectric constant ranging between 4.3 and 5. In this analysis, a dielectric constant of 4.7 was considered. Thus, the effect of the change in the height, which invariably increase the air trapped inside the casing that contained the antenna on the performance of the antenna is considered.

The first plot in Fig. 4.9 shows that the resonating frequencies of the loop antenna

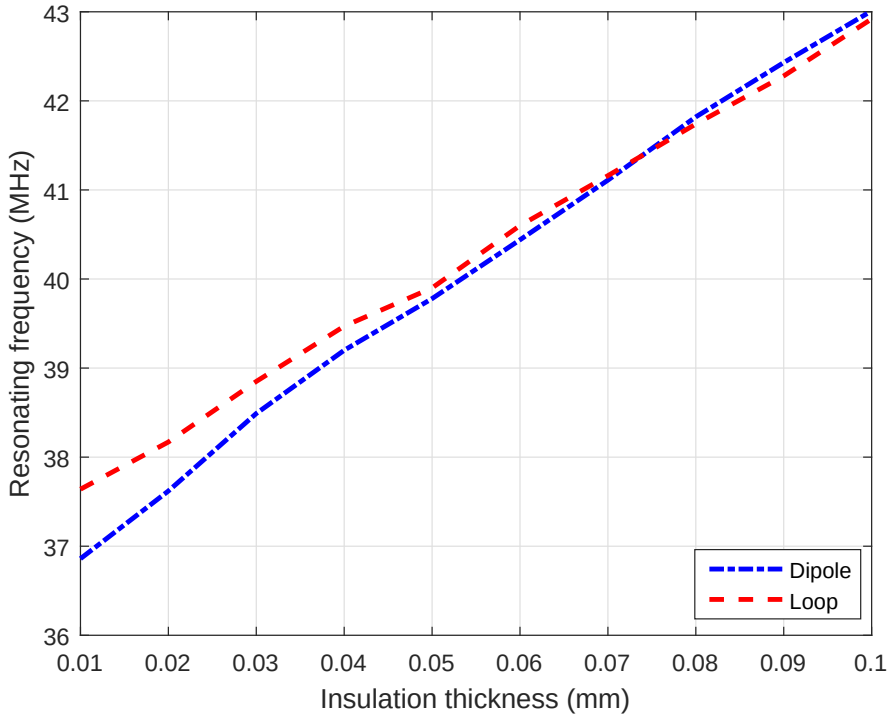

Figure 4.6: Resonance frequency as a function of coating thickness

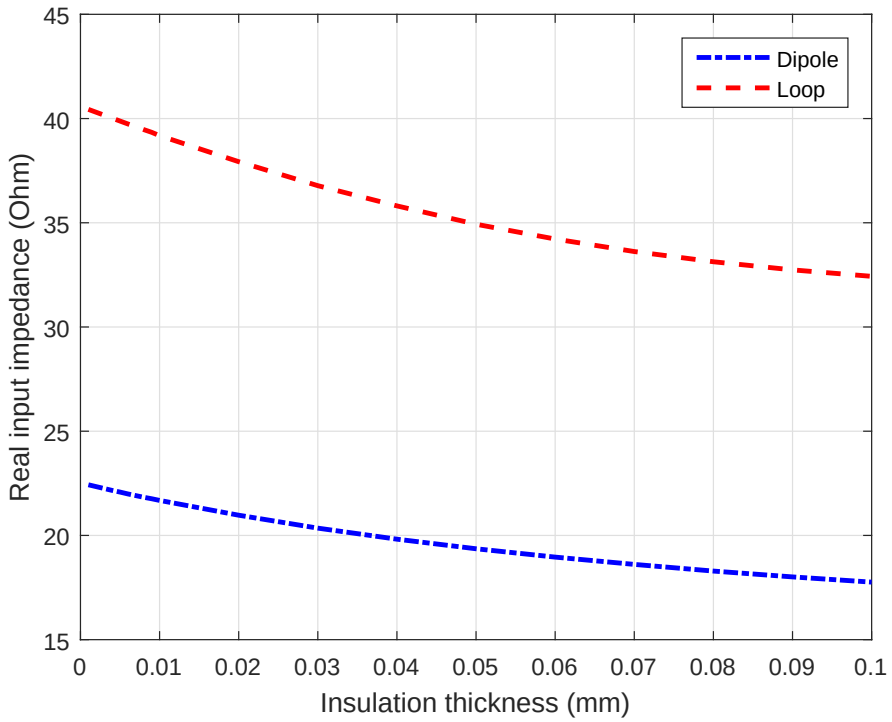

Figure 4.7: Real part input impedance as a function of coating thickness

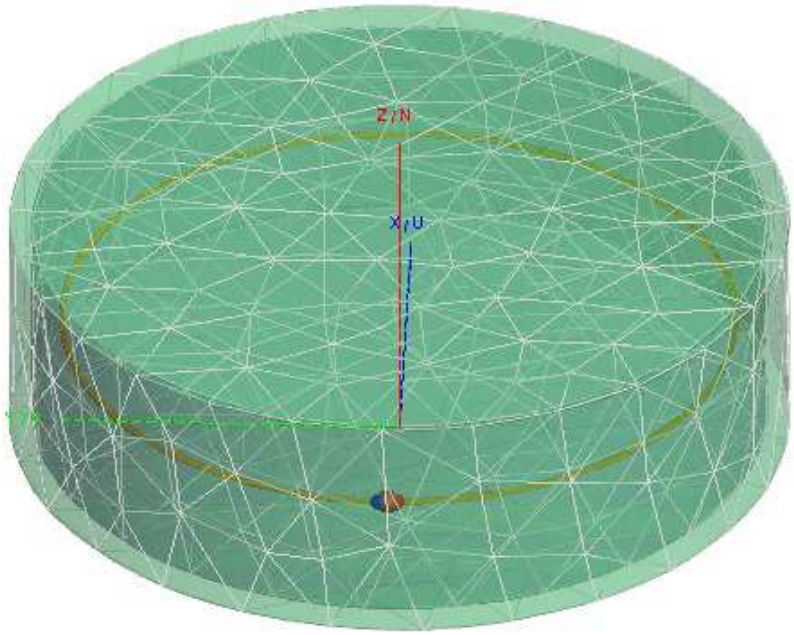

(a) Antenna inside air-filled casing

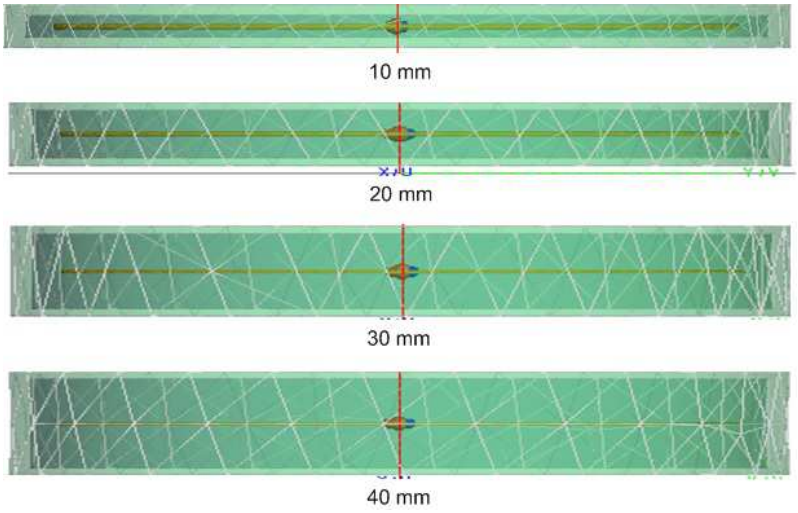

(b) Different sizes of air-filled casing with antenna

Figure 4.8: Antenna inside air-filled casing

in the two containers increases from about 250 MHz and 258 MHz for glass and plastics respectively until it reaches an optimum value after which the frequency remains unchanged with further increase in the container's height. This implies that the frequency when the antenna is inside the containers is about 6 times that of resonating frequency when the antenna is simulated in water with coating material only. In the second plot Fig. 4.9, the input impedances obtained when the antenna is simulated in both plastics and glass almost overlap on one another. It is also seen that the input impedance at the lowest height of the containers is closer to 200 Ω, which dropped below 100 Ω as the height of

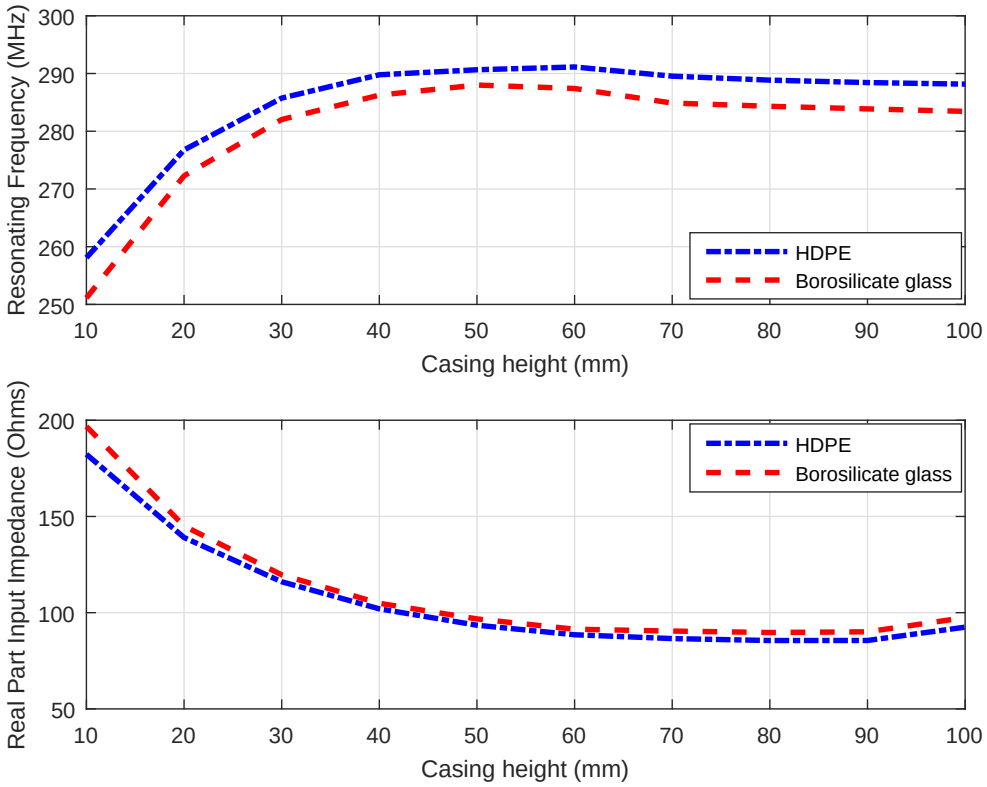

Figure 4.9: Resonating frequency and input impedance as a function of casing size

the containers increases. It can be concluded that despite the difference in the dielectric constant of the two materials, their performance is somewhat similar. Hence, when an antenna is designed and placed in an air-filled casing, the influence of the dielectric constant of the casing, make the results return high input impedance, which continue to reduce as the height of the casing increases, which allows more air to be trapped inside the container. On the other hand, as the air inside the container increases, the resonating frequency also increases, getting closer to resonating frequency of the antenna in air. It can therefore be concluded that, the medium (water) plays limited role, when an antenna is placed in an air-filled casing and lowered into it, as the resonating frequency and input impedance is closer to what is obtainable for the same antenna in air. In addition, the permittivity of the container will also affect the expected results.

4.4 Bandwidth and Directivity of Underwater Antennas

4.4.1 Performance Evaluation of the Dipole, Folded Dipole and Loop Antennas

Based on the analyses of these antennas, corresponding to the model presented in Fig. 4.2, three of the antennas namely; dipole, folded dipole, and loop antennas were simulated in fresh water (when $\sigma = 0.05\ S/m$) and sea water (when $\sigma = 4\ S/m$) scenarios. The thickness of the copper wire used is 3 mm and the coating thickness is 50 μm, J-pole, on the other hand, will later be simulated with other configurations of the antenna.

4.4.1.1 Simulation results: fresh water

At the design frequency of 40 MHz, the bandwidth, real part of input impedance and directivity characteristics obtained when the three antennas are immersed in fresh water are given in Table 4.3. Similarly, the reflection coefficient as a function of frequency for the antennas is presented in Fig. 4.10. The bandwidth is measured at -10 dB of the reflection coefficient, considering the antennas are matched to the source. Hence due to the input impedance of the dipole and loop antennas, matching circuits are required for these two antennas. A folded dipole antenna, on the other hand, has its input impedance close to 50 Ω, but at the same frequency, the imaginary part of the input impedance has a small magnitude of a capacitive reactance which is 3.49 Ω. Despite this, the antenna still has slightly higher bandwidth than other two antennas, while the loop, folded dipole and the dipole antennas have decreasing directivity in that order.

In addition, the 3d radiation pattern for the three antennas, as well as their 2d patterns in E and H planes are presented in Fig. 4.11 and 4.12 respectively. Here it is seen clearly that the dipole antenna has omnidirectional characteristics, meaning the radiated power is evenly distributed in all directions. Folded dipole, on the other hand, has a pattern that is slightly tilted to the direction of the port, though in 2d it shapes resemble that of a dipole antenna. On its part, the loop antenna has a bi-directional radiation pattern. It is important to add that radiation pattern of antennas submerged in fresh water is similar to

Table 4.3: Simulation results of the antennas in fresh Water

S /No.	Parameters	Dipole	Folded Dipole	Loop
1	Bandwidth (MHz)	12.84	22.12	15.76
2	Directivity (dBi)	2.22	2.61	3.80
3	Real part of Impedance (Ohm)	19.40	53.40	34.90

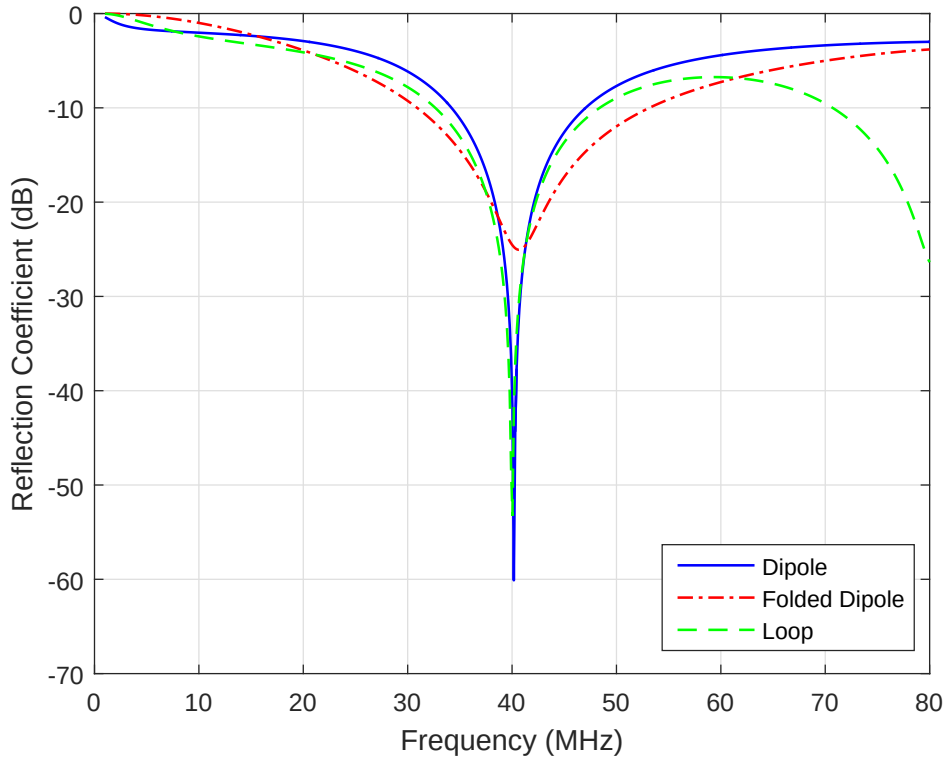

Figure 4.10: Reflection coefficient as a function frequency for the three antennas in fresh water

what is obtained when the same antenna is simulated in free space, this is due to the low conductivity of the medium.

4.4.1.2 Simulation results: sea water

Again the antennas were designed with the parameters defined in Table I associated with the sea water and the results obtained are tabulated in Table 4.4. The results obtained for the reflection coefficient as a function of frequency are presented in Fig. 4.13, while their respective 3D radiation pattern are shown in Fig. 4.14 In this medium, the loop antenna exhibits a higher bandwidth and directivity than other two antennas. In addition, the maximum directivity of the folded dipole antenna is towards the direction of the port only, whereas the loop and dipole antennas show a maximum in the opposite directions. An important result here is that the radiation pattern of the antennas changes significantly with conductivity. When going from fresh to sea water, the maximum directivity direction of the loop antenna changed 90°. Moreover, the dipole antenna which in fresh water exhibited an omnidirectional radiation pattern, now it became bi-directional. Therefore, the three antennas exhibit noticeable transition in their respective radiation pattern, when

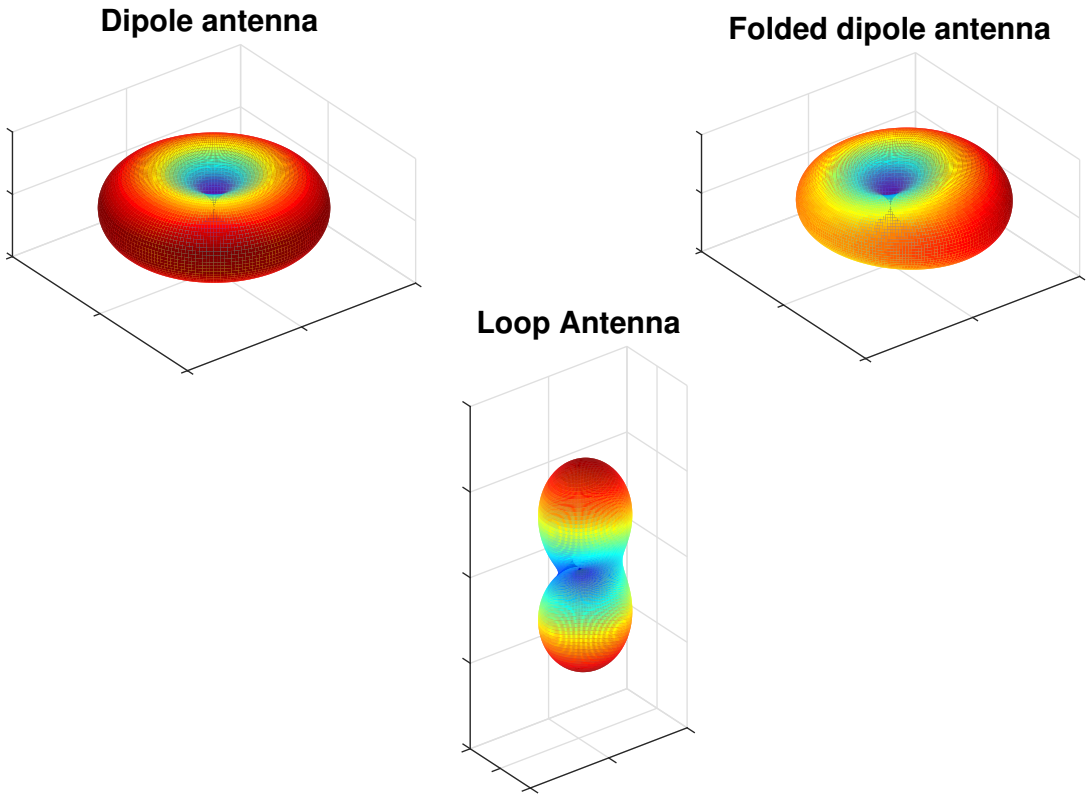

Figure 4.11: 3D radiation pattern of the antennas in fresh water

compared with the results obtained in fresh water. These changes is the effect of the different conductivity in fresh water and sea water. In addition it is also understood from Chapter 3 that sea water behaves as conductor at the operating frequency of the antennas, whereas fresh water operates as an insulator. Hence, it can be concluded that it is important to take into consideration the conductivity of the medium in the design of the antennas, because the major radiation parameters may change significantly with change in the conductivity. Thus, knowledge of the antenna characteristics in air or low conductivity mediums is not sufficient to design the antennas for operation in sea water.

Table 4.4: Simulation Results of the Antennas in sea Water

S /No.	Parameters	Dipole	Folded Dipole	Loop
1	Bandwidth (MHz)	11.89	22.12	13.94
2	Directivity (dBi)	2.22	2.61	3.80
3	Real part of Impedance (Ohm)	6.69	7.30	12.20

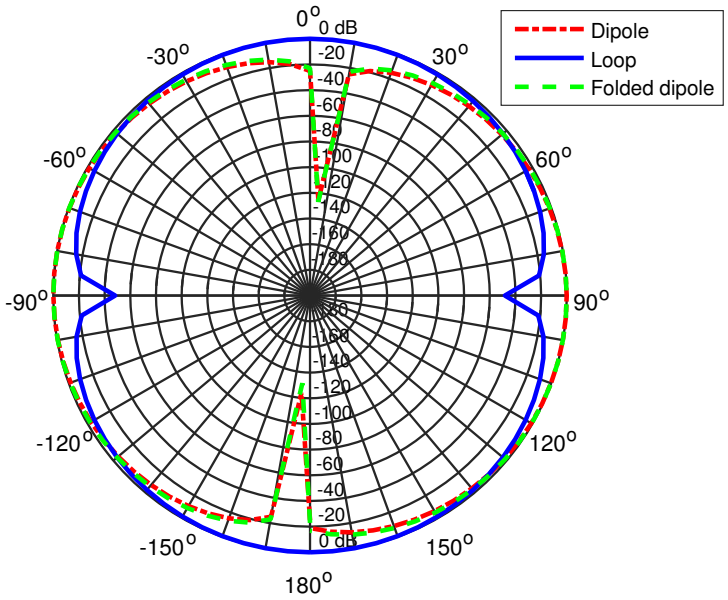

(a) E-plane

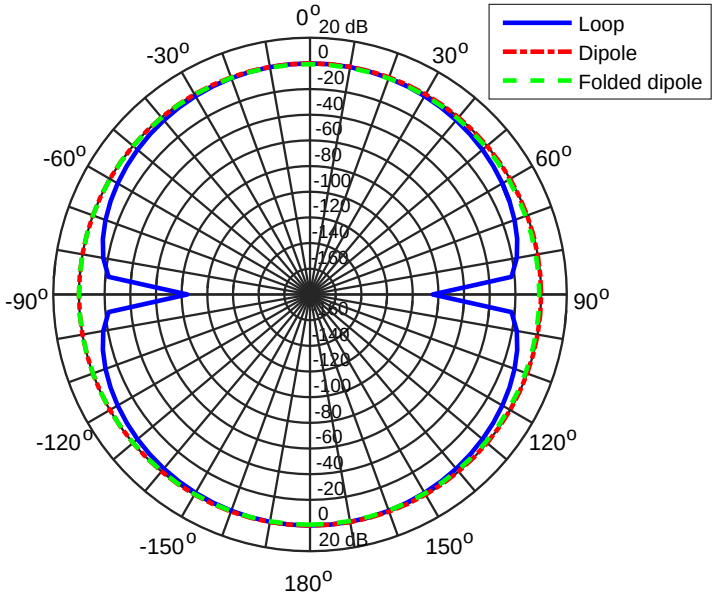

(b) H-plane

Figure 4.12: 2D radiation pattern for the three antennas

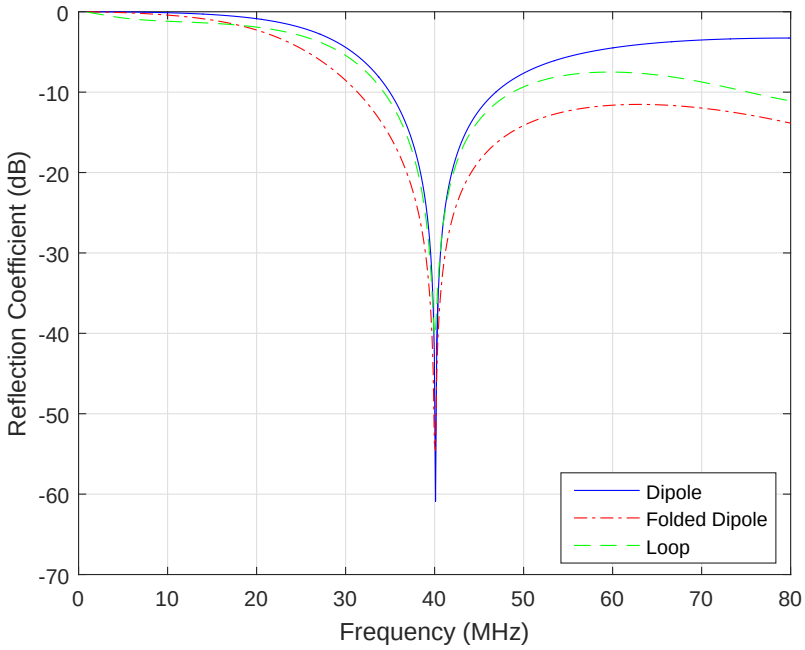

Figure 4.13: Reflection coefficient as a function frequency for the three antennas in sea water

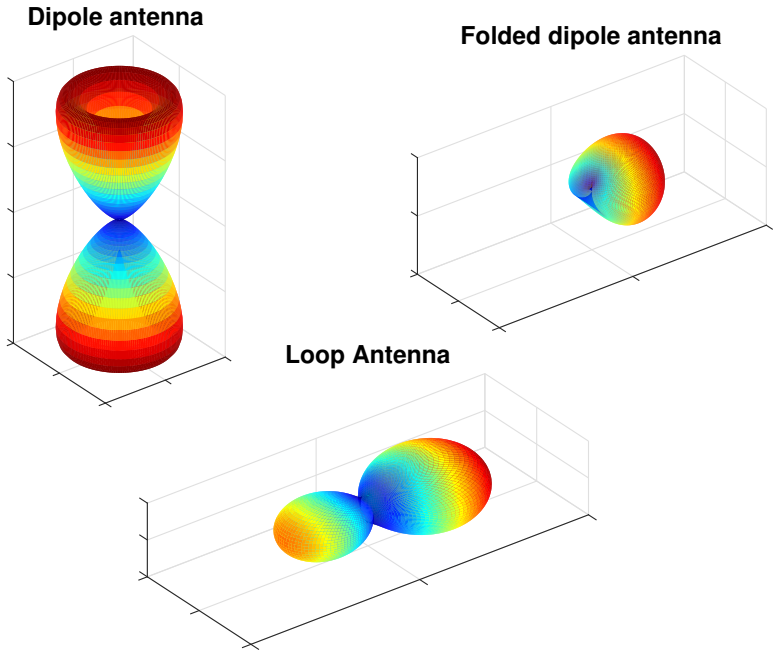

Figure 4.14: 3D radiation pattern of the antennas in sea water

4.4.2 J-pole Antenna Configurations

Apart from the J-pole antenna that has been presented in section III, other configurations of this antenna are super J-pole and collinear J-pole antennas which are depicted in Fig

4.15. One other configuration of J-pole antenna which is not considered in this work is Slim Jim antenna which, unlike the super J-pole and the collinear J-pole, does not have any performance advantage over the J-pole antenna or the other two variations [151].

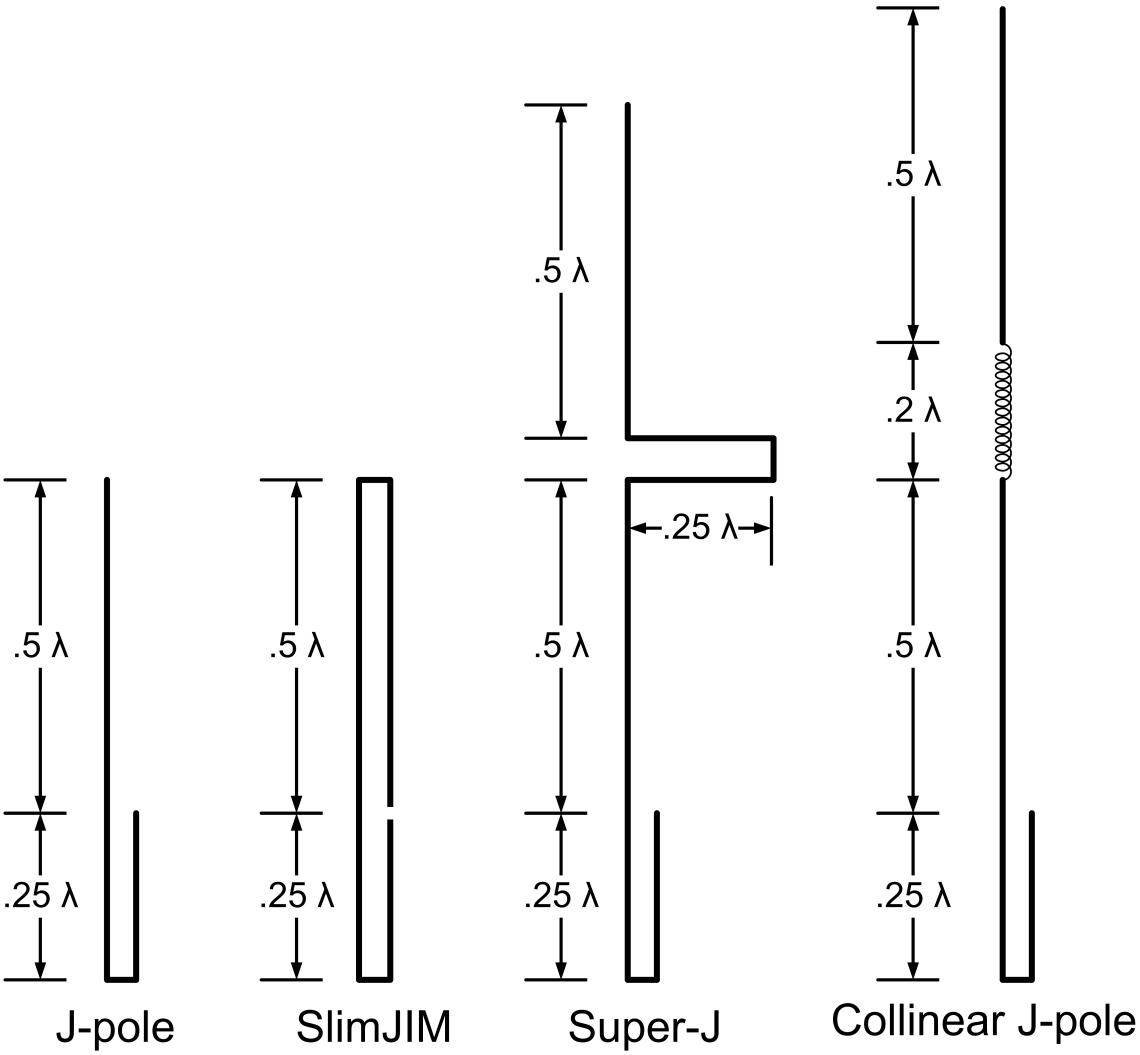

Figure 4.15: (a) J-pole (b) Super J-pole (c) Collinear J-pole antennas

1. **Super J-pole antenna** Super J-pole antenna is achieved by the addition of a phasing stub and half wavelength element to the long arm of an ordinary J-pole antenna.

2. **Collinear J-pole antenna** This is similar to the super J-pole antenna, only that the phasing stub is replaced by a phasing coil. The dimension of the phasing coil is calculated based on the analysis of helical antennas as specified in [152, 13]

4.4.2.1 Simulation Results and Interpretations in fresh water

These antennas were designed in FEKO software and its dimensions for usage in fresh water are given in Table 4.5; models are shown in Fig. 4.16. In the table, L1 is the sub-base of the antennas and this is the same for the three antennas; L2 is their respective quarter wavelength stub or simply short arm; L3 is their half wavelength element or long arm and L4 is the length of the phasing coil. In the super J-pole, the stub (stub base and quarter wavelength long) and half wavelength element added are of the same length, while in the collinear J-pole antenna, the phasing stub is replaced by a 0.2 λ phasing coil. Apart from the length of the coil, its radius is 9.69 mm.

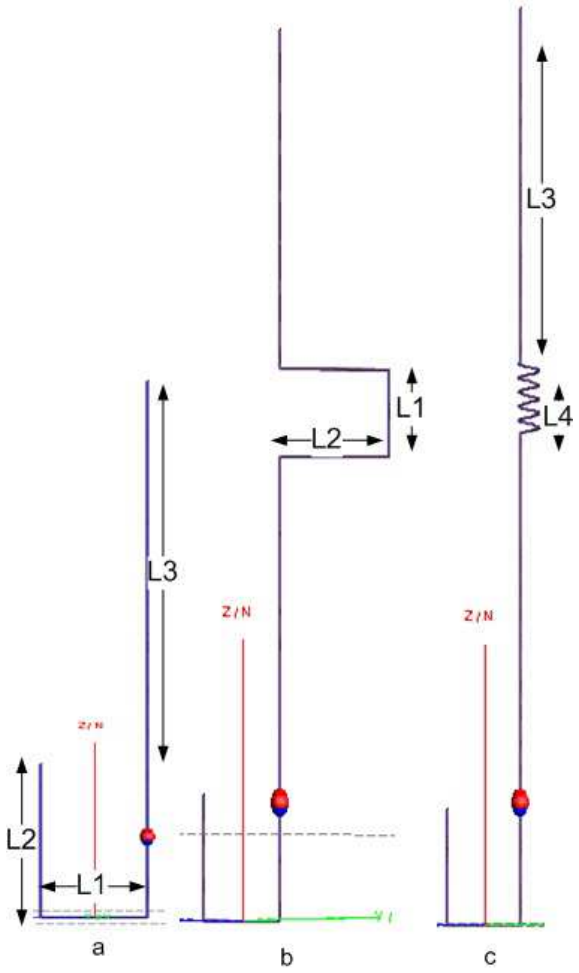

Figure 4.16: (a) J-pole (b) Super J-pole (c) Collinear J-pole antennas

The antennas are simulated with the ports represented in Fig. 4.16 by the dot located in along the long arm. Fig. 4.17 presents the results of the reflection coefficient when the input impedance of the antenna is matched to the source. Indeed, the ports were located on the antennas through parametric analysis, whereby the best position that favors the

Table 4.5: Dimension of the J-pole antenna configurations in freshwater

S /No.	Antennas	L1(mm)	L2(mm)	L3(mm)	L4(mm)
1	J-pole	80.00	161.13	402.26	-
2	Super J-pole	80.00	115.00	316.00	-
3	Collinear J-pole	80.00	135.00	350.00	70.00

bandwidth, directivity and the efficiency were taken into consideration. The super J-pole and the collinear J-pole antennas achieved a bandwidth above 40 MHz in the medium (freshwater). However, the J-pole antenna achieved better impedance matching than the other two antennas. The simulation results corresponding to the reflection coefficient as a function of frequency in this medium is presented in Fig. 4.17.

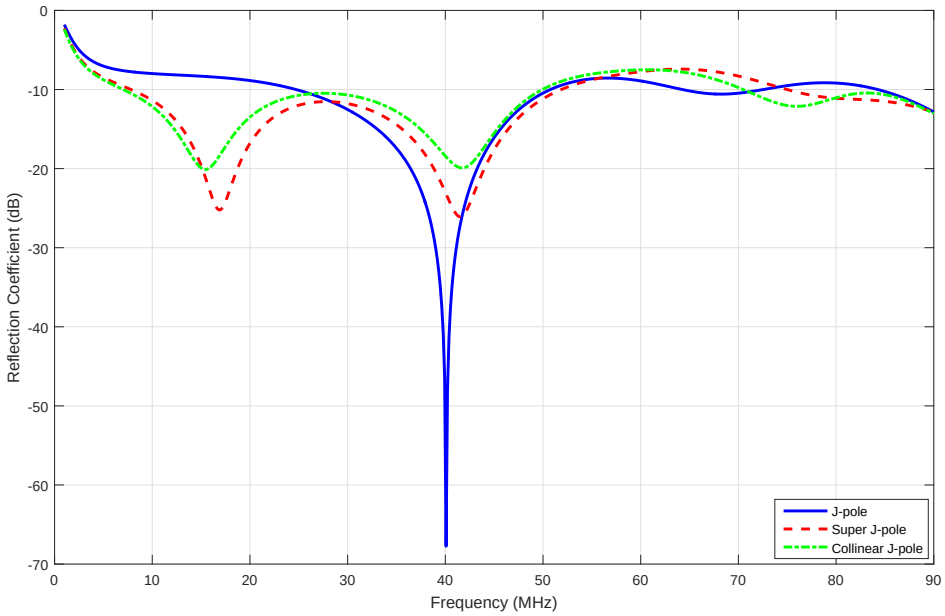

Figure 4.17: Reflection coefficient against frequency for the three antennas operating in freshwater

However, at the operating frequency, it was discovered that both the super J-pole and collinear J-pole antennas have inductive imaginary parts which can be canceled. Therefore, matching circuits were used to lower the reflection coefficient and therefore improve the radiation efficiency, albeit at the expense of reduced bandwidth. Based on this, capacitors are added to cancel the inductive load for the two antennas and their values are calculated as 0.57 nF and 0.29 nF for the super J-pole and collinear J-pole, respectively. Thus, the corresponding simulation results for the bandwidth (from the reflection coefficient measured at -10 dB) and directivity are given in Table 4.6.

In addition, modified simulation results when the capacitors have been used to lower the inductive imaginary part for the reflection coefficient as a function of frequency is presented in Fig. 4.18. It is seen in this figure that the three antennas achieved relatively the same bandwidth, with J-pole slightly higher than the other two antennas. In terms of directivity, the collinear J-pole and the super J-pole have higher directivity than the J-pole antenna. These are very encouraging results when considering the usage of these antennas mounting around bodies of AUVs, as the achievable bandwidth and directivity are higher than what is obtained for the loop and the dipole antennas in the previous section.

Table 4.6: Simulation results of the antennas in fresh water

S /No.	Parameters	J-pole	Super J-pole	Collinear J-pole
1	Bandwidth	25.82	24.96	23.56
2	Directivity (dBi)	4.65	7.13	8.02

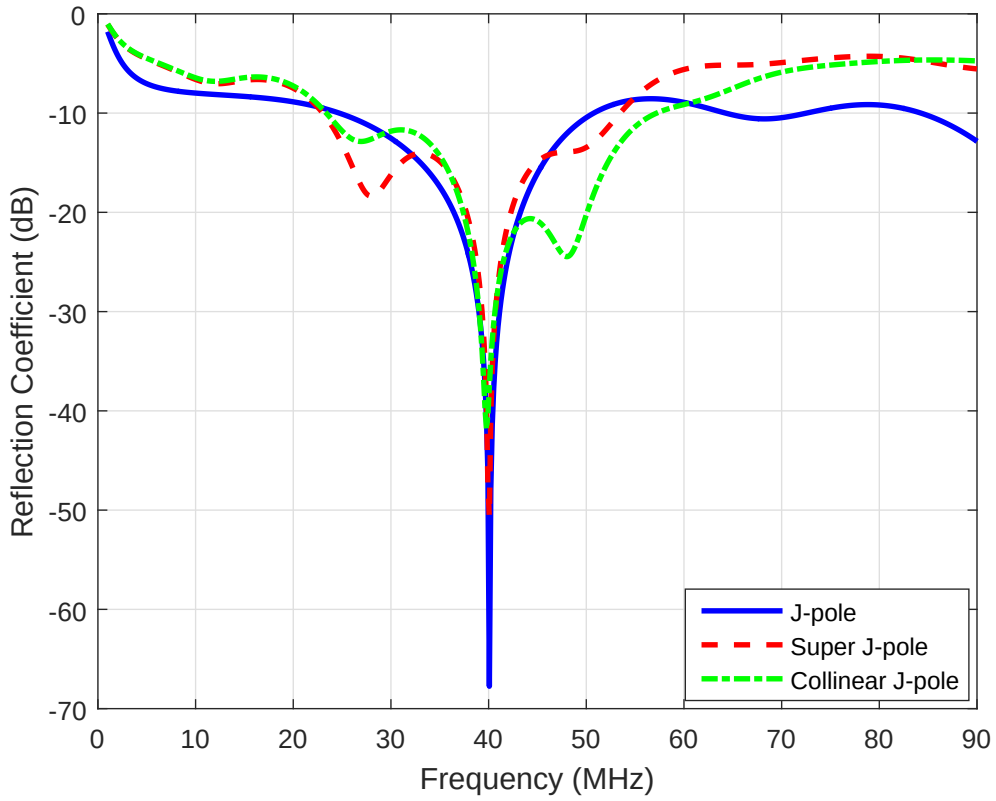

Figure 4.18: Modified Reflection coefficient against frequency for the antennas in fresh water

The circuits showing the addition of the capacitor as calculated, to cancel the inductive load are presented in Fig. 4.19a and 4.19b for the super J-pole and the collinear J-pole

antennas, respectively.

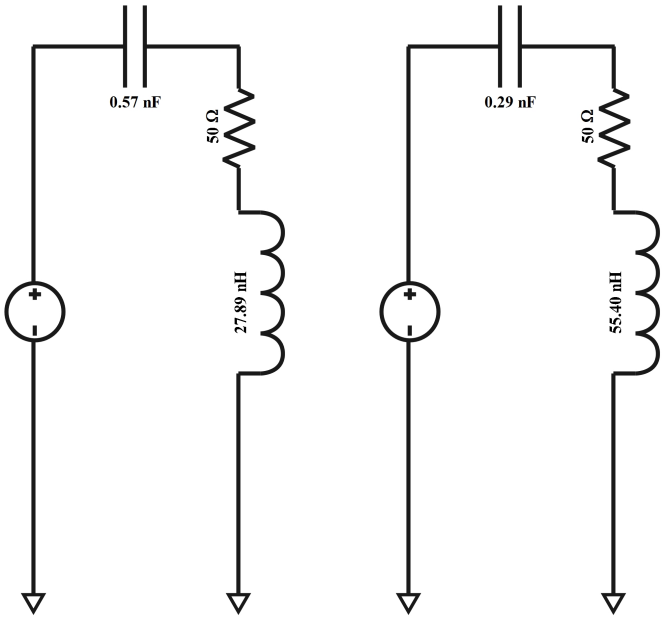

(a) Circuit for Super J-pole

(b) Circuit for Collinear J-pole

Figure 4.19: Circuits showing capacitors added to cancel inductive load for the antennas

4.4.2.2 Simulation results and interpretations in seawater

In this medium the conductivity plays an important role in determining the dimensions of the antennas. The calculated wavelength at the same operating frequency of 40 MHz is about one-quarter when compared with the one calculated in fresh water, taking a value of 244.44 mm. The dimensions of the antennas are as presented in Table 4.7. Simulation results corresponding to the bandwidth, input impedance and directivity characteristics of the antennas in this medium are presented in Table 4.8. Similarly, the results of the reflection coefficient is shown in Fig. 4.20. The input impedance of the antennas is very low in this medium due to change in the conductivity, and unlike fresh water, changing the ports locations for the antennas or sliding along the long arm does not improve the impedance in this medium. After several analysis of the antennas, the ports were located at 5% distance along the long arms of the three antennas. With their respective input impedances, it simply means that matching circuits are important for the three antennas. To this purpose, Advance Simulation System (ADS) software was used to design matching circuits and to calculate the corresponding lumped elements, which were optimized for maximum performance. The matching circuit of the J-pole antenna is presented in Fig. 4.21 and similar circuits were designed for the super J-pole and the

collinear J-pole antennas. The three antennas therefore exhibits a bandwidth that is closer to 30 MHz in this medium. This is an important results considering that often underwater applications are carried out in salt water than fresh water. The radiation pattern of the antennas in sea water is shown in Fig. 4.22. The super J-pole antenna has the highest maximum directivity in this medium, followed by the collinear J-pole and then the J-pole antenna in that order. It is seen that due to the conductivity the antennas become more directive than when operating in fresh water.

Table 4.7: Dimension of the J-pole antenna configurations in seawater

S /No.	Antennas	L1(mm)	L2(mm)	L3(mm)	L4(mm)
1	J-pole	80.00	73.00	290.00	-
2	Super J-pole	80.00	45.00	170.00	-
3	Collinear J-pole	80.00	44.80	223.20	34.00

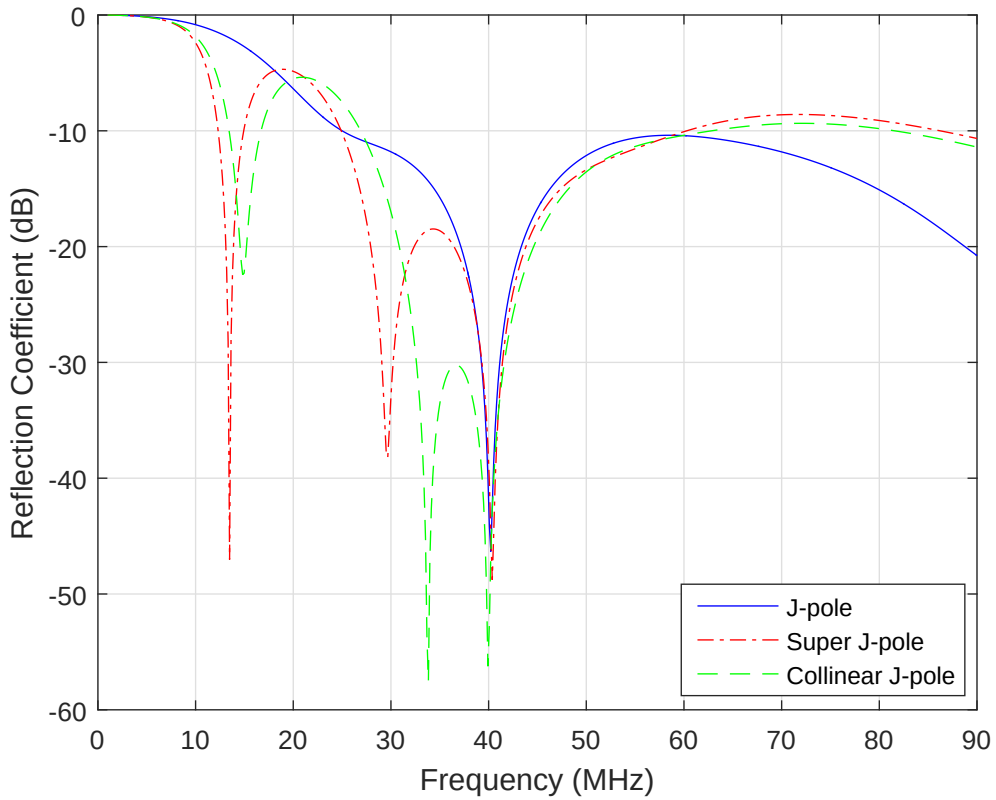

Figure 4.20: Reflection coefficient for the J-pole antenna configurations in seawater

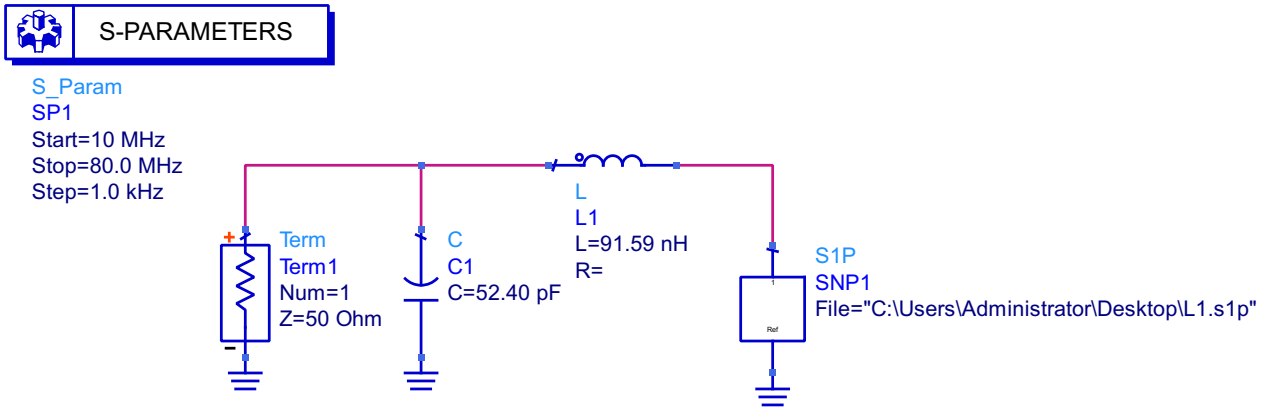

Figure 4.21: Matching circuit for the antennas in sea water

Table 4.8: Simulation results of the J-pole antenna configurations in Sea Water

S /No.	Parameters	J-pole	Super J-pole	Collinear
1	Bandwidth	27.92	35.32	28.45
2	Directivity (dBi)	14.05	25.81	19.52
3	Impedance (Ohm)	6.36	13.70	14.50

4.4.2.3 Experimental results in fresh water

Since the results of the super J-pole and the collinear J-pole antennas are similar, further analysis of the J-pole and super J-pole antennas were only considered. Their respective dimensions as presented in Table 4.5 were used in the fabrication of the antennas. However, the antennas were not tested with matching circuits, only with 1:1 current balun. The balun were added to ensure that the antenna characteristics remains stable in the medium. Also, their characteristics and performances were assessed through

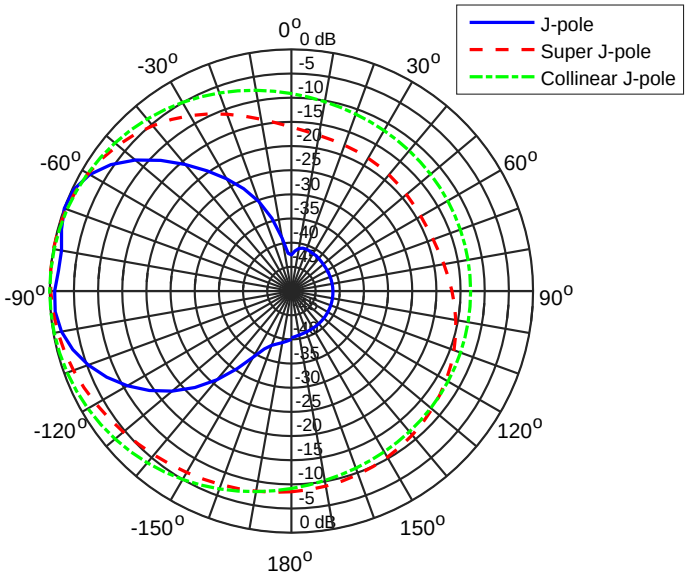

(a) E-plane

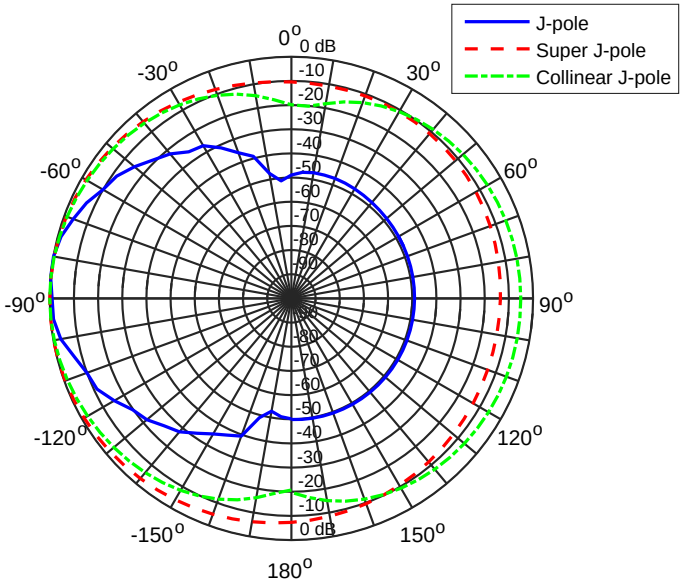

(b) H-plane

Figure 4.22: Radiation pattern of the antennas in sea water

measurements of the reflection coefficient and the radiation pattern in the E-plane and H-plane respectively. Pictures of the fabricated antennas and during their measurements in the pool are given in Fig. 4.24 and Fig. 4.25 respectively. The measurements of their

transmission coefficient (S_{21}) were painstakingly performed manually as there are no equipment similar to those used in anechoic chamber in the pool. In this regard, the reference antenna and the antenna to be measured are fixed to different plastic pipes to ensure stability and are lowered to the same depth in the water. These antennas are separated by a distance of 2 m, and are through their respective cables of 7 m long, are connected to the vector network analyzer (VNA). It is important to note that the far-field conditions for measuring S_{21} in water at 40 MHz requires antenna separation of about 0.8 m (this was determined theoretically and through simulation). Then, the antenna to be measured is rotated from 0° to 360° at a regular interval of 5°, with respect to the plane that is been considered. This is made possible with the help of a Protractor shown in Fig. 4.23 and a wire used as pointer to indicate each 5° changes. Hence, the measured and the simulated results for the two antennas in terms of the reflection coefficient as a function of frequency are presented in Fig. 4.26 and Fig. 4.27 for the J-pole and the super J-pole antenna respectively. It is seen that there is a good agreement between the simulations and measured results for the two antennas in the medium. Similarly, their respective radiation pattern in E and H-plane are presented in Fig. 4.28 and Fig. 4.29 respectively. These also confirmed that there is good agreement between numerical simulation and the measured results. Due to this, we can further conclude that these antennas exhibit improved performance when compared with those discussed in the previous section (loop and dipole antennas), in terms of both bandwidth and directivity.

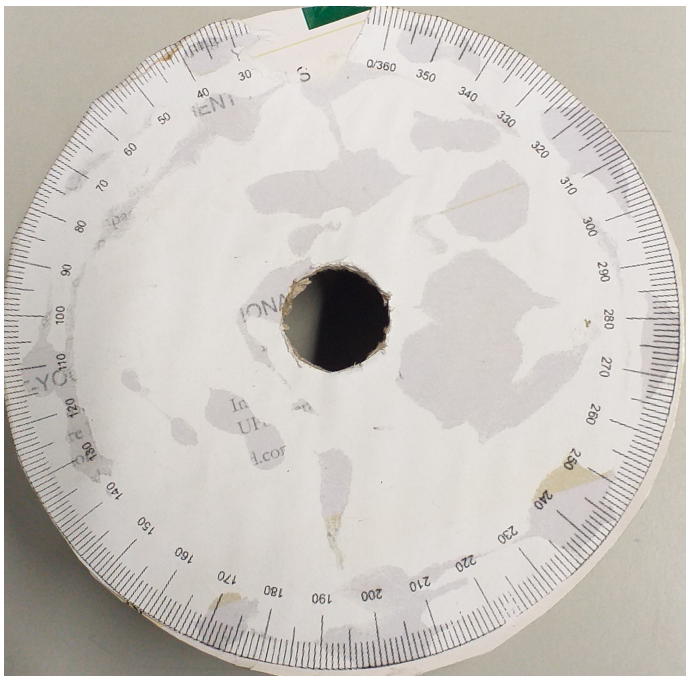

Figure 4.23: Protractor used in measurement of radiation pattern in freshwater

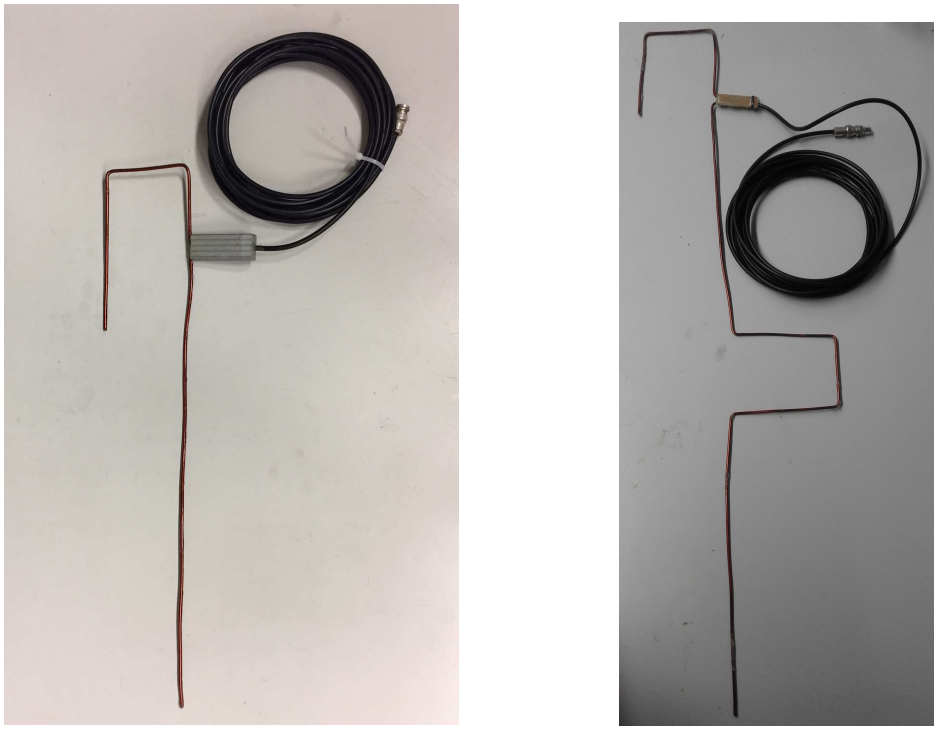

(a) [J-pole antenna (b) Super J-pole antenna

Figure 4.24: Fabricated J-pole and super J-pole antennas

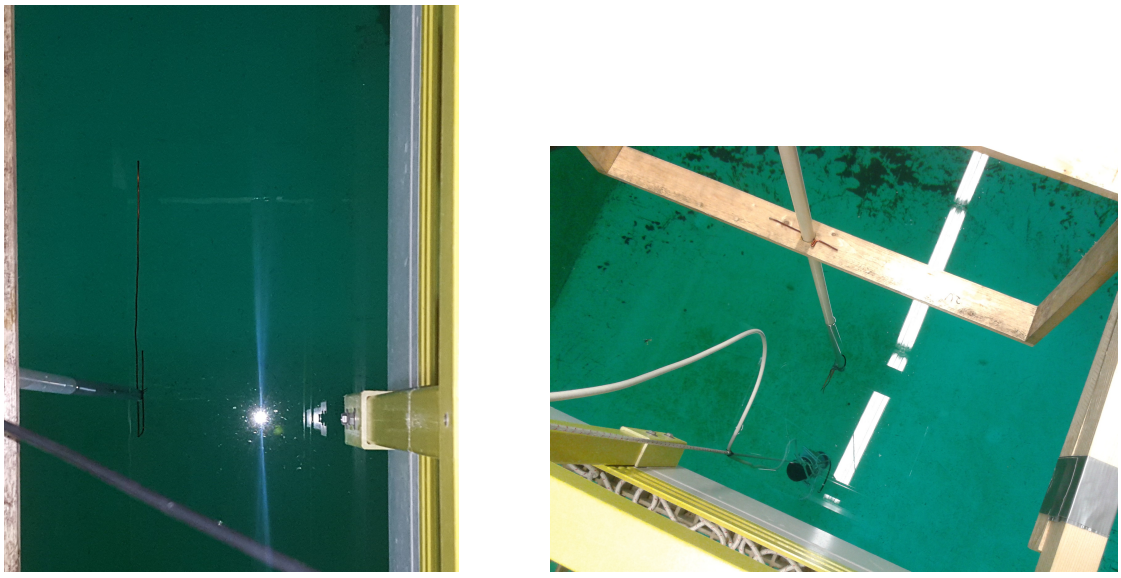

(a) J-pole antenna (b) Super J-pole antenna

Figure 4.25: Measurement setup showing the antennas inside the pool

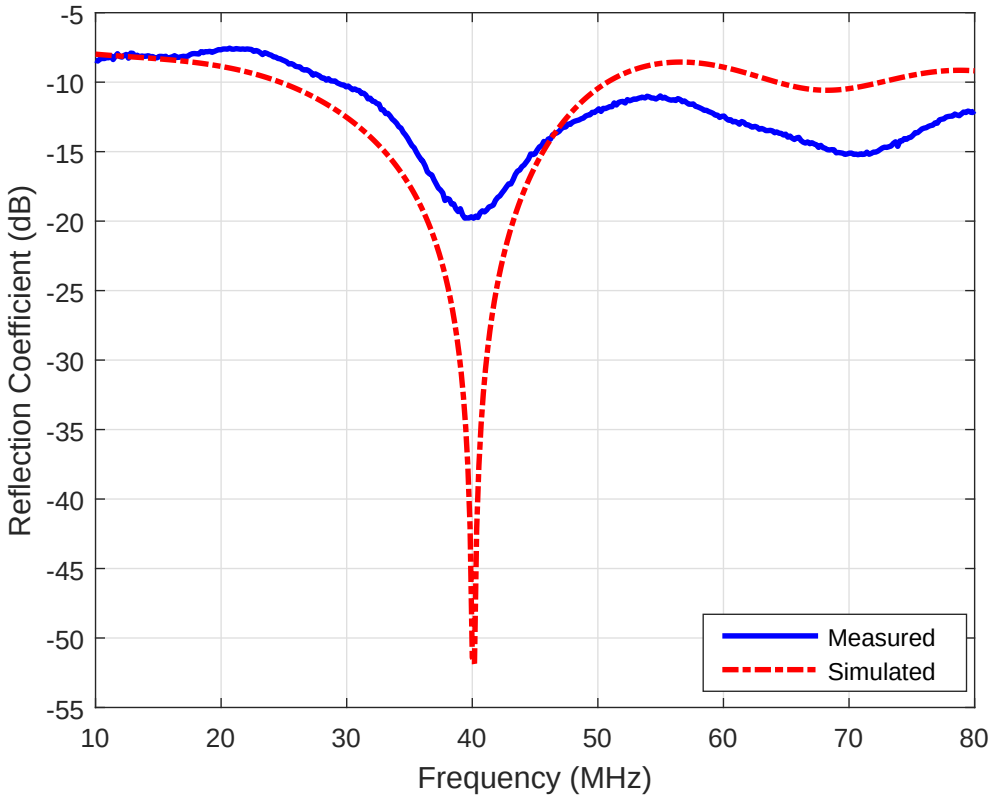

Figure 4.26: Reflection coefficient for the J-pole antenna

4.5 Modified Antennas for Installation on the Body of an AUV

Apart from the dipole, which does not need any modification and loop antenna which has a structure that cannot be modified to fit the required dimension, other antennas discussed in this chapter were remodeled such that they will be fitted around the body of an AUV. The AUV considered here is the one designed by the robotic unit of INESCTEC (Institute for Systems and Computer Engineering, Technology and Science) in conjunction with the Faculty of Engineering of the University of Porto (FEUP). The prototype of the designed AUV known as MARES (Modular Autonomous Robot for Sampling Environment), is presented in Fig. 4.30.

It is an autonomous underwater vehicle that has the capability of making 100 meters descending in water and similarly follow pre-defined trajectories and harvesting data through the onboard sensors. The characteristics of MARES as presented in [153] is given in Table 4.9. These characteristics are similar to ISURUS, which was an earlier design by the University of Porto in conjunction with her partners in the early 2000s

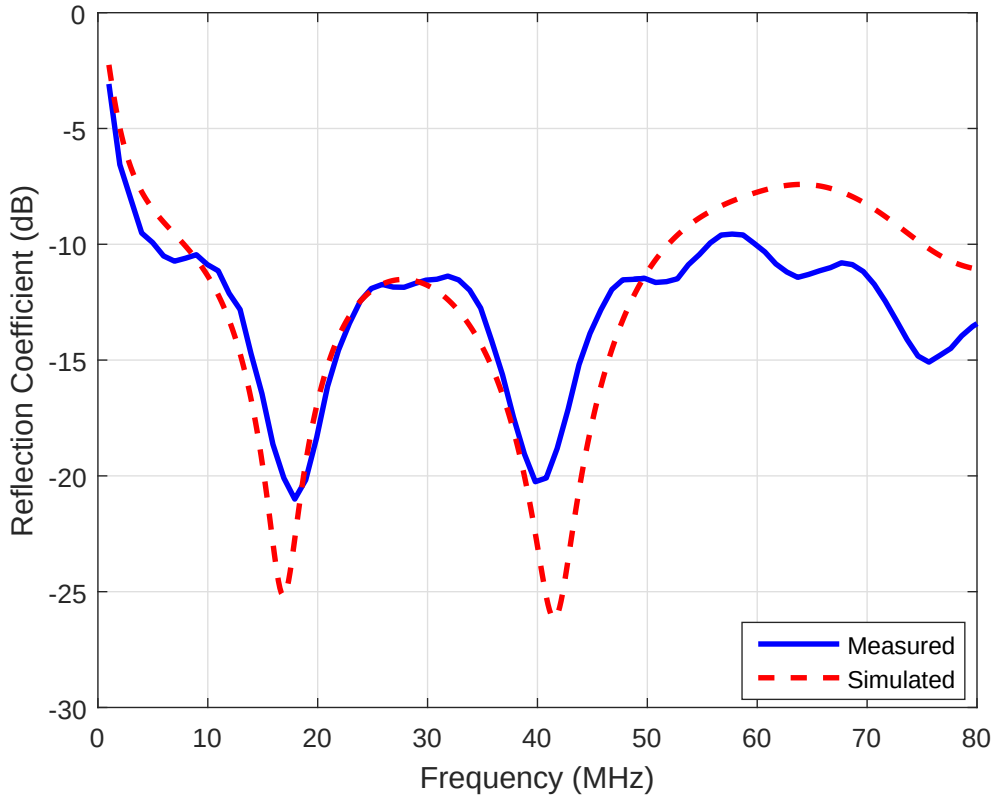

Figure 4.27: Reflection coefficient for the super J-pole antenna

[155]. Further in 2011, an advanced version of MARES was designed and manufactured, it is known as TriMARES robot. It has a high-resolution camera, sonar equipment and also with increased capacity to carry several sensors as presented in Fig. 4.31 [154].

Therefore, the initial plan is to install any of the modified antennas on MARES and the results obtained will be used to determine the most suitable antenna that can be installed on triMARES. Hence, a modular figure of MARES was designed in FEKO with the dimensions as MARES and presented in Fig. 4.32. It comprises three segments namely;

Table 4.9: MARES main characteristics [153]

Length	1.5 m
Diameter	20 cm
Deep rating	100 m
Weight in air	32 Kg
Propulsion	2 horizontal + 2 vertical thrusters
Horizontal velocity	0 - 2 m/s, variable
Energy	Li-Ion batteries, 600 Wh
Autonomy/Range	about 10 hrs / 40 km

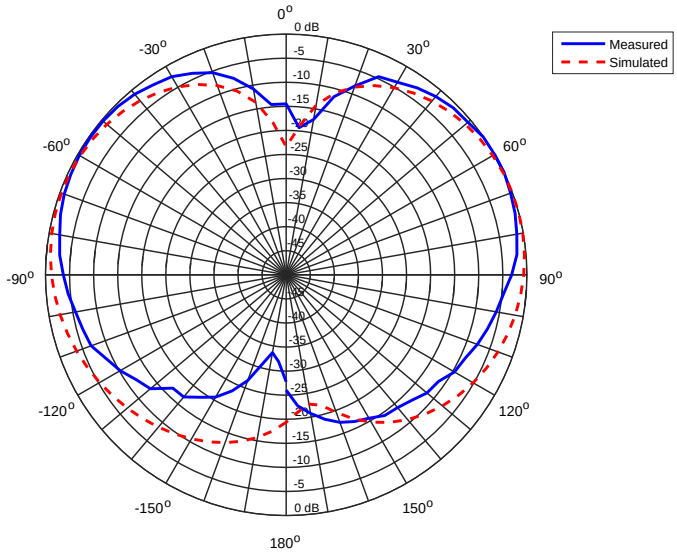

(a) E-plane

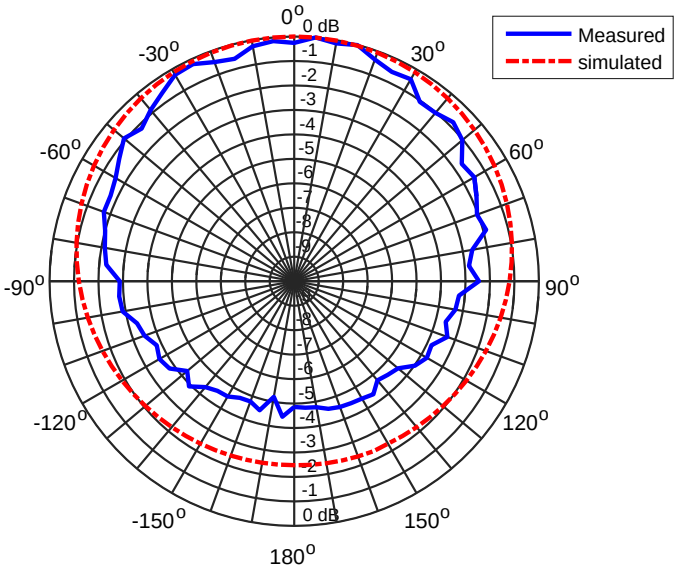

(b) H-plane

Figure 4.28: Radiation pattern for the Jpole antenna

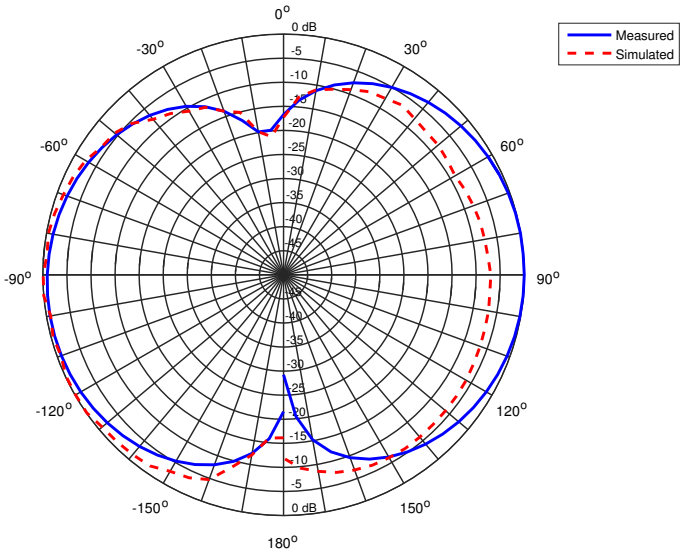

(a) E-plane

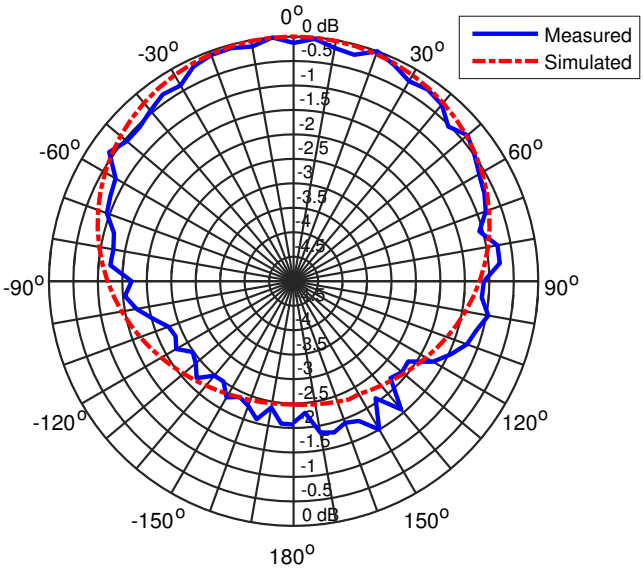

(b) H-plane

Figure 4.29: Radiation pattern for the super J-pole antenna

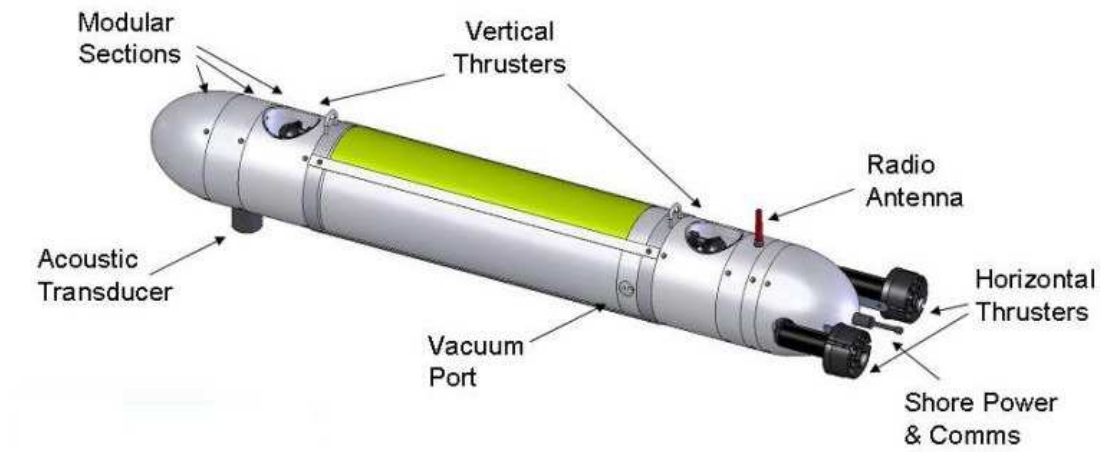

Figure 4.30: Prototype of MARES Autonomous Underwater Vehicle [153]

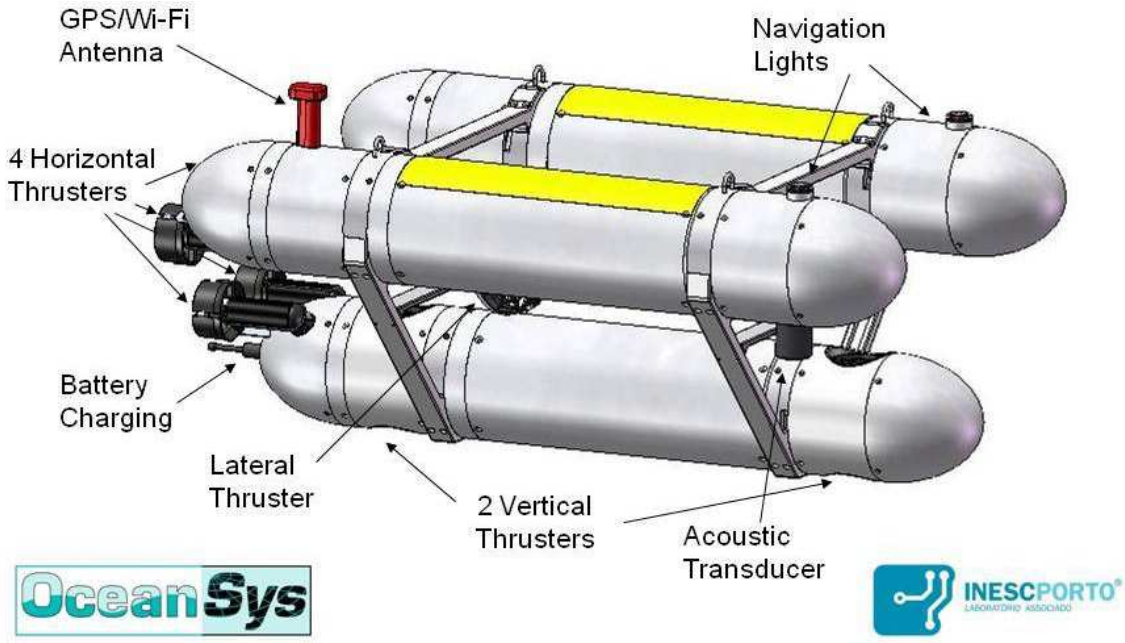

Figure 4.31: Prototype of TriMARES Autonomous Underwater Vehicle [154]

the upper segments, the middle and lower segments. The upper and lower segments are water compartment and areas for other electronic equipment that will be onboard, whereas the middle segment is an air compartment. Also, the length, inner and outer radius of the model are 1 m, 87.5 mm and 100 m respectively. The outer layer is made from materials with a relative permittivity of 3.7. For the inner layers, the permittivity depends if the compartment is air or water filled.

Based on this shape, three antennas namely; Folded dipole, J-pole, and super J-pole antennas were chosen and modified to ensure that each of them is perfectly fit around the

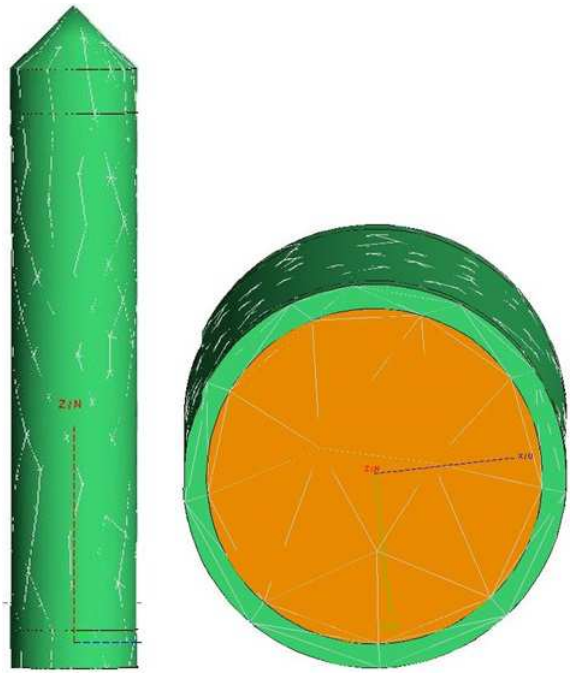

Figure 4.32: Model of Autonomous Underwater Vehicle

body of the AUV structure. In this sense; the base of the J-pole, the phasing stub of the super J-pole and the width of the folded dipole antenna became an arc of a circle whose radius is approximately the radius of the outer layer of the structure and subtending an angle of 30°. In addition, to ensure that these antennas still operate at the initial design frequency of 40 MHz, other dimensions were slightly altered, to accommodate for the change in the previously mentioned arcs. Thus, the modified antennas placed outside the AUV structure are presented in Fig. 4.33, with; a, b, c representing J-pole, folded dipole, and super J-pole antennas, respectively. The analyses do not include collinear J-pole antenna because it has already been shown that it has the relatively same performance as the super J-pole antenna and in addition because of its phasing coil, the antenna will not be able to fit around the wall of the AUV model in a similar version to the other antennas.

Table 4.10: Simulation Results for the modified Antennas with AUV models

S /No.	Parameters	Folded dipole	J-pole	Super J-pole
1	Bandwidth	17.00	16.20	22.77
2	Directivity (dBi)	2.17	4.65	7.13

The bandwidth and the directivity for each of these antennas is presented in Table 4.10. Comparing the results in this table with those previously obtained for each of the antennas without AUV model, it is obvious that the modification has little effect on the bandwidth as these are somewhat close to what was obtained when these were simulated

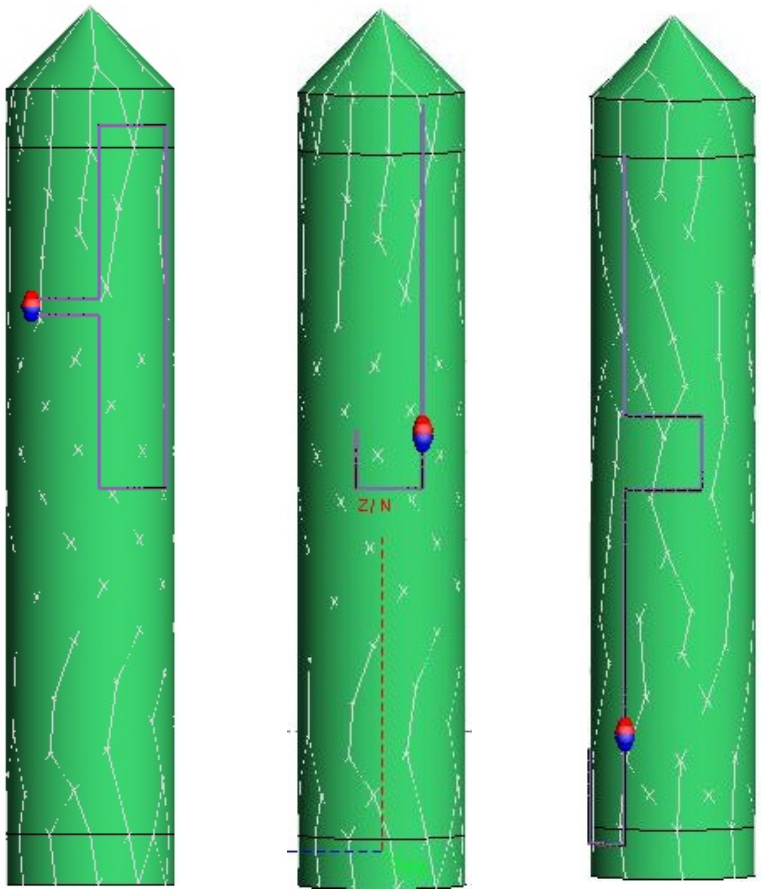

(a) Folded dipole (b) J-pole (c) Super-J-pole

Figure 4.33: Antennas placed outside the body of AUV model

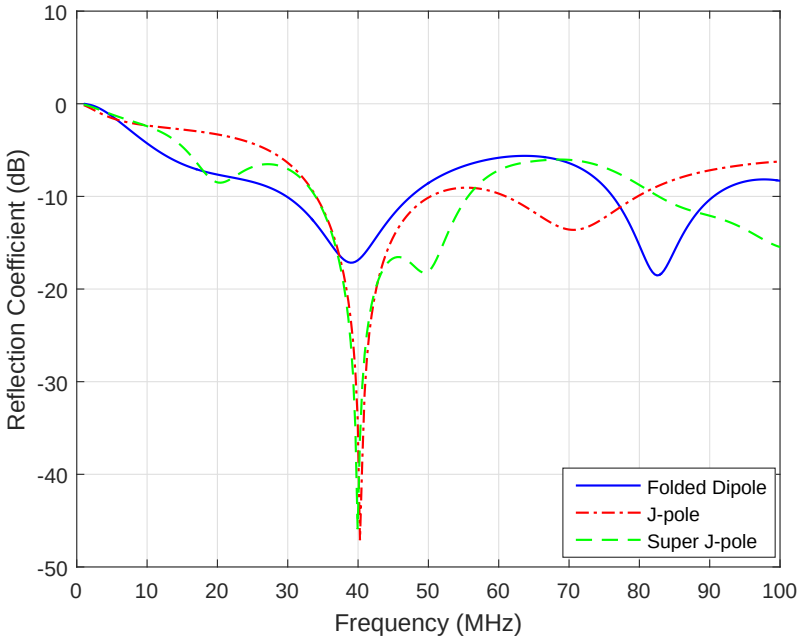

Figure 4.34: Reflection coefficient as a function of frequency for the antennas

without the AUV. Thus, the results of the reflection coefficient as a function of frequency is presented in Fig. 4.34. On the other hand, the values obtained for their directivities, are higher than those previously obtained for each of the antennas. This may be due to the AUV model preventing the antennas from radiating in all directions. To affirm this, the radiation pattern of the antennas in E and H plane are presented in Fig. 4.35.

Comparing these patterns with those presented for each of these antennas in the earlier sections, it simply shows that the presence of AUV model distorts these patterns. Each of the E-plane and H-plane pattern presented here are different from what was obtained originally for those antennas without AUV models. Only folded dipole antenna look somewhat close to the previously obtained and despite its directivity being lower than those of the other antennas, it is believed that if this antenna is tested on an AUV, its performance is predictable.

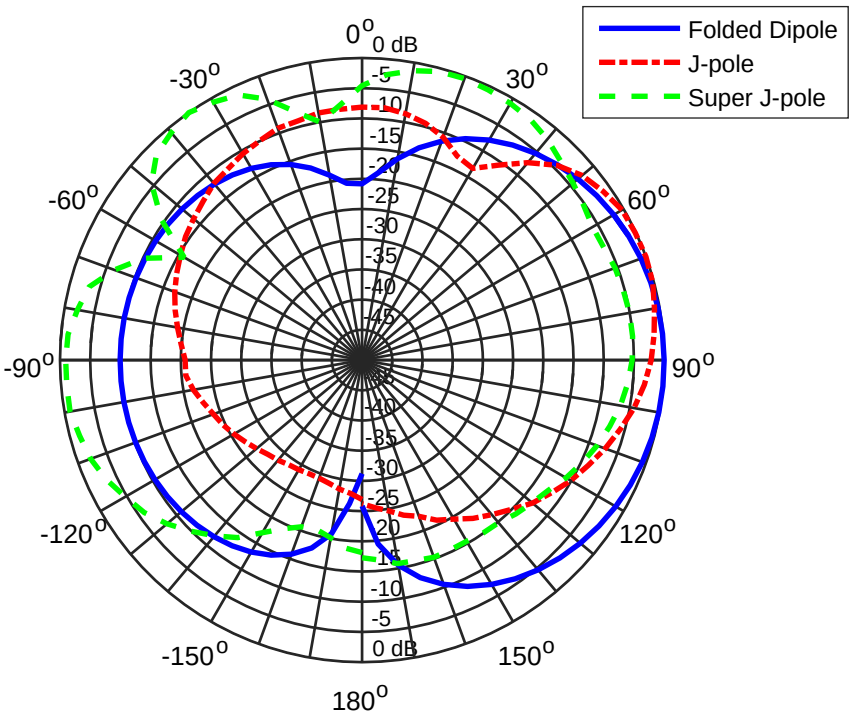

(a) E-plane

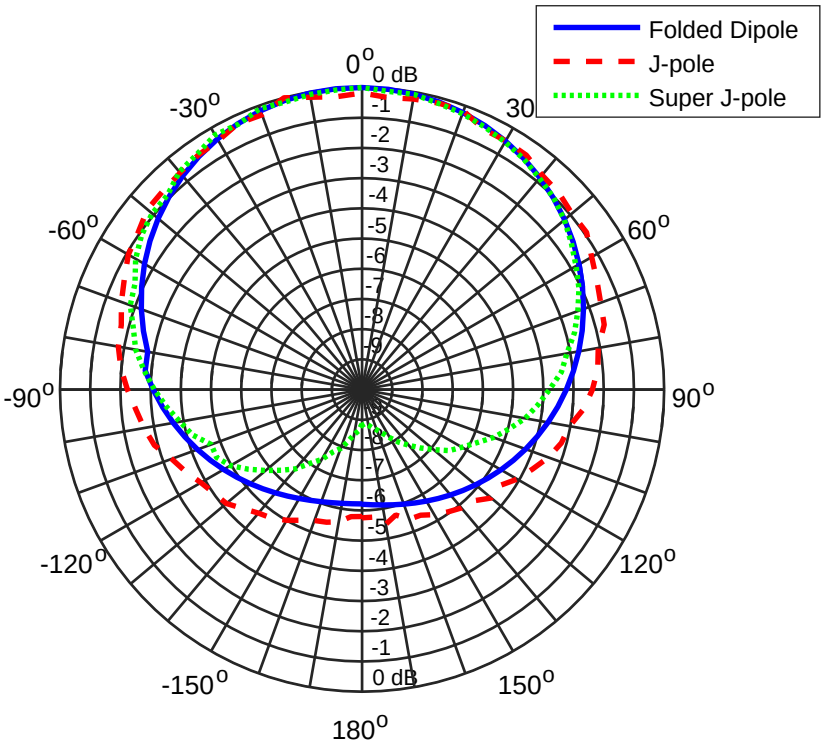

(b) H-plane

Figure 4.35: Radiation pattern for the antennas with AUV model

4.6 Conclusion

In this chapter, analyses of various parameters that can affect the design and development of underwater antennas were given. In addition, the performance of narrowband antennas with respect to the bandwidth and directivity has thus been presented. It is seen that super J-pole and collinear J-pole antennas have higher bandwidth and directivity when compared with other antennas presented in this chapter. Experimental results have been obtained of the reflection coefficient and radiation patterns, that match closely the numerical simulation.

The conclusion drawn is that due to the physical structure of some of the antennas presented in this chapter, it will be easier to fix such antenna around the body of an AUV model for onward data harvesting or communication with other underwater bodies. But fixing two antennas of the same type may enhance performance due to the noticeable effect of the AUV model on the radiation pattern of the antennas.

Chapter 5

Dual band and Wide band Underwater Antennas

5.1 Introduction

Apart from narrowband antennas, considered in the previous chapter, This chapter focuses on dual band and wideband underwater antennas, which are suitable to operate between 20 MHz and 200 MHz when the antennas are submerged in fresh water scenario. Also, the antennas designed specifically for ¡VAMOS! (Viable Alternative Mine Operating System) project was as well presented. These antennas required the addition of some materials with low permittivity and this altered the performance of the antennas in the medium. Finally in this chapter, realized the gain of underwater antennas were as well given, in which the expected received power of underwater systems was determined.

5.2 Dual band Dipole and J-pole Antennas

Dual band antennas introduced in this section are designed with extra arms attached to their respective ordinary half-wave dipole and J-pole antennas. These antennas are intended for dual communications at two different frequency bands, which is important when considering a scuba diver communicating with such antenna at a certain frequency and the same antenna is programmed to communicate with an underwater sensor nodes at another frequency. A gap band of more than 10 MHz is made to be between the two resonating frequencies, which is to ensure that the antenna serves it's purpose accordingly. In the case of the dual band dipole antenna, second arms are attached at a distance of 10 mm to the feeding point on either sides. The length of the extra arm is $\frac{\lambda}{4}$, which will ensure that the second resonating frequency is about 2 times the first one. The respective

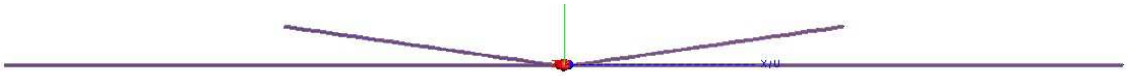

Figure 5.1: Dual band dipole antenna

dimensions of the arms are 450 mm and 225 mm for the resonating frequencies of 60 MHz and 30 MHz respectively. For the J-pole antenna on the other hand, it is designed by adding a parallel stub of $\lambda/8$ to the original J-pole antenna. The two resonating frequency for this antenna are 30 MHz and 55 MHz respectively. This additional stub will ensure that the antenna also resonates at almost 2 times the first resonating frequency. The port location and matching of this antenna are different from ordinary J-pole Antenna. Here the port is located between the long arm and $\lambda/8$ parallel stub, with which we ensured that the antenna is tuned for optimum performance in terms of the bandwidth, directivity, and the efficiency. The designed antennas are as presented in Fig. 5.1 and 5.2.

Figure 5.2: Dual band J-pole antenna

The initial results of the reflection coefficient as a function of frequency for the two antennas are displayed in Fig. 5.3

From these results, the dual-band dipole antennas have it minimum at the exact calculated resonating frequencies but that of the dual-band J-pole has a shift of 10 MHz in the lower resonating frequency, while the higher frequency conformed with the calculated one. This shift thereby affected the expected band gap between the lower and the higher

resonating frequencies. Hence, further analyses will only focus on the dual-band dipole antenna.

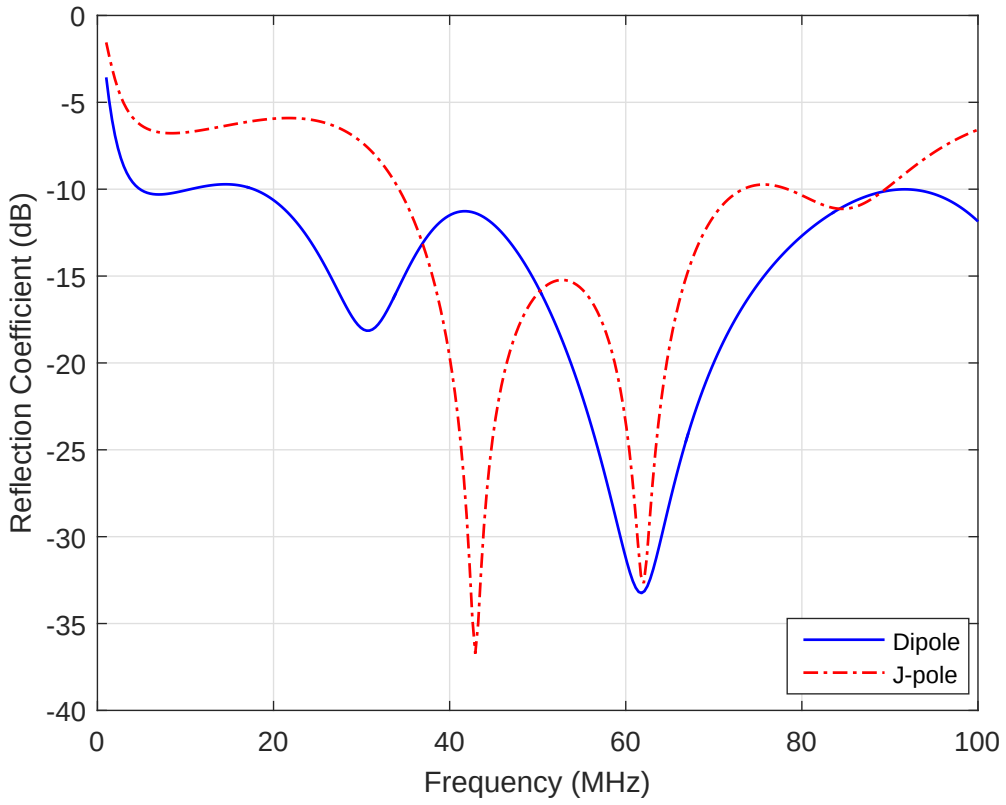

Figure 5.3: Dual band Dipole and J-pole antenna

5.3 Analyses Dual band Dipole

Two important parameters were considered in spacing the end of the short arm and the long arm, these are; the input impedance and the mismatch loss. At the lower resonating frequency of 30 MHz, the real part of the input impedance is 50 Ω and the imaginary part is -9.38 Ω, when the spacing is about 76.6 mm, whereas, for the second resonating frequency, the imaginary part is 8.68 Ω, for the same real part of 50 Ω when the spacing is reduced to 39.3 mm. These results are presented in Fig. 5.4. For the mismatch loss, the lowest value achieved at the two resonating frequencies occurs when the spacing is 60 mm and 40 mm for the resonance frequency of 30 MHz and 60 MHz respectively. This is also presented in Fig. 5.5. Thus, as a trade-off between the achievable bandwidth and other antenna parameters, a spacing of 48 mm between the two arms is used for designing and fabrication of the antenna. The preliminary conclusion arrived at this juncture is that

the closer the short arm is to the long arm, the antenna achieved more bandwidths but at the expense of increased mismatch loss. But a moderate spacing favors the mismatch loss at a fairly reduced bandwidth, These two parameters can be further affected as the spacing continue to increase.

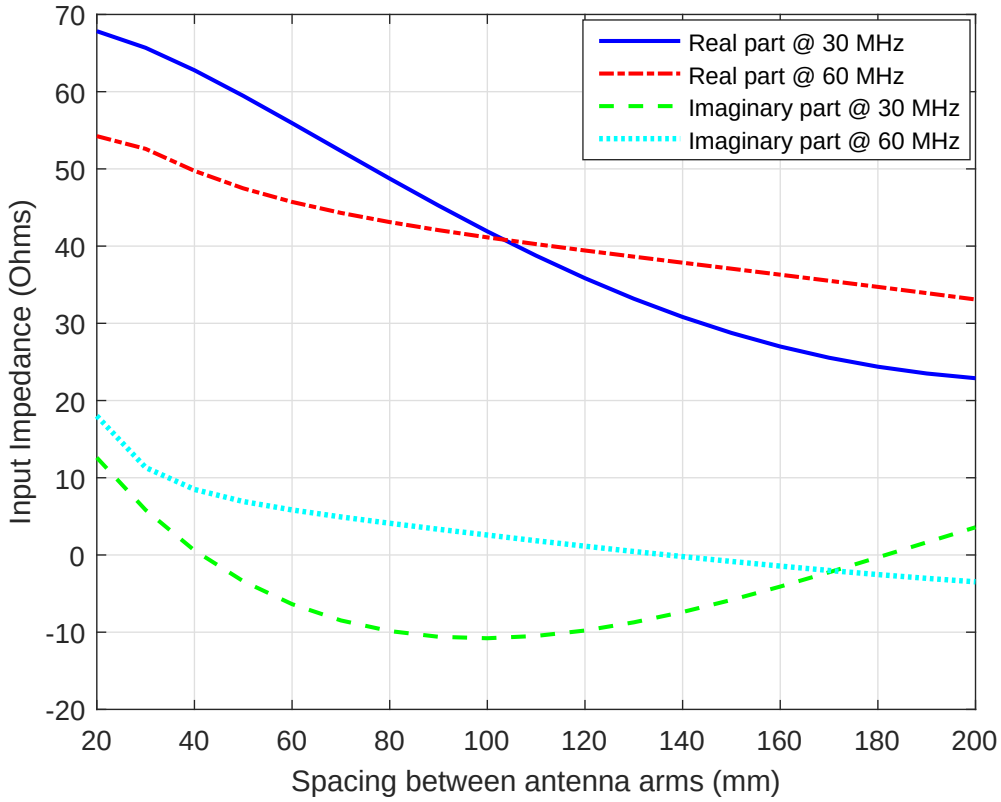

Figure 5.4: Input impedance as a function of spacing between antenna arms

5.3.1 Simulation and Experimental Results

The designed antenna is simulated in fresh water, the results of the reflection coefficient show that it achieved a bandwidth about 70 MHz, with the two lowest points of -18 dB and -33 dB occurs at 30 MHz and 60 MHz respectively. The designed antenna was fabricated and presented in Fig. 5.7. Similarly, the measurement set for this antenna is given in Fig. 5.6. Thus, the simulated and measured reflection coefficient as a function of operating frequency is compared and presented in Fig. 5.8.

Similarly, the measured and simulated radiation pattern in E-plane and H-plane at 30 MHz and 60 MHz are compared in Fig. 5.9 and 5.10. From these results, it is seen that the simulated and measured are in good agreement and exhibits omnidirectional pattern at the two resonating frequencies.

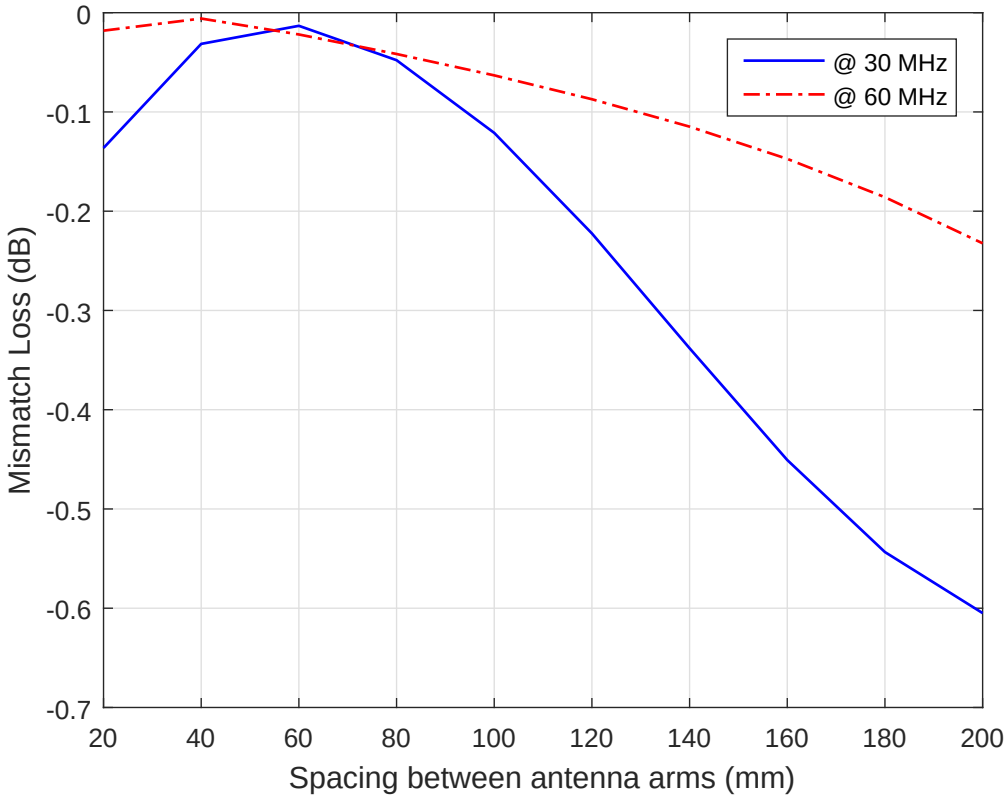

Figure 5.5: Mismatch loss as a function of spacing between antenna arms

Figure 5.6: Measurement set-up for dual band dipole antenna

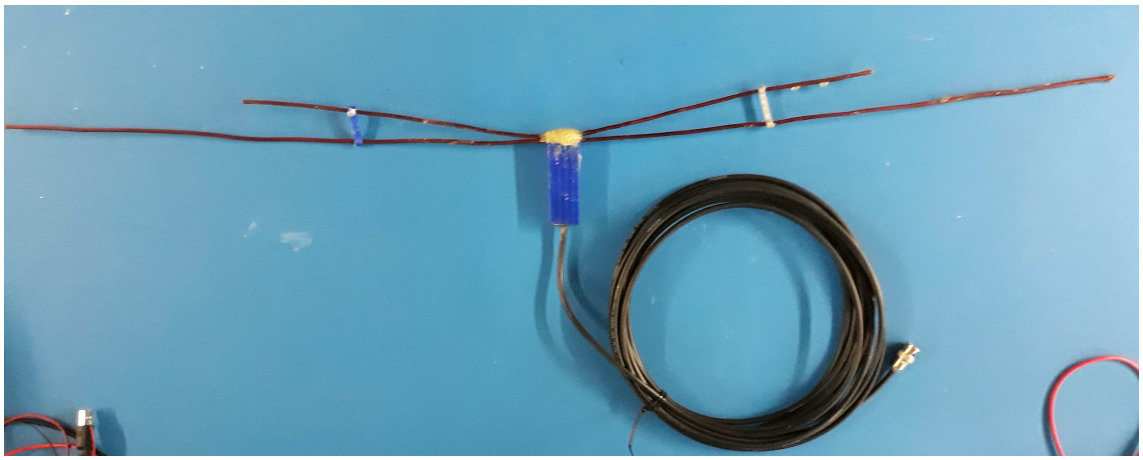

Figure 5.7: Fabricated dual band dipole antenna

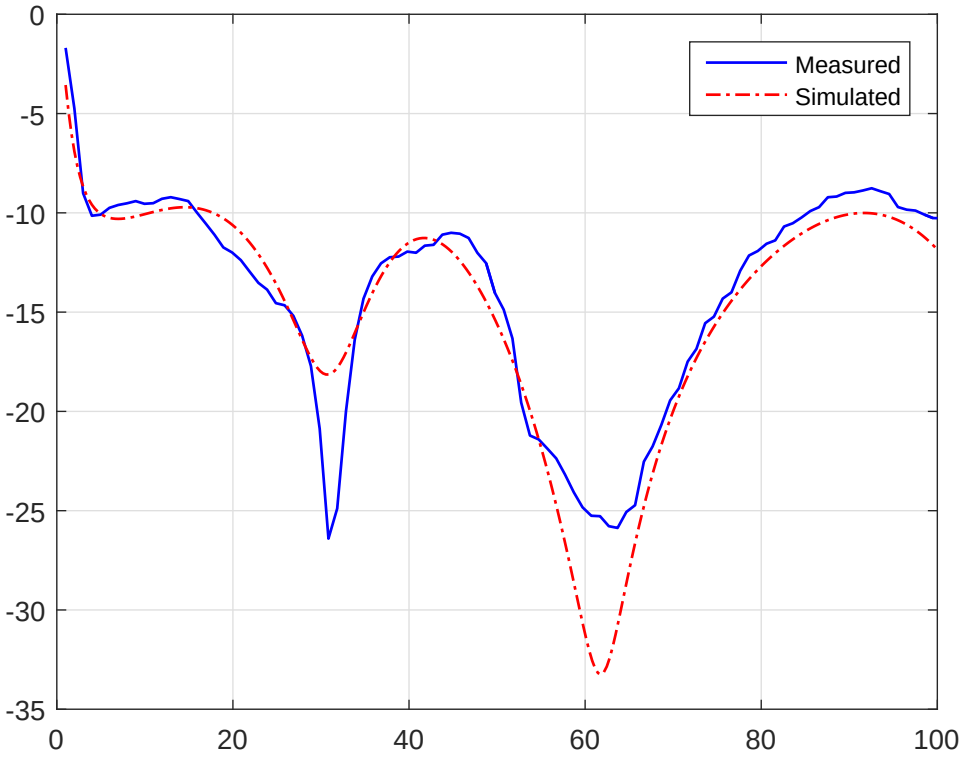

Figure 5.8: Reflection coefficient against resonance frequency for dual band dipole antenna

5.4 Dipole antenna with parasitic element

Apart from the loop antenna with ground reflector, another wideband antenna that has been considered in this work is the dipole with a parasitic element. This antenna will also

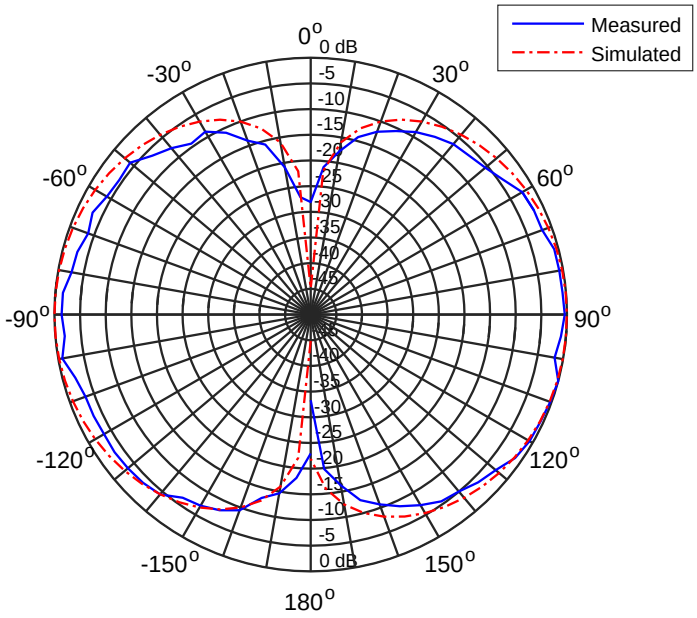

(a) E-plane

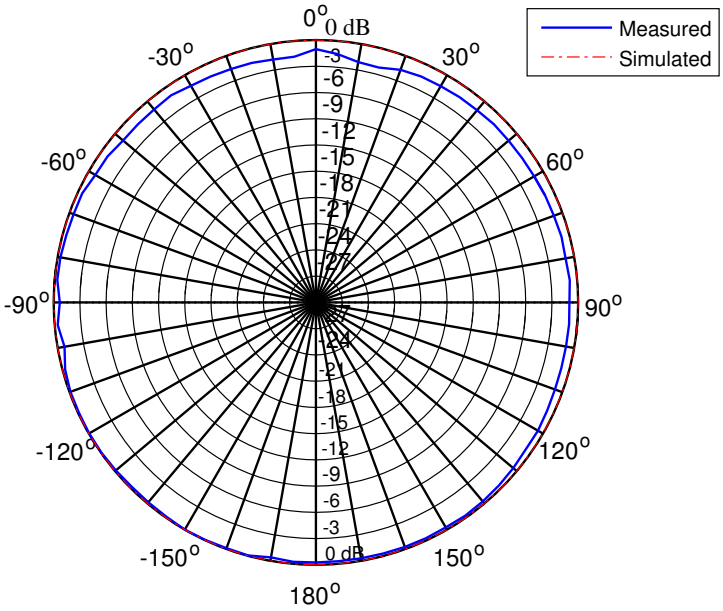

(b) H-plane

Figure 5.9: 2D radiation pattern for dual band dipole antenna at 30 MHz

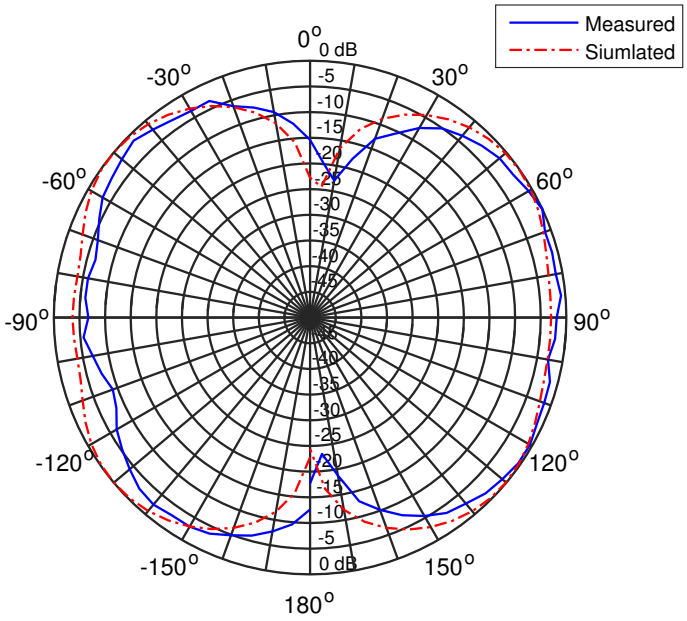

(a) E-plane

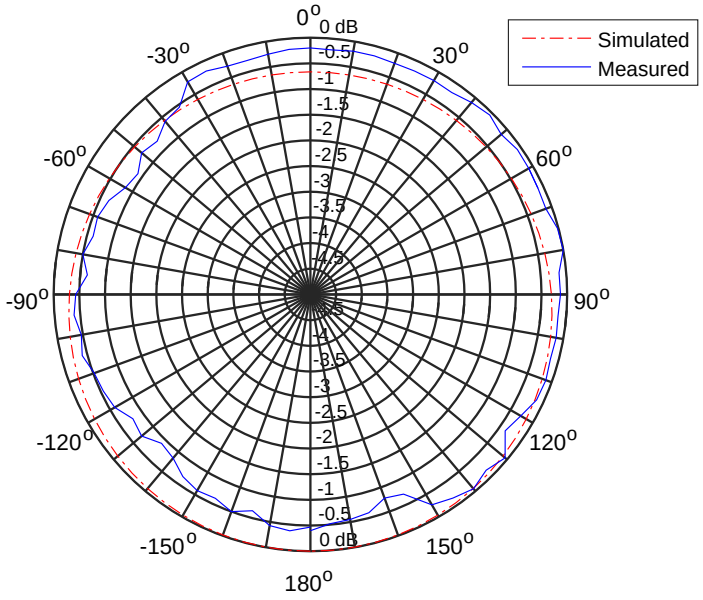

(b) H-plane

Figure 5.10: 2D radiation pattern for dual band dipole antenna at 60 MHz

guarantee improved bandwidth especially, when there is the need for higher throughput, for example, as in real-time video transmission, which may occur between underwater

sensor nodes and an AUV or between AUVs and a docking station, where narrowband antennas might not be able to sustain such data rates. It is therefore expediently important to construct underwater antennas that will meet the bandwidth requirements up to 60 MHz, for such defined operations. Thus, the performance of dipole antennas with two different parasitic elements was assessed in fresh water and measured in terms of bandwidth and directivity. The two forms of dipoles are the dipole antenna with an ordinary parasitic element (DipP) and the dipole antenna with a 'coily' (the parasitic element containing a coil) parasitic element (DipH).

The spacing of the parasitic elements to the antennas was carefully considered during the design of the antennas. From the simulation, it is observed that the closer the parasitic element to the dipole, the higher the bandwidth, but this comes at the expense of reducing efficiency. This is because the current flowing in the parasitic elements flows in opposite direction to the one flowing in the dipole, thereby reducing the efficiency of the antennas. Thus, after several parametric analysis in which both the antenna efficiency and the bandwidth were duly considered, the elements were placed at a distance of 2.5 cm from the antennas. The dimensions of the antennas is presented in Table 5.1, where D1 is the half wavelength element of the dipole arms for the two antennas, D2 is the quarter wavelength element of the parasitic arms of DipP antenna, D3 is the length of the coil added in DipH, and D4 is the $\lambda/16$ elements attached to the two ends of the coil. The dimension of this coil is calculated based on the analysis of helical antennas presented in [152, 13]. The thickness of the wires used in the design of the antennas is 3 mm and they are covered with insulating material with a thickness of 50 μm and relative permittivity of 3.

Table 5.1: Dimension of the Antennas

S /No.	D1	D2	D3	D4
1	475.00	237.50	72.00	82.75

5.4.1 Simulation Results

The two antennas were simulated in a freshwater scenario and the results corresponding to the reflection coefficient as a function of frequency for the antennas are presented in Fig. 5.12. In this respect at -10 dB of the reflection coefficient, DipP achieved 65 MHz bandwidth, between 10 MHz and 74 MHz, whereas DipH has a slightly higher bandwidth of 74 MHz, between 9 MHz and 83 MHz. These results show improvement when compared with the performance of the dipole antenna presented in the previous

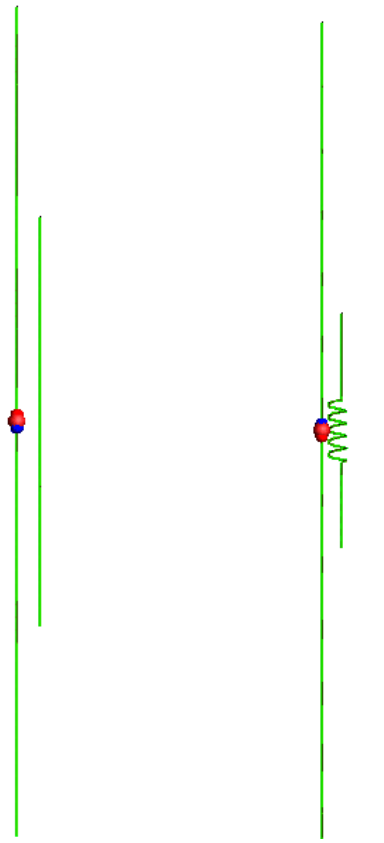

(a) [DipP antenna

(b) DipH antenna

Figure 5.11: Dipole antennas with parasitic elements

chapter and that of dual band dipole antenna presented in the previous section, when they were all simulated in the same medium.

Another important parameter that was simulated is the directivity which, at 25 MHz equals 10.70 dBi and 12.50 dBi and at 40 MHz equals 8.50 dBi and 9.92 dBi for DipP and DipH respectively. The radiation pattern of the antennas in E-plane, at 25 MHz and 40 MHz are presented in Fig. 5.13 and Fig. 5.14 respectively. It is clearly seen from the plots that at a lower frequency, they have similar behavior and thus their pattern overlap. But at 40 MHz, DipP is beginning to develop side lobes whereas pattern for DipH though narrower than what was obtained for the same antenna at 25 MHz, but no feasible side lobe seen on it. Similarly, the radiation pattern in H-plane at the two resonance frequencies are given in Fig. 5.15 and Fig. 5.16 respectively. Here, it is seen that the pattern shows that the presence of parasitic changed the shape of the plane when compared with the results obtained and presented in [138]. These are important results both for the data rates and the propagation distance.

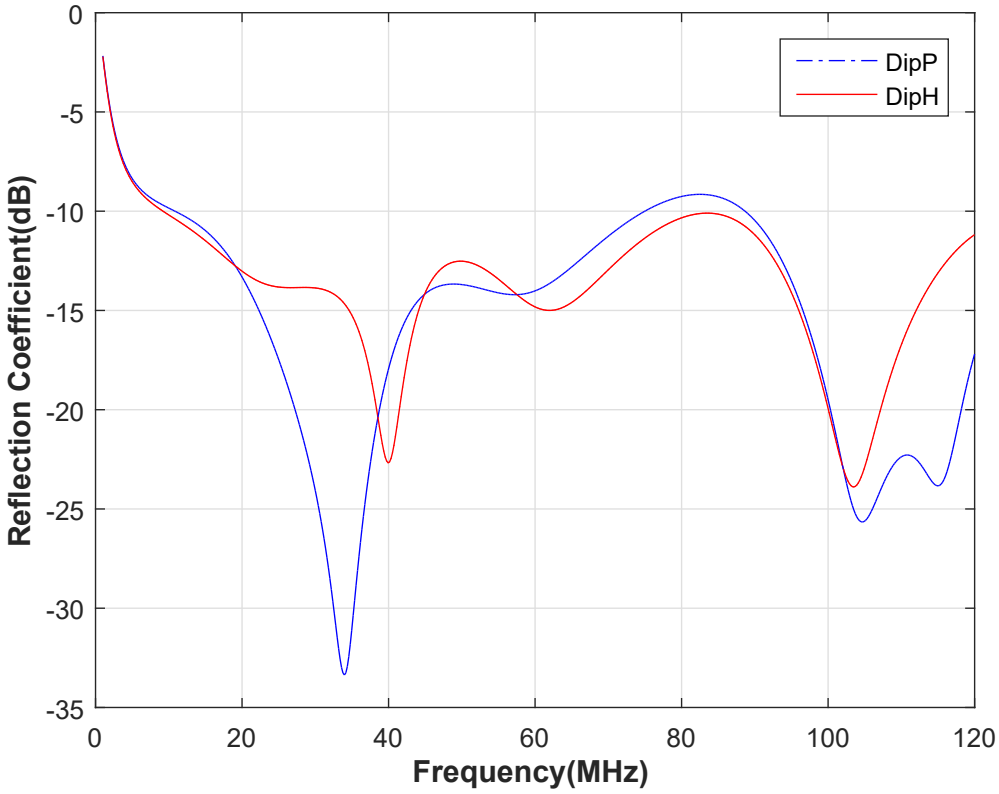

Figure 5.12: Reflection coefficient against frequency for the two antennas

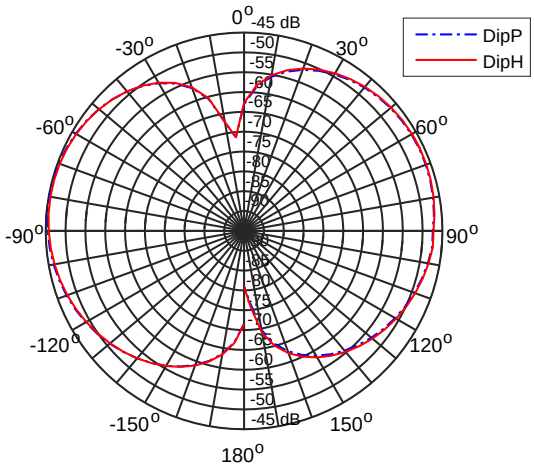

Figure 5.13: Radiation pattern of the antennas in E-plane at 25 MHz

Also measured is the S_{21} as a function of the distance between two antennas of each type (that is the distance between two of DipP antennas and two of DipH antennas) at 25 MHz and 40 MHz respectively, the results are presented in 5.17. The behavior of the

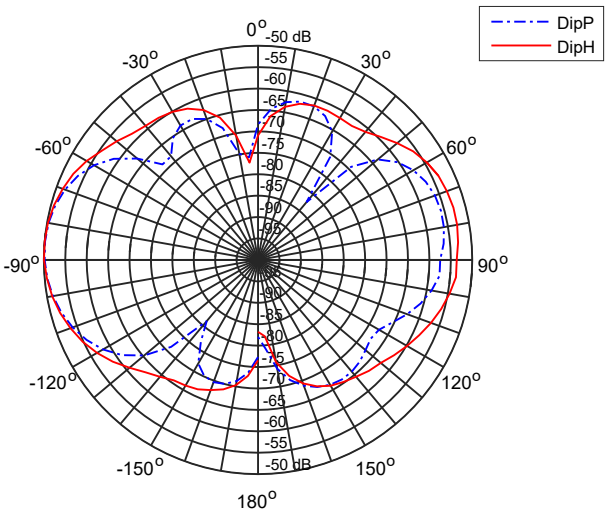

Figure 5.14: Radiation pattern of the antennas in E-plane at 40 MHz

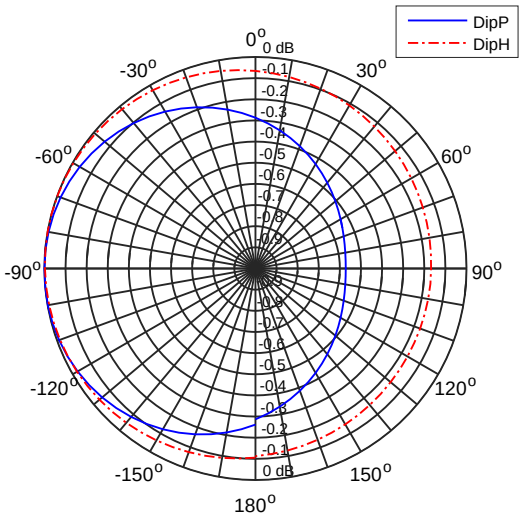

Figure 5.15: Radiation pattern of the antennas in H-plane at 25 MHz

two antennas is similar in this respect, as the plots seemingly overlap at the considered frequencies. Considering a transmission system operating in this medium, with a receiver having a sensitivity of 90 dBm and a transmitter with an output power of 10 dBm, the maximum expected a range of operation is around 7 m at 25 MHz and 6.4 m at 40 MHz, this is similar to the results presented in [138]. In all, the dipole with coily parasitic element relatively yielded higher performance than the one with an ordinary parasitic element. However, for reasons concerned with ease of fabrication and precision

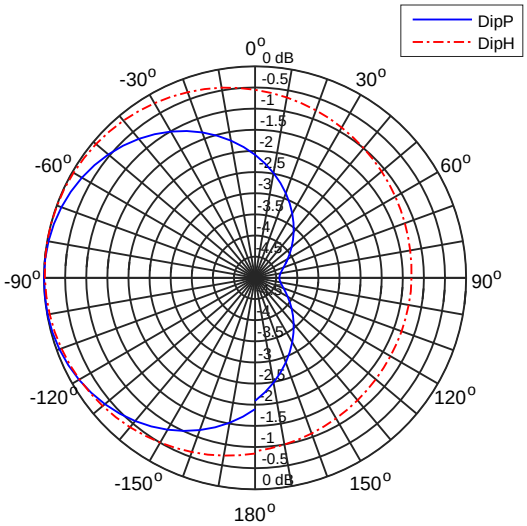

Figure 5.16: Radiation pattern of the antennas in H-plane at 40 MHz

of alignment of the elements, only the dipole antenna with ordinary parasitic element was manufactured and tested accordingly, to validate the simulated results with experimental measurements.

5.4.2 Experimental Results

The dipole antenna with ordinary parasitic element was manufactured using the dimension specified in Table 5.1. The thickness of the copper wire used in the fabrication is 3 mm and thereafter, the measurements were set up in the same freshwater pool located at INESC TEC. Pictures of the antenna and the measurement set-up are given in Fig. 5.18. The simulation results for the reflection coefficient against frequency are compared with the measured results in Fig. 5.19. The measured results agree well with the simulation and confirming that the antenna is wideband, achieving more than 60 MHz bandwidth in the medium.

Similarly, the radiation pattern of the antenna was also measured experimentally in the water at 25 MHz and 40 MHz. The results are shown in Fig. 5.20 and 5.21 respectively. it is seen that the results match quite well. Thus, one can summarily conclude that the achieved bandwidth and directivity for these antennas are important for underwater applications when considering the data rates and the propagation distance between two underwater bodies. Also, the spacing between the parasitic elements and the antennas must be carefully considered to ensure the efficiency is not affected while improving the bandwidth.

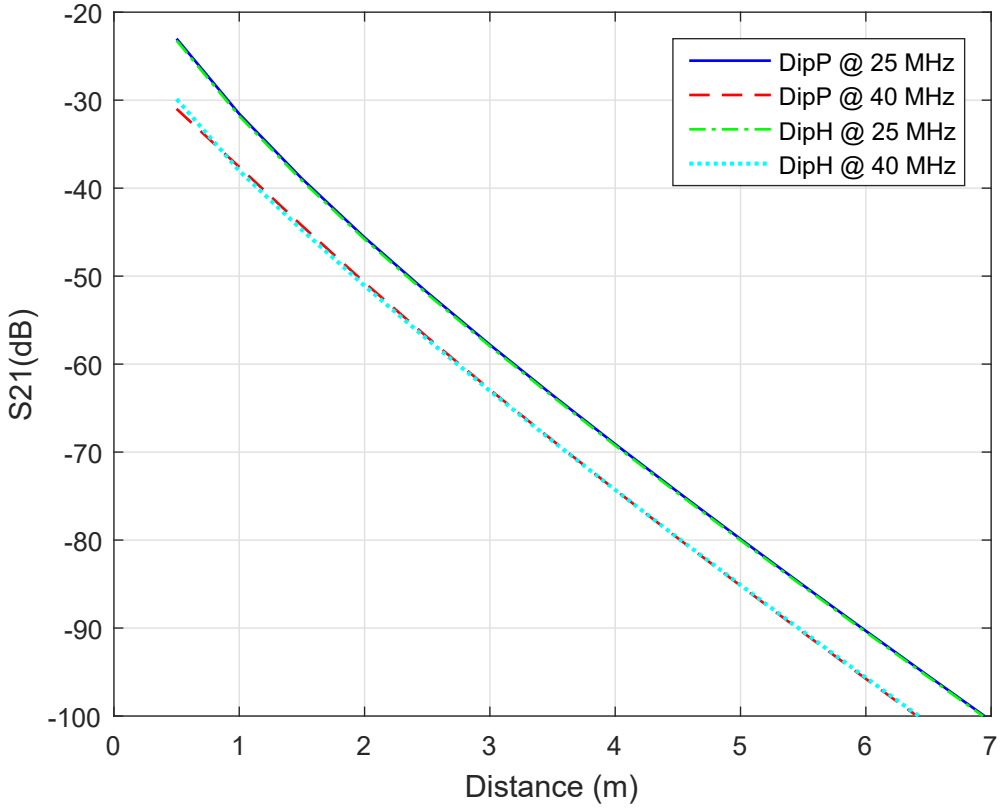

Figure 5.17: S_{21} as a function the distance between two antennas for both DipP and DipH

5.5 Loop Antenna with Ground Reflector

In the previous chapter, performance of the circular loop antenna have been duly analyzed, alongside dipole, folded dipole and J-pole antennas. In the analysis, the loop antenna has a bandwidth of 13.94 MHz and the maximum directivity of 5.2 dBi in fresh water, similarly, the radiation pattern is bi-directional in the plane perpendicular to the plane of the loop. But, to ensure that the antenna radiates in one direction only, thereby making it a highly unidirectional antenna with improved propagation distance in the chosen direction (that is the direction opposite where the grand plane is placed) [156] and also with higher bandwidth which is important for improved data rates, which is of great value to the scuba divers. The antenna is placed horizontally on a ground plane (reflector) through parametric analysis but at a distance not greater than $\lambda/4$ to reduce/cancel the back lobe that can be generated at a distance beyond this [157, 158]. Thus, three variations of the full wave loop antennas designed and analyzed in this paper are; the circular loop antenna, the square loop antenna and the delta loop antenna. Similarly, two dimensions of the ground plane used in this work are the circular and the square ground plane. Thus, the models

(a) Fabricated antenna

(b) Antenna during measurements

Figure 5.18: Photographs of the DipP antenna after fabrication and during measurement

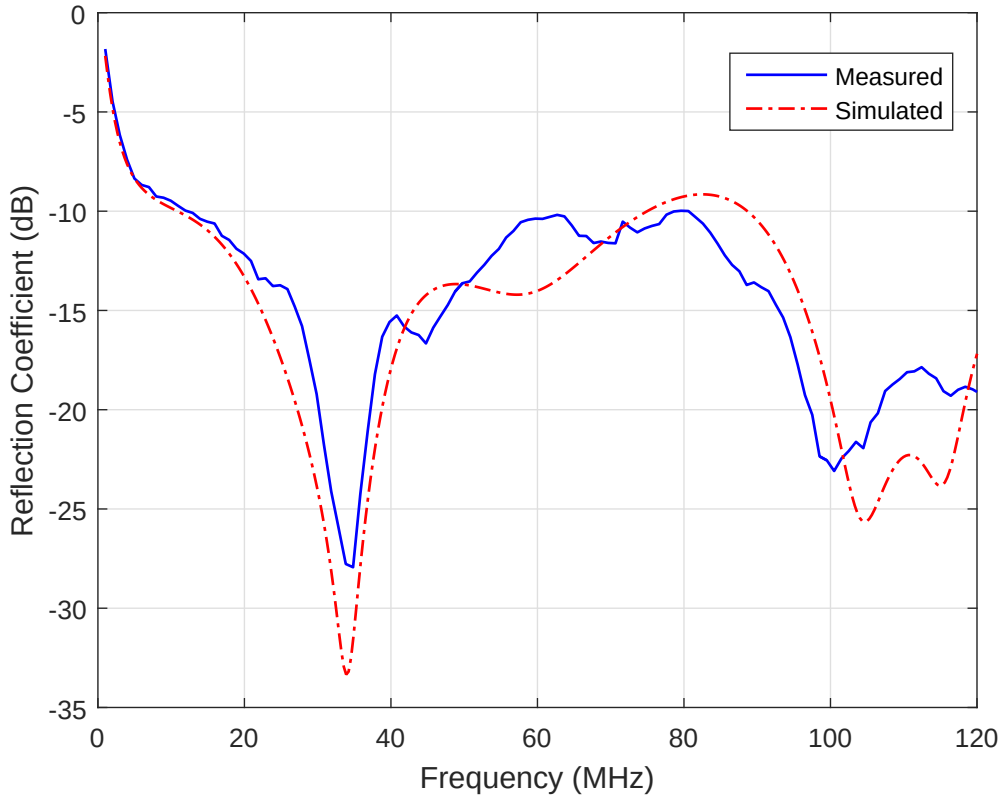

Figure 5.19: Simulation versus measurement for the DipP Antenna

of these antennas are presented in Fig. 5.22 & 5.23 showing the circular, square and the delta loops placed perpendicular on circular and square ground plane respectively with a distance of 14 cm apart, which the the calculated $\lambda/4$ distance from the antenna. The three antennas designed to propagate at the same operating frequency, in that respect, the circumference of the circular loop antenna is equivalent to the perimeter of; the square loop and delta loop antennas. Likewise, the circumference of the circular ground plane is equal to the perimeter of the square ground plane.

Table 5.2: Dimension of loop antenna with ground reflector

S /No.	Parameters (mm)	Dimensions (mm)
	Antennas	
1	Radius of Circular Loop Antenna	136.87
2	Side of the Square loop Antenna	215.00
3	Side of the Delta Loop Antenna	286.63
	Ground Planes	
4	Radius of Circular Ground Plane	258.00
5	side of the Square Ground Plane	400.00

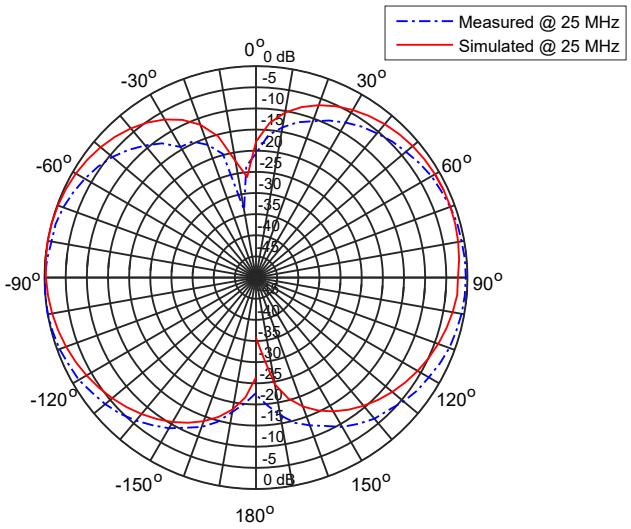

(a) E-plane

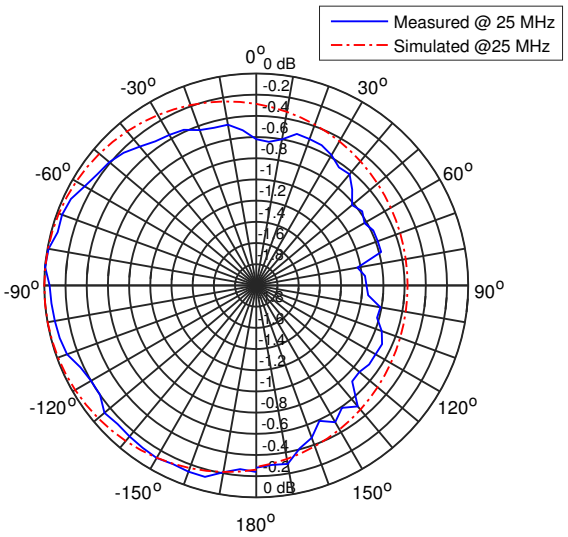

(b) H-plane

Figure 5.20: Simulation versus measurement of the 2-D radiation pattern at 25 MHz

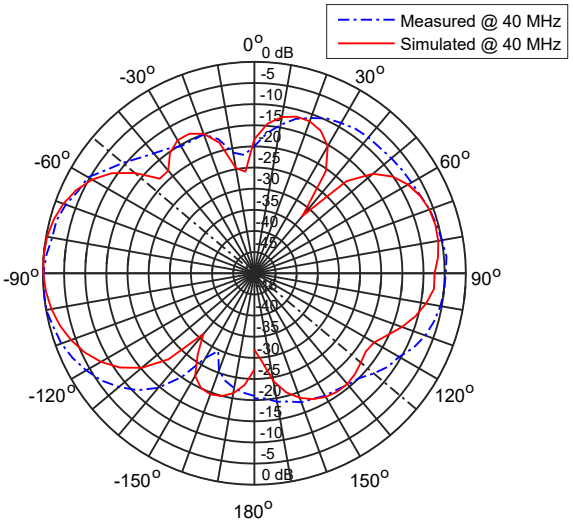

(a) 25 MHz

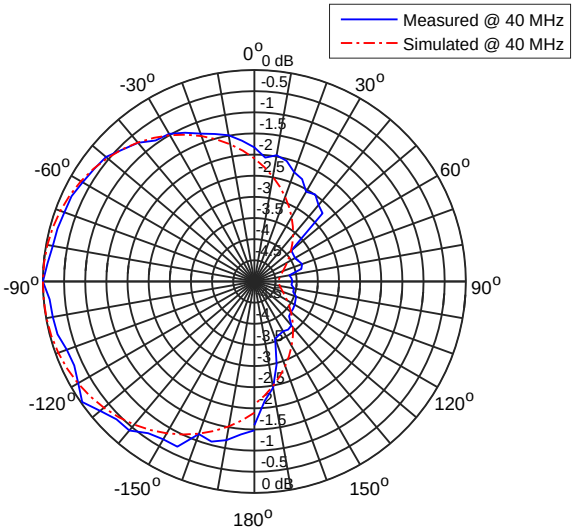

(b) 40 MHz

Figure 5.21: Simulation versus measurement of the 2-D radiation pattern at 40 MHz

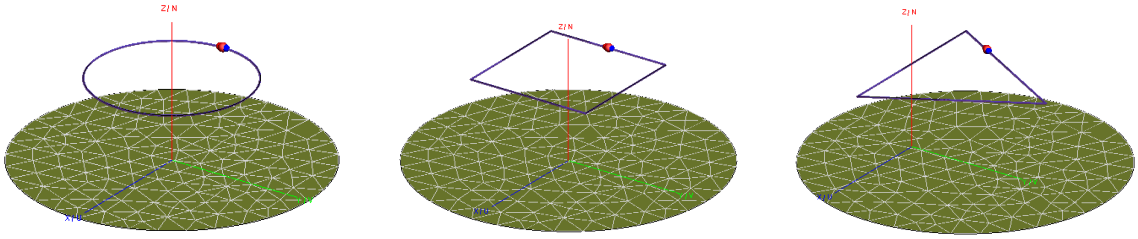

Figure 5.22: The antennas placed horizontally to circular ground planes

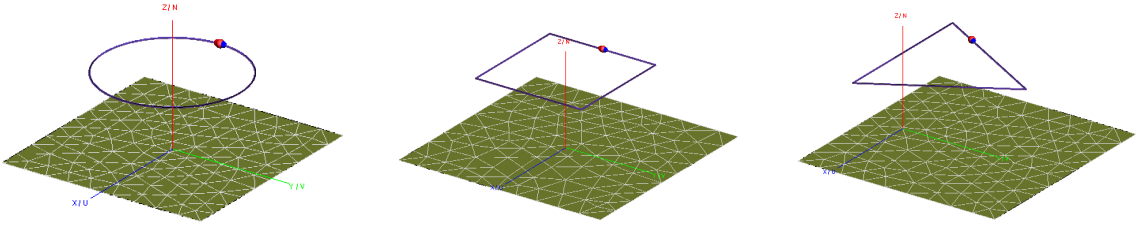

Figure 5.23: The antennas placed horizontally to square ground planes

The antennas are designed at the operating frequency of 50 MHz, at this frequency, it has been shown in [159] and chapter 3 that the attenuation is minimal at lower frequencies. If the antennas are to be operated in both fresh and sea water, different dimensions will be required as the operating frequency depends on the conductivity of the medium. But the concern of this work is operating the antennas in a freshwater scenario only at first and later extends the work to water with higher conductivity. Thus, the dimensions of the antennas are given in Table 5.2. Here, the radius of the circular loop antenna is given as 136.67 mm, the length of each side of the square loop antenna is given as 215 mm and the length of each side of the delta loop antenna is given as 286.63 mm. Similarly, the radius of the circular ground plane is given as 258 mm and the length of each side of the square ground plane is 400.00 mm.

5.5.1 Simulation Results

The antennas were simulated in a freshwater scenario and the results corresponding to the reflection coefficient as a function of frequency, when the antennas were simulated with a circular ground plane and square ground plane are presented in Fig. 5.24 and Fig. 5.25 respectively. The terms CC, SC, and DC in Fig. 5.24 is used to represent the Circular loop antenna on Circular ground plane, Square loop antenna on Circular ground plane and Delta loop antenna on Circular ground plane respectively. Similarly, the terms CS, SS and DS in Fig. 5.25 are used to represent Circular loop antenna on Square ground plane, Square loop antenna on a Square ground plane and Delta loop antenna on a Square ground plane respectively. The bandwidth is measured at -10 dB and the results show that

Table 5.3: Directivities of the antennas versus operating frequencies

		Directivity (dBi)		
S /No.	Frequencies (MHz)	CS	SS	DS
1	40.00	15.38	16.84	14.41
2	50.00	16.73	18.22	15.69
3	60.00	16.98	18.79	16.01
4	70.00	16.12	17.82	15.24
5	80.00	14.62	16.15	14.36
6	90.00	14.11	15.78	13.64
7	100.00	13.79	15.18	13.21

antennas achieved wideband which spanned between 32 MHz and 167 MHz both on the antennas with the circular ground plane and the square ground plane in the three antennas. It is also clearly observed that change in the ground plane shape (circular to square) has little or no effect on the performance of the antennas as the reflection coefficient results obtained for the antennas in both ground planes are very similar.

Based on these analyses, the antennas on the square ground plane were further analyzed to determine their directivity characteristics in the frequency bands from 40 MHz and 100 MHz incrementing by 10 MHz and the results are presented in Table 5.3. The results in the table were used to generate plots of directivity as a function of frequency, which is presented in Fig. 5.26. These results show that the directivities of the antennas within the frequencies of observation are higher than what was obtained for the J-pole antenna in the same medium, which was presented in 4 and [33]. Also, the three antennas have their respective highest directivity at 60 MHz and the Square loop Antenna has slightly higher directivity than other antennas. This is important results when considering the usage of these antennas for underwater operations, especially when both data rates and propagation distance are been considered.

The simulated 3D radiation pattern of the square loop antenna on a square ground plane at 50 MHz, 60 MHz, and 70 MHz are given in Fig. 5.27, showing that the antenna has a stable radiation pattern over these frequencies with large main lobe and minimal back lobe. Also, the directivity obtained at these frequencies is 15.24 dBi, 15.97 dBi, and 15.15 dBi at the three operating frequencies mentioned earlier.

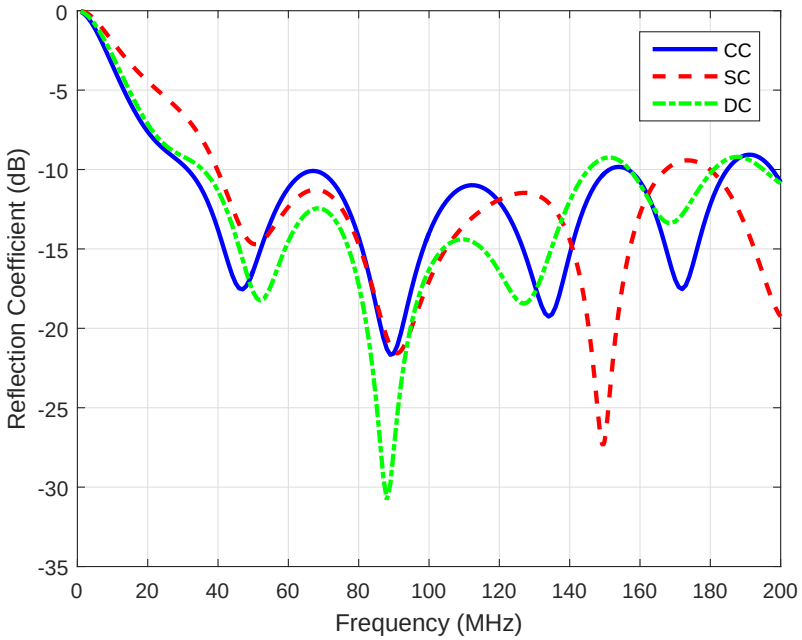

Figure 5.24: Reflection coefficient against frequency for the antennas on circular ground plane

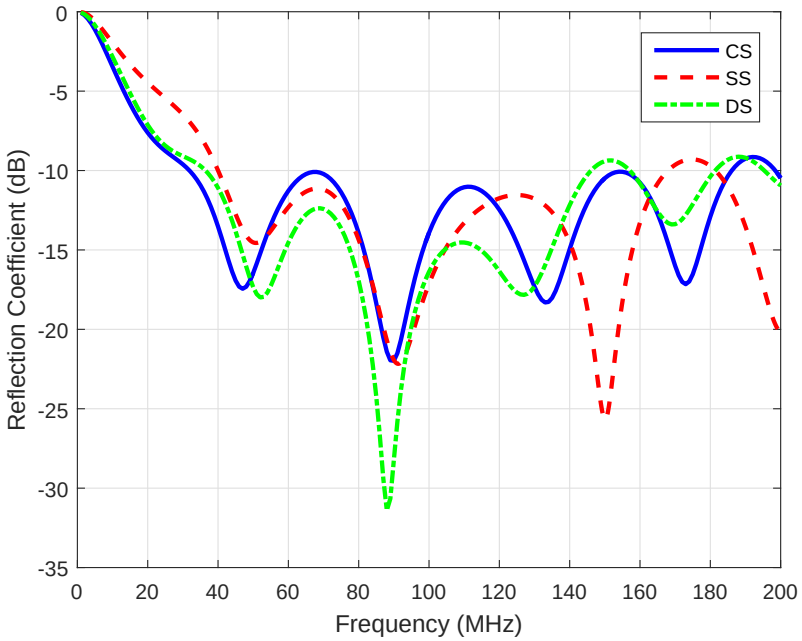

Figure 5.25: Reflection coefficient against frequency for the antennas on square ground plane

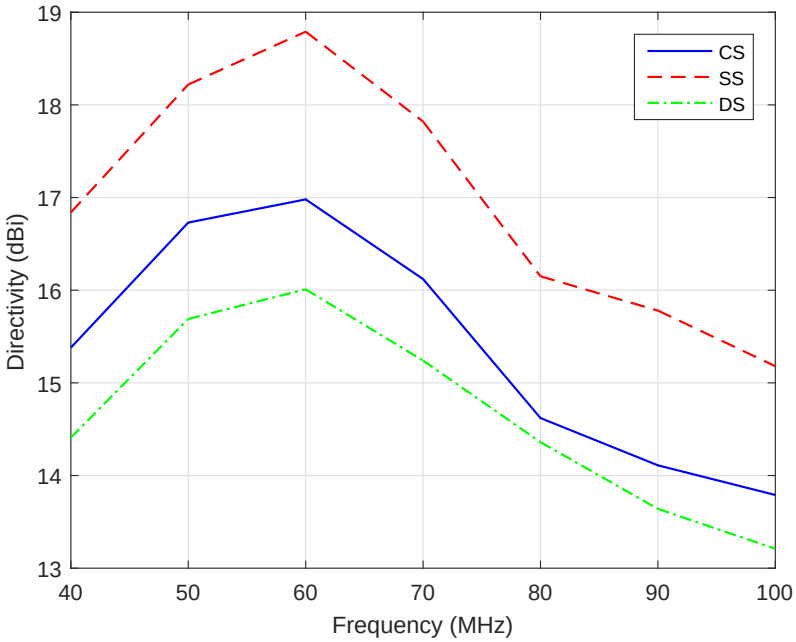

Figure 5.26: Directivity against frequency for the antennas

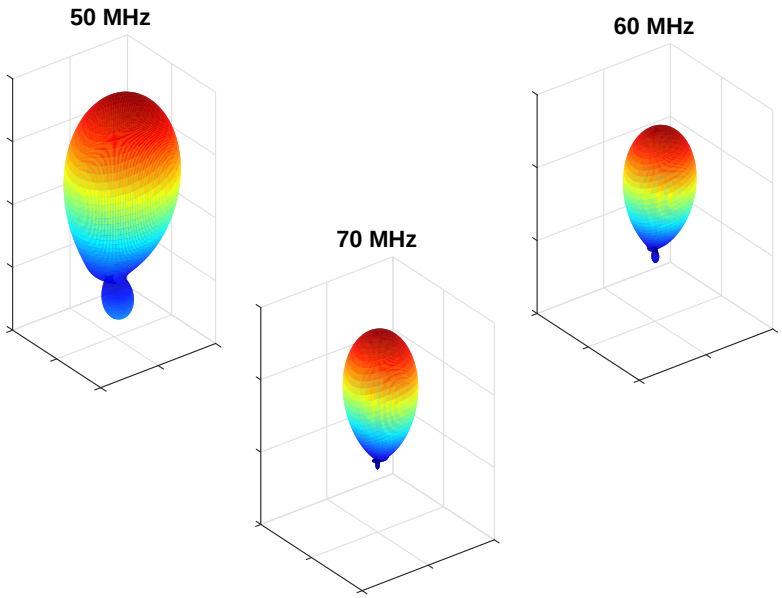

Figure 5.27: 3D radiation pattern of the antenna at 50 MHz, 60 MHz, and 70 MHz respectively

5.5.2 Experimental Results

In manufacturing the square loop antenna on the square ground plane, the simulation results and ease of fabrication were taken into consideration. Thus, the antenna was fabricated using the dimensions as presented in Table 5.2; thickness of copper wires used is 3 mm and thickness of the aluminum ground plane is 5 μm. Baluns (1:1) were added to the manufactured antenna which is presented in Fig 5.28, this is to reduce undesired radiation on the coaxial cables, which could interfere with the radiation of the antennas and thereby altering the radiation characteristics of the antennas.

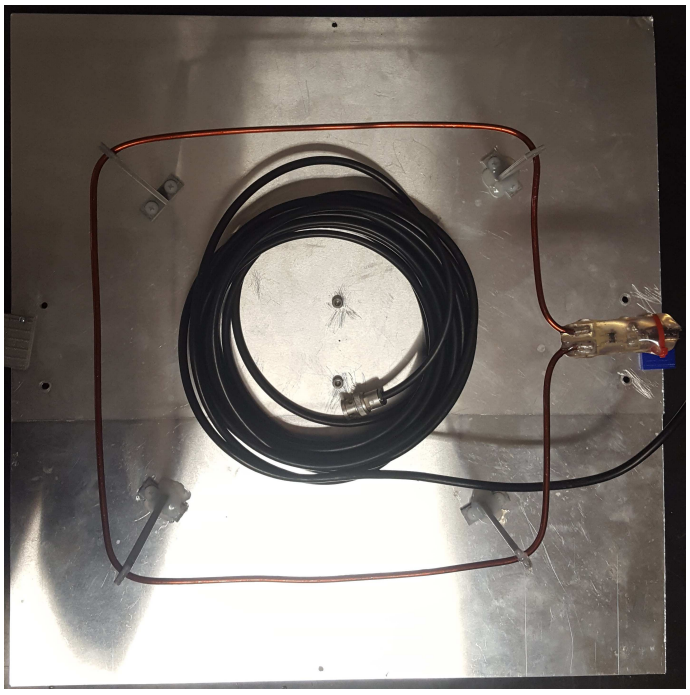

Figure 5.28: Manufactured square loop antenna with square ground plane

The experimental measurements for the bandwidths and radiation pattern was set up in a freshwater pool owned by INESC TEC, with the antennas at a depth of 2.5 m from the surface and placed on the center of the tank (which has dimensions of 10 m $\times$ 6 m $\times$ 5.5 m and the conductivity of water was 0.0487 S/m at 25°C). Thus, the entire set up used in the measurements are presented in Fig. 5.29. The simulation results for the reflection coefficient as a function of operating frequencies are compared with the measured results, which are presented in Fig. 5.30. These results confirmed that Loop antenna with ground plane actually achieved wideband. The difference between the measured and the simulated can be due the attenuation through cable loss or as a result of reflection from the wall of the freshwater tank. Similarly, the measured and simulated radiation pattern in for the antenna at 50 MHz, 60 MHz and 70 MHz were presented in Fig.5.31, 5.32 and 5.33

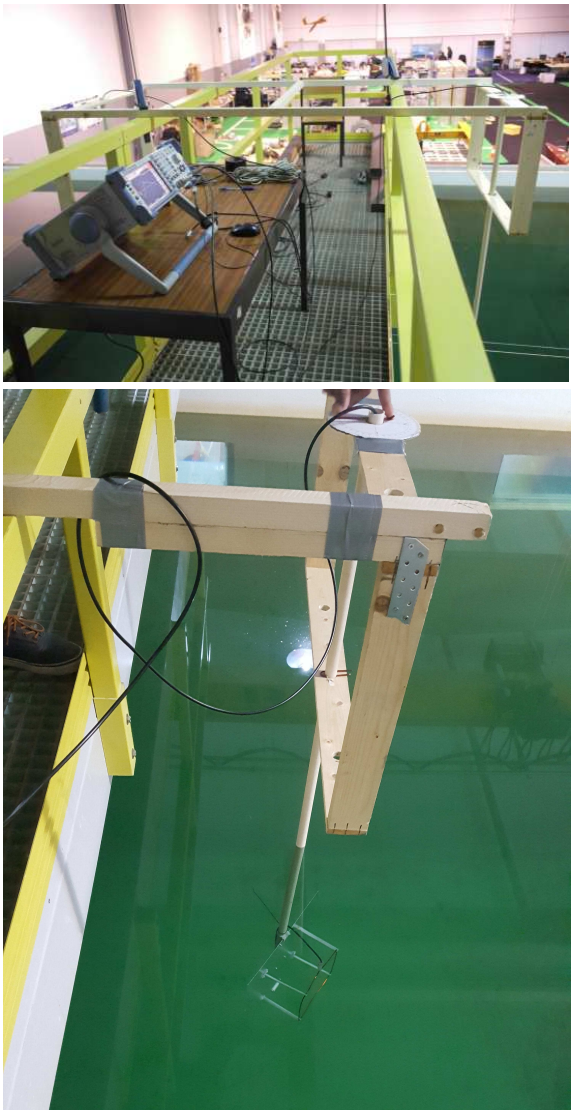

Figure 5.29: Set up for the measurements

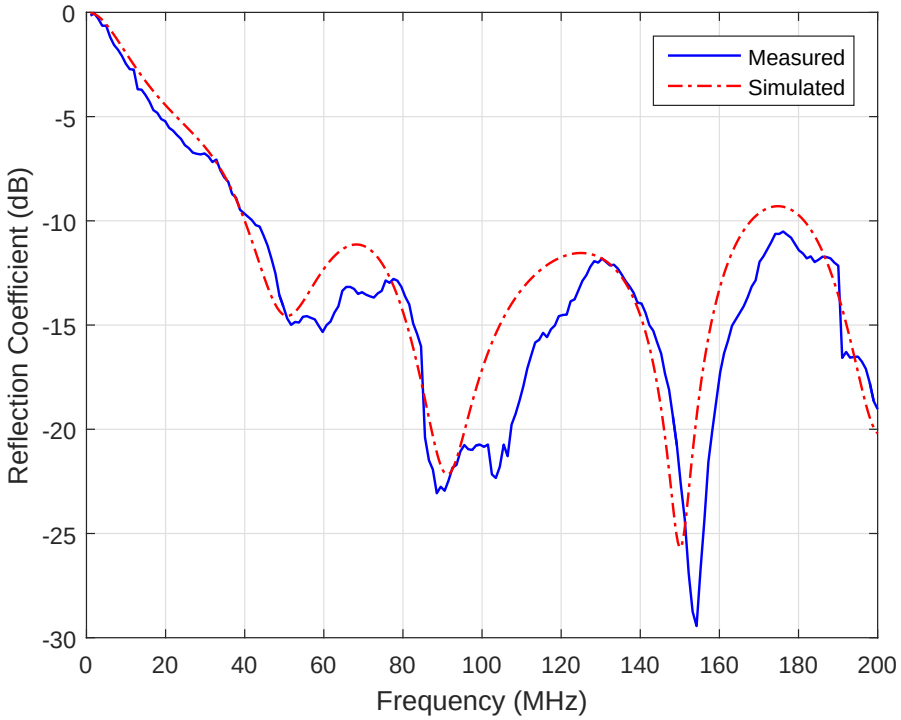

Figure 5.30: Simulation versus Measurement Square Loop Antenna with Reflector

respectively. It is seen here that at the three frequencies, the simulated and the measured are in good agreement and also with minimal back lobe.

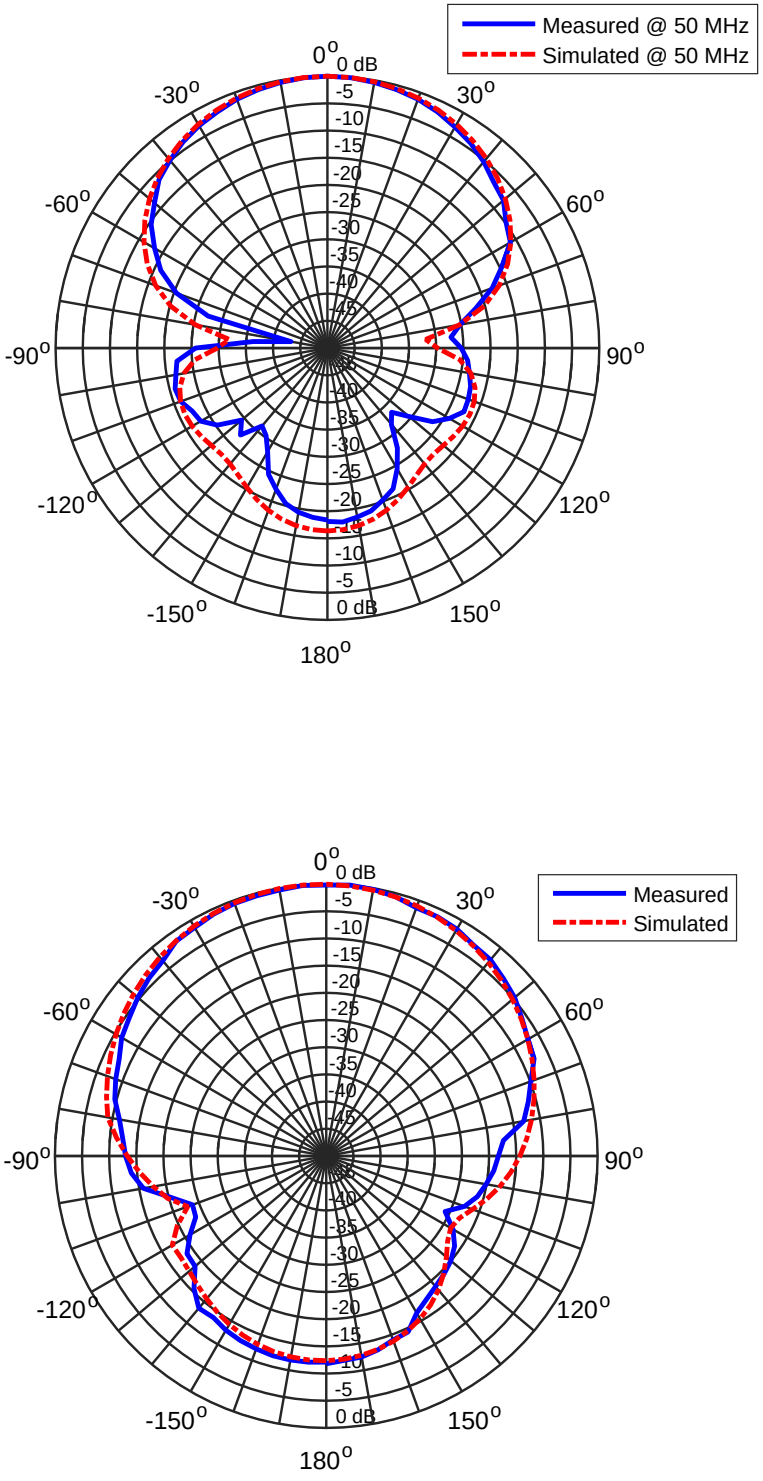

Figure 5.31: Radiation pattern of the antenna at 50 MHz (a) E-plane, (b) H-plane

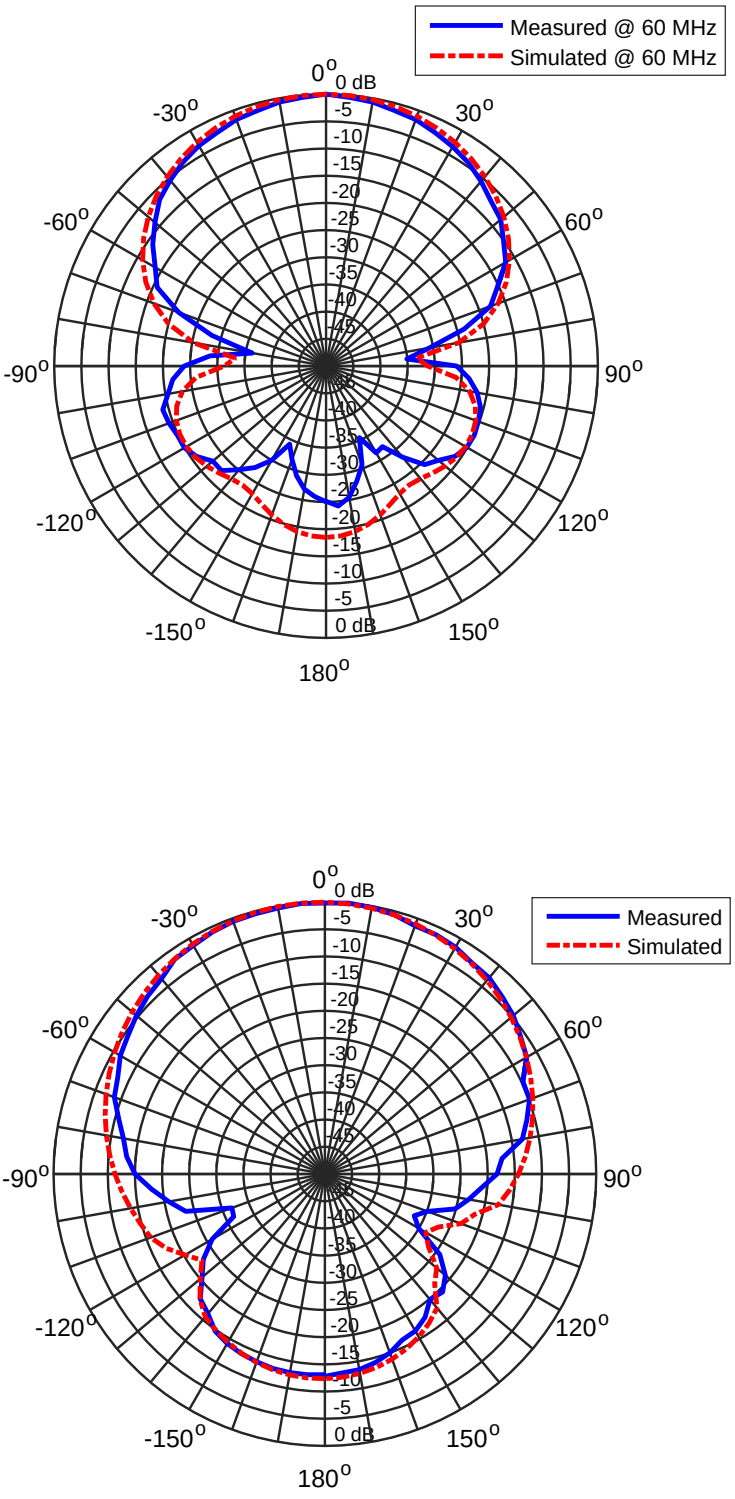

Figure 5.32: Radiation pattern of the antenna at 60 MHz (a) E-plane, (b) H-plane

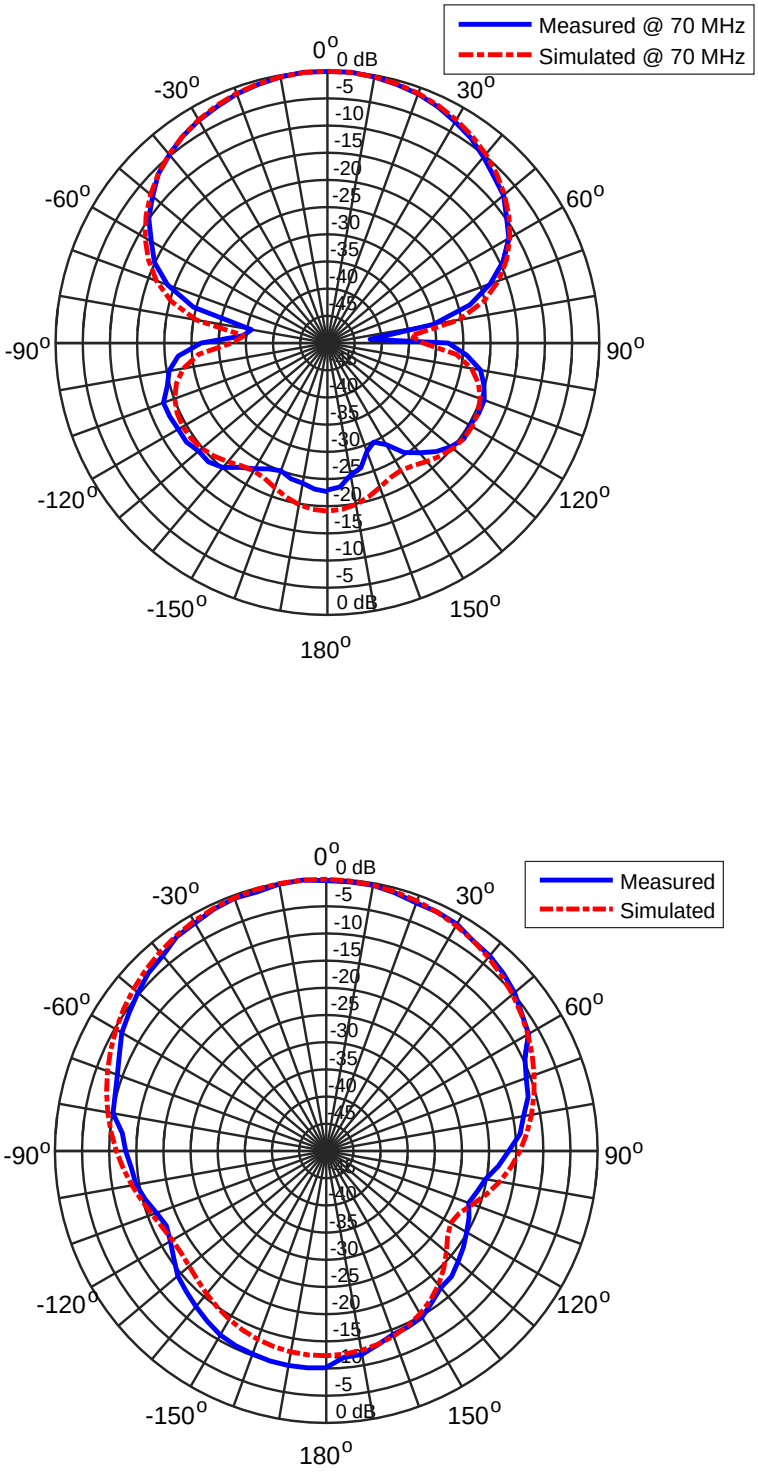

Figure 5.33: Radiation pattern of the antenna at 70 MHz (a) E-plane, (b) H-plane

5.6 ¡VAMOS! Project

¡VAMOS! known as Viable Alternative Mine Operating System is a European Union's Horizon 2020 (H2020) research and innovation funded project for developing novel approach based on robotics technologies for exploring, extraction and processing of ores in the underwater mines. Through this project high grade European reserves of deep seated minerals will be accessed thereby resulting in the provision of safe, clean and low visibility mining technique [160, 161, 162].

The project brought together about 17 partners and the task giving to our team is to provide real-time communication through underwater electromagnetic transmission in freshwater between AUV and robot for possible transference of imagery from the mine site. Prototype of the communication unit of this project is presented in Fig 5.34. This is a two way communication in which Wi-Fi frequency of 2.4 GHz is down-converted 100 MHz, which is the resonating frequency for the underwater antennas and up-converted back to 2.4 GHz. In the transmitting part the system includes; commercial Wi-Fi card known as bullet, which is an IEEE 802.11 N (also compatible with IEEE 802.11b/g) operating at 2.4 GHz, up/down converter that receive 2.4 GHz at the input and produce 100 MHz at the output and the directional antenna resonating at this down frequency. Similarly in the receiving part, the system includes the directional antenna, the up/down converter for converting 100 MHz to 2.4 GHz and the bullet. It is important to state that both the up/down converting systems and the bullet are securely protected in a glass cylinder designed for the purpose.

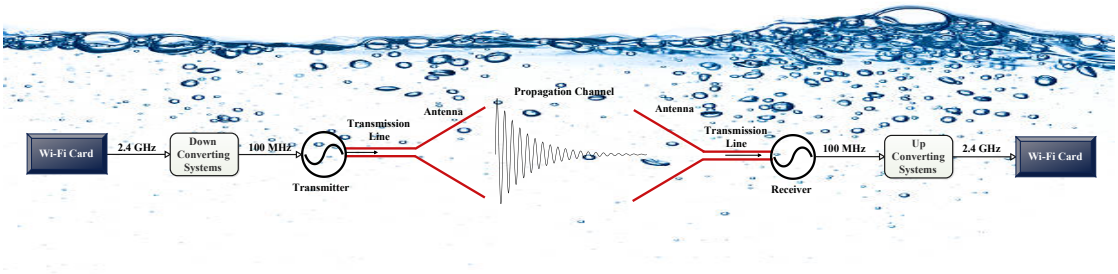

Figure 5.34: Prototype of communication unit for ¡VAMOS! project

5.6.1 Antennas for ¡VAMOS! Project

To improve propagation distance of underwater antennas, it is important to employ a highly directional antenna such as the helical antenna presented in Fig. 5.35.

Alternatively, by adding ground reflector to the antennas such as loop or dipole antennas, which will change their original radiation characteristics to the desired one.

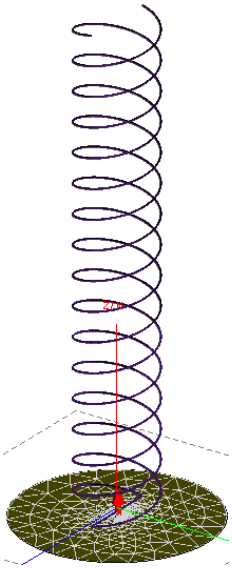

Figure 5.35: Isometric view of double helical antenna

In ¡VAMOS!, dipole and loop antennas with ground reflector were preferred to helical antenna, due to the constraints of space both on the robot and the AUV. These antennas are similar in design to the one presented in the previous section as they were also placed horizontally on the ground plane at a distance of $\lambda/4$ to the plane. But for the stability of these antennas against the water current/waves, which can result in damaging of the antennas or been totally lost to the waves in turbulent situation and also considering that the antennas will remain in the underwater mines for long term usage, the designs include encasing plastics (drilled appropriately with required diameter to contain the wire) made from High-density polyethylene (HDPE) with bracing lengths for the required space between the antennas and the ground plane. The relative permittivity and loss tangent of the HDPE used is 2.3 and 0.0004, respectively. In addition to ensure that these antennas are completely protected from falling off from the frame or against corrosion due to long usage in water, they were completely covered with epoxy material whose relative permittivity is 3.6.

5.6.2 Design Methods of the Antennas

Based on the space available for the antennas on the robot and the AUV, the initial calculation was made to ensure that both loop and dipole antennas resonate at 42 MHz. To this end, the radius of the loop antenna is 150 mm and the length of the half-wave dipole antenna is 424 mm, respectively. But to ensure adequate protection of the antennas from

water waves and also for the stability of the antennas when placed in the robot and the AUV, a plastics frames were designed for the antennas. For the loop antenna, a circular, flat HDPE plastics with thickness, inner, and outer radius of 20 mm, 140 mm and 160 mm, respectively is placed horizontally on four plastics braces, each of 20 mm thickness and 105 mm length. These are finally placed on another flat plastic of the same dimensions with the initial one, and a circular, thin aluminum ground reflector of radius 160 mm and thickness 500 μm is added. These dimensions are carefully calculated to ensure that the separation between the antenna and the ground reflector remains $\lambda/4$, which is 140 mm. In a similar manner, a rectangular frame was designed for the dipole antenna. The thickness, width, and length of the plastic are 20 mm, 20 mm and 464 mm, respectively. Also, two braces of equal length 135 mm and the same thickness with those used for the loop antenna were placed at the opposing ends of the length of the plastics. Thereafter a rectangular aluminum sheet (which has 464 mm long, 50 mm width and thickness of 500 μm) is added to the design. Since the thickness of the wire is 3 mm, trenches of 6 mm wide and 5 mm deep were made in the respective flat circular and rectangular plastics for the loop and the dipole antennas, respectively. Each antenna is placed in the appropriate trench and simulated accordingly. The simulation results in this respect shows that the initial resonating frequency of 42 MHz, is shifted to 50 MHz. This is due to the relative permittivity of the plastic added to the design. It is important to note that the frequency shift is minimal because water still filled the immediate environment of the drilled section of the plastic, where the antennas are placed. The isometric and top views of the designs showing the antennas in red are presented in Fig. 5.36.

For further protection of these antennas from wear and tear due to long usage in the underwater mines, as well as avoiding it from falling off from the plastics, epoxy resin were used to cover the antennas. These inherently fill up the space surrounding the antennas and are showing in green colour in Fig. 5.37. With this inclusion, the frequency of the antennas further shifted to 100 MHz. These change in resonating frequency is due to the relative permittivity of materials around the antennas that is altered from 81, which is the relative permittivity of water to 2.3 and 3.6 for the HDPE and epoxy resin, respectively. Indeed, the same antennas would have resonated at 250 MHz in the air, therefore, when the relative permittivities of the materials around the antennas is lowered then the resonating frequency increases. The simulation results of the reflection coefficient as a function of frequency in fresh water without and with an epoxy resin are presented in Fig. 5.38 and 5.39, respectively.

Some important observations that were noticed through the results in the previous section about the addition of the ground plane to an ordinary loop antenna include: the antenna does not require a matching circuit as seen in the simulations results of Fig. 5.38

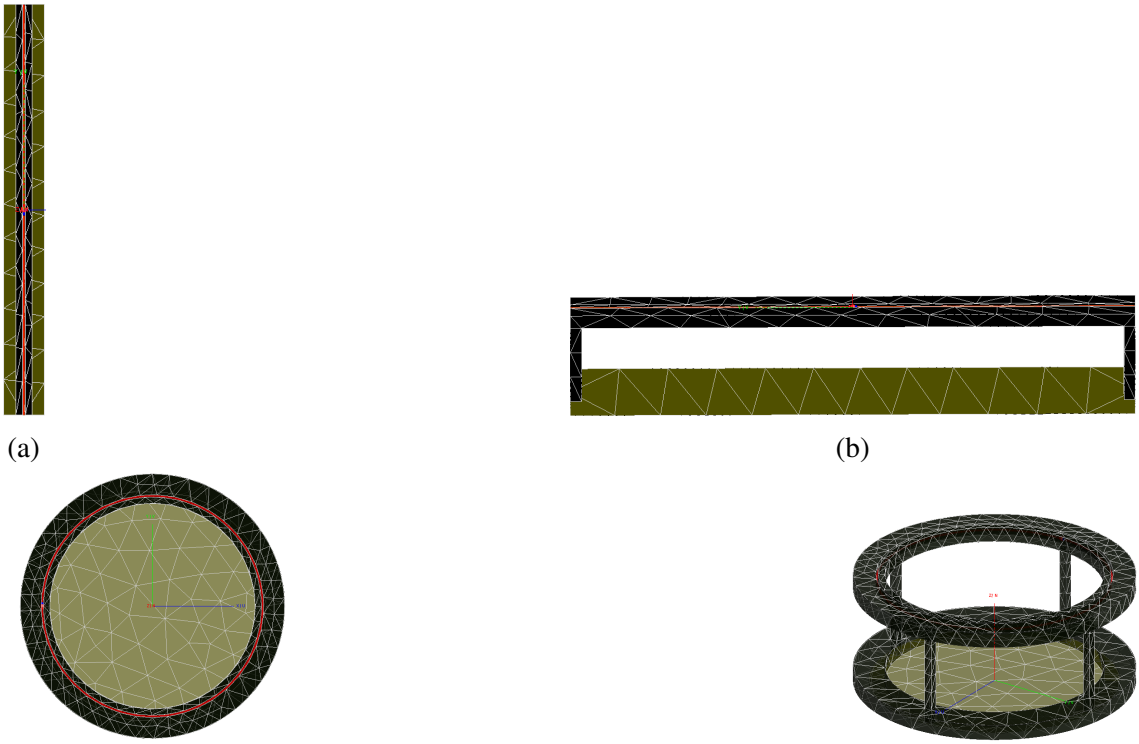

(a) (b)

(c) (d)

Figure 5.36: Antennas inside frame with ground reflector without epoxy

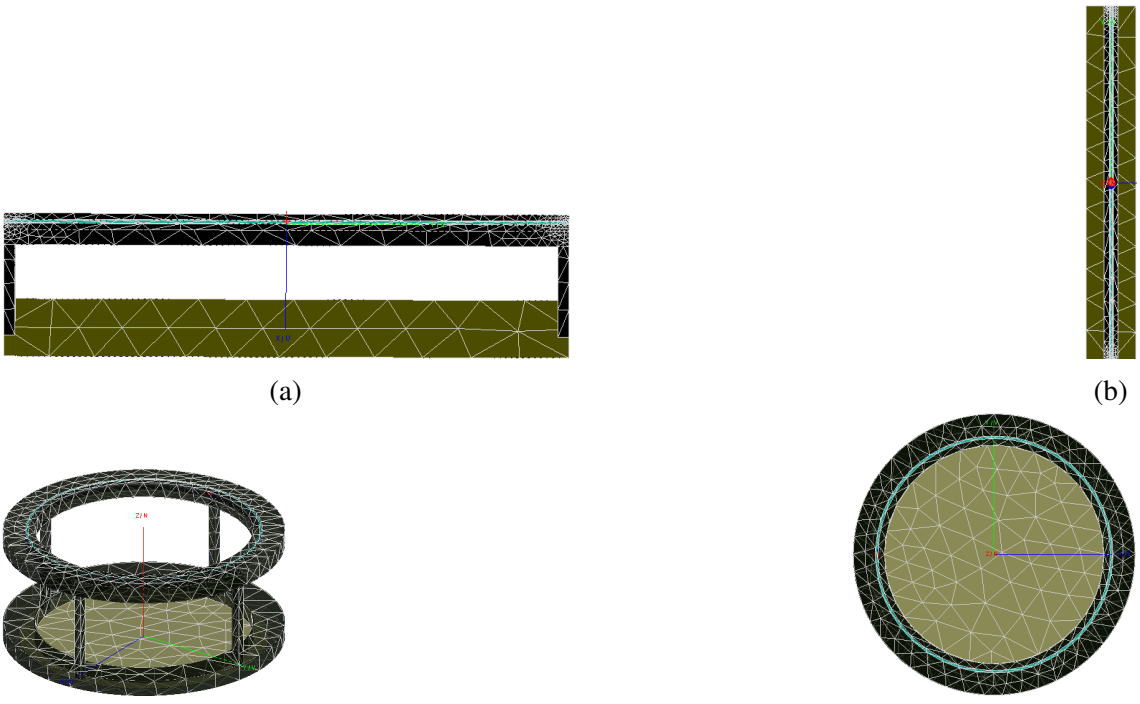

(a) (b)

(c) (d)

Figure 5.37: Antennas covered by epoxy inside frame with ground reflector

and 5.39, also the radiation characteristics of the antennas with ground reflector changes from bi-directional to a directional and the pattern is stable over a wide bandwidth. But with inclusion of plastics, the antennas experienced sharp reduction in their respective achievable bandwidths. After the epoxy resin which wholly covered the wires, the bandwidth of dipole antenna remained unchanged while that of the loop antenna reduced marginally. The conclusion can be drawn that encasing the antennas in the plastics materials is responsible for the change in their respective bandwidth.

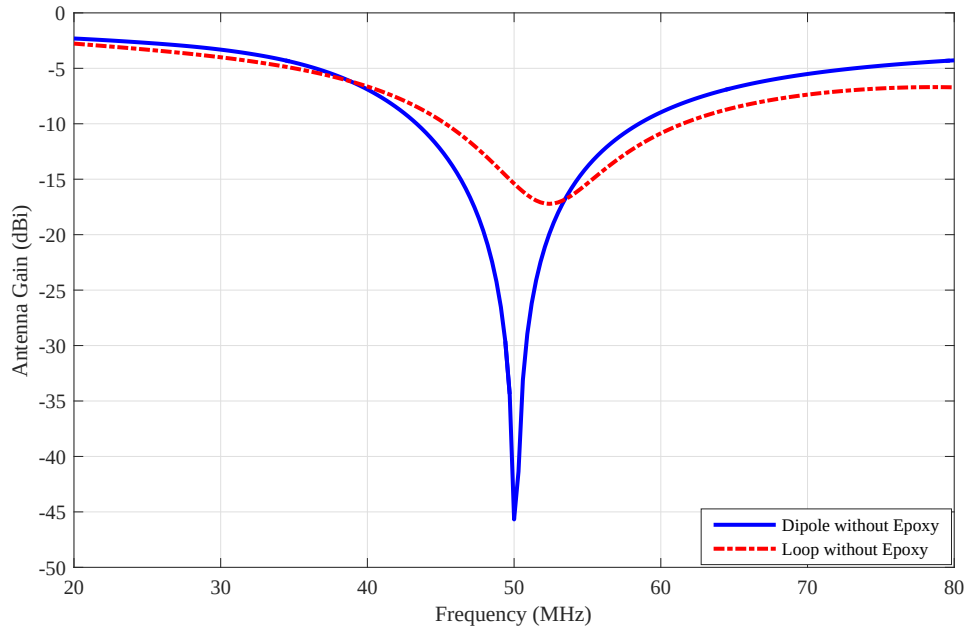

Figure 5.38: Reflection coefficient against frequency for the antennas without epoxy

The radiation pattern of the antennas appeared affected by the presence of other materials though it is still very certain that despite these materials, the antennas still remain directional. Hence, the radiation characteristics in E and H-plane of the antennas are presented in Fig. 5.40 and 5.41, respectively.

Based on the results obtained from the simulator, the antennas were fabricated accordingly. Computer Numerical Control (CNC) machine was used to make smooth trenches on the HDPE plastics. The pictures of the fabricated antennas are given in Fig. 5.42 and 5.43 for the dipole and the loop antennas, respectively.

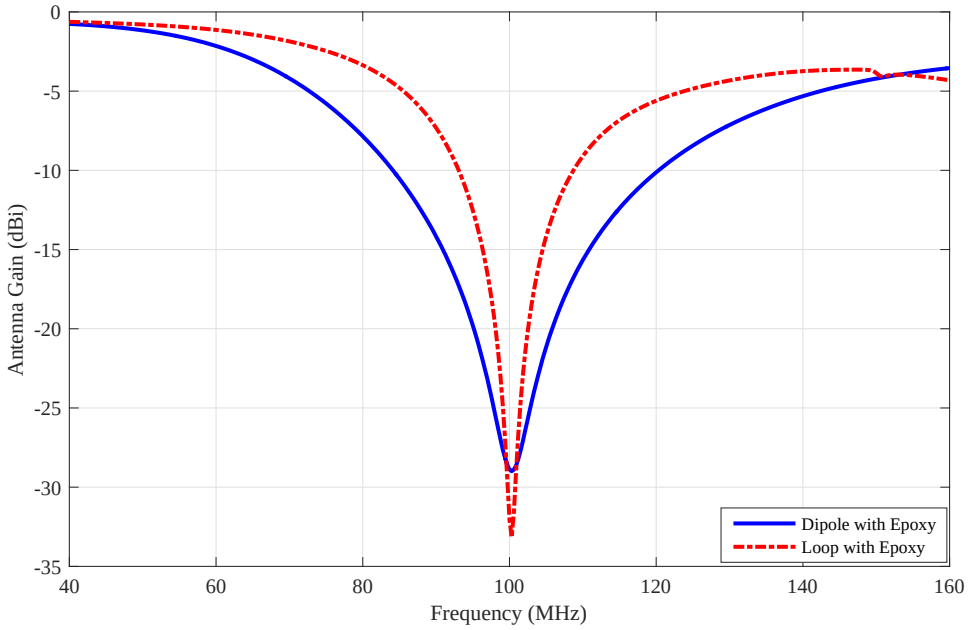

Figure 5.39: Reflection coefficient against frequency for the antennas with epoxy

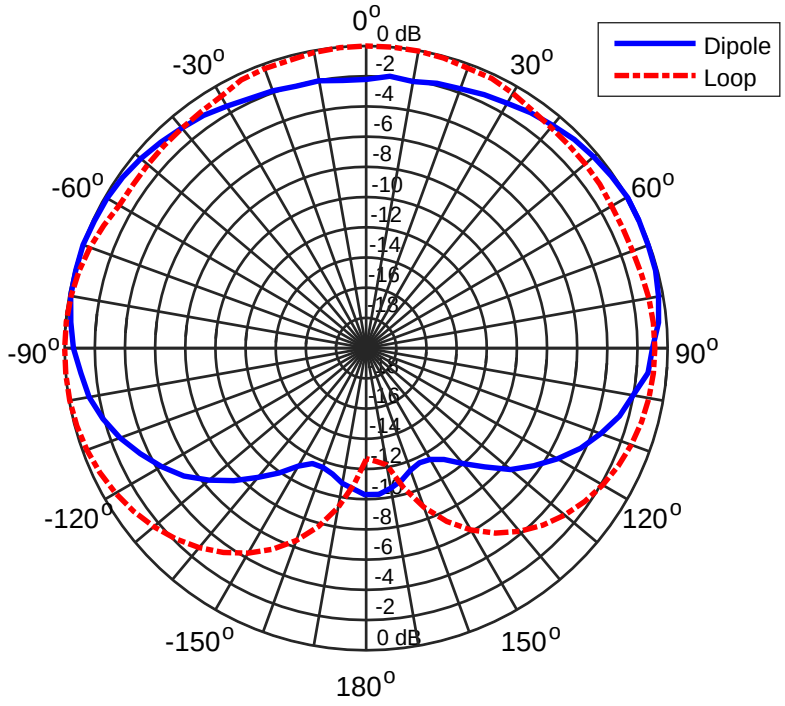

Figure 5.40: Radiation pattern of the antennas in E-plane

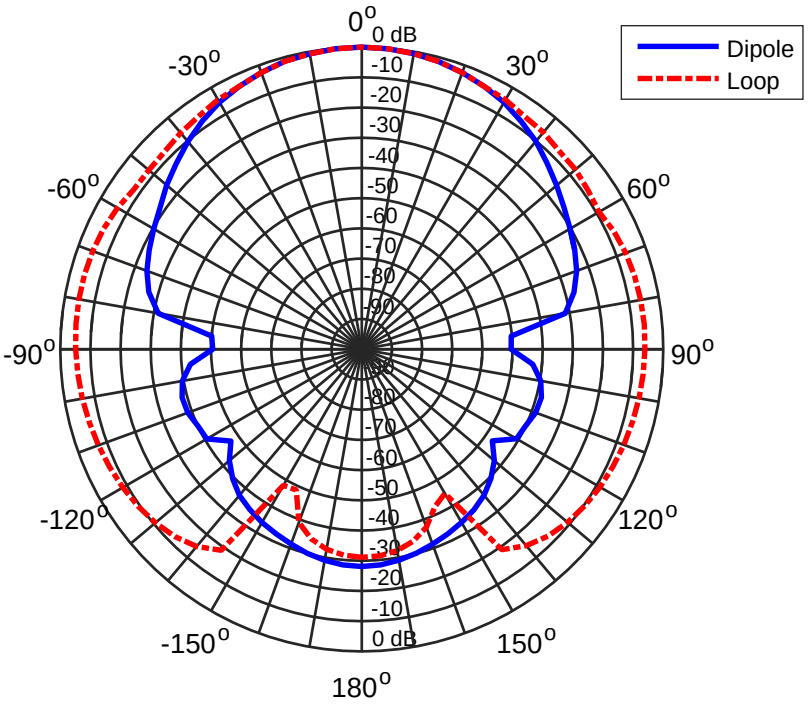

Figure 5.41: Radiation pattern of the antennas in H-plane

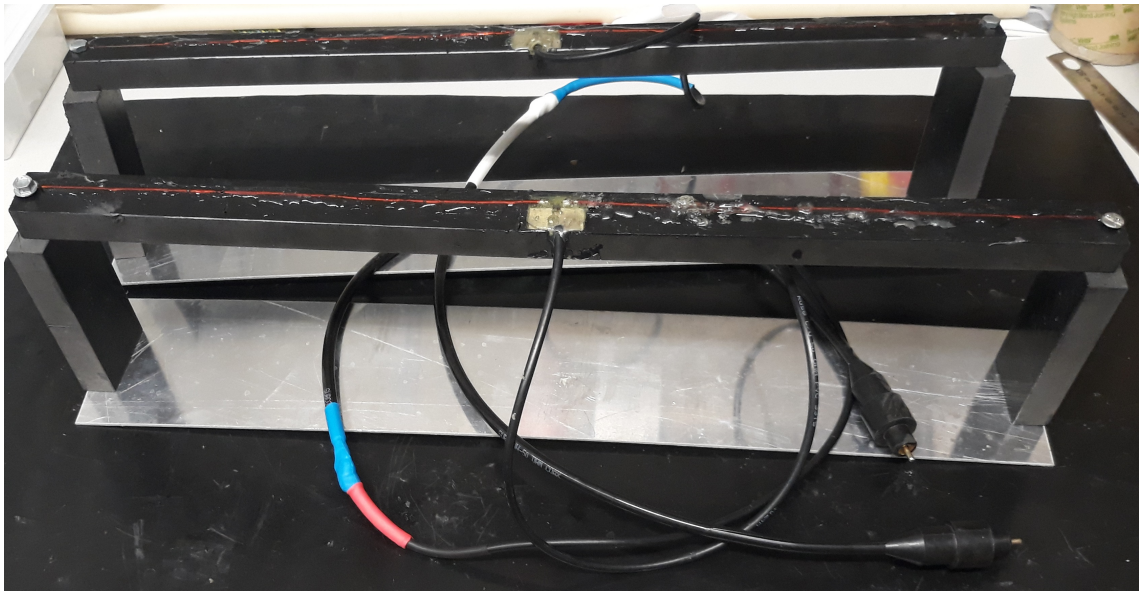

Figure 5.42: Fabricated dipole antenna for the project

Figure 5.43: Fabricated loop antenna for the project

5.6.3 Confirmation of the Achievable Data Rates of ¡VAMOS! Antennas

In the Masters' project submitted by Ricardo Pereira to the faculty of Engineering, University of Porto, titled "Project of an up-down converter and antenna for Underwater Wi-Fi Communications", antennas developed for ¡VAMOS! project was tested with up-down converter designed by the author [163]. His work centered on improving the down-converting and up-converting signals from and to the WIFI card. Through this work, it is affirmed that at a distance of 5 m between the transmitting and the receiving antennas, the achievable data rates if 9 Mb/s, when the propagation distance increased to 6 m, the data rates dropped to 4 Mb/s.

The results presented were when the wires of the antennas were only held in the plastics before and after applying epoxy. From the simulation results, the inclusion of plastics degrades the achievable bandwidth from the wideband to a seemingly narrowband, but the radiation pattern remains unchanged. Also, after applying the resin to cover the antennas, without reducing the antenna size, the resonating frequency drifted from the initial 50 MHz to 90 MHz, still the radiation pattern remains unaffected.

5.7 Friis Equation for Underwater Antennas

One of the fundamental equation in antenna technology is the Friis equation (Friis formula), which is used to calculate the received power when two antennas are separated by a distance $R > \frac{2D^2}{\lambda}$. Once the gain of the antennas are known, then the received power (P_r) can be calculated as presented in [10]:

$$P_r = \frac{P_t G_t G_r \lambda^2}{(4\pi d)^2}, \tag{5.1}$$

where P_t is the transmitted power, G_t is the gain of the transmitting antenna, G_r is the gain of the received antenna, and $R = d$ is the distance between the transmitting and the receiving antennas. The term $(\frac{\lambda}{4\pi d})^{-2}$ is known as the free-space loss (FSL), which takes into consideration losses due to spherical spreading of the energy by the antenna [13]. This is written as:

$$FSL = \left(\frac{4\pi d}{\lambda}\right)^2. \tag{5.2}$$

In free-space, this parameter is dependent on the wavelength and the distance between the transmitting and the receiving antennas. However, in water electromagnetic spreading is through a medium with conductivity and high permittivity, hence losses in water are dependent on the distance between the transmitter and the receiver, water itself and its conductive level, which increases with the resonating frequency.

To that purpose the previous equation is modified, by replacing the wavelength λ with $\frac{2\pi}{\beta}$ and the equation becomes:

$$FSL = (2d\beta)^2. \tag{5.3}$$

In decibel, FSL is given as:

$$FSL = 20\log_{10}(2d\beta). \tag{5.4}$$

For antennas that are wholly submerged in fresh or sea water, the path loss, L_p, equals the loss through the medium (water) which can be determined by considering equation 3.42 in terms of its cosine functions as:

$$\gamma = \omega\sqrt{\frac{\mu\varepsilon'(1-\cos\delta_e)}{2\cos\delta_e}} + j\omega\sqrt{\frac{\mu\varepsilon'(1+\cos\delta_e)}{2\cos\delta_e}}m, \tag{5.5}$$

Given that the attenuation constant is the real part of this equation, then path loss is given as:

$$L_p = 20.\log_{10}\left(e^{\alpha d}\right) = 8.68\alpha d. \tag{5.6}$$

in linear form, this is given as

$$L_p = 10^{(8.68\alpha d/10)}. \tag{5.7}$$

Consequently, the Friis equation for underwater antenna communication with the inclusion of the attenuation through the medium is presented as:

$$P_r = P_t G_t G_r L_p FSL. \tag{5.8}$$

Therefore, equation 5.8 will be used to determine the "**gains**" of underwater antennas and can also be the link budget for underwater communication systems, but this is not included in this thesis.

5.7.1 Realized Gains of Underwater Antennas

To determine the realized gain of underwater antennas from equation 5.8, the following equivalents were used from the S-parameters

- Transmitted power P_t relative to the incident is measured by the mismatch loss through the system, hence
$$P_t = |1 - S_{11}|^2; \tag{5.9}$$
- Received power P_r is the modulus of transmission coefficient given as

$$P_r = |S_{21}|^2. \tag{5.10}$$

Also, if the transmitting and the receiving antennas are of the same type (for instance two dipole antennas) and operating at the same frequency, then their respective gains are also equal and equation 5.8 becomes

$$|S_{21}|^2 = |1 - S_{11}|^2 G^2 L_p FSL, \tag{5.11}$$

this can be rearranged to determine the realized gains as:

$$G = \sqrt{\frac{|S_{21}|^2}{|1 - S_{11}|^2} . \frac{1}{L_P . FSL}}, \tag{5.12}$$

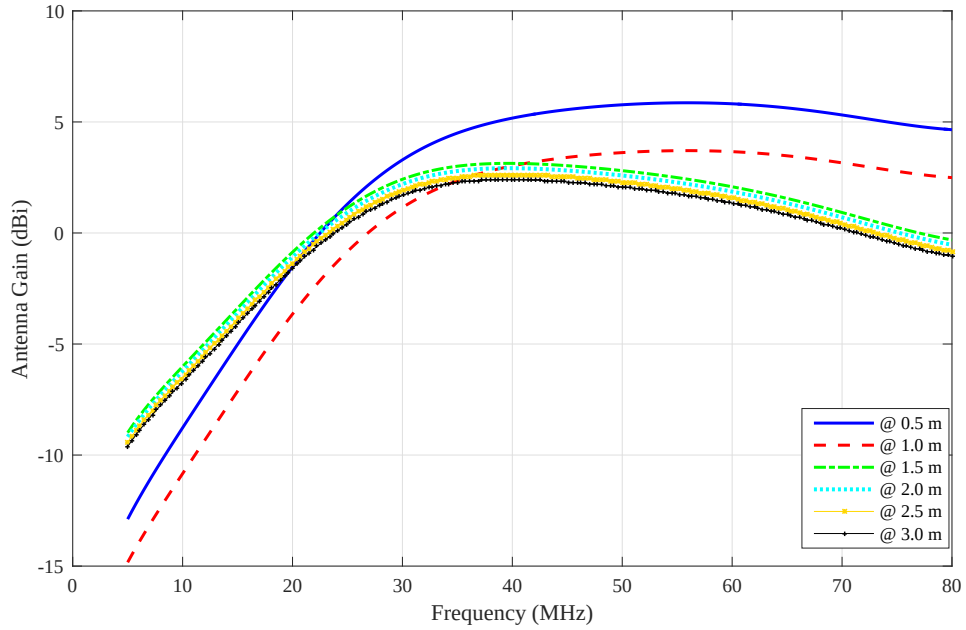

Figure 5.44: Gain against frequency for dipole antenna

It is important to note that S_{21}, the transmission coefficients and S_{11}, the reflection coefficients are obtained from the FEKO simulator, which may also be obtained from measurements.

Based on the last equation, the realized gains of some antennas were plotted as a function of frequency. The antennas considered are dipole, dipole with parasitic element, J-pole and collinear J-pole antennas:

1. Dipole antenna: The design frequency of this antenna is 40 MHz, and the plot of gain vs frequency is presented in Fig. 5.44.

   From this plot it is seen that at a distance of 0.5 m and 1.0 m between the two antennas, the gains has optimum values around 60 MHz, which is not the design frequency, but from a distance of 1.5 m, the gain reaches a maximum value at the desired operation frequency. This means that although a somewhat higher gain is obtained at closer distance, the antenna is still operating at the reactive near field, which is responsible for the noticeable shift.

2. Dipole antenna with parasitic element: This antenna is a wideband, but the frequencies of interest are 25 MHz and 40 MHz. Gain as a function of frequency for this antenna is presented in Fig. 5.45.

   This plot similarly show that at closer distances, seemingly at a reactive near field, the gain is higher at 40 MHz and 70 MHz. But at the distance of 1.5 m, is a good

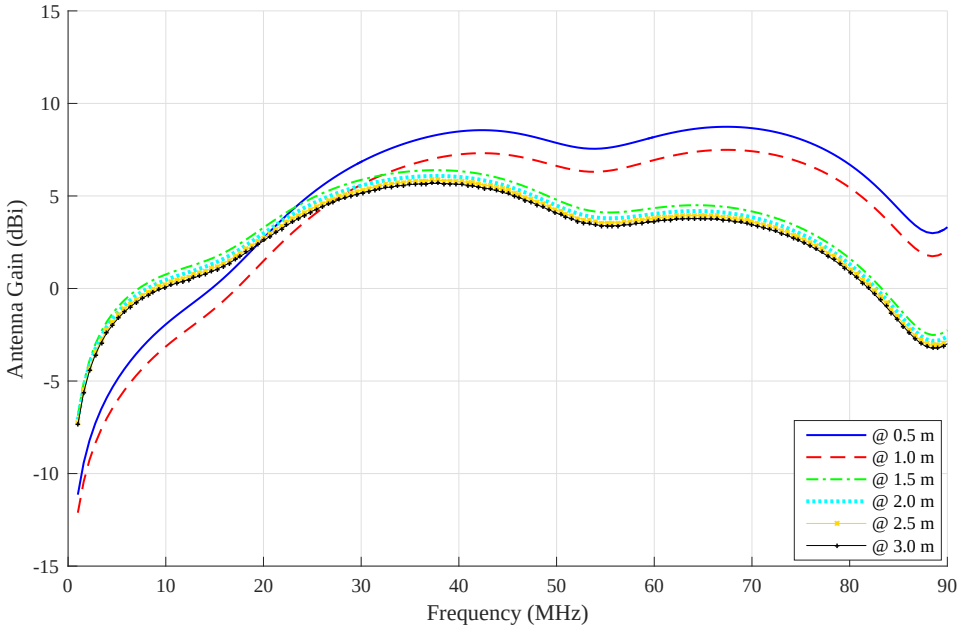

Figure 5.45: Gain against frequency for dipole antenna with parasitic element

compromise between gain and distance, the gain being 6 dB at 40 MHz, compared to 8 dB at 1 m.

3. J-pole antenna: This antenna is also design to operate at 40 MHz and the corresponding gain plot is presented in Fig. 5.46.

   Unlike the first two antennas, at the reactive near field, the antenna gain is optimum at around 30 MHz, and at higher distances, the optimum is around 35 MHz and not at 40 MHz, precisely.

4. Collinear J-pole antenna: this antenna has the same resonating frequency as the J-pole antennas and the realized gain as a function of frequency is presented in Fig. 5.47.

   Similar to the performance of J-pole antenna, the collinear J-pole also its optimum gain at 15 MHz and 35 MHz at distances equivalent to that of the reactive near field but at a further distances, only at around 40 MHz that the optimum gain occur.

The conclusion here is that for half-wave antennas, the optimum gain occur at an higher frequency than the resonating frequency when the antennas are at reactive near field region, but for a full-wave antenna, the optimum gain occur at seemingly lower frequency than the desired operating frequency in the same region.

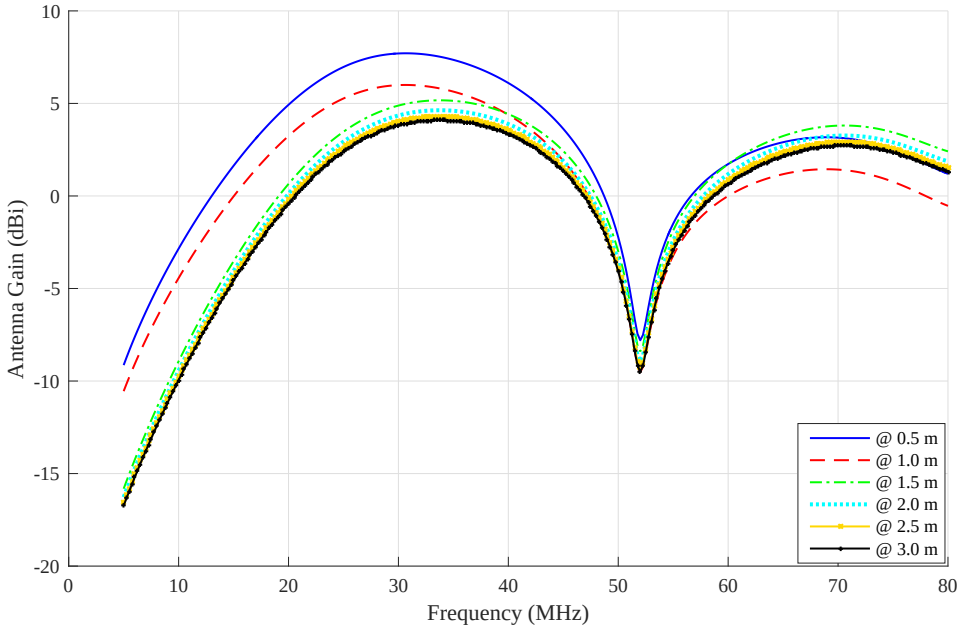

Figure 5.46: Gain against frequency for J-pole antenna

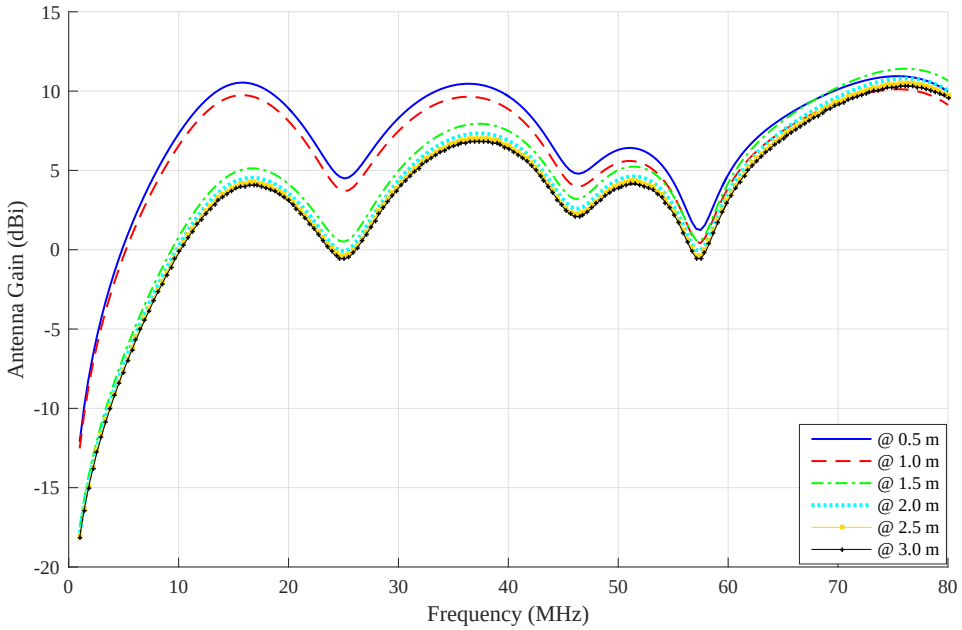

Figure 5.47: Gain against frequency for collinear J-pole antenna

5.8 Conclusion

In this chapter, dual band and wideband underwater antennas have been duly presented in this thesis. These antennas have improved bandwidth when compared with those

presented in the previous chapter. In addition, to achieve improved propagation distance in the medium, ground reflectors were calculated and placed horizontally at a specified distance from the antennas, which helped to improved radiation characteristics in the chosen direction only. When other materials like plastics and epoxy resin were used to place the antennas in containers which are materials with low permittivity, the performance of the antennas were altered entirely. Finally in this chapter, Friis equation was modified to fit usage in underwater environments. Through this equation, realized gain were eventually calculated and presented.

Chapter 6

Conclusions and Future Works

6.1 Introduction

In this last chapter of this thesis, here is the conclusion is drawn from various works presented in the entire thesis as well as the future works.

6.2 Conclusion

In this thesis, a number of antennas suitable for short-range communication in underwater scenario have been duly presented through design, simulation, construction, and measurements. These antennas are designed to operate at a high-frequency band, where the effect of attenuation in the medium is minimal and will provide reliable communication at short distances between two or more underwater bodies. With respect to bandwidth, antennas presented are narrow, dual or wideband which can be deployed depending on the requirement for data rates in its usage. In addition, structures of some selected antennas were modified to ensure their suitability to fit around an AUV, for a possible body mounting in the outer layer of an AUV. Similarly, when there is a need for improved propagation distance in a specified direction, an aluminum sheet, the tagged ground reflector can be placed horizontally at a distance not greater than $\frac{\lambda}{4}$ from the loop and dipole antennas to improve the directivity, which will consequently improve the propagation distance in that direction. Examples of these are the antennas designed for a communication unit of VAMOS project, which nonetheless has other materials around the antennas that altered their performances. Indeed, it shows the effect of permittivity on underwater antennas. It has also been shown through experimental measurements that data rates of 9 Mb/s is achievable, when the propagation distance is 5 m Finally, realized the gain for underwater antenna communications were presented, which shows

that transmission and reception of signals in the underwater environment through radio waves is possible at short propagation distance.

6.3 Future Work

For the furtherance of the work in underwater environments where submarines will have diverse communications with satellite networks and terrestrial facilities, underwater robots will on one hand harvest data from sensor nodes and instantaneously transmit such to locations above the water surface. Also, scuba divers will able to have real-time video, data and voice communications exchange with High Altitude Platform Stations (HAPS), all these will require a hybrid network of at least two of the underwater technologies. Thus, if radio waves communication is deployed as part of the hybrid network, therefore some antennas are been proposed to be used in the network.

6.3.1 Miniaturized Underwater Antenna

A compact sized, self-similar antenna been proposed is fractal antennas. These can be categorized as deterministic or random types [13]. A particular type of deterministic fractal antenna been suggested for this application is known as snowflake fractal antenna. From an ordinary square loop (generator) to the 1st iteration, where outer lengths are about 1.5 of the inner lengths, such that 8 outer lengths are equivalent to 12 inner lengths. Hence, 1st iteration has a total of 24 inner lengths if all the lengths are expressed in terms of inner lengths. A similar relationship exists between the lengths at the 4 edges and the inner lengths in the 4 wings of the 2nd iteration. Hence, generator, 1st iteration and 2nd iteration as designed using FEKO software are presented in Fig. 6.1. It is worth noting that 2nd iteration will occupy about 15.4% of the cross-sectional area of the generator and details of the analyses of the lengths of these antennas are as presented in [164]. Additionally, with the inclusion of ground reflector to this antenna, it can be made a highly directional in the medium, which will, therefore, improve the achievable propagation distance.

6.3.2 Highly Directional Antenna

The double helical antenna presented in Fig. 5.35 of chapter 5 is a highly directional antenna, which has exhibits high gain in the air. It is believed that the use of this type of antenna in the underwater environment can enhance air-water cross-boundary communication. Indeed, the system will suffer from interface loss, which is dependent

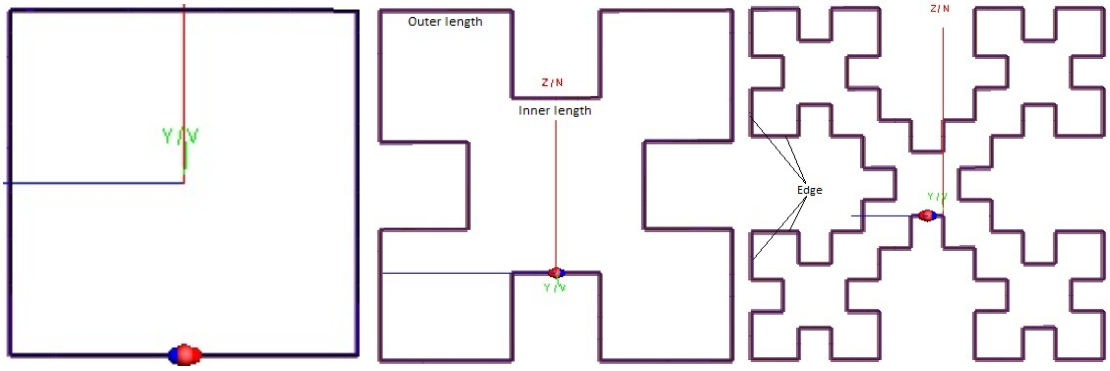

(a) Generator (b) First iteration (c) Second iteration

Figure 6.1: Two iterations snowflake fractal antenna

on the frequency, hence deploying a highly directional antenna will ensure smooth communication. It is believed that a hybrid system comprising underwater and satellite communication will benefits immensely when such antenna like this is deployed to provide the cross-boundary signal either in the transmitting or the receiving ends.

Appendix A

BALUN

A.1 Definition

Balun is the codename for balance to unbalance. It is an electrical transformer or device that converts a balanced signal to unbalanced signal. It is also defined as a three-port power splitter, which is similar to resistive power divider or Wilkinson. It has two output, which is equal in magnitude but has a 180 deg phase shift. In other words, it means the voltages in the balance line are equal but with opposite signs. Balun is a reciprocal device, which implies that it can be used in the bidirectionally. Depending on the configuration, outputs of a balun may or may not have the same impedance as the input. For instance, a 1:1 balun is expected to have an input impedance the same with the outputs, whereas a 4:1 balun sill have outputs impedances that are different from the input.

A.2 Balun in Underwater Antennas

In the designing of underwater antennas, a balun is used in two different ways. The first is to ensure matching of the input impedance to the desired 50 Ω source. But in some cases, due to the effect of the high permittivity of water, the input impedance is almost matched, a balun is still very important in the design to reduce the undesired radiation on the coaxial cable that could change some of the characteristics of the antennas by interfering with the measured parameters. Thus, current baluns were used

References

[1] L. M. Pessoa, M. R. Pereira, H. M. Santos, and H. M. Salgado, "Simulation and experimental evaluation of a resonant magnetic wireless power transfer system for seawater operation," in *OCEANS 2016 - Shanghai*, April 2016, pp. 1–5.

[2] J. Lloret, S. Sendra, M. Ardid, and J. J. Rodrigues, "Underwater wireless sensor communications in the 2.4 ghz ism frequency band," *Sensors*, vol. 12, no. 4, pp. 4237–4264, 2012.

[3] S. Jiang and S. Georgakopoulos, "Electromagnetic wave propagation into fresh water," *Journal of Electromagnetic Analysis and Applications*, vol. 3, no. 07, p. 261, 2011.

[4] J. Goh, A. Shaw, and A. Al-Shamma'a, "Underwater wireless communication system," in *Journal of Physics: Conference Series*, vol. 178, no. 1. IOP Publishing, 2009, p. 012029.

[5] Z. Hao, G. Dawei, Z. Guoping, and T. A. Gulliver, "The impact of antenna design and frequency on underwater wireless communications," in *Proceedings of 2011 IEEE Pacific Rim Conference on Communications, Computers and Signal Processing*, Aug 2011, pp. 868–872.

[6] X. Che, I. Wells, G. Dickers, and P. Kear, "Tdma frame design for a prototype underwater rf communication network," *Ad Hoc Networks*, vol. 10, no. 3, pp. 317–327, 2012.

[7] S. Cerwin, *Mobile and Maritime Antennas - The Super-J Maritime Antenna* , 21st ed., D. Straw R, Ed. ARRL Amateur Radio, 2007.

[8] D. K. Cheng *et al.*, *Field and wave electromagnetics*. Pearson Education India, 1989.

[9] B. C. Hacker, "The machines of war: western military technology 1850–2000," *History and Technology*, vol. 21, no. 3, pp. 255–300, 2005.

[10] R. E. Sheriff and Y. F. Hu, *Mobile satellite communication networks*. John Wiley & Sons, 2003.

[11] P. Sharma, "Evolution of mobile wireless communication networks-1g to 5g as well as future prospective of next generation communication network," *International*

Journal of Computer Science and Mobile Computing, vol. 2, no. 8, pp. 47–53, 2013.

[12] "Ieee standard for definitions of terms for antennas," *IEEE Std 145-2013 (Revision of IEEE Std 145-1993)*, pp. 1–50, March 2014.

[13] C. A. Balanis, "Antenna theory: analysis and design," *third edition, John wiley & sons*, 2005.

[14] W. L. Stutzman and G. A. Thiele, *Antenna theory and design*. John Wiley & Sons, 2012.

[15] T. A. Milligan, *Modern antenna design*. John Wiley & Sons, 2005.

[16] J. D. Kraus, *Antennas*. {McGraw-Hill Education}, 1988.

[17] Y. Huang and K. Boyle, *Antennas: from theory to practice*. John Wiley & Sons, 2008.

[18] "Radio spectrum," https://en.wikipedia.org/wiki/Radio_spectrum, accessed: 2010-09-07.

[19] D. Roddy, *Satellite Communications, (Professional Engineering)*. McGraw-Hill Professional: New York, 2006.

[20] H. Griffiths, L. Cohen, S. Watts, E. Mokole, C. Baker, M. Wicks, and S. Blunt, "Radar spectrum engineering and management: Technical and regulatory issues," *Proceedings of the IEEE*, vol. 103, no. 1, pp. 85–102, 2015.

[21] R. Regulations, "International telecommunication union," *Radiocommunication Sector. ITU-R. Geneva*, 2016.

[22] "QWH Series: Standard Gain Horn Antennas, howpublished = https://www.rfglobalnet.com/doc/qwh-series-standard-gain-horn-antennas-0002," accessed: 2018-05-30.

[23] V. Midasala and P. Siddaiah, "Microstrip patch antenna array design to improve better gains," *Procedia Computer Science*, vol. 85, pp. 401–409, 2016.

[24] E. Ebeleke, "'how nigcomsat will help achieve 30posted 07-March-2018. [Online]. Available: https://www.vanguardngr.com/2018/03/nigcomsat-will-help-achieve-30-broadband-target/

[25] X. Che, I. Wells, G. Dickers, P. Kear, and X. Gong, "Re-evaluation of rf electromagnetic communication in underwater sensor networks," *IEEE Communications Magazine*, vol. 48, no. 12, pp. 143–151, 2010.

[26] A. Gkikopouli, G. Nikolakopoulos, and S. Manesis, "A survey on underwater wireless sensor networks and applications," in *Control & Automation (MED), 2012 20th Mediterranean Conference on*. IEEE, 2012, pp. 1147–1154.

[27] C. Gussen, P. Diniz, M. Campos, W. A. Martins, F. M. Costa, and J. N. Gois, "A survey of underwater wireless communication technologies," *J. Commun. Inf. Sys.*, vol. 31, no. 1, pp. 242–255, 2016.

[28] M. R. Frater, M. J. Ryan, and R. M. Dunbar, "Electromagnetic communications within swarms of autonomous underwater vehicles," in *Proceedings of the 1st ACM international workshop on Underwater networks*. ACM, 2006, pp. 64–70.

[29] Z. Xiao, H. Xiao, Y. Jingwei, and S. Xueli, "Study on doppler effects estimate in underwater acoustic communication," *The Journal of the Acoustical Society of America*, vol. 133, no. 5, pp. 3463–3463, 2013.

[30] X. Guo, M. R. Frater, and M. J. Ryan, "A propagation-delay-tolerant collision avoidance protocol for underwater acoustic sensor networks," in *OCEANS 2006 - Asia Pacific*, May 2006, pp. 1–6.

[31] Z. Zeng, S. Fu, H. Zhang, Y. Dong, and J. Cheng, "A survey of underwater optical wireless communications," *IEEE Communications Surveys Tutorials*, vol. 19, no. 1, pp. 204–238, Firstquarter 2017.

[32] L. Lanbo, Z. Shengli, and C. Jun-Hong, "Prospects and problems of wireless communication for underwater sensor networks," *Wireless Communications and Mobile Computing*, vol. 8, no. 8, pp. 977–994, 2008.

[33] O. Aboderin, L. M. Pessoa, and H. M. Salgado, "Performance evaluation of antennas for underwater applications," in *2017 Wireless Days*, March 2017, pp. 194–197.

[34] A. Palmeiro, M. Martín, I. Crowther, and M. Rhodes, "Underwater radio frequency communications," in *OCEANS 2011 IEEE - Spain*, June 2011, pp. 1–8.

[35] U. Chakraborty, T. Tewary, and R. Chatterjee, "Exploiting the loss-frequency relationship using rf communication in underwater communication networks," in *Computers and Devices for Communication, 2009. CODEC 2009. 4th International Conference on*. IEEE, 2009, pp. 1–4.

[36] A. H. Taylor, "Short wave reception and transmission on ground wires (subterranean and submarine)," *Proceedings of the Institute of Radio Engineers*, vol. 7, no. 4, pp. 337–361, Aug 1919.

[37] W. H. Secor, "American greatest war invention," *Electrical Experimenter*, vol. 6, no. 11, p. 5, 1919.

[38] R. Batcher, "Loop antenna for submarines," *Wireless age*, vol. 7, p. 28, 1920.

[39] R. Llamas, *Curved spiral antennas for underwater biological applications*. The University of Iowa, 2015.

[40] K. C. Rao, P. M. Rao, and A. S. S. Rao, "Submarine based communication over years: A review," *International Journal of Innovative Research in Science, Engineering and Technology*, vol. 5, no. 12, pp. 20 983–20 995, 2016.

[41] V. R. Fisher, "The submerged receiving aerials," *The wireless Age*, vol. 7, no. 6, p. 2, March 1920.

[42] G. O. Squier, "Transmission of high frequency waves over bare wires in water," *The wireless Age*, vol. 7, no. 10, p. 2, July 1920.

[43] J. R. Wait, "The magnetic dipole over the horizontally stratified earth," *Canadian Journal of Physics*, vol. 29, no. 6, pp. 577–592, 1951.

[44] J. R. Wait, "Current-Carrying Wire Loops in a Simple Inhomogeneous Region," *Journal of Applied Physics*, vol. 23, no. 4, pp. 497–498, 1952.

[45] J. Wait, "Electromagnetic Fields of Current-Carrying Wires in a Conducting Medium," *Canadian Journal of Physics*, vol. 30, pp. 512–523, Sep. 1952.

[46] J. R. Wait and L. L. Campbell, "The fields of an electric dipole in a semi-infinite conducting medium," *Journal of Geophysical Research*, vol. 58, no. 1, pp. 21–28, 1953. [Online]. Available: <GotoISI>://WOS:A1953XX13300002

[47] J. R. Wait, "Insulated loop antenna immersed in a conducting medium," *Journal of Research of the National Bureau of Standards*, vol. 59, no. 2, 1957.

[48] A. Banos Jr and J. P. Wesley, "The horizontal electric dipole in a conducting half-space," Universi.ty of California, Tech. Rep., 1953.

[49] H. Wheeler, "Fundamental limitaions of a small vlf antenna for submarines," *IRE Transactions on Antennas and Propagation*, vol. 6, no. 1, pp. 123–125, January 1958.

[50] W. Weeks and R. Fenwick, "Submerged antenna performance," in *1958 IRE International Convention Record*, vol. 10, March 1962, pp. 108–135.

[51] R. W. Turner, "Submarine communication antenna systems," *Proceedings of the IRE*, vol. 47, no. 5, pp. 735–739, May 1959.

[52] W. Anderson and R. Moore, "Frequency spectra of transient electromagnetic pulses in a conducting medium," *IRE Transactions on Antennas and Propagation*, vol. 8, no. 6, pp. 603–607, November 1960.

[53] R. Moore and W. Blair, "Dipole radiation in a conducting half-space," *J. Res. NBS*, vol. 65, no. 6, pp. 547–563, 1961.

[54] S. Durrani, "Air-to-undersea communication with electric dipoles," *IRE Transactions on Antennas and Propagation*, vol. 10, no. 5, pp. 524–528, September 1962.

[55] R. Hansen, "Radiation and reception with buried and submerged antennas," *IEEE Transactions on Antennas and Propagation*, vol. 11, no. 3, pp. 207–216, May 1963.

[56] R. King and K. Iizuka, "The complete electromagnetic field of a half-wave dipole in a dissipative medium," *IEEE Transactions on Antennas and Propagation*, vol. 11, no. 3, pp. 275–285, May 1963.

[57] G. Hasserjian and A. Guy, "Low-frequency subsurface antennas," *IEEE Transactions on Antennas and Propagation*, vol. 11, no. 3, pp. 225–231, May 1963.

[58] R. Fenwick and W. Weeks, "Sumberged antenna characteristics," *IEEE Transactions on Antennas and Propagation*, vol. 11, no. 3, pp. 296–305, May 1963.

[59] R. Moore, "Effects of a surrounding conducting medium on antenna analysis," *IEEE Transactions on Antennas and Propagation*, vol. 11, no. 3, pp. 216–225, May 1963.

[60] R. K. Moore, "Radio communication in the sea," *IEEE Spectrum*, vol. 4, no. 11, pp. 42–51, Nov 1967.

[61] S. Durrani, "Air to undersea communication with magnetic dipoles," *IEEE Transactions on Antennas and Propagation*, vol. 12, no. 4, pp. 464–470, July 1964.

[62] R. King, B. Sandler, and T. Wu, "Cylindrical antennas immersed in arbitrary homogeneous isotropic media," *Journal of Applied Physics*, vol. 40, no. 13, pp. 5049–5065, 1969.

[63] M. Siegel and R. King, "Radiation from linear antennas in a dissipative half-space," *IEEE Transactions on Antennas and Propagation*, vol. 19, no. 4, pp. 477–485, Jul 1971.

[64] C. Tsao, "Radiation resistance of antennas in lossy media," *IEEE Transactions on Antennas and Propagation*, vol. 19, no. 3, pp. 443–444, May 1971.

[65] M. Burrows and C. Niessen, "Elf communication system design," in *Ocean 72 - IEEE International Conference on Engineering in the Ocean Environment*, Sept 1972, pp. 95–109.

[66] M. Siegel and R. King, "Electromagnetic propagation between antennas submerged in the ocean," *IEEE Transactions on Antennas and Propagation*, vol. 21, no. 4, pp. 507–513, Jul 1973.

[67] J. R. Wait, "Project sanguine," *Science*, vol. 178, no. 4058, pp. 272–275, 1972.

[68] B. Keiser, "Early development of the project sanguine radiating system," *IEEE Transactions on Communications*, vol. 22, no. 4, pp. 364–371, April 1974.

[69] R. Moore, "A simplified estimate of sanguine performance," in *Ocean 72 - IEEE International Conference on Engineering in the Ocean Environment*, Sept 1972, pp. 136–143.

[70] B. Kruger, “Sanguine system overview,” in *Ocean 72 - IEEE International Conference on Engineering in the Ocean Environment*, Sept 1972, pp. 91–94.

[71] C. Fessenden and D. Cheng, “Development of a trailing-wire e-field submarine antenna for extremely low frequency (elf) reception,” *IEEE Transactions on Communications*, vol. 22, no. 4, pp. 428–437, Apr 1974.

[72] J. Merrill, “Some early historical aspects of project sanguine,” *IEEE Transactions on Communications*, vol. 22, no. 4, pp. 359–363, Apr 1974.

[73] J. Wait, “Historical background and introduction to the special issue on extremely low frequency (elf) communications,” *IEEE Transactions on Communications*, vol. 22, no. 4, pp. 353–354, April 1974.

[74] S. L. Bernstein, M. L. Burrows, J. E. Evans, A. S. Griffiths, D. A. McNeill, C. W. Niessen, I. Richer, D. P. White, and D. K. Willim, “Long-range communications at extremely low frequencies,” *Proceedings of the IEEE*, vol. 62, no. 3, pp. 292–312, March 1974.

[75] S. Wolf, J. Davis, and M. Nisenoff, “Superconducting extremely low frequency (elf) magnetic field sensors for submarine communications,” *IEEE Transactions on Communications*, vol. 22, no. 4, pp. 549–554, Apr 1974.

[76] H. Momma and T. Tsuchiya, “Underwater communication by electric current,” in *OCEANS ’76*, Sept 1976, pp. 631–636.

[77] J. Davis, R. Dinger, and J. Goldstein, “Development of a superconducting elf receiving antenna,” *IEEE Transactions on Antennas and Propagation*, vol. 25, no. 2, pp. 223–231, March 1977.

[78] J. Wait, “Propagation of elf electromagnetic waves and project sanguine/seafarer,” *IEEE Journal of Oceanic Engineering*, vol. 2, no. 2, pp. 161–172, Apr 1977.

[79] R. Decesari, “Buoyant module vhf antenna design for submerged systems/aircraft communications,” in *OCEANS ’79*, Sept 1979, pp. 366–372.

[80] A. Arutaki and J. Chiba, “Communication in a three-layered conducting media with a vertical magnetic dipole,” *IEEE Transactions on Antennas and Propagation*, vol. 28, no. 4, pp. 551–556, Jul 1980.

[81] M. Callaham, “Submarine communications,” *IEEE Communications Magazine*, vol. 19, no. 6, pp. 16–25, November 1981.

[82] D. L. Jones, “Sending signals to submarines,” *New Scientist*, vol. 106, no. 1463, pp. 37–41, 1985.

[83] L. B. VK5BR, “Underwater radio communication,” *Originally published in Amateur Radio*, 1987.

[84] R. M. Dunbar, “A surface-contour electromagnetic wave antenna for short-range subsea communications,” in *Sixth International Conference on Electronic Engineering in Oceanography, 1994.*, Jul 1994, pp. 117–123.

[85] B. Benhabiles, P. Lacour, M. Pellet, C. Pichot, and A. Papiernik, “A study of vlf antennas immersed in sea water: theoretical, numerical, and experimental results,” *IEEE Antennas and Propagation Magazine*, vol. 38, no. 5, pp. 19–29, Oct 1996.

[86] R. W. P. King, C. W. Harrison, and V. A. Houdzoumis, “Electromagnetic field in the sea due to an omnidirectional vlf antenna,” *Radio Science*, vol. 32, no. 1, pp. 103–112, Jan 1997.

[87] R. W. P. King, “Directional vlf antenna for communicating with submarines,” *Radio Science*, vol. 32, no. 1, pp. 113–125, Jan 1997.

[88] B. Aldridge, “Elf history: extremely low frequency communication,” PLRCPacific Life Research Center, Tech. Rep. PLRC-941005B, 2001.

[89] A. Monin, “Submarine floating antenna model for loran-c signal processing,” *IEEE Transactions on Aerospace and Electronic Systems*, vol. 39, no. 4, pp. 1304–1315, Oct 2003.

[90] A. I. Al-Shamma’a, A. Shaw, and S. Saman, “Propagation of electromagnetic waves at mhz frequencies through seawater,” *IEEE Transactions on Antennas and Propagation*, vol. 52, no. 11, pp. 2843–2849, Nov 2004.

[91] A. Karlsson, “Physical limitations of antennas in a lossy medium,” *IEEE Transactions on Antennas and Propagation*, vol. 52, no. 8, pp. 2027–2033, Aug 2004.

[92] C. A. Altgelt, “The world’s largest "radio" station,” *accessed from internet*, 2005.

[93] R. Tamas, “Evaluation of the mutual coupling between shipborne antennas,” in *Europe Oceans 2005*, vol. 2, June 2005, pp. 1343–1346 Vol. 2.

[94] A. Shaw, A. i. Al-Shamma’a, S. R. Wylie, and D. Toal, “Experimental investigations of electromagnetic wave propagation in seawater,” in *2006 European Microwave Conference*, Sept 2006, pp. 572–575.

[95] F. Plonski and C. M. Gyenes, “Efficient hf submarine antennas,” in *2008 IEEE Antennas and Propagation Society International Symposium*, July 2008, pp. 1–4.

[96] C. Liu, L.-G. Zheng, and Y.-P. Li, “Study of elf electromagnetic fields from a submerged horizontal electric dipole positioned in a sea of finite depth,” in *Microwave, Antenna, Propagation and EMC Technologies for Wireless Communications, 2009 3rd IEEE International Symposium on*. IEEE, 2009, pp. 152–157.

[97] Y. Cai and R. Ding, "Application of superconductor in elf communication," in *2009 International Conference on Applied Superconductivity and Electromagnetic Devices*, Sept 2009, pp. 77–80.

[98] B. Austin, "Signalling to submarines at extremely low frequencies," *Radio Bygones*, no. 118, pp. 10–17, 2009.

[99] A. Garcia Miquel, "Uwb antenna design for underwater communications," Ph.D. dissertation, Universitat Politecnica de Catalunya, 2009.

[100] R. M. Dunbar, M. R. Frater, M. J. Ryan, and G. N. Milford, "Undersea electromagnetic networking," in *2011 Military Communications and Information Systems Conference*, Nov 2011, pp. 1–9.

[101] G. Thompson, H. Widmer, K. Rice, R. Ball, and J. Sweeney, "Buoyant cable antenna technology for enhancing submarine communications atspeed and depth," *Johns Hopkins APL technical digest*, vol. 20, no. 3, pp. 285–296, 1999.

[102] A. M. Karim, S. J. Stafford, and R. Benjamin Baker, "Global positioning system over fiber for buoyant cable antennas," *Johns Hopkins APL Technical Digest*, vol. 30, no. 4, pp. 309–320, 2012.

[103] B. Kelley and K. Naishadham, "High data rate undersea broadband radio-frequency communications," in *2014 IEEE Antennas and Propagation Society International Symposium (APSURSI)*, July 2014, pp. 695–696.

[104] M. Manteghi and A. A. Y. Ibraheem, "On the study of the near-fields of electric and magnetic small antennas in lossy media," *IEEE Transactions on Antennas and Propagation*, vol. 62, no. 12, pp. 6491–6495, Dec 2014.

[105] H. Wang, K. Zheng, K. Yang, and Y. Ma, "Electromagnetic field in air produced by a horizontal magnetic dipole immersed in sea: Theoretical analysis and experimental results," *IEEE Transactions on Antennas and Propagation*, vol. 62, no. 9, pp. 4647–4655, Sept 2014.

[106] M. Manteghi, "An electrically small antenna for underwater applications," in *2016 IEEE International Symposium on Antennas and Propagation (APSURSI)*, June 2016, pp. 1745–1746.

[107] A. Massaccesi and P. Pirinoli, "Analysis of antennas for underwater applications," in *2017 11th European Conference on Antennas and Propagation (EUCAP)*, March 2017, pp. 1907–1910.

[108] G. S. Saran and G. Held, "Field strength mesurements in fresh water," *Journal of Research of the National Bureau of Standards D*, vol. 52, pp. 435–437, 1960.

[109] M. Siegel and R. W. King, "Electromagnetic fields in a dissipative half-space: A numerical approach," *Journal of Applied Physics*, vol. 41, no. 6, pp. 2415–2423, 1970.

[110] L. Shen, R. W. King, and R. Sorbello, "Measured field of a directional antenna submerged in a lake," *IEEE Transactions on Antennas and Propagation*, vol. 24, no. 6, pp. 891–894, Nov 1976.

[111] L. C. Shen, K. M. Lee, and R. W. P. King, "Coupled horizontal-wire antennas over a conducting or dielectric half space," *Radio Science*, vol. 12, no. 5, pp. 687–698, Sept 1977.

[112] H. M. Hafez, W. J. Chudobiak, and J. S. Wight, "The attenuation rate in fresh water at vhf frequencies," *IEEE Transactions on Instrumentation and Measurement*, vol. 28, no. 1, pp. 71–74, March 1979.

[113] L. N. An and G. S. Smith, "The horizontal circular loop antenna near a planar interface," *Radio Science*, vol. 17, no. 03, pp. 483–502, May 1982.

[114] G. S. Smith and L. N. An, "Loop antennas for directive transmission into a material half space," *Radio Science*, vol. 18, no. 05, pp. 664–674, Sept 1983.

[115] G. Smith, "Directive properties of antennas for transmission into a material half-space," *IEEE Transactions on Antennas and Propagation*, vol. 32, no. 3, pp. 232–246, March 1984.

[116] F. Travade, P. Bomassi, J. Bach, C. Brugel, P. Stein-bach, J. Luquet, and G. Pustelnik, "Use of radiotracking in france for recent studies concerning the edf fishways program," *Hydroécologie Appliquée*, vol. 1, pp. 33–51, 1989.

[117] J. W. Beeman, C. Grant, and P. V. Haner, "Comparison of three underwater antennas for use in radiotelemetry," *North American Journal of Fisheries Management*, vol. 24, no. 1, pp. 275–281, 2004.

[118] R. Zhou, H. Zhang, and H. Xin, "A compact water based dielectric resonator antenna," in *2009 IEEE Antennas and Propagation Society International Symposium*, June 2009, pp. 1–4.

[119] C. Conessa and A. Joisel, "Active wideband antenna for underwater tomography (1 ghz)," *Electronics Letters*, vol. 45, no. 4, pp. 193–194, February 2009.

[120] K. P. Hunt, J. J. Niemeier, and A. Kruger, "Short paper: Antennas for mussel-based underwater biological sensor networks in rivers," *WUWNET, ACM*, 2010.

[121] H. F. G. Mendez, C. Gac, F. L. Pennec, and C. Person, "High performance underwater uhf radio antenna development," in *OCEANS 2011 IEEE - Spain*, June 2011, pp. 1–5.

[122] A. A. Abdou, A. Shaw, A. Mason, A. Al-Shamma'a, J. Cullen, and S. Wylie, "Electromagnetic (em) wave propagation for the development of an underwater wireless sensor network (wsn)," in *2011 IEEE SENSORS Proceedings*, Oct 2011, pp. 1571–1574.

[123] S. Kumar, "Design and comparison of modified circular bow-tie antenna for under water radio communication by optimized parameters," *International Journal of Innovative Research in Technology & Science (IJIRTS)*, 2012.

[124] A. Abdou, A. Shaw, A. Mason, A. Al-Shamma'a, J. Cullen, S. Wylie, and M. Diallo, "A matched bow-tie antenna at 433mhz for use in underwater wireless sensor networks," in *Journal of Physics: Conference Series*, vol. 450, no. 1. IOP Publishing, 2013, pp. 1–7.

[125] S. Sendra, J. Lloret, J. J. P. C. Rodrigues, and J. M. Aguiar, "Underwater wireless communications in freshwater at 2.4 ghz," *IEEE Communications Letters*, vol. 17, no. 9, pp. 1794–1797, September 2013.

[126] E. A. Karagianni, "Electromagnetic waves under sea: bow-tie antennas design for wi-fi underwater communications," *Progress In Electromagnetics Research*, vol. 41, pp. 189–198, 2015.

[127] H. Yoshida, N. Iwakiri, T. Fukuda, M. Deguchi, and S. Onogi, "Measurements of underwater electromagnetic wave propagation," in *2015 IEEE Underwater Technology (UT)*, Feb 2015, pp. 1–5.

[128] R. A. Llamas, J. J. Niemeier, and A. Kruger, "Curved spiral antennas for freshwater applications," in *2015 IEEE Radio and Wireless Symposium (RWS)*, Jan 2015, pp. 53–55.

[129] A. Massaccesi and P. Pirinoli, "Preliminary results on cylindrical antennas for underwater communication," in *2016 IEEE International Symposium on Antennas and Propagation (APSURSI)*, June 2016, pp. 1895–1896.

[130] D. M. Pozar, *Microwave Engineering*. John Wiley & Sons, 2011.

[131] M. R. S. Pereira, *Inverse Scattering Techniques for the Synthesis of Microwave Structures*. Universidade do Porto, 2014.

[132] R. E. Collin, *Foundations for Microwave Engineering*. John Wiley & Sons, 2007.

[133] K. S. Cole and R. H. Cole, "Dispersion and absorption in dielectrics i. alternating current characteristics," *The Journal of chemical physics*, vol. 9, no. 4, pp. 341–351, 1941.

[134] F. Franks, *The physics and physical chemistry of water*. Springer Science & Business Media, 2012, vol. 1.

[135] R. Somaraju and J. Trumpf, "Frequency, temperature and salinity variation of the permittivity of seawater," *IEEE Transactions on Antennas and Propagation*, vol. 54, no. 11, pp. 3441–3448, Nov 2006.

[136] F. T. Ulaby, U. Ravaioli, and E. Michielssen, *Fundamentals of applied electromagnetics*. Prentice Hall, 2014.

[137] L. Klein and C. Swift, "An improved model for the dielectric constant of sea water at microwave frequencies," *IEEE Journal of Oceanic Engineering*, vol. 2, no. 1, pp. 104–111, 1977.

[138] S. I. Inácio, M. R. Pereira, H. M. Santos, L. M. Pessoa, F. B. Teixeira, M. J. Lopes, O. Aboderin, and H. M. Salgado, "Antenna design for underwater radio communications," in *OCEANS 2016 - Shanghai*, April 2016, pp. 1–6.

[139] L. M. Pessoa, M. R. Pereira, O. Aboderin, H. M. Salgado, and S. I. Inácio, "Antenna for underwater radio communications," patentep 3 291 364A1.

[140] P. A. Mendez and R. James, "A comparative study of underwater wireless optical communication for three different communication links," *Journal of Electronics and Communication Engineering*, vol. 10, no. 3, pp. 40–48, 2015.

[141] F. Teixeira, P. Freitas, L. Pessoa, R. Campos, and M. Ricardo, "Evaluation of ieee 802.11 underwater networks operating at 700 mhz, 2.4 ghz and 5 ghz," in *Proceedings of the International Conference on Underwater Networks & Systems*. ACM, 2014, p. 11.

[142] A. Netchaev, J. Klein, C. Thurmer, B. Carver, and J. Evans, "Medium range underwater communication development system," in *2016 IEEE SENSORS*, Oct 2016, pp. 1–3.

[143] C. A. Balanis, "Antenna theory: a review," *Proceedings of the IEEE*, vol. 80, no. 1, pp. 7–23, Jan 1992.

[144] Y. Rahmat-Samii, L. I. Williams, and R. G. Yaccarino, "The ucla bi-polar planar-near-field antenna-measurement and diagnostics range," *IEEE Antennas and Propagation Magazine*, vol. 37, no. 6, pp. 16–35, Dec 1995.

[145] A. H. F. S. Simulator, "Version 10.0," *Ansoft Corporation*, 2005.

[146] A. Boyer, "Getting started with feko software," *National Institute of Applied Sciences Toulouse*, 2008.

[147] S. I. Inácio, M. R. Pereira, H. M. Santos, L. M. Pessoa, F. B. Teixeira, M. J. Lopes, O. Aboderin, and H. M. Salgado, "Dipole antenna for underwater radio communications," in *2016 IEEE Third Underwater Communications and Networking Conference (UComms)*, Aug 2016, pp. 1–5.

[148] M. Rhodes, "Underwater electromagnetic propagation: re-evaluating wireless capabilities," *Hydro International*, vol. 10, no. 10, pp. 28–31, 2006.

[149] V. Bhavsar, N. Blas, H. Nguyen, and A. Balandin, "Measurement of antenna radiation patterns laboratory manual," *EE117 Laboratory Manual, UC-Riverside, Retrieved on April*, vol. 20, no. 2010, pp. 1–42, 2000.

[150] H. Beggerow, "Zeppelin antenna," 1909.

[151] J. S. Huggins, “Improving the super j-pole antenna,” 2012.

[152] A. R. Djordjević, A. G. Zajić, M. M. Ilić, and G. L. Stüber, “Optimization of helical antennas,” *IEEE Antennas and Propagation Magazine*, vol. 48, no. 6, pp. 107–115, 2006.

[153] N. A. Cruz and A. C. Matos, “The mares auv, a modular autonomous robot for environment sampling,” in *OCEANS 2008*, Sept 2008, pp. 1–6.

[154] N. A. Cruz, A. C. Matos, R. M. Almeida, B. M. Ferreira, and N. Abreu, “Trimares-a hybrid auv/rov for dam inspection,” in *OCEANS 2011*. IEEE, 2011, pp. 1–7.

[155] A. Matos, N. Cruz, and F. L. Pereira, “Post mission trajectory smoothing for the isurus auv,” in *Oceans 2003. Celebrating the Past ... Teaming Toward the Future (IEEE Cat. No.03CH37492)*, vol. 2, Sept 2003, pp. 683–687 Vol.2.

[156] A. Ayorinde, S. Adekola, A. I. Mowete, and W. Island, “Performance characteristics of loop antennas above a ground plane of finite extent,” in *PIERS Proceedings*, 2013, pp. 769–744.

[157] D. Jefferies, “Experiments on loops above ground,” *antenneX Online*, no. 106, p. 8, 2006.

[158] J. Iwashige, “Analysis of loop antenna with circular reflector and its properties,” *Electronics and Communications in Japan (Part I: Communications)*, vol. 63, no. 11, pp. 44–50, 1980.

[159] O. Aboderin, S. I. Inacio, H. M. Santos, M. R. Pereira, L. M. Pessoa, and H. M. Salgado, “Analysis of j-pole antenna configurations for underwater communications,” in *OCEANS 2016 MTS/IEEE Monterey*, Sept 2016, pp. 1–5.

[160] J. Almeida, A. Ferreira, B. Matias, A. Dias, A. Martins, F. Silva, J. Oliveira, P. Sousa, M. Moreira, T. Miranda *et al.*, “Air and underwater survey of water enclosed spaces for vamos! project,” in *OCEANS 2016 MTS/IEEE Monterey*. IEEE, 2016, pp. 1–5.

[161] C. Sword, B. Bodo, S. Kapusniak, F. Bosman, J. Rainbird, and E. Silva, “¡ vamos! (viable alternative mine operating system) - a ’horizon 2020’ project,” in *EGU General Assembly Conference Abstracts*, vol. 19, 2017, p. 348.

[162] M. Bleier, A. Dias, A. Ferreira, J. Pidgeon, J. Almeida, E. Silva, K. Schilling, and A. Nüchter, “Real-time 3d Mine Modelling in the ¡vamos! Project,” pp. 1–12, 2017.

[163] J. R. Pereira, “Projeto de up-down converter e antena para comunicações wi-fi sub-aquáticas,” 2018.

[164] F. Hughes, “Fractal type antennas,” *http://www.vk6fh.com/vk6fh/fractal.htm*, 2013, accessed: 2018-07-15.